# The Role of the Coagulation Cascade in Liver Injury

**Gemma Susan Petts**

**PhD**

**Imperial College London, Department of Medicine**

**Abstract**

Liver disease affects approximately 600,000 people in England and Wales and is the third biggest cause of premature death. Acute and chronic liver injury occur due to a number of aetiologies and affect the function of the liver in the short and long term through pathological inflammation and fibrosis. Given the variety of aetiologies and growing burden of disease in the population, there is a need to find universal therapies that alter the progression of liver injury and fibrosis beyond the initiating insult.

This work focuses on investigating the role of the coagulation cascade, specifically Tissue Factor Pathway Inhibitor (TFPI), in liver injury and it's use as a potential therapeutic target for altering the progression of acute and chronic liver injury.

Using two transgenic strains of mice, expressing TFPI in a cell specific manner I have shown that TFPI decreases the extent and progression of liver injury in models of acute liver injury but does not modify the development of liver fibrosis in a model of chronic liver injury.

In the models of acute liver injury there was decreased liver injury associated with decreased fibrin deposition, decreased hepatic stellate cell activation, decreased total liver macrophage content and decreased PAR2 expression. The pattern of changes suggests that TFPI acts early in the injury process, limiting total hepatocyte injury and resulting in a decrease in hepatic stellate cell activation and macrophage recruitment, rather than the other way round.

Further work should focus on defining the inflammatory cytokine profile of the liver of these transgenic mice in acute liver injury with the aim of describing the biological mechanism for the action of TFPI in acute liver injury and taking forward the trial of TFPI administration to control mice in a manner that could be carried forward to human studies.

**Declaration of Originality**

I confirm that the work described in this thesis is my own and all else is appropriately referenced.

Gemma Susan Petts

July 2016

**For Freddy**

**Acknowledgments**

I would like to thank my supervisors Professor Robert Goldin and Professor Mark Thursz for their guidance and support throughout the time I spent carrying out this research and building up to it.

I would like to acknowledge the financial support from the NIHR Academic Clinical Fellowship scheme that allowed me the time and opportunity to start on this body of work and the Jean Shanks Foundation and The Pathological Society of Great Britain and Ireland who generously supported the me through their 3 year Research Training Fellowship.

I would like to show my appreciation to the fantastic group of postgraduate researchers with whom I was privileged to share an office space during this work. Their insight, queries and own struggles helped me develop my work and analytical thought processes. I would particularly like to acknowledge Hiromi Kudo, Dr Lucia Possamai, Dr Fouzia Sadiq, Dr Susanne Knapp and Dr Wafa Khamri who guided me through many of the challenges I faced with laboratory techniques. I would also like to acknowledge the support and guidance of the dedicated team of biomedical scientists in the histology department at St Mary's Hospital; the NACWOs, ATs and NVSs in CBS throughout Imperial College London but specifically at the St Mary's Campus and Dr Fiona Oakley at Newcastle University.

Finally, I would like to thank my parents Linda and Robert Petts, Oscar Kelly and Freddy for their personal support.

**Project hypotheses**

This work sought to investigate the role of TFPI in liver injury using transgenic mice that selectively expressed TFPI creating local, cell specific over expression.

The overall hypothesis was:

*Cell specific expression of TFPI in acute and chronic liver injury would limit the progression and extent of liver injury.*

Specifically that:

1. *Expression of TFPI on αSMA positive cells in the liver would decrease the degree of acute hepatocellular injury and fibrosis via PAR associated modification of hepatic stellate cell activity and decreased microvascular clot formation.*

2. *Expression of TFPI on CD31 positive cells in the liver would decrease the degree of acute hepatocellular injury and fibrosis via PAR associated modification of CD31 positive myeloid cell activity and decreased microvascular clot formation.*

**Chapters**

**Detailed Contents**

## List of Figures

## List of Tables

**List of Abbreviations**

- ‘a’ activated form of coagulation factor (e.g FVIIa)
- ACK Ammonium-Chloride-Potassium
- ActB Beta actin
- ANIT Alpha-naphthylisothiocyanate
- APAP N-acetyl-p-aminophenol or paracetamol
- aPTT activated partial thromboplastin time
- ATP Adenosine triphosphate
- CCD Charge coupled device
- $CCl_4$ Carbon tetrachloride
- CCL Chemokine (c-c motif) ligand
- CCR Chemokine receptor
- CD31 Cluster of differentiation 31
- cDNA complementary DNA
- CMV Cytomegalovirus
- $C_T$ Cycle threshold
- CV Coefficient of variance
- CXCL Chemokine (c-x-c motif) ligand
- DAB 3,3’ Diaminobenzidine
- DAMPs Danger associated molecular patterns
- DMAB Dimethylamine borane
- DNA Deoxyribonucleic acid
- dNTP Deoxyribose nucleotide triphosphates
- EBV Epstein Barr virus
- EDTA Ethylenediaminetetraacetic acid

- EGF Epidermal growth factor
- EGFR Epidermal growth factor receptor
- EPI Extrinsic pathway inhibitor
- ErB2 Oestrogen receptor b2
- ERK1/2 Extracellular signal regulated kinases ½
- ETP Endogenous thrombin potential
- ETP + TM Endogenous thrombin potential in the presence of TM
- FAK focal adhesion kinase
- FFPE Formalin fixed, paraffin embedded
- FgL2 Fibrinogen-like protein 2
- FMO Fluorescence minus one
- GAPDH Glyceraldehyde-3-phosphate dehydrogenase
- GPI Glycophosphatidylinositol
- GTPase guanosine triphosphate hydrolase enzymes
- HELLP Haemolysis, elevated liver enzymes & low platelet count
- HER2 Human epidermal growth factor receptor 2
- HIE Heat induced epitope retrieval
- HIF Hypoxia inducible factors
- HLA human leukocyte antigen
- $HPC^{\Delta TF}$ Hepatocyte specific TF inactivation
- HPF High power field (typically x400 magnification)
- HRP Horseradish peroxidase
- HSC Hepatic stellate cells
- IFNγ Interferon gamma
- IL-1, etc Interleukin-1, 8, etc

- $IP_3$ Inositol 1,45-triphosphate
- IPEC Immortalised porcine endothelial cells
- LACI lipoprotein-associated coagulation inhibitor
- LPS Lipopolysaccharide
- LRP lipoprotein receptor-related protein
- LSEC Liver sinusoidal endothelial cells
- MAPK Mitogen-activated protein kinase
- MCM4 Minichromosome maintenance complex component 4
- MCP-1 Monocyte chemo-attractant protein-1 (also known as CCL2)
- MHV Mouse hepatitis virus
- MIP Macrophage inflammatory protein (MIP-1α and 2α also known as CCL3 and CXCL2 respectively)
- MMP Matrix metalloproteinase
- NADPH Nicotinamide adenine dinucleotide phosphate, reduced
- NAPQI N-acetyl-*p*-benzoquinone imine
- NF-kB Nuclear factor kappa beta
- NK cell Natural Killer cell
- NKG2D Natural killer group 2D
- NO Nitric oxide
- PAI-1 Plasminogen activator inhibitor-1
- PAR Protease Activated Receptors
- PBS Phosphate buffered solution
- PCA Pro-coagulant activity
- PCNA Proliferating cell nuclear antigen
- PDGF Platelet derived growth factor

- PMA Phorbol myristate acetate
- Rac1 Ras-related C3 botulinum toxin substrate 1
- RGB Red green blue
- RhoA Ras homolog gene family, member A
- RNA Ribonucleic acid
- ROI Region of interest
- RT Reverse transcriptase
- TAA Thioacetamide
- TAFI Thrombin-activatable fibrinolysis inhibitor
- TAT Thrombin-anti-thrombin complex
- TBST Tris-buffered saline and Tween 20
- TF Tissue Factor
- TF / FVIIa Tissue Factor – Factor VIIa complex
- TFI tissue factor inhibitor
- TFPI Tissue Factor Pathway Inhibitor
- TGF-β1 Transforming growth factor beta 1
- TIMP Tissue inhibitor of matrix metalloproteinase
- TM Thrombomodulin
- TNF-α Tumour necrosis factor alpha
- TRAIL TNF-related apoptosis inducing ligand
- Vol Volume
- αSMA alpha smooth muscle actin

## 1. Introduction

Approximately 60,000 people in England and Wales have cirrhosis and ten times that have some form of liver disease. Liver disease is currently the third biggest cause of premature mortality in England and Wales and worryingly mortality rates from liver disease have been increasing over the past 30 years (Williams et al. 2014). Acute and chronic liver injury occurs due to a number of aetiologies. Acute liver injury can immediately affect the function of the liver and in chronic liver injury a state of chronic inflammation initiates pathological repair where damaged functional tissue is replaced by fibrous scar tissue. This scaring process can then affect the function of the liver in the longer term. Given the variety of aetiologies and growing burden of disease in the population, there is a need to find universal therapies that alter the progression of liver injury and fibrosis beyond the initiating insult.

Epidemiological studies on a variety of populations have demonstrated that procoagulant / prothrombotic states are associated with more advanced liver fibrosis (of varying aetiology) compared to age/sex matched controls. (Papatheodoridis et al. 2003; Papatheodoridis et al. 2009; Wright et al. 2003; Poujol-Robert, Rosmorduc, et al. 2004; Poujol-Robert, Boelle, et al. 2004). Subsequent animal studies have confirmed that mouse models with pro-thrombotic tendencies also demonstrate accelerated fibrosis. In mouse models it has also been shown that anticoagulation can be used to alter/halt the progression of liver fibrosis (Anstee et al. 2008). A discussion of the role of the coagulation cascade in chronic liver injury is covered in more detail in section 1.4.

In humans the role of the coagulation cascade in the progression of acute liver injury has not been widely researched and animal models have predominantly been used to investigate the role of the coagulation cascade in acute liver injury due to specific causative agents. A discussion of the role of the coagulation cascade in acute liver injury is covered in more detail in section 1.3.

This body of work sought to further the understanding of role of the coagulation cascade, specifically Tissue Factor Pathway Inhibitor (TFPI), and it's potential as a therapeutic target in the progression of acute and chronic liver injury.

TFPI is a serine protease inhibitor that regulates the activation of the extrinsic arm of the coagulation cascade. The first part of this introduction provides background information on the coagulation cascade and TFPI (section 1.1) before exploring the existing literature on the role of the coagulation cascade in acute and chronic liver injury (sections 1.2, 1.3, 1.4). The final part of this introduction covers the mouse models used in this body of work, including models of liver injury (section 1.5) and the transgenic strains of mice unique to this work (section 1.6).

## 1.1. The coagulation cascade

The coagulation cascade describes a series of reactions where a precursor of a serine protease and it's glycoprotein co-factor are activated, catalyzing the next reaction and creating a cascade of subsequent reactions resulting in fibrin clot formation. The cascade is traditionally split into an intrinsic or contact activation pathway and an extrinsic or tissue factor pathway, both converging on a common factor X activating pathway (Figure 1-1).

The extrinsic pathway is associated with clot formation after vascular injury (and is measured using prothrombin time). The intrinsic pathway associated with clot formation secondary to contact with charged surfaces in disease states such as inflammation and in the propagation of clot formation after cessation of extrinsic pathway activation. The intrinsic pathway is measured using the activated partial thromboplastin time (aPTT). (Gailani & Renné 2007; van Montfoort & Meijers 2013).

*In-vivo* it is useful to consider the coagulation cascade split into the functional steps of initiation and propagation because of the considerable overlap in activation of the intrinsic and extrinsic pathways. Initiation of clotting occurs after vascular injury when the tissue factor - factor VIIa (TF / FVIIa) complex initiates activation of factor X. At the same time it activates factor IX (at a similar rate to factor X). After initiation there is propagation of factor X activation through factor IXa and thrombin (Mann, Krudysz-Amblo, & Butenas, 2012; Osterud & Rapaport, 1977) (Figure 1-1).

After activation, homeostatic control of the coagulation cascade is dependent upon regulators that inhibit the serine protease factors. These regulators include Protein C, antithombin and TFPI. Fibrinolytic agents such as plasmin are also important in homeostasis.

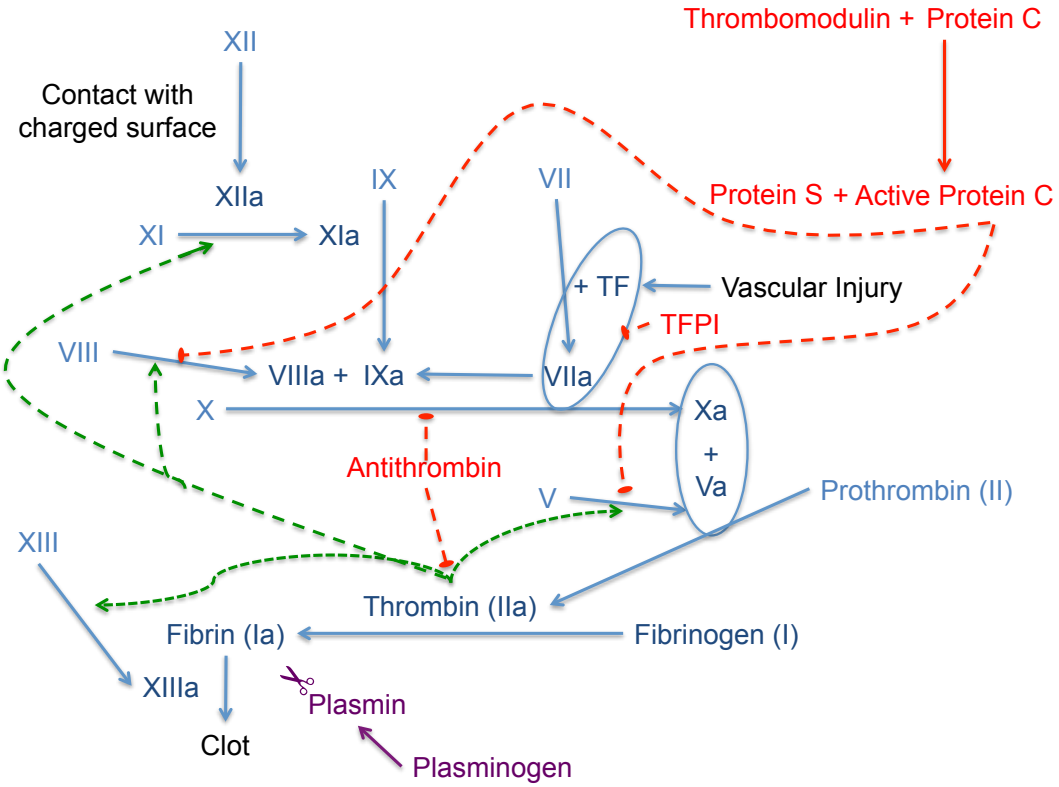


**Figure 1-1: Schematic of the coagulation cascade**

Blue arrow / Text – coagulation cascade activation.
Green arrow, broken line – thrombin propagation of coagulation cascade activation.
Red arrow, solid line – Inhibitors / Regulators of the coagulation cascade, direction of action.
Red broken line – Site of inhibition.
Purple – fibrinolytic system.
'a' denotes the activated form of the factor.

### *1.1.1. Tissue factor (TF)*

Tissue factor (also known as thromboplastin) is a transmembrane glycoprotein. Structurally the extracellular domain of tissue factor is composed of 219 residues with fibronectin type 3 domains containing 3 potential glycosylation sites and multiple residues important to its interaction with factor VIIa and factor X. The factor VIIa interaction sites are near the tip of the molecule and the factor X interaction sites are near the membrane attachment site (Drake et al. 1989; Mann et al. 2012; Spicer et al. 1987).

Tissue factor (TF) is expressed on adventitial fibroblasts where it forms the haemostatic envelope (Drake et al. 1989). These cells are not normally exposed to flowing blood but when there is damage to the intimal endothelial lining they are exposed to blood that contains low levels of circulating factor VIIa (approximately 1% of circulation factor VII is present in its cleaved, activated, protease form). The binding of Factor VIIa (in the presence of calcium ions) to the extracellular portion of TF forms a complex that proteolytically cleaves factor X to Xa. This reaction simultaneously triggers the expression of TFPI which forms an inactivating quaternary complex with the TF / VIIa / Xa complex (Broze Jr. 1995).

As well as expression on adventitial fibroblasts TF is found on circulating activated monocytes. Un-activated macrophages are negative for TF (Osterud 2010; Drake et al. 1989). TF is also expressed on microparticles and in certain disease settings the proportion of microparticles carrying TF is elevated (Owens 3rd & Mackman 2011). The activity of the circulating blood

cell / microparticle bound TF is dependent upon cofactors and oxidation associated conformational change (V. M. Chen et al. 2006; Mann et al. 2012). Literature describing the expression of TF on platelets, neutrophils and eosinophils is not conclusive (Osterud 2010; Drake et al. 1989).

Tissue factor is also expressed in a large number of tissues outside of the vasculature, including low-levels of expression in the liver. In the liver TF is expressed on hepatocytes, bile duct epithelial cells, hepatic stellate cells and Kupffer cells (Sullivan et al. 2013; Stephenne et al. 2007; Willingham & Matschiner 1989; Arai et al. 1995; Luyendyk et al. 2009; Flossel et al. 1994; Bataller et al. 2005; Mackman et al. 1993; Drake et al. 1989). The main role of TF in the liver physiology is not completely understood. In injury states, the literature suggests that TF is responsible for the majority of coagulation cascade activation with liver. Importantly, 90% of the TF expressed on hepatocytes is 'encrypted' and unable to activate the clotting cascade prior to un-encryption. This encryption is likely to be vital to maintaining coagulation cascade homeostasis in the uninjured liver as plasma (carrying coagulation factors) passes freely through the fenestrations of the liver sinusoidal epithelial cells and interacts with hepatocytes which are a major source of many coagulation factors including factor VII (Sullivan et al. 2013; Kopec & Luyendyk 2014).

The role of TF in liver injury is discussed in more detail in sections 1.3.3 and 1.4.3.

### *1.1.2. Tissue factor pathway inhibitor (TFPI)*

Tissue factor pathway inhibitor (TFPI) was first described in the 1950's and sequenced in 1987. The molecule was initially called lipoprotein-associated coagulation inhibitor (LACI) and has also been known as anti-convertin, extrinsic pathway inhibitor (EPI), tissue factor inhibitor (TFI) and TFPI-1. TFPI is a 32-38-kDa plasma glycoprotein composed of three tandem kunitz-type domains flanked by a negatively charged N-terminal region and a positively charged c-terminal tail (Wun et al. 1988).

TFPI is a serine protease inhibitor and the main homeostatic brake that is able to immediately inhibit the tissue factor (TF) dependant initiation phase of the coagulation cascade (Lwaleed & Bass 2006). In the coagulation cascade tissue factor, factor VIIa and factor Xa form a large complex (TF / VIIa / Xa) anchored by tissue factor to a plasma membrane. Each TFPI molecule irreversibly binds a TF / VIIa / Xa complex. First the second kunitz-type domain binds to factor Xa, this then facilitates the binding of the first kunitz-type domain to the active site of TF / Xa. The TFPI / TF / VIIa / Xa quaternary molecule prevents further interaction of the bound TF, VIIa and Xa in the coagulation cascade (McVey 1994; Broze Jr. et al. 1988; Girard et al. 1989).

The third kunitz-type domain is probably involved in the association with lipoproteins or cell surface localization but its exact function is not known (Abumiya et al. 1995; Piro & Broze Jr. 2004). The c-terminal is required for the binding of TFPI to cell surfaces and allows for the internalisation and

degradation of factor X and down regulation of TF / VIIa activity (Lwaleed & Bass 2006; Han et al. 1999).

TFPI is found in two alternatively spliced isoforms, TFPIα and TFPIβ. TFPIα is the full length protein described above and TFPIβ lacks the third kunitz-type domain and contains an alternative c-terminal region that contains a glycophosphatidylinositol (GPI) attachment signal. Both bind TF / VIIa in a factor Xa dependent manner (Broze Jr. et al. 1988; Girard et al. 1989). TFPIα is a soluble form of TFPI and TFPIβ is exclusively found anchored to the cell membrane (Piro & Broze Jr. 2005; Zhang et al. 2003). TFPIβ accounts for 20% of total surface TFPI (Piro & Broze Jr. 2005). Importantly, although TFPIα and TFPIβ mRNA is found in the mouse (with a similar tissue distribution) TFPIβ protein has not been detected in the mouse (Chang et al. 1999).

In the circulation TFPI is distributed in three pools – the endothelium, platelets and the plasma. Approximately 80-85% of TFPI is constitutively produced by microvascular endothelium and expressed on their luminal surface (with expression also noted in the Golgi apparatus and endocytic compartments) (Hansen et al. 1997). This is the most biologically active pool of TFPI and is predominantly TFPIα (Mast et al. 2000; Ameri et al. 1992).

Between 2-10% of TFPI is present in platelets and expression on the platelet surface is seen in un-activated platelets and following activation by collagen

and thrombin (Novotny et al. 1988; Maroney & Mast 2008; Ott et al. 2001; Werling et al. 1993). Again, this is predominantly TFPIα.

Approximately 10% of TFPI is found in the blood plasma. Circulating TFPI is almost exclusively TFPIα (Zhang et al. 2003). Most (80-90%) of the circulating TFPI is bound to lipoproteins (HDL, LDL and VLDL) and only a small proportion is uncomplexed and freely circulating (Novotny et al. 1989; Lwaleed & Bass 2006; Werling et al. 1993; Sandset 1996). The uncomplexed plasma TFPI has greater anticoagulant activity than the complexed TFPI and there is evidence that this (uncomplexed) fraction is responsible for the anticoagulant activity of TFPI in plasma (Lindahl et al. 1992; Hansen et al. 1997; Broze Jr. et al. 1994). The uncomplexed TFPI is likely to originate from TFPI released by endothelial cells and platelets (Novotny et al. 1988; Ameri et al. 1992).

In addition to these three pools, vascular smooth muscle cells have been shown to demonstrate expression of TFPI (Bajaj, Kuppuswamy, et al. 1999; Wojtukiewicz et al. 1999). Un-activated monocytes (and macrophages) demonstrate weak TFPI expression and bone marrow megakaryocytes also show TFPI expression (Ott et al. 2001; Werling et al. 1993). TFPI expression has not been seen on erythrocytes, neutrophils and lymphocytes, although in atherosclerotic lesions T cell expression of TFPI has been identified (Caplice, Mueske, Kleppe & Simari 1998; Crawley et al. 2000; Bajaj, Steer, et al. 1999; Osterud et al. 1995). TFPI expression has also been identified in laryngeal

squamous epithelial cells, astrocytes and in small amounts in lung fibroblasts (Bajaj, Kuppuswamy, et al. 1999; Wojtukiewicz et al. 1999).

Examination of a range of human tissues shows that expression of TFPI varies in different organs. High levels of TFPI mRNA are found in both the lung and heart while the liver (hepatocytes and bile duct epithelial cells) express moderate amounts of TFPI (Bajaj, Kuppuswamy, et al. 1999; Shimokawa et al. 2000; Uhlén et al. 2015). *In-vitro* TFPI expression has been detected on the human hepatoma cell line HepG2 but is not seen in cultured hepatocytes (Broze Jr. & Miletich 1987; Bajaj et al. 1990).

Phorbol myristate acetate (PMA), endotoxin, interleukin-1, TNF-$\alpha$, epidermal growth factor, platelet-derived growth factor and heparin are all upregulators of TFPI expression *in-vitro* and thrombin is associated with the cell surface expression and release of TFPI from cultured endothelium (Lupu, Kruithof, et al. 1999; Lupu, Poulsen, et al. 1999; Lupu et al. 1995; Caplice, Mueske, Kleppe, Peterson, et al. 1998; Ameri et al. 1992).

Therapeutically, heparins and tissue plasminogen activator stimulate this release of TFPI into the plasma from endothelium and platelets and total plasma TFPI is increased 1.5-to 3-fold. This occurs without depleting the cell surface membrane, suggesting rapid replacement of membrane TFPI by intracellular stores (Lupu, Poulsen, et al. 1999; Hansen et al. 2000; McVey 1994; Sandset et al. 1988; Gori et al. 1999).

TFPI is cleared by the liver and the kidneys. In hepatocytes the low density lipoprotein receptor-related protein (LRP), a cell surface glycoprotein, mediates the endocytosis and degradation of TFPI (Palmier et al. 1992; Warshawsky et al. 1994).

While the role of the liver in the homeostasis of TFPI is understood, there is very little literature on the role of TFPI in liver homeostasis and liver disease. In the uninjured liver, TFPI is likely to play a role in coagulation cascade homeostasis. In patients with cirrhosis and cirrhosis with portal vein thrombosis, plasma levels of TFPI are known to be reduced compared to controls (Oksuzoglu et al. 1997). This body of work sought to address this gap in the literature.

Of note, TFPI is not to be confused with TFPI-2. TFPI-2 is also a kunitz-type serine protease inhibitor with weak inhibition of TF / VIIa, factor Xa and other serine proteases. However it is encoded by *TFPI2* on chromosome 7 (compared to TFPI which is encoded by *TFPI* on chromosome 2) and its main function is as a tumour suppressor gene. This body of work refers to TFPI, not TFPI-2.

## 1.2. The Coagulation cascade and liver injury

Since the 1980's the coagulation cascade has been linked with the progression of liver injury (Levy et al. 1982; Levy et al. 1983; Wanless, Liu, et al. 1995; Wanless, Wong, et al. 1995). These early papers correlated the extent of microthrombi in the hepatic microcirculation with severity of liver fibrosis and the term parenchymal extinction was coined by Wanless et al to describe the replacement of areas of functional parenchyma with fibrous tissue between veno-occlusive lesions (Wanless, Wong, et al. 1995). Later, the role of receptors activated by coagulation cascade proteases (Protease Activated Receptors, PAR) were added to the pathogenesis of the coagulation cascade in liver injury.

### *1.2.1. Parenchymal extinction*

Levy et al observed microthrombi, microcirculatory changes and associated tissue necrosis in the livers of mice infected with mouse hepatitis virus (MHV). They noted that one strain of mouse (A/J) did not develop these changes and that this appeared to be related to this strains' lack of expression of a pro-coagulant protein on monocytes in response to MHV infection. The protein (later identified as Fibrinogen-like protein 2, FgL2) cleaved prothrombin to thrombin and resulted in fibrin microthrombi formation in other strains (Levy et al. 1982; Levy et al. 1983).

Later Wanless et al studied post-mortem and ex-planted cirrhotic human livers, mapping veno-occlusive lesions and areas of fibrous septa. He found that hepatic vein veno-occlusive lesions mapped to areas with dense fibrous tissue replacing parenchyma. He also found that the extent of these fibrous lesions was proportional to the frequency and extent of medium sized hepatic vein veno-occlusive lesions. He termed this appearance parenchymal extinction (Wanless, Wong, et al. 1995).

Wanless proposed that the patchy distribution of veno-occlusive lesions in hepatic veins was due to multiple associated thrombotic events starting in the sinusoids and propagating into the hepatic veins causing local tissue ischaemia, hepatocellular loss and fibrosis. Wanless theorised that the sinusoidal thrombi occurred due to stasis or vascular injury caused by parenchymal inflammation. (Wanless, Liu, et al. 1995; Wanless, Wong, et al. 1995).

### *1.2.2. Protease Activated Receptors (PAR)*

Protease activated receptors (PAR) are G-protein linked transmembrane receptors. The receptors are activated by the irreversible cleavage of an extracellular amino-terminal by a protease, often a coagulation cascade protease. This exposes another amino-terminal (called the tethered ligand) that acts intra-molecularly to activate downstream intracellular signalling.

The intracellular signalling cascades activated by PAR are dependent upon G-protein subunits (and β-arrestin in PAR-2). Intracellular signalling cascades activated by PAR include (Adams et al. 2011):

- Phospholipase C generation of diacyl glycerol and inositol 1,45-triphosphate ($IP_3$) and the mobilisation of calcium from the endoplasmic reticulum into the cytosol (seen in conjunction with PAR-1 and PAR-2 in fibroblasts (Ossovskaya & Bunnett 2004)).
- Mitogen-activated protein kinase (MAPK) pathway proliferative activity.
- Nuclear factor-kB (NF-kB) pathway inflammation (most prominent in PAR-2 signalling).
- RhoA GTPase or Rac1 activation induced focal adhesion kinase (FAK) tyrosine phosphorylation dependant cell migration.
- Transactivation of other receptor systems such as ErB2, HER2 and EGFR.
- G-protein independent signalling via β-arrestin1 and 2 resulting in regulation/termination of G-protein signalling and ERK1/2 pathway activation.

There are four known PAR, PAR-1 to 4 (see Table 1-1). PAR 1-4 are detectable (mRNA and protein) in the uninjured liver (Jesmin et al. 2006).

PAR-1 is constitutively expressed in the liver (on sinusoidal endothelium) and is upregulated during liver injury with expression in non-parenchymal cells associated with portal infiltrates and areas of regeneration (Marra et al. 1998; Fiorucci et al. 2004; Gaca et al. 2002). The principle activator of PAR-1 is thrombin.

PAR-2 is activated by the TF / VIIa complex and by TF / VIIa generated Xa. In addition PAR-2 can be trans-activated by the interaction of thrombin with PAR-1 (Brien et al. 2000). In the uninjured liver PAR-2 expression is seen in hepatocytes, hepatic stellate cells, Kupffer cells, the endothelium of large vessels and bile duct epithelium (Knight et al. 2012; Borensztajn et al. 2008).

PAR-3 is expressed on platelets and neutrophils but work has so far not identified liver specific staining (Coughlin 2000; Rullier et al. 2006). In the mouse it is likely that PAR-3 does not independently transduce intracellular signalling but acts as a co-factor for PAR-4 activation (Nakanishi-Matsui et al. 2000).

PAR-4 is expressed on platelets, macrophages, B cells, endothelial cells and in the injured liver, activated hepatic stellate cells (Fiorucci et al. 2004; Gaca et al. 2002; Rullier et al. 2006; Miyakawa et al. 2015; Rezaie 2014). PAR-4 is

important in the thrombin mediated activation of platelets (Miyakawa et al. 2015).

The wide range of cells that PAR are expressed upon, their reliance on proteases for activation and the range of intracellular signalling cascades initiated by PAR activation means that their role in normal tissue is difficult to define, as demonstrated by a lack of published literature on the topic. Conversely, the role of PAR in disease states has been widely investigated, particularly with the aid of mouse models. The role of PAR in acute and chronic liver injury is covered in detail in sections 1.3.3, 1.3.4, 1.4.3 and 1.4.4.

| PAR | Protease interaction (Adams et al. 2011) | Liver expression |
|---|---|---|
| 1 | **Activating**<br>Thrombin<br>Plasmin<br>Factor Xa<br>tissue kallikreins<br>Activated protein C<br>endothelial receptor complex<br>Granzyme A<br>Cathepsin G<br>MMP-1<br><br>**Disarming**<br>Plasmin<br>Tissue kallikreins<br>Elastase<br>Cathepsin G | Hepatic stellate cells (quiescent and activated) (Fiorucci et al. 2004; Gaca et al. 2002; Marra et al. 1998)(Rullier et al. 2006)<br><br>Endothelial cells (Martinelli et al. 2008)(Rullier et al. 2006)<br><br>Macrophages (Kallis et al. 2014)<br>Monocytes (Martinelli et al. 2008)<br>Dendritic cells (Martinelli et al. 2008)<br>T cells (Rullier et al. 2006)<br><br>Not present on mouse platelets (is present on human platelets) (Coughlin 2000) |
| 2 | **Activating**<br>TF/VIIa complex<br>TF/VIIa generated Xa<br>Tissue kallikreins<br><br>**Disarming**<br>Plasmin<br>Elastase<br>Protease 3<br>Cathepsin G | Hepatocytes (Knight et al. 2012; Borensztajn et al. 2008)<br>Hepatic stellate cells (Knight et al. 2012; Fiorucci et al. 2004)<br>Bile duct epithelium (Knight et al. 2012; Borensztajn et al. 2008)<br><br>Kupffer cells (Knight et al. 2012; Borensztajn et al. 2008)<br><br>Endothelial cells of large vessels (Knight et al. 2012; Borensztajn et al. 2008) |
| 3 | **Activating**<br>Thrombin<br><br>**Disarming**<br>Cathepsin G | Mouse platelets (Coughlin 2000)<br><br>Occasional neutrophils (Rullier et al. 2006) |
| 4 | **Activating**<br>Thrombin<br>Plasmin<br>Factor Xa<br>tissue kallikreins<br>Cathepsin G<br><br>**Disarming**<br>KLK14 (Kallikrein) | Activated hepatic stellate cells (Fiorucci et al. 2004; Gaca et al. 2002)<br><br>Platelets (Miyakawa et al. 2015; Coughlin 2000)<br><br>Macrophages (Rullier et al. 2006)<br>B cells (Rullier et al. 2006)<br><br>Endothelial cells (Rezaie 2014) |

**Table 1-1: Protease activate receptors, activating proteases and liver specfic expression**

### 1.3. The coagulation cascade in acute liver injury

Drug induced liver injury is the main cause of acute liver failure in the developed world. In the UK (as well as northern Europe and the US) paracetamol toxicity induced liver injury is the most common cause of acute liver failure. Prescription drugs, over the counter and herbal medications are also associated with drug induced acute liver failure but diseases such as autoimmune hepatitis, viral hepatitis (Hepatitis A-E, EBV, varicella zoster, CMV), HELLP syndrome, Wilson's Disease and Budd-Chiari syndrome can also cause acute liver failure. In 15% of cases the cause is never elucidated (Singanayagam & Bernal 2015).

In humans the role of the coagulation cascade in the progression of acute liver injury has not been widely researched, probably due to the coagulopathy seen in acute liver injury and the difficulty this presents in dissecting out effector pathways and molecules. In addition patients with acute liver failure often present in extremis with either an unknown cause for their liver injury or with multiple confounding causes (e.g. multi-drug overdoses). These limitations are reflected in the variable outcomes in trials of anti-coagulants in acute liver failure. Papers from the 1970's and 1980's describes benefits of anti-coagulant (heparin and antithrombin III) treatment of patients with acute liver failure (Rake et al. 1971; Weerasinghe et al. 2011; Fujiwara et al. 1988) whereas a paper from the 1990's describes a lack of effect of anticoagulation (using antithrombin III) on mortality in fulminant hepatic failure (Langley et al. 1993).

### *1.3.1. Coagulopathy of acute liver injury*

The focus of this work is the role of the coagulation cascade in the propagation and progression of liver injury, not the role of liver injury in coagulopathy. However as this may be drawn into the discussion of the work; I have summarised two recent studies comparing the coagulation factors and clotting potential of blood from patients with acute liver injury as a brief overview.

During acute liver injury there is a marked coagulopathy. The cause and effect are not clear-cut and there are a number of theories regarding the coagulopathy in acute liver injury (reduced synthesis of coagulation factors, increased consumption, reduced clearance).

Kerr et al and Habib et al found that when blood from patients with acute liver failure (paracetamol toxicity only and all causes, respectively) was compared to healthy controls, there were consistent decreases in factors II (thrombin), V, VII, and X but elevated levels of factor VIII and decreased functional anti-thrombin (Kerr 2003; Habib et al. 2014).

Kerr also found relative preservation of factors IX and XI levels, elevated levels of soluble tissue factor (TF) but also elevated thrombin-anti-thrombin (TAT) complexes. He hypothesized that the relative preservation of factors IX and XI and increased factor VIII suggested that synthesis of coagulation factors was not impaired by liver damage and that, along with normal platelet counts and levels of fibrinogen, disseminated intravascular coagulation

associated consumption was also unlikely. Rather, the increase in soluble TF and decrease in factors activated (directly or indirectly) by TF supported the central role of TF generation in acute liver injury with a predominantly thrombin mediated amplification of fibrin deposition (decreased functional anti-thrombin and increased TAT complexes) (Kerr 2003).

Later Habib et al focused on thrombin generation and found that despite the low levels of clotting factors, low fibrinogen, low platelets and the resulting low endogenous thrombin potential (ETP), the endogenous thrombin potential in the presence of thrombomodulin (ETP+TM) was preserved and the ETP ratio (ETP : ETP+TM) actually elevated. This provided evidence for Kerr's hypothesis and the theory of re-balanced coagulation seen in acute liver injury (Habib et al. 2014).

### *1.3.2. Effector cells in acute liver injury*

The pattern, progression and biological pathways involved in acute liver injury vary greatly depending on the cause of the injury. However activation of the immune system, the production of inflammatory cytokines, recruitment of monocytes, T cells, B cells, NK cells, and neutrophils to the liver plus activation of tissue resident macrophages (Kupffer cells), hepatic stellate cells and sinusoidal endothelial cells is universally seen.

An in depth review of these effector cells goes beyond the scope of this work (centred on tissue factor pathway inhibitor (TFPI) and tissue factor (TF) dependent activation of the coagulation cascade), however below I have briefly summarised the current role of some key effector cells with reference to more comprehensive review articles.

**Neutrophils**

Neutrophils represent the early immune response to liver injury. Neutrophil invasion of the liver during acute liver injury often exacerbates liver injury. After hepatocyte injury and death, neutrophils accumulate in the liver sinusoids under the influence of TNFα, IL-1 and CXC chemokines. Neutrophils then extravasate into the surrounding liver along a chemotactic gradient of CXC chemokines (IL-8 and MIP-2), complement, reactive oxygen species and contact with fragments of apoptotic hepatocyte fragments. Activated neutrophils then release potent chemotactic agents (such as Leukotriene $B_4$), recruiting more neutrophils to the site of injury (Ramaiah & Jaeschke 2007).

Neutrophils engage with their target through $\beta_2$ integrins, releasing NADPH oxidase, myeloperoxidase and serine proteases that directly and indirectly contribute to hepatocyte damage and trigger pro-inflammatory cytokine production by macrophages. Thus creating a self perpetuating pro-inflammatory microenvironment and cycle of liver parenchymal damage (Ramaiah & Jaeschke 2007).

**Macrophages and monocytes**

After acute liver injury there is expansion of the hepatic macrophage population through recruitment of circulating monocytes. By 48 hours after the initial insult macrophages account for 10-12% of total hepatic cells. This recruitment is predominantly due to Kupffer cell and injured hepatocyte expression of Monocyte chemo-attractant protein-1 (MCP-1) in the first 12 hours after injury. MCP-1 is a chemokine that acts on chemokine receptor 2 (CCR2) expressed on monocytes, macrophages, T cells and NK cells (Possamai 2010).

Hepatic macrophages (recruited or tissue resident) appear to then be activated to either an inflammatory phenotype or a pro-resolution phenotype (see 1.4.2 for more detailed description of these phenotypes) (Zimmermann et al. 2012).

**T cells**

The role of T cells in acute liver injury varies considerably depending on the mode of injury and the T cell subset. Cytotoxic T cells are a key effector cell in virus (hepatitis B, etc) associated acute liver injury and regulatory T cells play a role in controlling the immune response to TGFβ dependent pathways (Wu et al. 2010).

**B cells**

The role of B cells in acute liver injury is not well understood and much of the work is based on mice with combined immune deficiencies. It was previously thought that B cells and immunoglobulin production (IgM) were important in shaping the response to acute liver injury, however a recent paper suggest that the impact of IgM and B cells is dependent upon their interplay with T cells (Richards et al. 2015).

**NK cells**

In acute liver injury NK cells are regulated by Kupffer cell / macrophage derived cytokines (IL-12, IL-18) and produce IFNγ. NK cells modulate T cell responses and can promote cell death / lysis in endothelial cells, hepatic stellate cells and hepatocytes through death receptor and perforin / granzyme pathways (Wu et al. 2010).

**Hepatic stellate cells**

The activation of hepatic stellate cells (HSC) results ultimately in the production of collagen that, unchecked can lead to a fibrotic response to liver injury. Although the role of the HSC in the extent of acute liver injury is unclear many of the activated / recruited effector cells initiate HSC activation and HSC secrete a number of cytokines that amplify the inflammatory response (Scott L Friedman 2008).

**Liver sinusoidal endothelial cells**

As well as acting as a barrier between blood borne factors and the hepatic parenchyma, liver sinusoidal endothelial cells (LSEC) also clear pro-inflammatory substances (such as LPS) through production of anti-inflammatory mediators and reduced expression of adhesion molecules. LSEC also induce T cell tolerance. Loss of LSEC and their protective function is thought to contribute to acute parenchymal liver injury (Wu et al. 2010).

### *1.3.3. TF and PAR-2 in acute liver injury*

Tissue factor (TF) expression in the liver is low compared to other organs such as the lung (Mackman et al. 1993). In the liver TF is found on hepatocytes (Sullivan et al. 2013; Stephenne et al. 2007; Willingham & Matschiner 1989), bile duct epithelial cells (Luyendyk et al. 2009; Flossel et al. 1994), hepatic stellate cells (Bataller et al. 2005) and Kupffer cells (Arai et al. 1995).

In a paracetamol model of acute liver injury the pro-coagulant activity (PCA, a measure of TF activity) of the liver initially increases (at 30 minutes) but returns to normal after 2 hours. In contrast plasma thrombin-anti-thrombin (TAT) levels only increase after 2 hours and return to normal after 6 hours. PAI-1 (the major inhibitor of fibrinolysis) increases after paracetamol administration, reaching significant levels at 6 hours. Parenchymal fibrin deposition occurs from 2 hours after paracetamol administration and an increase in fibrin deposition was associated with increased liver parenchymal injury (Ganey et al. 2007).

In a paracetamol model of acute liver injury low-TF mice and $HPC^{\Delta TF}$ mice (with hepatocyte specific TF inactivation) have lower thrombin generation at 2 hours than control mice. In combination this suggests that TF is key to early coagulation cascade activation in early paracetamol induced liver injury and that hepatocytes are the major source of TF in a paracetamol model of acute liver injury (Sullivan et al. 2013; Ganey et al. 2007).

Low-TF mice also demonstrate a reduction in liver injury in the first 6 hours after paracetamol administration. However they reach the same level of injury by 24 hours as control mice. These low-TF mice do have some expression of TF and therefore fibrin deposition still occurs with time. These results suggests that the delay in liver injury seen in low-TF mice is due to the role of TF dependent coagulation in early acute liver injury but that with time and fibrin accumulation there is progression of the liver injury independent of low levels of TF (Ganey et al. 2007).

In a cholestatic model (alpha-napthiosthiocyanate, ANIT) of acute liver injury there is increased TF expression, thrombin generation (plasma TAT), fibrin deposition and increased plasma fibrinogen associated with elevation in serum ALT, ALP and bile acid levels (at 24 hours and increasing at 48 hours). Thrombocytopenia is observed at 48 hours after the initial coagulation cascade activation and is associated with liver parenchymal platelet accumulation (Sullivan, Wang, et al. 2010; Luyendyk et al. 2011; Luyendyk et al. 2009). Of note, liver parenchymal injury in this model is thought to be driven by neutrophils following the initiating bile duct injury from direct ANIT toxicity as opposed to direct hepatocyte injury seen in the paracetamol model of acute liver injury (Kodali et al. 2006).

In a cholestatic model of acute liver injury, low-TF mice demonstrate less liver injury, less thrombin generation, less hepatic parenchymal fibrin deposition and less elevation in serum ALT, ALP and bile acids compared to control mice. The difference was most pronounced at 48 hours after ANIT administration

(Luyendyk et al. 2009). This suggests that TF contributes to the later progression of acute liver injury in acute cholestatic liver injury.

In addition to causing cellular injury and initiating the coagulation cascade activation, paracetamol and ANIT are known to have additive effects that worsen the pro-coagulant state of the liver in a TF dependant manner. Glutathione binds the extracellular sulfhydryl group of TF, impairing its activity (Reinhardt et al. 2008; Stephenne et al. 2007). Paracetamol and ANIT deplete glutathione levels (Carpenter-Deyo et al. 1991; Jaeschke & Bajt 2006), thereby removing inhibitory binding of TF and increasing the potential for TF dependent coagulation.

PAR-2 is expressed by hepatocytes, Kupffer cells, large vessel endothelium and bile duct epithelium in the uninjured liver. PAR-2 activation is associated with a pro-inflammatory, pro-proliferation and pro-migratory response (Adams et al. 2011). During acute (LPS induced) liver injury PAR-2 expression is strongly increased in Kupffer cells and weakly increased in endothelium and bile duct epithelium. PAR-2 is activated by the TF/VIIa complex and TF/VIIa generated Xa (Adams et al. 2011) and it has been suggested (in chronic liver injury models) that PAR-2 is responsible for the pro-inflammatory effect of factor Xa (Borensztajn et al. 2010).

There is little published work on the role of PAR-2 in xenobiotic induced acute liver injury. Kataoka et al demonstrated that PAR-2 deficient mice had a decreased neutrophilic infiltrate in paracetamol induced liver injury compared

to wild type mice. However no difference in the magnitude of liver injury or the recruitment of monocytes was seen (Kataoka et al. 2014).

In a rat model of sepsis and mouse models of inflammation; inhibition or deficiency of PAR-2 reduced inflammation, limited TNF-α production and improved outcome (Jesmin et al. 2006). Together these results build on the chronic liver injury data and suggest that PAR-2 activation plays a pro-inflammatory role in acute liver injury.

### *1.3.4. Thrombin, PAR-1, -3 & -4 in acute liver injury*

Thrombin is one of the final steps in the coagulation cascade before fibrin clot formation. Thrombin activates PAR-1, 3 and 4 signalling.

Inhibition of the action of thrombin through the administration of heparin (that potentiates the action of anti-thrombin), lepirudin (a thrombin inhibitor) or the loss of PAR-1 signalling (PAR-1 knockout mouse models) has been shown to limit early (< 6 hours) paracetamol induced liver injury damage associated with decreased fibrin deposition (Ganey et al. 2007; Miyakawa et al. 2015; Weerasinghe et al. 2011). This suggests a role for thrombin and PAR-1 activation in early acute liver injury.

However, at 24 hours after paracetamol administration, loss of PAR-1 signalling and the inhibition of thrombin through heparin administration (as well as the low-TF model discussed above) is associated with control / wild type level fibrin deposition and liver injury. This suggests that, like TF and PAR-2, the role of thrombin and PAR-1 inhibition is limited to early acute liver injury and that this too is probably due to alternative thrombin generation and fibrin clot formation later in the progression of acute liver injury as well as alternate PAR activation and / or pro-inflammatory signalling (Ganey et al. 2007).

In work somewhat contrary to the work on TF, thrombin, PAR-1 and PAR-2, Hugenholtz et al demonstrated that a hyperfibrinolytic state caused by deficiency of thrombin-activatable fibrinolysis inhibitor (TAFI, a thrombin-

thrombomodulin complex activated inhibitor of the fibrinolytic tissue plasminogen activator), resulted in reduced parenchymal necrosis and fibrin deposition at 6 hours but increased parenchymal necrosis (and control equivalent fibrin deposition) at 24 hours after paracetamol induced acute liver injury. The authors hypothesised that in early acute liver injury (six hours) the hyperfibrinolytic state protected the liver but, as the injury developed and the inflammatory cell infiltrate becomes more significant in disease progression, the loss of TAFI's anti-inflammatory function outweighed the protective effects of a hyperfibrinolytic state (Hugenholtz et al. 2013).

Also contrary to the literature on TF, thrombin, PAR-1 and PAR-2; Rullier et al found that in a carbon tetrachloride ($CCl_4$) model of acute liver injury (with a similar reactive metabolite induced membrane damage mode of injury as paracetamol) there was no difference in the extent of liver injury when PAR-1 deficient mice were compared to control mice (Rullier et al. 2008). However this work only looked at a single 48 hour time point and, as previous work has shown, the role PAR-1 is likely to be significant in early acute liver injury.

In an ANIT model of acute liver injury PAR-1 deficiency was not found to protect against cholestatic liver injury at 24 and 48 hours (Luyendyk et al. 2011) . The authors did not give a reason for the lack of effect in this model compared to other xenobiotic models, however it could be hypothesised that lack of expression of PAR-1 on bile duct epithelium (the cell type injured directly by ANIT) may be a factor.

The role of platelets in acute liver injury is complex and goes beyond this works centred on tissue factor pathway inhibitor (TFPI) and tissue factor (TF) dependent activation of the coagulation cascade. However, PAR-3 and PAR-4 are expressed on mouse platelets and PAR-4 is responsible for thrombin mediated platelet activation.

Platelet depletion (with an anti-CD41 antibody) and the global loss of PAR-4 expression in PAR-4 knockout mice was associated with less platelet accumulation in the liver, less thrombin generation and a sustained reduction (up to 24 hours) in a paracetamol model of acute liver injury (Miyakawa et al. 2015). Bone marrow chimera experiments showed that the importance of PAR-4 signalling in this model was not through platelet PAR-4 but was likely to be due to PAR-4 expressed on liver sinusoidal endothelial cells (Miyakawa et al. 2015).

In an ANIT model of acute cholestatic liver injury inhibition of platelet activation through administration of clopidogrel (a $P2Y_{12}$ receptor antagonist) was associated with reduced liver injury and reduced platelet and neutrophil accumulation at 48 hours. However, antibody mediated platelet depletion in the same model was associated with accelerated liver injury with increased parenchymal necrosis, peliosis and serum ALT (but no change in ALP) at 24 hours but with little or no progression at 48 hours (by which time control mice had developed the same degree of liver injury) (Sullivan, Wang, et al. 2010). The authors attributed these opposing effects to the role of the coagulation

cascade (TF and thrombin) and PAR in modulating both platelet and effector immune cell activation and accumulation, independent of the platelets themselves.

Later work partially confirmed this. Luyendyk et al demonstrates that global PAR-4 deficiency (PAR-4 knockout model) and early administration (2 hours after ANIT administration) of a PAR-4 inhibitor was associated with a similar pattern of accelerated liver injury in the ANIT model. However, when the PAR-4 inhibitor was administered at 8 hours after ANIT administration the mice demonstrated less parenchymal injury at 24 and 48 hours (and reduced plasma ALP and bile acids). These results suggest that in cholestatic acute liver injury PAR-4 plays a protective role early on but is involved later on in the progression of injury (Luyendyk et al. 2011).

There is little work on the role of PAR-3 in liver injury. Jesmin et al detail the gene and protein expression of PAR-3 in rat liver after LPS administration. They showed that PAR-3 protein and gene expression had an early peak at 1 hour after LPS administration, decreased at 3 hours after LPS administration but then steadily increased thereafter (up to 10 hours, the end of their experiment) (Jesmin et al. 2006). They found that PAR-3 expression mirrored PAR-4 expression which corroborates the theory that, in the mouse, PAR-3 does not independently transduce intracellular signalling but acts as a co-factor for PAR-4 activation (Jesmin et al. 2006; Nakanishi-Matsui et al. 2000).

## 1.4. The coagulation cascade in chronic liver injury

Approximately 60,000 people in England and Wales have cirrhosis and ten times that have some form of liver disease. The mortality rates from liver disease have been increasing over the past 30 years (Williams et al. 2014).

Chronic liver injury occurs due to a number of aetiologies including chronic viral hepatitis, autoimmune hepatitis, biliary disease and drug / toxin induced damage. These disease processes create a state of chronic inflammation and pathological repair where damaged functional tissue is replaced by fibrous scar tissue. With chronicity there is progressive replacement of functional parenchyma by non-functional fibrous scar tissue (liver fibrosis).

The fibrous scar tissue is composed of connective tissue / extra cellular matrix that is laid down and removed under the influence of a milieu of cells and cytokines. Hepatic fibrosis is reversible (Bonis et al. 2001; Desmet & Roskams 2004), but with on going injury and impaired resolution, can lead to cirrhosis. Histologically, cirrhosis of the liver describes nodules of hepatocytes surrounded by fibrous bands. Functionally the liver is impaired and features of end stage liver disease may be present, including portal hypertension, ascites, encephalopathy and impaired synthetic and metabolic activity.

Epidemiological studies on a variety of populations have demonstrated that procoagulant states (protein C deficiency/resistance, anti-thrombin III deficiency, plasminogen deficiency and factor V Leiden) are associated with more advanced liver fibrosis (of varying aetiology) compared to age / sex

matched controls (Papatheodoridis et al. 2003; Papatheodoridis et al. 2009; Wright et al. 2003; Poujol-Robert, Rosmorduc, et al. 2004; Poujol-Robert, Boelle, et al. 2004).

Subsequent animal studies have confirmed that mouse models with the prothrombotic Factor V Leiden mutation demonstrate accelerated fibrosis and that anticoagulation can be used to counter this (Anstee et al. 2008).

However, these findings are not universal and one study of 210 women who contracted Hepatitis C from a single contaminated batch of anti-D immunoglobulin showed no significant correlation between liver fibrosis status and thrombophilia (Goulding et al. 2007). The reason for this may be due to the low rates of factor V Leiden and prothrombin mutation in this group and the all female gender. Wright et al showed that when individuals with prothrombotic tendencies were separated by gender there was a strong significant association with fibrosis progression in males but a non-significant association in females (Wright et al. 2003).

Martinelli et al studied the relationship between liver fibrosis and three known protease activated receptor 1 (PAR-1) polymorphisms, one of which (-506I/D) has been shown to be protective against thromboembolism and one (IVS-14A/T) which results in decreased PAR-1 expression. Both of these polymorphisms showed no effect on rates of fibrosis, however the third polymorphism (-1426C/T) showed a link between allele type and rate of

fibrosis in males (Martinelli et al. 2008). As with the work by Wright et al, this association was present but not as strong in females.

The recognition of the difference in liver fibrosis progression between males and females is not specific to coagulation status and large cohort studies has previously identified that male gender is a risk factor for fibrosis progression (Poynard et al. 1997; Poynard et al. 2001). The cause for this difference has been attributed to the antifibrogenic / protective effect of female sex hormones (oestrogen and progesterone) as demonstrated in carbon tetrachloride induced liver fibrosis in rats (Xu et al. 2002; Shimizu 2003) and in menopausal women with hepatitis C (Codes et al. 2007). Equally, it has been demonstrated that endometrial PAR-1 gene expression is down-regulated by progestogens (Hague et al. 2002). This led me to conduct all the work in male mice only.

### *1.4.1. Coagulopathy of chronic liver injury*

The focus of this work is the role of the coagulation cascade in the propagation and progression of liver injury. However humans with cirrhosis have multiple defects in a variety of coagulation cascade factors and as this may be drawn into the discussion of the work I have given a brief overview of these defects below.

In the cirrhotic patient defects in the coagulation cascade resulting in a relative procoagulant phenotypes include elevated thrombin generation with resistance to thrombomodulin, elevated levels of factor VIII and reduced levels of protein C, protein S and antithrombin (Tripodi et al. 2009; Muciño-Bermejo et al. 2013). However relative anticoagulant phenotypes are also present such as decreased production of fibrinogen, factors II, V, X, VII, IX, XI, XII and hyperfibrinolysis due to increased plasma tissue-plasminogen activator (t-PA) and decreased plasma thrombin activated fibrinolysis inhibitor (TAFI) (Ferro et al. 2009; Muciño-Bermejo et al. 2013). The reason for a deficiency in coagulation cascade factors could be due to decreased hepatocellular production of these factors, secondary to the decrease in the functional hepatocyte mass in cirrhosis. However factor VIII shows an opposite trend, possibly because it is also produced by pulmonary vascular endothelium, and there may be an increase in production from this source as a compensatory mechanism (Jacquemin et al. 2006).

Defects in the coagulation system are not limited to the coagulation cascade. Briefly, cirrhotic patients have also been found to have features of reduced

platelet plug formation with decreased plasma thrombopoietin, accelerated platelet turnover, and reduced platelet production indicating both increased platelet clearance (consumption) and impaired thrombopoiesis (Pradella et al. 2011). Again, this is countered by features of a pro-thrombotic / pro-platelet plug formation phenotype with increased levels of von Willebrand factor and reduced levels of ADAMTS13 that may counteract this relative platelet deficiency (Mannucci et al. 2001).

### *1.4.2. Effector cells and mechanisms of liver fibrosis*

Key effector cells in liver fibrosis are the collagen producing activated hepatic stellate cell and cells of the innate and adaptive immune system. An in depth review of these effector cells goes beyond the scope of this work (centred on TFPI and TF dependent activation of the coagulation cascade), however below I have briefly summarised the current role of some key effector cells with reference to more comprehensive review articles.

**Hepatic stellate cells**

In the normal liver hepatic stellate cells (also known as the Ito cell or Vitamin A cell) are found in the perisinusoidal space of Disse. Hepatic stellate cells store retinoids (including vitamin A). At rest, hepatic stellate cells express glial fibrillary protein and desmin (cytoskeletal proteins).

During chronic liver injury the hepatic stellate cell is activated to a myofibroblast phenotype and is the major source of the extra cellular matrix that forms the fibrous scar tissue in liver fibrosis. Other cells undergoing myofibroblast differentiation in the context of chronic liver injury include bone marrow derived cells, portal fibroblast and fibroblasts derived from epithelial-mesenchymal transition (Lemoinne et al. 2013).

Activation of the hepatic stellate cell to a myofibroblast phenotype has been split into two phases, initiation and perpetuation (overview from (S L Friedman 2008)).

Initiation is the ‘pre-inflammatory stage’ where early change in gene expression and phenotype make the cells responsive to other stimuli. Paracrine signalling (including reactive oxygen species and apoptotic cell fragments from damaged hepatocytes and Kupffer cells, TGF-β1 from Kupffer cells and endothelial cells, fibronectin from endothelial cells and PDGF, TGF-β1 and EGF from platelets) is the major stimulatory factor in initiation.

Perpetuation of hepatic stellate cell activation involves six cell behaviours:

1. Proliferation.
2. Chemotaxis (release of chemo-attractants from inflammatory cells and other hepatic stellate cells).
3. Fibrogenesis (increasing collagen I production).
4. Contractility.
5. Matrix degradation.
6. Retinoid loss (observed but of unknown significance).

Resolution of hepatic stellate cell activation is associated with cessation of extracellular matrix deposition and the reversal of fibrosis. Resolution of hepatic stellate cell activation occurs in two ways (overview from (S L Friedman 2008)):

1. Reversion of the activated hepatic stellate cell to a quiescent state
2. Apoptosis of the activated hepatic stellate cell. NK cells appear to be the main effector cell in this step and this has been attributed to TRAIL-mediated pathways and the expression of the NK cell activating NKG2D receptor (Radaeva et al. 2006).

Intimately, although not exclusively, associated with hepatic stellate cells are the matrix metalloproteinases (MMPs) and their inhibitors (tissue inhibitors of metalloproteinases, TIMPs). MMPs and TIMPs are involved in the progression and resolution of collagen deposition in the liver. MMP-1 (not found in mice, but murine MMP-13 amino acid sequence and function is similar), MMP-2, MMP-3, MMP-9, MMP-14, TIMP-1 and TIMP-2 have all been identified as important in liver fibrosis. Three of these, MMP-2, MMP-9 and TIMP-1 were examined in this work and therefore I have given a brief overview of their function in liver fibrosis (overview from (Hemmann et al. 2007) with additional key references).

MMP-2 (also known as gelatinase A) is responsible for extra-cellular matrix degradation. MMP-2 is not readily identified in the normal liver, however during liver injury and fibrosis it is expressed by activated hepatic stellate cells. MMP-2 expression increases and stays elevated in fibrosis. As well as its role in extracellular matrix degradation MMP-2 has a number of autocrine regulatory functions in hepatic stellate cells including proliferation, migration and apoptosis (Hartland et al. 2009).

MMP-9 (also known as gelatinase B) is responsible for extracellular matrix degradation. MMP-9 is expressed by Kupffer cells, hepatic stellate cells, lymphocytes and neutrophils during liver fibrosis. The expression of MMP-9 appears to be affected by the duration and frequency of liver injury as a single dose of $CCl_4$ has been shown to increase MMP-9 activity (but not mRNA

expression) at 24 hours whereas in chronic $CCl_4$ administration no change in MMP-9 activity or mRNA expression from baseline is seen (Knittel et al. 2000)(Hemmann et al. 2007). MMP-9 is important in the activation of hepatic stellate cells, as it is able to activate latent TGF-β that results in collagen production by hepatic stellate cells. It is also likely that MMP-9 has an autocrine and paracrine role in the down regulation of further MMP-9 expression.

TIMP-1 is a tissue inhibitor of matrix metalloproteinases. TIMP-1 is predominantly expressed by activated hepatic stellate cells, although expression by Kupffer cells has also been described. During liver fibrosis TIMP-1 up regulation inhibits MMPs leading to the accumulation of extracellular matrix. As well as its role in extracellular matrix turnover TIMP-1 also inhibits programmed cell death in hepatic stellate cells via its MMP inhibition (Murphy et al. 2002)(Hemmann et al. 2007). TIMP-1 has also been shown to inhibit apoptosis in B cells (Arthur 2000).

**Macrophages and monocytes**

Macrophages have been described as a Jekyll and Hyde cell as they play major roles in both the promotion and resolution of liver injury and fibrosis (Duffield 2003). Two types of macrophage have been described based on *in vitro* work. The classically activated, pro-inflammatory M1 macrophage and the alternatively activated, immune-modulatory M2 macrophage.

The pro-inflammatory macrophage releases pro-inflammatory cytokines and chemokines such as TNF, IL-1β, IL-12 and reactive oxygen species. It is associated with extracellular matrix breakdown. The immune-modulatory macrophage secretes mediators such as TGFβ, IL-10, IL-4 and IL-13 and is associated with extracellular matrix deposition through its close association with hepatic stellate cells (activated hepatic stellate cell M-CSF secretion = recruitment and activation of macrophages, macrophage TGFβ secretion = activation of hepatic stellate cells) (Henderson & Iredale 2007; Tacke & Zimmermann 2015; Wynn & Barron 2010).

In the setting of liver fibrosis the *in vitro* work has not translated directly to the *in vivo* model. Current understanding of the diverse role of the macrophage in liver fibrogenesis and resolution in mouse models is succinctly summed up in a review article by Pellicoro et al (Pellicoro et al. 2014). They define a pro-fibrotic macrophage with high Ly6C expression that is responsible for:

- Recruitment, activation (TGFβ driven), proliferation (PDGF driven) and survival (TNF and IL-1β driven) of hepatic stellate cells.
- Recruitment of inflammatory cells (TNF and IL-1β driven).

This macrophages population can subsequently undergo a phenotypic switch to become pro-resolution macrophages with low expression of Ly6C that are responsible for:

- Promotion of hepatic stellate cell apoptosis (TRAIL and MMP-9 driven).
- Extracellular matrix breakdown (MMP-12 and MMP-13 driven).
- Phagocytosis of profibrogenic stimuli (cellular debris, etc).

**Neutrophils**

Although neutrophils play an important role in acute liver injury, their role in chronic liver injury and fibrosis is less well defined, with many studies suggesting that they do not significantly impact fibrogenesis (Henderson & Iredale 2007).

**T cells**

There is evidence to suggest that the balance of T cell subsets ($T_H1$ to $T_H2$) might influence liver fibrosis. $T_H2$ subsets are pro-fibrogenic, predominantly through IL-13 signalling and $T_H1$ subsets are anti-fibrotic through IFNγ and IL-12 signalling. However, the expansion of the vast array of T cell subsets including $T_H17$, $T_{Reg}$ and cytotoxic T cells has produced an often conflicting view of the role of these cells depending on the stage of liver injury and the initiating insult (Pellicoro et al. 2014).

**B cells**

Mice deficient in B cells have shown decreased collagen deposition after chronic carbon tetrachloride and α-naphthylisothiocyanate administration. This is likely to be due to lack of autoantibodies and other antibody independent mechanisms such as secretion of pro-fibrotic cytokines (IL-4, IL-6, IL-13) and direct cell-cell interaction with other immune cells (CD40 mediated) (Marra et al. 2009).

**NK cells**

NK cells have a primarily pro-resolution role in liver fibrosis via IFNγ production and their role in killing activated hepatic stellate cells (Pellicoro et al. 2014; Marra et al. 2009).

### *1.4.3. TF and PAR-2 in chronic liver injury*

Tissue factor (TF) expression in the liver is low compared to other organs such as the lung (Mackman et al. 1993). In the liver TF is found on hepatocytes (Sullivan et al. 2013; Stephenne et al. 2007; Willingham & Matschiner 1989), bile duct epithelial cells (Luyendyk et al. 2009; Flossel et al. 1994), hepatic stellate cells (Bataller et al. 2005) and Kupffer cells (Arai et al. 1995).

In an α-naphthylisothiocyanate (ANIT) model of chronic cholestatic liver injury, mice with low levels of tissue factor (low-TF mice) demonstrated reduced coagulation cascade activation and decreased liver fibrosis. The mechanism of action was demonstrated to be decreased MCP-1 expression, decreased integrin β6 mRNA expression and decreased αVβ6 dependent activation of TGFβ signalling (as demonstrated by decreased SMAD2 phosphorylation but not related to decreased TGFβ expression). These results were recapitulated when wild type mice were administrated a function blocking anti-αVβ6 antibody and a recombinant fusion protein that decreased TGFβ signalling, confirming the role of TGFβ and αVβ6 integrin signalling in chronic cholestatic liver injury and as a possible mechanism for the role of TF in liver fibrosis (Sullivan, Weinreb, et al. 2010).

Although this group looked into the mechanistic pathway of these results they concluded that the impact of TF was through the generation of thrombin and PAR-1 activation (see below) but did not explore the possibility of the role of TF and PAR-2 signalling.

PAR-2 is expressed by hepatocytes, Kupffer cells, large vessel endothelium and bile duct epithelium in the uninjured liver. However, during liver fibrosis PAR-2 expression stays static in hepatocytes but increases in proliferating bile duct epithelial cells, proportional to the degree of fibrosis. PAR-2 expression is also seen in the endothelium, vascular smooth muscle, some inflammatory cells and myofibroblasts of fibrous liver septa. This differs from the PAR-2 expression profile in acute liver injury. PAR-2 activation on a variety of cell types in the liver during fibrosis results in the production of pro-inflammatory cytokines (IL-6, IL-8, MCP-1), sinusoidal endothelial capilarisation and activation of hepatic stellate cells and portal fibroblasts to a myofibroblast phenotype. PAR-2 activation is thought to be responsible for the profibrotic effect of factor Xa (Borensztajn et al. 2010; Borensztajn et al. 2008).

PAR-2 exerts its regulatory effect on hepatic stellate cells by promoting proliferation, migration and collagen production via activation of the MAP kinase cascades (ERK1/2 phosphorylation) and FAK/Src pathway and promoting TGFβ expression (Gaca et al. 2002; Knight et al. 2012). This correlates with findings in fibroblast cell lines and other models of tissue fibrosis and remodelling (Borensztajn et al. 2008).

In a carbon tetrachloride model ($CCl_4$) of liver fibrosis PAR-2 knockout mice developed fibrosis at a similar rate to controls over a five week time frame but did not demonstrate progression beyond this when the model was continued to eight weeks (unlike the control mice who developed more severe fibrosis). This was associated with a similar pattern of hepatic stellate cell activation

(αSMA expression) and number of CD68 positive hepatic macrophages (same at 5 weeks, less at 8 weeks). In addition, there were less F4/80+ macrophages in the livers of PAR-2 knockout mice at both 5 and 8 weeks. In keeping with these findings, at eight weeks PAR-2 knockout mice demonstrated less TGFβ expression and decreased MMP2 and TIMP1 gene expression than controls. The time dependent progression of liver fibrosis was attributed to a compensatory increase in PAR-1 expression (pro-fibrotic) in PAR-2 knockout mice during the first five weeks of injury only. (Knight et al. 2012).

### *1.4.4. Thrombin, PAR-1, -3 & -4 in chronic liver injury*

Thrombin generation in chronic liver injury is associated with fibrosis progression. Duplantier et al demonstrated that, using a thrombin antagonist in rats, liver fibrosis and hepatic stellate cell activation were decreased after seven weeks of $CCl_4$. They also showed that in rats culled earlier in disease progression (3 weeks of $CCl_4$) there was a decrease in hepatic stellate cell activation and TIMP1 gene expression but no difference in fibrosis (Duplantier et al. 2004).

Thrombin activates PAR including PAR-1. PAR-1 activation in a variety of cell types (in and outside the liver) promotes inflammatory cell recruitment and a pro-fibrotic microenvironment. In a bile duct ligation model of chronic liver injury PAR-1 (as well as PAR-2 and PAR-4) expression was upregulated in activated hepatic stellate cells. PAR-1 exerts a regulatory effect on hepatic

stellate cells, promoting proliferation and collagen production via Shc phosphorylation, Shc / Grb2 complex formation and activation of the MAP kinase cascade and ERK1/2 phosphorylation (Fiorucci et al. 2004; Gaca et al. 2002).

As mentioned above, Sullivan et al explored the mechanism linking coagulation cascade proteases, PAR signalling and liver fibrosis using a low-TF mouse model (discussed above) and a PAR-1 knockout model. The PAR-1 knockout model, like the low-TF model, demonstrated decreased liver fibrosis in an ANIT model of chronic cholestatic liver injury associated with decreased MCP-1 expression, decreased integrin β6 mRNA expression and decreased αVβ6 dependent activation of TGFβ signalling (Sullivan, Weinreb, et al. 2010).

Rullier et al and Kallis et al also demonstrated decreased fibrosis and hepatic stellate cell activation / less myofibroblasts in PAR-1 knockout mice after $CCl_4$ induced chronic liver injury. Kallis et al noted that in this model, PAR-1 knockout mice had a reduced number of scar associated macrophages. Using a bone marrow transplant model and *in vitro* migration assays they concluded that this was due to the role of PAR-1 on bone marrow derived macrophages and their recruitment / migration from the bone marrow to the liver after injury. They concluded that this occurred independent of MCP-1 signalling and that PAR-1 played no role in macrophage proliferation (Kallis et al. 2014). Rullier et al noted that PAR-1 knockout mice had a significant decrease in liver T cell infiltrate (Rullier et al. 2008).

There is very little in the published literature relating to the role of PAR-3 and PAR-4 in chronic liver injury. Recently Joshi et al demonstrated that PAR-4 exerted a protective effect in ANIT induced chronic cholestatic liver injury, via its role in platelet activation. They demonstrated that, compared to wild type controls, PAR-4 knockout mice developed increased liver fibrosis and demonstrated increased hepatic expression of profibrogenic factors (collagen1α1, ITGB6 and TIMP-1) as well as more activated hepatic stellate cells (α SMA expression). PAR-4 knockout mice also demonstrated increased serum bilirubin, ALT and ALP as well as worse bile duct proliferation and accumulation of CD3+ lymphocytes in portal tracts compared to wild type controls (Joshi et al. 2015).

Thrombin, in a complex with thrombomodulin, activates thombin-activatable fibrinolysis inhibitor (TAFI) that inhibits tissue plasminogen activator mediated fibrinolysis. Hugenholtz et al demonstrated that deficiency of TAFI (creating a hyperfibrinolytic state with initially normal levels of fibrin) resulted in accelerated fibrosis and liver injury (increase hepatic stellate cell activation, pro-collagen gene expression and plasma ALT) after three weeks of $CCl_4$ induced chronic liver injury. However, there was no difference in the fibrin deposition in the livers of TAFI deficient mice compared to wild type controls and a more marked infiltrate of neutrophils was identified in TAFI deficient mice compared to wild type controls. This led the authors to conclude that the major role for TAFI in chronic liver injury was not via its potentially protective

fibrinolytic properties, but via it's known anti-inflammatory properties. (Hugenholtz et al. 2013).

## 1.5. Murine models of liver injury

### *1.5.1. Comparative physiology, anatomy and histology of the liver*

The liver in the mouse and human has a similar physiological role and in general the anatomy and histology are also similar. The main anatomical differences are the more prominent lobation of the mouse liver compared to humans and the increase in percentage of total body weight in mice (2% vs. 6% in humans and mice respectively).

The main histological differences are:

- More prominent central and portal veins and less conspicuous portal tracts in mice compared to humans.
- Less connective tissue (in health and disease) in the livers of mice compared to humans.

There are a number of murine models of acute and chronic liver injury. Four models of liver injury, two chronic and two acute, were used in this work. Their mechanisms of cellular injury are detailed below.

### *1.5.2. Acute liver injury model: Paracetamol toxicity*

Paracetamol, also known as acetaminophen, N-acetyl-p-aminophenol or APAP is a commonly used, over the counter analgesic. Paracetamol overdose accounts for 54% of cases of acute liver failure in the UK (O'Grady 2005). The mechanisms of cellular injury in paracetamol toxicity centres on the cytochrome P450 pathway and glutathione antioxidant activity.

Cytochrome P450 enzymes located in the smooth endoplasmic reticulum of hepatocytes metabolise paracetamol to the highly reactive N-acetyl-*p*-benzoquinone imine (NAPQI). This is then detoxified by conjugation with glutathione. The conjugation of NAPQI by glutathione prevents it from binding to other cellular proteins. Glutathione is an antioxidant with a reducing thiol group that acts to reduce unstable molecules such as NAPQI, free radicals and reactive oxygen species. Cells can synthesise glutathione de novo from amino acids but recycling of reduced and oxidized forms plays an important role in maintaining physiological levels.

Where there is an excess of the starting molecule to be metabolised (as in paracetamol overdose) this pathway becomes overwhelmed/saturated and the unstable NAPQI causes cellular damage. The mitochondria of a cell are particularly vulnerable and increased mitochondrial membrane permeability from NAPQI damage decreases their functionality and leads to the release of more reactive oxygen species. This further increases oxidative stress and limits the cells ability to produce ATP resulting in cell death/necrosis and apoptosis via the pro-apoptotic BAX protein (Jaeschke et al. 2014; Hinson et

al. 2010). NAPQI also forms the basis of the hapten model of cell death in paracetamol toxicity. In this model antigen presenting cells present NAPQI-protein adducts via the human leukocyte antigen (HLA), activating T cells. Cytotoxic T cells in turn express FasL and release TNF-α, perforin and granzyme, mediating apoptosis in target cells (hepatocytes) (Krenkel et al. 2014).

In the mouse, administration of high levels of paracetamol causes hepatocellular damage and cell death. In addition to hepatocellular damage there is injury to liver sinusoidal endothelium. The pattern of hepatocellular damage can vary from centrilobular hepatocellular swelling, to circumscribed centrilobular necrosis and finally confluent necrosis of large areas of liver parenchyma.

### *1.5.3. Acute liver injury model: Alpha-naphthylisothiocyanate (ANIT)*

Alpha-naphthylisothiocyanate (ANIT) is an isothiocyanate that is commonly used as an insecticide. When administered to rodents it produces a cholangiolitic hepatitis resembling that seen in humans with drug induced cholestatic injury. Morphological changes in portal bile duct lining epithelial cells precede morphological changes in hepatocytes (described in rats). Six hours after treatment with ANIT the first features of damage are evident by light microscopy; there is some portal edema and loss of gamma-glutamyl transpeptidase (γGT) activity from the bile duct lining cells. Eight hours after treatment many ducts show clear-cut damage, with bile plug formation and cells exfoliating into the ducts. Twenty-four hours after treatment the majority

of bile ducts are destroyed and there is focal hepatocellular necrosis (Connolly et al. 1988).

The damage to bile ducts and liver parenchyma is accompanied by a marked neutrophilic inflammatory cell infiltrate. In the setting of experimental induced neutropenia there is virtually no liver damage after ANIT treatment, indicating the central role of neutrophils in this form of experimental acute liver injury (Dahm et al. 1991; Kodali et al. 2006).

ANIT induced liver injury, like paracetamol induced liver injury, involves glutathione. However, unlike paracetamol induced liver injury decreased glutathione levels are associated with decreased ANIT associated liver injury and vice versa. In ANIT induced liver injury glutathione forms a reversible conjugate with ANIT that allows it to be transported from the bloodstream, through hepatocytes, leading to concentration in the bile where it causes toxic damage to bile duct epithelium (Dahm & Roth 1991; Carpenter-Deyo et al. 1991).

### *1.5.4. Chronic liver injury model: Carbon tetrachloride ($CCl_4$)*

Carbon tetrachloride ($CCl_4$) is a commonly used hepatotoxin for the experimental induction of liver injury in mice. $CCl_4$ administration leads to hepatocellular damage through its metabolism by the cytochrome P450 pathway to toxic trichloromethyl that causes cell membrane damage. Membrane damage to Kupffer cells results in the secretion of pro-inflammatory mediators such as TNF-α, IL-1, IL-6, IL-8, IL-18, eicosanoids, and NO. These factors promote the recruitment and activation of inflammatory cells (Liu et al. 2013; Novobrantseva et al. 2005). The resulting damage has a centrilobular distribution and repeated dosing leads to progressive hepatic fibrosis.

Progressive hepatic fibrosis in this model relies on repeated dosing (repeated acute insults). Cessation of the acute insult results in resolution. In order to study the role of experimental interventions in this resolution phase animals need to be culled at different time points after the last dose. Ramachandran et al have described the pattern of hepatic stellate cell activation and fibrosis progression and resolution in C57BL6 mice in the $CCl_4$ model of chronic liver injury up to 256 hours after the last dose of $CCl_4$, Figure 1-2 summarises their findings (Ramachandran et al. 2012).

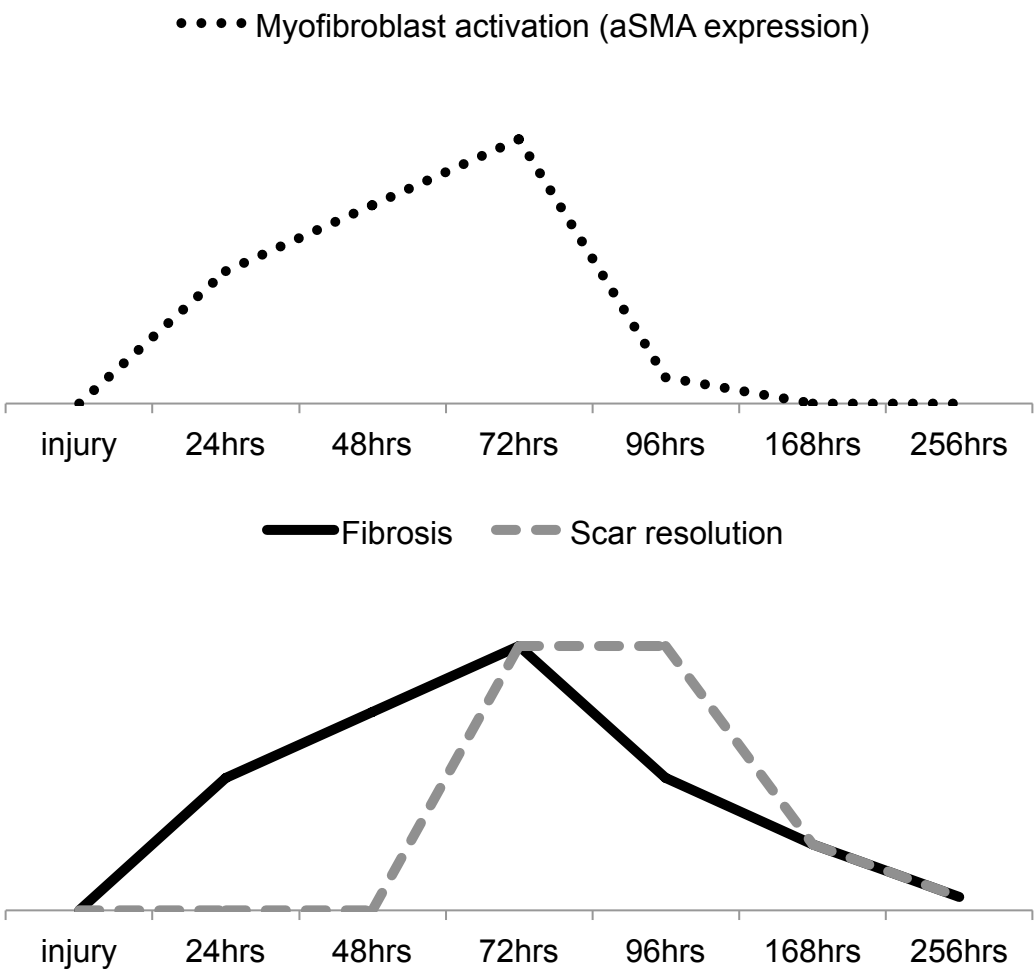


Myofibroblast activation occurs between the start of injury and 96 hours after cessation of the injury, maximal activation occurs between 48 and 72 hours with maximal fibrogenesis at 24 hours.

Maximal extracellular matrix deposition occurs between 48 and 72 hours.

Scar resolution occurs after reduction in liver injury (decreased plasma ALT and AST) and is associated with reduced IL-1β, MCP-1, MIP-1α and MIP-2α (suggesting a change in macrophage phenotype).

**Figure 1-2: Resolution of liver fibrosis after chronic $CCl_4$ induced liver injury**

Graphs created from data published in Ramachandran et al (Ramachandran et al. 2012).

## 1.6. The Transgenic Mouse Model

This section details the development of two transgenic mouse models that were utilised in this work. The mice express TFPI in a cell specific manner and have been used in tissue inflammation and injury research previously.

### *1.6.1. Development of in vitro transgenic TFPI expression*

Initially human TFPI$\alpha$, modified by the addition of a membrane anchor consisting of domains 3 and 4 plus the carboxy-terminal sequence of human CD4, was successfully expressed in mouse fibroblasts. This was achieved by fusing cDNA coding for TFPI (full-length or truncated - lacking the third kunitz domain and the C-terminal) with cDNA coding for domains 3 and 4 and the C-terminal of human CD4 using a cassette cloning strategy. Surface expression and functionality (factor Xa, factor VIIa and TF binding assays) of the transfected TFPI was confirmed by flow cytometry (Riesbeck et al. 1997).

Later, the construct was successfully transvected into immortalised porcine endothelial cells (IPEC) and modified by the addition of P-selectin to the CD4 cytoplasmic tail of the construct (Riesbeck et al. 1998; Chen, Reisbeck, McVey, et al. 1999; Chen, Reisbeck, Kemball-Cook, et al. 1999). P-selectin is a membrane glycoprotein found in secretory granules of platelets (α-granules) and endothelial cells (Weibel-Palade bodies). After platelet/cellular activation the membrane of these granules fuse with the plasma membrane, releasing their contents and resulting in surface expression of P-selectin (Johnston et al. 1989). This modification allowed for the intracellular storage of the fusion protein with expression only on activated cell; avoiding (anti-coagulant)

complications associated with constitutive expression. The successful intracellular storage and expression of the fusion protein, as well as the ability of the fusion protein to inhibit human and non-human, free and membrane bound coagulation factors, including TF was confirmed in a series of *in vitro* experiments (Chen, Reisbeck, McVey, et al. 1999; Chen, Reisbeck, Kemball-Cook, et al. 1999).

Finally, sub-fragments of human CD31 or α-smooth muscle actin (αSMA) were added to the construct. These acted as promoters to target transgene expression to CD31 or αSMA expressing cells respectively (Chen, Giannopoulos, et al. 2004; Daxin Chen et al. 2006).

CD31 (also known as platelet endothelial expression molecule, PECAM-1) is a protein expressed on the surface of platelets, monocytes, macrophages, Kupffer cells, megakaryocytes, neutrophils and some T cells and makes up part of the endothelial cell intercellular junction. It is a member of the immunoglobulin super family and is involved in leukocyte migration, angiogenesis and integrin activation (Pruitt et al. 2012).

αSMA (also known as actin, alpha-actin-2, ACTA2) is a protein expressed predominantly on vascular smooth muscle. It is a member of the actin family of proteins that play a role in cell motility, structure and integrity. αSMA is a major constituent of the contractile apparatus of a cell. αSMA is also a marker of myofibroblast differentiation.

### *1.6.2. Development of in vivo transgenic murine models*

Using these P-selectin-CD4-TFPI constructs transgenic founder mice were generated by microinjection (herein referred to as αSMA-TFPI mice and CD31-TFPI mice). The background strain was C57BL/6. Both heterozygous and homozygous mice were viable, bred normally and had normal baseline bleeding times. No circulating soluble anticoagulant activity was detected (Chen, Giannopoulos, et al. 2004; Daxin Chen et al. 2006).

### *1.6.3. αSMA-TFPI mice*

In the αSMA-TFPI mice *ex vivo* cultured vascular smooth muscle cells expressed the fusion protein and inhibited clotting in recalcified mouse plasma. The smooth muscle cells also failed to show normal proliferation after incubation with activated clotting factors, indicating that the fusion protein was biologically active (Daxin Chen et al. 2006).

In a neointimal (wire-induced) injury model the αSMA-TFPI mice demonstrated a markedly decreased macrophage infiltrate in acute injury and were resistant to post-injury neointimal hyperplasia compared to controls. Bone marrow reconstitution/chimera studies identified that the lack of neointimal hyperplasia was attributable to the expression of the transgenic TFPI on infiltrating bone marrow-derived αSMA expressing neointimal CD34+ cells (Daxin Chen et al. 2006).

Investigation of the mechanistic pathway behind this finding revealed that in control mice circulating CD34+ cells, present after wire-induced vascular

injury, expressed TF and protease activated receptors (PAR) 1, 2 and 4. In addition it was demonstrated that thrombin acted directly on these cells to cause intimal hyperplasia and that the cell type found in the neointima was a mixed phenotype CD34+ αSMA+ CD31+ progenitor cell population which was actively recruited to the neointima from the bone marrow. Selective antagonism of PAR-1 and PAR-4 and CXCR4 suggested that these thrombin-induced changes were at least partly mediated by PAR-1. In αSMA-TFPI mice the absence of these cells suggested that expression of the transgenic TFPI promoted their maturation to endothelial cell or vascular smooth muscle cell phenotypes and in turn promoted the regenerative repair of the damaged arteries (Chen et al. 2008).

This was confirmed in an aortic transplantation model. Recipient αSMA-TFPI mice did not develop the intimal hyperplasia seen in recipient control mice despite the same adaptive and innate immune response. This was associated with a lack of TF expression on αSMA+ cells compared to control mice. However the transgenic TFPI expression did not prevent or delay graft rejection. Bone marrow reconstitution/chimera models showed that bone marrow derived cells from αSMA-TFPI mice, PAR-1 deficient (knockout) mice or cells incubated with a PAR-1 antagonist prior to transplantation had the same effect on intimal hyperplasia in aortic transplantation models using control mice. Reduced intimal hyperplasia was also seen with bone marrow reconstitution from PAR-4 deficient (knockout) mice, but to a lesser extent (Chen et al. 2012).

In addition circulating CD34+ cells in the αSMA-TFPI mice had the same proportion of TF, PAR-1, αSMA and CD31 expression but there were significantly fewer CD45+ myeloid progenitors (CD45+, CD68+, F4/80+, Ly6C+, CD11b+ and CD115+ cells) compared to controls. This difference was ameliorated by the administration of anti-hTFPI or anti-PAR-1 antibodies (but not anti-PAR-2 antibodies), suggesting that in the αSMA-TFPI mice TFPI inhibition of TF altered the proportion of circulating CD45+ myeloid progenitors via PAR-1 signalling (Chen et al. 2012).

### *1.6.4. CD31-TFPI mice*

In the CD31-TFPI mice resting endothelial cells were negative for the fusion protein however *ex vivo* cytokine activated endothelial cells inhibited clot formation in clotting assays with recalcified mouse plasma. Activation of platelets and monocytes (with thrombin and LPS) also lead to expression of the fusion protein in this strain. Activated (concanavalin A stimulated) CD31 negative splenic immune cells did not express the fusion protein (Chen, Giannopoulos, et al. 2004).

In a LPS-endotoxaemia model these CD31-TFPI mice demonstrated a modified response compared to control mice, with less thrombocytopenia, consumptive coagulopathy and intravascular thrombosis. This was thought to be due to limitation of the propagation phase of the coagulation cascade in the transgenic mice, mostly associated with expression of the transgenic TFPI on endothelial cells (Chen, Giannopoulos, et al. 2004). In a xenotransplantation model of acute humoral rejection (mouse-heart-to-rat

model) CD31-TFPI mice showed delayed xenograft rejection compared to controls. This was attributed to the inhibition of systemic xenograft induced intravascular coagulation in the transgenic mice {Chen, 2004 #499} (Chen, Weber, et al. 2004).

## 1.7. Project hypotheses

This work sought to investigate the role of TFPI in liver injury using transgenic mice (described in section 1.6) that selectively expressed TFPI creating local, cell specific over expression.

The overall hypothesis for the work was:

*Cell specific expression of TFPI in acute and chronic liver injury would limit the progression and extent of liver injury.*

On review of the literature and given the data gathered from these mice in the models discussed above, it was hypothesised that:

3. *Expression of TFPI on αSMA positive cells in the liver would decrease the degree of acute hepatocellular injury and fibrosis via PAR associated modification of hepatic stellate cell activity and decreased microvascular clot formation.*

4. *Expression of TFPI on CD31 positive cells in the liver would decrease the degree of acute hepatocellular injury and fibrosis via PAR associated modification of CD31 positive myeloid cell activity and decreased microvascular clot formation.*

## 2. Methods

### 2.1. Animal husbandry

All research using live animals was approved by the local ethics committee and carried out under Home Office supervision in accordance with the Animal (Scientific Procedures) Act 1986.

All animals were housed under standard conditions (12 hour light/dark cycle, 21+/-2°C temperature, 55+/- 10% humidity, with a standard diet and access to drinking water *ad libitum*).

### 2.2. Transgenic mouse colonies

Breeding trios of two transgenic strains was gifted from Prof Dorling at Kings College London. Breeding colonies were established and inbred to optimise the number of male transgene positive animals available for experimentations. After 4-5 generations transgenic animals were backcrossed with bought in wild type controls (C57/BL6 J, Harlan UK) to limit genetic drift from the background control animal strain.

### *2.2.1. Genotyping transgenic mice*

Carriage of the transgene was confirmed using DNA extracted from ear biopsies and polymerase chain reaction (PCR) followed by gel electrophoresis of the PCR product.

Primer pairs were specific to the unique region of the transgene construct that coded for the human TFPI - CD4 - P-selectin fusion protein.

#### *2.2.1.1. DNA extraction*

Ear punch biopsy samples (maximum 3mm diameter) were digested in 100µL of buffer solution made up of 100mMTrisHCl (pH8), 5mM EDTA, 200mM NaCl and 0.1% SDS (all Sigma-Aldrich); plus 2µL of 20mg/mL proteinase K (Life Technologies). Samples were placed in a thermomixer (Fisher Scientific) overnight at 55°C and 400rpm. After digestion samples were centrifuged (Sorvall Biofuge Fresco) at 13,000rpm for 5 minutes at 4°C followed by Proteinase K inactivation by heating to 95°C for 5 minutes.

#### *2.2.1.2. PCR and Gel electrophoresis*

PCR conditions were optimised to custom made primer specific conditions (see table Table 2-1). 1µL of ear biopsy DNA was added to a mixture of PCR primers (custom oligos, Sigma-Aldrich) and master mix (GoTaq® Green Master Mix, Promega) and placed in a thermocycler (Applied Biosystems).

| Primer name | Sequence, 5'-3' | | Product length | Conc in PCR mix | Annealing temp and cycles |
|---|---|---|---|---|---|
| | Forward: | Reverse (complementary): | | | |
| **XCON 1/2** | atgtggcagtgtctgctgag | aggatccggacaggtctctt | 350 | 1.2μM | 55°C 30 cycles |
| **XCON 3/4** | *tccctgactccgcaatcaac* | *tcgtggtgctagctttccag* | 384 | 1.2μM | 55°C 35 cycles |
| **XCON 5/6** | *tcgtccgaatggtttccagg* | *ggggaacaggtggagttctc* | 852 | 1.2μM | 55°C 35 cycles |
| **ActB** | cccatctacgagggctatgc | atgtcacgcacgatttccct | 146 | 1μM | 55°C 30 cycles |
| **GAPDH** | accacagtccatgccatcac | caccaccctgttgctgtagcc | 450 | 1.2μM | 55°C 30 cycles |

**Table 2-1: Genotyping PCR primer information.**
Conc = concentration; temp = temperature

PCR product was run on a 2% agarose (w/v, Invitrogen) gel made with 1x TAE buffer and 4% ethidium bromide at 140A for 30 minutes. Gels were viewed on a UV illuminator and the presence or absence of a band at the appropriate molecular weight was recorded.

## 2.3. Animal models of liver injury

A power calculation based on pilot data or experience from researchers in the group was used to calculate the number of animals required per experimental arm. The following calculation was used:

$$n = 1+2C(s/d)^2$$

$n$ = number per group

$s$ = standard deviation

$d$ = difference to be detected (2 standard deviations)

$C$ = constant, calculated based upon the $\alpha$ (probability of a type I error) and 1-$\beta$ (probability of making a type II error) values. For this study $\alpha = 0.05$ and $1-\beta = 0.9$ and $C = 10.51$ (Dell et al. 2002).

### *2.3.1. Acute liver Injury*

#### *2.3.1.1. Paracetamol induced liver injury*

Under Home Office Licence 70/7578, 8-10 week old transgenic and background strain matched wild type controls (C57BL6/J, Harlan UK) were fasted (with free access to water) overnight for twelve hours prior to administration of 300-325mg/kg of paracetamol (Sigma) dissolved in 0.9% saline (Baxter UK) at a concentration of 20mg/mL. The solution was administered by intraperitoneal injection.

Mice maintained for less than 24 hours were administered 325mg/kg and mice maintained for 24 hours or more were administered 300mg/kg. This dosing regimen was based on work carried out by Dr Lucia Possamai looking at the strain dependant susceptibility of mice to paracetamol (Possamai 2015).

Vehicle only treated mice were administered saline only.

Mice were monitored frequently using minimally invasive parameters (observation of body condition, minimal handling) and in accordance with guidance set out in the licence.

Mice were culled at set time points as defined by the experimental conditions and within the remit of the licence.

A power calculation based on early cohort liver hepatocellular necrosis data suggested 6 animals per experimental arm.

#### *2.3.1.2. Alpha-naphtylisothiocyanate (ANIT) induced liver injury*

Under Home Office Licence 70/7578, 8-10 week old transgenic and background strain matched wild type controls (C57BL6/J, Harlan UK) were fasted (with free access to water) overnight for twelve hours prior to administration of 60mg/kg of ANIT (Sigma) dissolved in corn oil (Mazola) at a concentration 6mg/mL. The solution was administered by oral gavage.

ANIT dosing was determined by existing literature (Luyendyk et al. 2011; Sullivan, Weinreb, et al. 2010). Strain tolerance to the hepatotoxin at this dose was tested in a small number of animals (n=2 per strain) and this data was included in subsequent experiments to reduce the number of animals used overall.

Vehicle only treated mice were administered corn oil only.

Mice were monitored frequently using minimally invasive parameters (observation of body condition, minimal handling) and in accordance with guidance set out in the licence.

Mice were culled at set time points as defined by the experimental conditions and within the remit of the licence.

A power calculation based on early cohort liver hepatocellular injury data suggested 6 animals per experimental arm.

### *2.3.2. Chronic Liver Injury*

#### *2.3.2.1. Carbon tetrachloride ($CCl_4$) induced liver injury*

Under Home Office Licence 70/6493 and 70/8060, 6-8 week old transgenic and background strain matched wild type controls (C57BL6/J, Harlan UK) administered $CCl_4$ (Sigma) dissolved in corn oil (Mazola).

Initial work administering 2mL/kg of a solution containing 33.3% v/v $CCl_4$ (a dose of 0.5mL/kg of $CCl_4$) [personal communication - Dr F Oakley, (Moles A Fau - Sanchez et al. 2013)] was poorly tolerated by the transgenic and wild type strains of mice. An incremental dosing regimen over 4 weeks, based on previous work by Dr Anstee (Anstee et al. 2008), was better tolerated.

In the incremental regimen mice were administered 4mL/kg of a solution by intraperitoneal injection 3 times a week. The solution was changed on a weekly basis, each week containing a greater dose of $CCl_4$ than the last. Week 1 solution contained 3.2% v/v $CCl_4$ (a dose of 0.125mL/kg of $CCl_4$); week 2 solution contained 6.7% v/v $CCl_4$ (a dose of 0.25mL/kg of $CCl_4$); week 3 solution contained 14.3% v/v $CCl_4$ (a dose of 0.5mL/kg of $CCl_4$) and week 4 solution contained 33.3% v/v $CCl_4$ (a dose of 1mL/kg of $CCl_4$).

Vehicle only treated mice were administered corn oil only.

Mice were monitored using minimally invasive parameters (observation of body condition and weight, minimal handling) and in accordance with guidance set out in the licence.

Mice were culled at set time points after the last dose of $CCl_4$ as defined by the experimental conditions and within the remit of the licence. These time points were guided by the literature and based on the phases of hepatic stellate cell activation, development and resolution of fibrosis as described in Figure 1-2. Briefly, after administration of $CCl_4$, myofibroblast / hepatic stellate cell activation is seen to increase to a maxima around 72 hours, returning to a baseline level of activation around 96-168 hours. Intrinsically linked to this is the deposition of collagen to produce fibrous scar tissue (peak deposition at 72 hours) and the resolution of this scar tissue (peak 72-96 hours). These measurable parameters provide reproducible indices for assessing any changes in the liver microenvironment.

A power calculation based on pilot cohort Sirius red collagen staining data suggested 6 animals per experimental arm.

## 2.4. Tissue and blood harvest, processing and storage

### *2.4.1. Tissue and blood harvest*

Mice were culled with an overdose of pentobarbitone administered by intraperitoneal injection.

#### *2.4.1.1. Tissue and blood harvest without fresh liver collection*

A midline incision was made to visualise the abdominal and thoracic cavity. Cardiac puncture (right ventricle) was performed with a 23 gauge needle and at least 200µL of blood collected. The blood was transferred into heparinised container (Sarstedt) for later processing.

The liver was isolated and removed from the abdominal cavity and dissected as shown in Figure 2-1.

Any other organs required for control tissue were harvested at the same time and stored/processed as detailed below.

#### *2.4.1.2. Tissue and blood harvest with fresh liver collection*

A midline incision was made to visualise the abdominal and thoracic cavity. Cardiac puncture (right ventricle) was performed with a 23 gauge needle and at least 200µL of blood collected. The blood was transferred into heparinised container (Sarstedt) for later processing.

The left ventricle was then cannulated with a 23 gauge needle and 30mL of PBS perfused through the entire circulation.

The liver was isolated and removed from the abdominal cavity and dissected as shown in Figure 2-1.

Any other organs required for control tissue were harvested at the same time and stored/processed as detailed below.

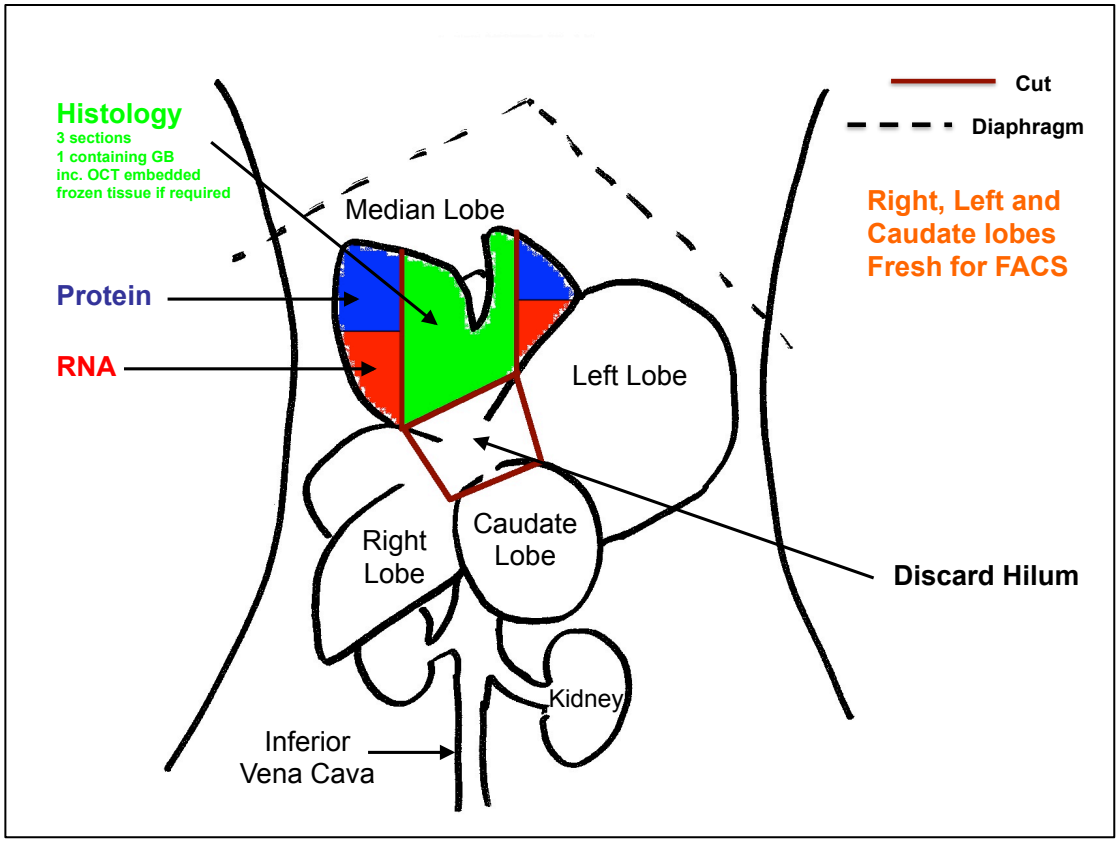


**Figure 2-1: Liver tissue harvest**

Based on diagram from plate 60 from the web adapted version of the The Anatomy of the Laboratory Mouse by Margaret J. Cook (Mouse Genome Informatics 2008).

### *2.4.2. Blood processing*

Heparinised tubes containing up to 200µL of blood were centrifuged at 3,000rpm for 10 minutes. The blood plasma supernatant was removed and stored at -20°C.

The analysis and interpretation of the small volumes of plasma harvested from mouse models requires specialist expertise. Within the research group there was an existing relationship with Dr Tertius Hough at the Clinical Pathology Laboratory, Medical Research Council Harwell (Oxford), an institute specialising in mouse genetics and phenotyping and a member of the International Mouse Phenotyping Consortium (IMPC). Blood plasma samples were batched and sent to Dr Hough to be analysed on a Beckman Coulter AU680 clinical chemistry analyser.

### *2.4.3. Frozen tissue processing*

Tissue for RNA and protein extraction was snap frozen in liquid nitrogen and stored at -80°C.

### *2.4.4. Formalin fixed tissue processing*

Tissue for paraffin embedding and sectioning was fixed in 10% formalin. Fixed tissue was processed on a tissue processor for automated dehydration and paraffin infiltration before embedding in paraffin blocks.

Tissue sections were cut at 5-8µm on a microtome with one section per slide. Slides were placed in a drying oven at 65°C for at least 30 minutes.

### *2.4.5. Fresh tissue processing and liver immune cell isolation*

Fresh liver was collected for immune cell isolation. Fresh liver was placed in chilled PBS and transported on ice.

Immune cell isolation was carried out in a sterile cell culture environment.

The fresh liver from each mouse was individually processed.

Fresh liver was placed in a petri-dish with PBS and dissociated using a scalpel and forceps. This solution was then passed through a 100μm filter into a 50mL tube. The solution was centrifuged at 60g for 1 minute to pellet the hepatocytes/parenchymal cells. The supernatant was transferred to a new tube and centrifuged at 1400rpm to pellet the non-parenchymal cells.

The non-parenchymal cell pellet was resuspended in 10mL of PBS and carefully layered over 5mL of a 27% optiprep (v/v with PBS, Sigma-Aldrich) solution in a 15mL tube and centrifuged at 800rpm for 15mins at 22°C (brake off). This created a density gradient to separate non-viable cells (bottom fraction) from viable cells (top fraction). The top fraction was harvested and transferred to a fresh tube and centrifuged at 1400rpm to pellet the viable non-parenchymal cells.

ACK lysis buffer (Lonza) was added to the pellet to lyse red blood cells. After 1 minute PBS was added to stop the ACK lysis reaction and cells were centrifuged twice at 1400rpm to wash and pellet the non-parenchymal cells.

The non-parenchymal cell pellet was then resuspended in 500µL of PBS and the cells counted using a Malassez haemocytometer and trypan blue (Life Technologies).

## 2.5. Histochemical staining of FFPE sections

### *2.5.1. Deparafinisation*

Paraffin sections were deparaffinsed and rehydrated by passing through xylene and ethanol at varying concentrations.

### *2.5.2. Haematoxylin and Eosin staining*

After deparafinisation sections were stained using an automated Tissue Tek staining machine. Briefly the protocol was:

- Nuclear staining with Harris haematoxylin (CellPath), 5 minutes.
- Wash in tap water.
- Differentiate with 1% acid alcohol (1% HCl, 70% alcohol, Sigma), 30 seconds or as required.
- Wash in tap water.
- 'Blue' in Scotts water (Sodium bicarbonate, Magnesium sulphate 7-hydrate, tap water), 30 seconds or as required.
- Wash in tap water.
- Stain with 1% eosin Y (1% v/v in tap water), 5 minutes.
- Wash in tap water.
- Dehydrate by passing through varying concentrations of ethanol.
- Clear in xylene (Sigma)
- Mount using automated cover-slipping machine (Tissue Tek).

### *2.5.3. Sirius Red staining*

After deparafinisation sections were stained with Sirius red (Sigma) for 1 hour. Sections were then washed and blotted dry before dehydration in industrial methylated spirit and clearing in xylene. Sections were covered slipped by hand using a resin-based mounting media (DPX mountant, Sigma).

## 2.6. Immunohistochemistry on FFPE tissue sections

Immunohistochemical staining was optimised to individual antibodies (see Table 2-2) however the outline protocol was as follows:

### *2.6.1. Deparafinisation*

Paraffin sections were deparaffinsed and rehydrated by passing through xylene and ethanol or industrial methylated spirit at varying concentrations.

### *2.6.2. Antigen retrieval*

Where required antigen retrieval was performed using heat-induced epitope retrieval in a suitable buffer:

- 1mM EDTA, pH8 (Sigma)
- or 10mM Sodium Citrate with 0.05% Tween 20, pH 6.0 (Sigma)

### *2.6.3. Endogenous peroxidase and other protein block*

Where required endogenous peroxidase block was performed using a hydrogen peroxide buffer solution (hand staining, Abcam; automated staining, Leica Bond Max).

Where required non-specific protein binding was blocked by incubating the sections with a suitable protein block:

- 1% Bovine serum albumin in PBS or TBST,(Sigma)
- or Abcam Rodent block (Abcam)

### *2.6.4. Indirect immunolabelling*

After washing, sections were incubated with primary antibody.

### *2.6.5. Detection systems*

After washing, sections were incubated with secondary antibody (specific to the host species of the primary antibody). In some cases the secondary antibody was biotinylated for use with a streptavidin-biotin complex (LSAB) detection system (biotinylated secondary plus streptavidin-peroxidase) and other secondary antibodies were directly conjugated with horseradish peroxidase (immunoenzyme method).

After washing, the chromogen 3,3' Diaminobenzidine (DAB) was applied. DAB forms a brown precipitate in the presence of peroxidase enzymes that is insoluble in alcohol.

### *2.6.6. Counter staining*

After washing, sections were counterstained with haematoxylin (Harris haematoxylin followed by blueing agents, acid alcohol and Scotts Water, various suppliers see 2.5.2), dehydrated (by passing through varying concentrations of ethanol and xylene) and coverslipped by hand or using an automated coverslipper (Tissue Tek).

### *2.6.7. Controls*

Appropriate controls are important to ensuring quality control of immunohistochemical staining. For each batch of staining a positive control and a secondary only control were used.

Positive controls were used to confirm that the staining had worked, ensuring that negative staining represented true negative results. Positive controls were either sections of tissue known to stain positive with the antibody (placenta in fibrin immunohistochemistry), internal positive controls (blood vessel smooth muscle αSMA immunohistochemistry) or sections positive in previous batches.

Secondary only controls are a form of negative control that ensures that there is no non-specific staining due to cross-reaction with the secondary antibody and tissue antigens. It is expected that these sections will not show any positive staining. In each batch a known positively staining section, preferable of the same tissue type, went through the entire immunohistochemical staining process but the primary antibody solution was replaced with a dilutent only solution.

Additional positive and negative controls were used in the TFPI immunohistochemistry. As well as a tissue positive and secondary only control, a known transgene negative and transgene positive control were processed with each batch.

| Primary antibody | Antigen retrieval | Primary antibody incubation conditions* | Secondary antibody | Chromogen | Notes |
|---|---|---|---|---|---|
| **αSMA Abcam, ab5694 Rabbit polyclonal anti-human** | HIE with citrate buffer<br><br>20 minutes | 0.0005mg/mL (1 in 400 dilution)<br><br>60 minutes incubation | DAKO REAL Envision HRP rabbit/ mouse<br><br>10 minutes | DAB<br><br>10 minutes | Copper sulphate enhancement<br><br>2 minutes |
| **MCM4 Abcam, ab84153 Rabbit polyclonal anti-human** | HIE with EDTA buffer<br>Primary antibody 1 in 100 dilution<br>Leica (Leica Bond Max) automated immunohistochemistry system – Mouse 30 program | | | | Copper sulphate enhancement<br><br>2 minutes |
| **F4/80 Santa Cruz, sc-25830 Rabbit polyclonal anti-mouse F4/80 (M-300)** | HIE with EDTA buffer<br><br>20 minutes | 0.002mg/mL (1 in 100 dilution)<br><br>Overnight incubation at 4°C | DAKO REAL Envision HRP rabbit/ mouse<br><br>15 minutes | DAB<br><br>15 minutes | Copper sulphate enhancement<br><br>2 minutes |
| **TFPI Abcam, ab117628 Mouse monoclonal anti-human** | HIE with citrate buffer<br><br>(20 minutes, water bath at 95°C) | 0.01 mg/mL<br><br>Overnight incubation at 4°C | Abcam mouse on mouse HRP polymer<br><br>60 minutes | DAB<br><br>10 minutes | TBST wash/diluent |
| **Fibrin Sekisui, REF 350 Mouse monoclonal anti-human fibrin β chain** | None | 0.02 mg/mL<br><br>60 minutes incubation | Abcam mouse on mouse HRP polymer<br><br>60 minutes | DAB<br><br>10 minutes | |

**Table 2-2: Immunohistochemistry conditions by primary antibody.**

* Incubation at room temperature unless otherwise stated. HIE = heat induced epitope retrieval.

## 2.7. Histology section image analysis

Histology section images were acquired using the Nuance multispectral imaging system 3.0.2 (PerkinElmer) and a light microscope (Olympus BX50).

### *2.7.1. Nuance multispectral imaging system*

The Nuance multispectral imaging system works using a high resolution CCD image sensor (CCD = charge coupled device; the light sensitive element found in modern digital cameras, the 'digital retina') with a unique solid state liquid crystal wavelength tuning element. This liquid crystal wavelength tuning element acts like an emission filter in fluorescent microscopy and can be applied to transmitted bright field microscopy. The liquid crystal wavelength tuning element allows transmitted visible light to be recorded on the CCD in more than the standard 3 channels (Red/Green/Blue).

The liquid crystal wavelength tuning element allows for multiple colours with a similar transmission spectrum to be individually defined by narrowing the portion of the visible light spectrum detected and increasing the number of portions of the visible light spectrum that are recorded (e.g. data acquired at 10nm steps throughout a defined wavelength range). The data collected from this acquisition is called an image cube.

The image analysis software accompanying the system can use the data from the image cube to identify specific portions of the visible light spectrum recorded and manipulate the image using false colours to enhance detection

and quantification of differentially stained elements within the imaged sections (PerkinElmer 2012).

In some instances (e.g. use of immunohistochemical chromogens in dual staining that are close in the visible light spectrum) this allows for a more detailed analysis of images compared to a standard RGB image where data is recorded at only the 3 standard Red/Green/Blue wavelengths (450nm, 530nm and 610nm approximately).

When acquiring a cube the multispectral imaging system allows the user to define the binning (the combining of pixel data to reduce exposure time and image size but reducing resolution), region of interest (ROI) from the entire field of interest, the wavelength range for acquisition and the exposure time. In this work the default settings for an image cube were:

- Binning – 1x1 (i.e. no reduction in pixels)
- ROI – 2/3
- Wavelength range – 420nm to 720nm, narrow band mode, 10nm steps
- Exposure - autoexposure

A 2/3 (two-thirds) ROI was used for technical reasons. Briefly, the adaptor used to attach the Nuance imaging system to the microscope was slightly too short, creating a circular ‘shadow’ around the edge of the acquired images. To eliminate this artefact the inner two-thirds of the CCD sensor (2/3 ROI) was selected for image acquisition.

### *2.7.2. Sirius red staining image analysis*

Sirius red histochemical staining detects type I and Type III collagen in formalin fixed paraffin embedded (FFPE) tissue on light microscopy. Collagen is the predominant extracellular matrix protein deposited in liver (during health and disease) and as such is often used as a surrogate for liver fibrosis. Other methods of detecting fibrosis in the liver include trichrome stains and immunohistochemistry using antibodies to specific collagen types. However Sirius red is generally favoured in the published literature and quantification of collagen via image analysis of tissue stained with Sirius red has been shown to correlates with hepatic hydroxyproline content (James et al. 1990). Technically the contrast between the red stained collagen fibres and the yellow non-collagen containing tissue in Sirius red stained tissue is good for digital image analysis.

To quantify Sirius red staining in both the carbon tetrachloride and thioacetamide models of chronic liver injury Sirius red stained sections of FFPE liver were photographed using the Nuance multispectral imaging system with a x4 light microscope objective (x40 magnification).

RGB images were acquired and saved as JPEG files. Images were analysed using ImageJ (1.46r (Rasband 2014)). Images were converted into RGB stacks and the Green image selected for analysis. The ImageJ Threshold tool was used to select regions of the tissue stained red and the overall area of tissue in each section in a semi-automated method. See Figure 2-2.

Field diameter and image quality were used to calculate a scale of 201.3 pixels : 1mm and therefore each image a field area of 15.76mm$^2$. The area of Sirius red staining (collagen) was determined as a percentage of tissue present in each section.

A cumulative mean calculation was performed on two samples, one with extensive Sirius red staining and one with less pronounced staining. Taking into account results from both samples, the cumulative mean showed that images of two entire sections of liver were required.

**Figure 2-2: ImageJ quantification of Sirius Red staining**

***See over for figures.***

Figure legend

All images x40 original magnification

**Image 1:** Sirius Red stained liver section in a αSMA-TFPI mouse, 72 hours after last administration of $CCl_4$.

**Image 2:** ImageJ RGB stacked images, Green channel image used for threshold quantification.

**Image 3:** ImageJ threshold image and automated quantification of red stained (collagen) area.

**Image 4:** ImageJ threshold image and automated quantification of total tissue in image.

**Image 1**

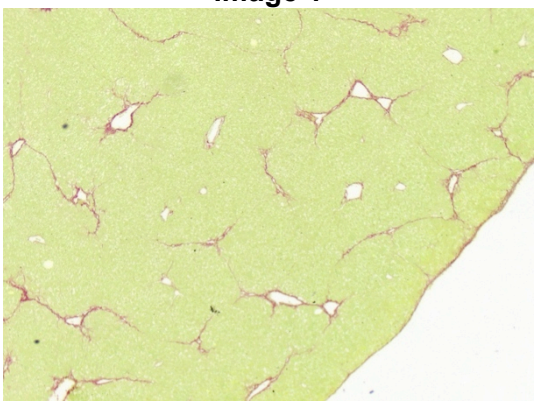

**Image 2**

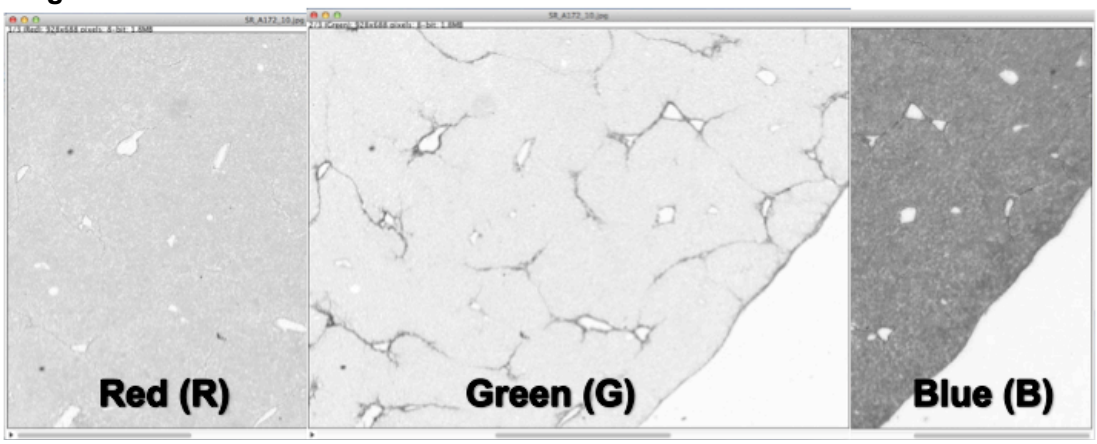


**Image 3**

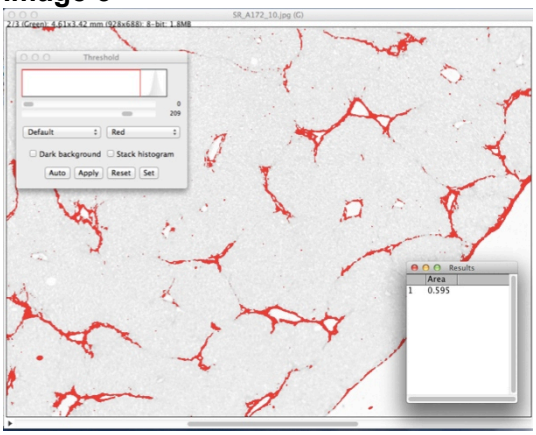

**Image 4**

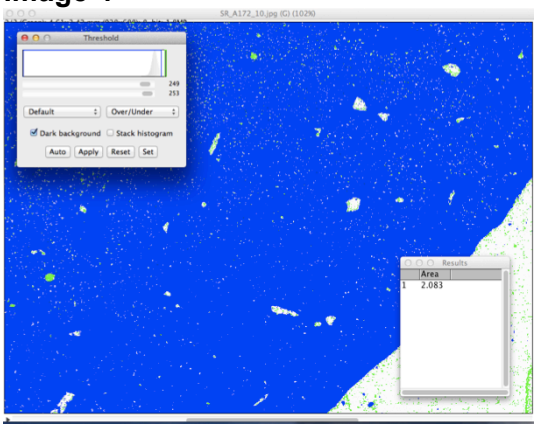

**Figure 2-2: ImageJ quantification of Sirius Red staining**

See previous page for figure legend.

### *2.7.3. Percentage liver parenchymal (hepatocellular) injury*

To quantify liver parenchymal hepatocellular injury in both the paracetamol and ANIT models of acute liver injury H&E stained sections of FFPE liver were photographed using the Nuance multispectral imaging system with a x10 light microscope objective (x100 magnification).

RGB images were acquired and saved as JPEG files. Images were analysed using ImageJ (1.46r (Rasband 2014)). The ImageJ Region of Interest (ROI) Manager was used to manually delineate and measure areas of necrosis (see Figure 2-3). This method was also used to manually delineate and quantify non-hepatocellular tissue (e.g. central vein lumen).

Field diameter and image quality were used to calculate a scale of 502.57 pixels : 1mm and therefore each image a field area of 2.52mm$^2$. The area of necrosis was determined as a percentage of liver hepatocellular tissue present in each section. Liver hepatocellular tissue was defined as the total field area minus non-hepatocellular tissue.

A cumulative mean calculation was performed on two samples, one with extensive parenchymal injury and one with less pronounced parenchymal hepatocellular injury. Taking into account results from both samples, the cumulative mean plateaued at 15 consecutive x10 objective fields.

**Image 1 – Original Image**

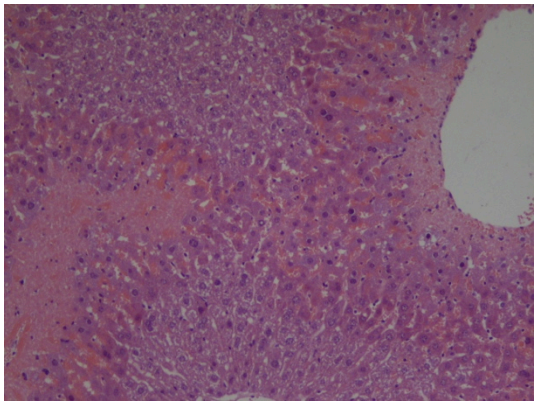

**Image 2**

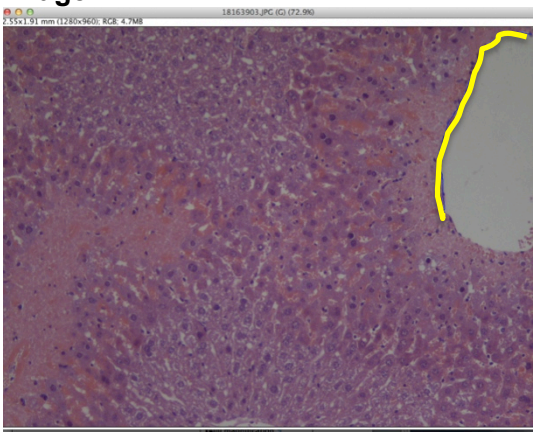

**Image 3**

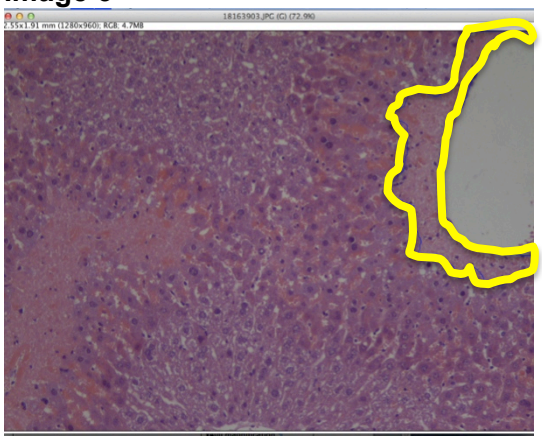

**Image 4**

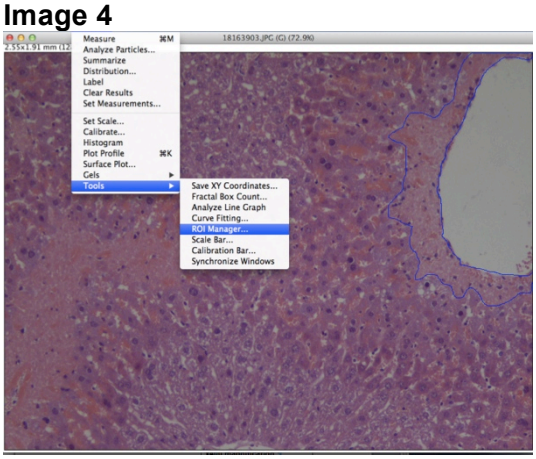


**Image 5**

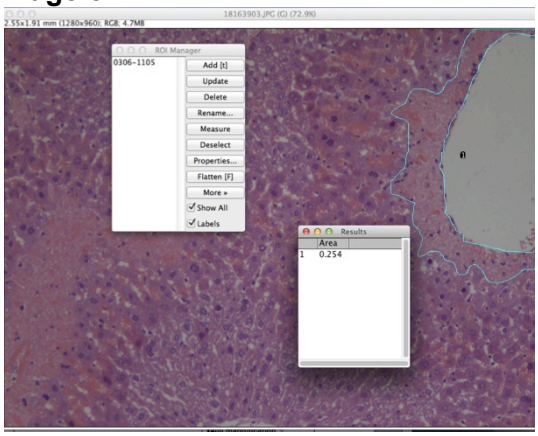


**Image 6**

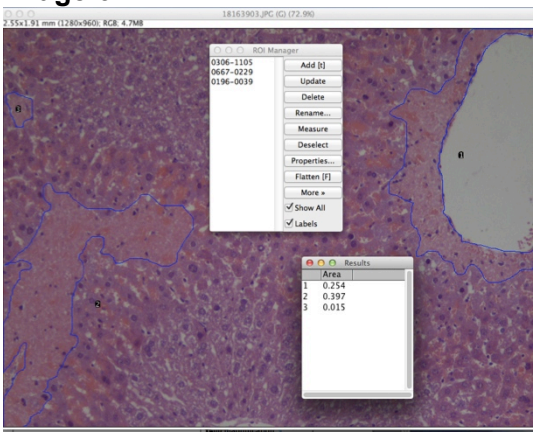


**Figure 2-3: ImageJ quantification of hepatocellular necrosis**

Images and figure legend continued on next page.

**Image 7**

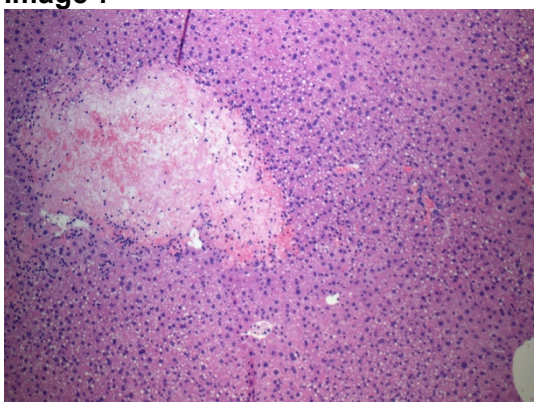

**Image 8**

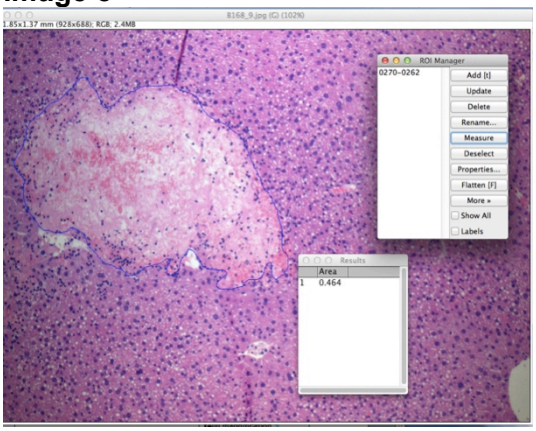


**Figure 2-3: ImageJ quantification of hepatocellular necrosis, continued**

All images, original x100 magnification.

**Image 1:** Paracetamol induced liver injury in a αSMA-TFPI mouse, 6 hours after administration of paracetamol. Original image.

**Image 2 and 3:** Manual delineation of area of hepatocellular injury. (Highlighted with yellow overlay).

**Image 4 and 5:** ImageJ ROI manager automated quantification of area of hepatocellular necrosis based on manually selected area. (Yellow overlay removed, original ImageJ outline blue).

**Image 6:** ImageJ ROI manager automated quantification of area of hepatocellular necrosis based on all manually selected area. (Original ImageJ outline blue).

**Image 7:** ANIT induced liver injury in a CD31-TFPI mouse, 48 hours after administration of ANIT. Original image.

**Image 8:** Using ImageJ manual delineation of area of hepatocellular injury and ROI manager automated quantification of area. (Original ImageJ outline blue).

### *2.7.4. αSMA Immunohistochemical staining image analysis*

Activated hepatic stellate cells are the predominant collagen producing cell in the liver during homeostasis and fibrosis. Activated hepatic stellate cells express αSMA. Immunohistochemistry for αSMA in FFPE liver tissue sections is widely used in the literature as a surrogate for hepatic stellate cell activation. Other markers, including desmin, GFAP and Vitamin A, are expressed by hepatic stellate cells but αSMA has been described as the "single most reliable marker of stellate cell activation" because in both normal and injured liver the only other cell type known to express it is the vascular smooth muscle cell (Scott L Friedman 2008). These have a characteristic vascular distribution that can be easily distinguished from activated hepatic stellate cells.

To quantify the proportion of cells staining positive for αSMA in chronic liver injury models sections of FFPE liver stained with αSMA were photographed using the Nuance multispectral imaging system with a x40 light microscope objective (x400 magnification).

Images cubes were acquired. Spectra for haematoxylin and DAB were defined using sections individually stained with haematoxylin or DAB. This spectral library was used to unmix the image cube. False colouring of the two elements and the formation of a composite image allowed for better definition and identification of DAB positive (αSMA positive) cells.

The unmixed composites were saved as a JPEG files and analysed using ImageJ (Rasband 2014). As the aim of this test was to quantify the number of αSMA positive activated hepatic stellate cells the ImageJ cell counter was used to manually select (and automatically count) positive cells so that αSMA positive vascular smooth muscle cells could be excluded from the count. Results were expressed as DAB positive (αSMA positive) cells per high power field (HPF).

A cumulative mean calculation was performed on two samples, one with many DAB positive (αSMA positive) cells and one with few positive cell. Taking into account results from both samples, the cumulative mean plateaued at 10 consecutive x40 objective fields.

### *2.7.5. MCM4 immunohistochemical staining image analysis*

Mini-chromosome maintenance (MCM) proteins are essential for cellular replication. MCM4 forms part of the MCM complex that has DNA helicase activity. Immunohistochemistry for MCM4 in liver FFPE sections is used to identify cells that are in a pre-replication state. Increased MCM4 staining can be used as a surrogate marker for increased cellular proliferation. Other cellular markers of proliferation include Ki-67 (present throughout cellular replication) and PCNA (proliferating cell nuclear antigen, present during the synthesis stage of cellular replication). Automated immunohistochemcal staining produces a more consistent staining pattern and both Ki-67 and MCM4 markers of cell proliferation have been optimised for automated immunohistochemical staining in the research group. Ki-67 staining can be affected by formalin fixation (Hitchman et al. 2011) and therefore MCM4 was selected as the preferred proliferation marker for this work.

To quantify MCM4 nuclear staining in the paracetamol acute liver injury model sections of FFPE liver stained with MCM4 were photographed using the Nuance multispectral imaging system with a x40 light microscope objective (x400 magnification).

RGB images were acquired and saved as JPEG files. Images were analysed using ImageJ (1.46r (Rasband 2014)). The ImageJ Find Maxima tool was used to automatically count peaks in DAB staining. Results were expressed as DAB positive (MCM4 positive) cells per high power field (HPF).

A cumulative mean calculation was performed on two samples, one with many DAB positive (MCM4 positive) cells and one with few positive cells. Taking into account results from both samples, the cumulative mean plateaued at 10 random x40 objective fields.

**Image 1**

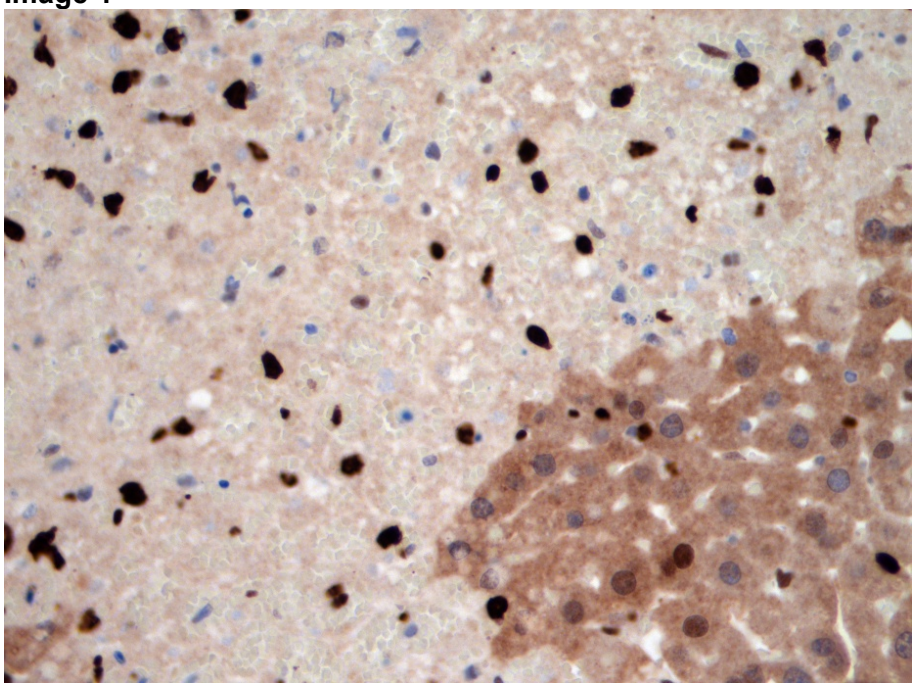

**Image 2**

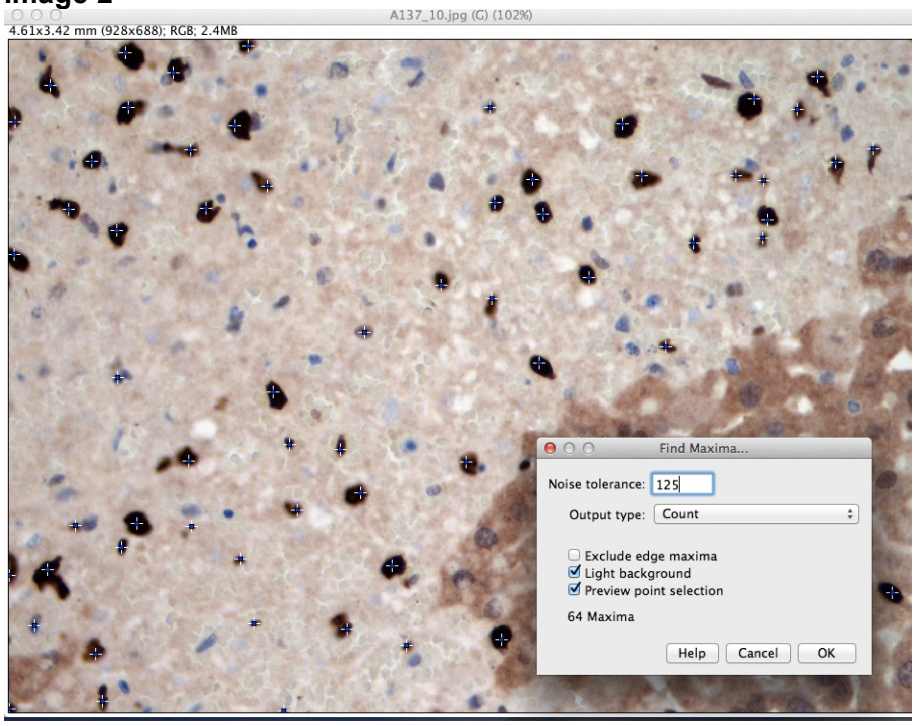


**Figure 2-4: ImageJ quantification of MCM4 nuclear staining**

All images original x400 magnification.

**Image 1:** MCM4 DAB stained section of liver in control mouse, 24 hours after administration of paracetamol.

**Image 2:** ImageJ Find Maxima selection of darkly stained nuclei (blue/white mark on image) and automated count ("64 maxima" in "Find Maxima" box).

### *2.7.6. F4/80 immunohistochemical staining image analysis*

A single marker for macrophages in injured and uninjured FFPE liver was required for the screening of models in this work. CD68, CD163 and F4/80 are cell surface markers commonly used in the detection of macrophages by immunohistochemistry. All are expressed on most tissue macrophages in the mouse (Murray & Wynn 2011; Rehg et al. 2012). CD68 or macrosialin in mice is a glycoprotein that binds low density lipoprotein. Some studies have shown that it is expressed on non-myeloid cells including lymphocytes and fibroblasts (Gottfried et al. 2008). CD163 is scavenger receptor expressed on monocytes and resident macrophages of normal tissues, high levels of expression are seen in liver Kupffer cells (Schaer et al. 2001). F4/80 is a cell surface marker encoded by *Emr1*. It is widely used in the identification of monocytes and macrophages in mice and variation in expression has been used to define monocyte / macrophage subsets in flow cytometry (Holt et al. 2008; Zigmond et al. 2014; Yona et al. 2013; Ramachandran et al. 2012; Murray & Wynn 2011). Therefore F4/80 was selected as the FFPE marker of choice in this work because of its specificity and overlap with work carried out by flow cytometry.

To quantify F4/80 staining, sections of FFPE liver stained with F4/80 were photographed using the Nuance multispectral imaging system with a x40 light microscope objective (x400 magnification).

Images cubes were acquired. Spectra for haematoxylin and DAB were defined using sections individually stained with haematoxylin or DAB. This

spectral library was used to unmix the image cube. False colouring of the two elements and the formation of a composite image allowed for better definition and identification of DAB positive (F4/80 positive) cells.

The unmixed composites were saved as a JPEG files and analysed using ImageJ (Rasband 2014). The ImageJ cell counter was used to manually select and automatically count positive cells. Results were expressed as DAB positive (F4/80 positive) cells per high power field (HPF).

A cumulative mean calculation was performed on two samples, one with many DAB positive (F4/80 positive) cells and one with few positive cell. Taking into account results from both samples, the cumulative mean plateaued at 10 random x40 objective fields.

### *2.7.7. Fibrin immunohistochemical staining image analysis*

To quantify fibrin deposition sections of FFPE liver stained with a fibrin antibody were photographed using the Nuance multispectral imaging system with a x4 light microscope objective (x40 magnification).

RGB images were acquired and saved as JPEG files. Images were analysed using ImageJ (1.46r (Rasband 2014)). The ImageJ Threshold tool was used, with color space Lab. Adjustment of the L threshold was used to determine the liver tissue area in each image and the b threshold was used to determine the DAB stained fibrin area in each image.

Field diameter and image quality were used to calculate a scale of 201.3 pixels : 1mm and therefore each image a field area of 15.76mm$^2$. The area of fibrin staining was determined as a percentage of tissue present in each section.

Taking into account the similarities between this method for analysing fibrin staining and the analysis of Sirius red staining, two entire sections of liver were used to calculate the percentage fibrin staining.

## 2.8. Flow Cytometry

Flow cytometry was performed on isolated live liver cells using a BD LSRFortessa™ cell analyser. Panels of primary conjugated fluorophore labelled antibodies was used to phenotype cell populations.

### *2.8.1. Staining protocol*

After the immune cells had been isolated as described previously (Section 2.4.1.2) the cells were incubated with 1% normal mouse serum for 20 minutes at 4°C to block non-specific protein binding by antibodies.

After blocking the cells were washed twice and resuspended at a concentration of 100,000 cells per 100µL PBS. Alliquots of 200,000 cells were separated from each sample for the panels described below (Section 2.8.2) and any remaining cells were pooled for control staining.

Cells were incubated with antibody panels as described below for 30 minutes at 4°C. Where Fixed Viability Dye was used cells were pre-stained with this (at a concentration of 1µL of Dye per 1mL of cell solution) and washed prior to incubation with antibodies.

Beads were used for compensation controls (ArC Amine Reactive beads for Fixed Viabilty Dye and OneComp beads for all antibodies) and incubated as per manufacturer instructions.

Fluorescence minus one (FMO) controls were used for antibodies/fluorochromes where data spread from other flurochromes in a panel affected gating boundaries.

After incubation with antibody panels, cells were washed and resuspended in FACs staining buffer (BD) before analysing on the flow cytometer.

### *2.8.2. Flow cytometry phenotyping panels*

Over the course of this work the flow cytometry phenotyping panel was developed. Below are the panels used as defined by the experimental model being assessed.

#### *2.8.2.1. Chronic liver injury immune cell phenotyping panel v.1*

| Laser | Filter | Fluorochrome | Antibody | Titrated vol (µL) | Supplier information |
|---|---|---|---|---|---|
| **Violet (405nM)** | 405-450/50 | eFluor 450 | CD45.2 | 1 | eBioscience 48-0454 |
| | 405-525/50 | eFluor 506 | Fixed Viability Dye | 1µL/mL | eBioscience 65-0866 |
| | 405-610/20 | Brilliant Violet 605 | Ly6G | 5 | BD 563005 |
| **Blue (488nM)** | 488-530/30 | AlexaFluor 488 | F4/80 | 1 | Serotec MCA497A488T |
| | 488-780/60 | PE-Cy7 | Ly6C | 1 | eBioscience 25-5932 |
| **Red (640nM)** | 640-670/14 | APC | CD11B | 1 | eBioscience 17-0112 |
| | 640-780/60 | APC-eFluor 780 | CD3 | 1 | eBioscience 47-0032 |

**Table 2-3:Flow cytometry chronic liver injury immune cell phenotyping panel v.1, macrophage and T-cells**

Titrated vol = titrated volume per sample

| Laser | Filter | fluorochrome | Antibody | titrated vol (µL) | Supplier information |
|---|---|---|---|---|---|
| **Violet (405nM)** | 405-450/50 | eFluor 450 | CD45.2 | 1 | eBioscience 48-0454 |
| | 405-525/50 | eFluor 506 | Fixed Viability Dye | 1µL/mL | eBioscience 65-0866 |
| **Red (640nM)** | 640-780/60 | APC-eFluor 780 | NK1.1 | 1 | eBioscience 47-5941 |

**Table 2-4: Flow cytometry chronic liver injury immune cell phenotyping panel v.1, NK-cell panel**

| Laser | Filter | fluorochrome | Antibody | titrated vol (µL) | Supplier information |
|---|---|---|---|---|---|
| **Violet (405nM)** | 405-450/50 | eFluor 450 | CD45.2 | 1 | eBioscience 48-0454 |
| | 405-525/50 | eFluor 506 | Fixed Viability Dye | 1µL/mL | eBioscience 65-0866 |
| **Red (640nM)** | 640-780/60 | APC-eFluor 780 | B220/CD45R | 1 | eBioscience 47-0452 |

**Table 2-5: Flow cytometry chronic liver injury immune cell phenotyping panel v.1, B-cell panel**

### *2.8.2.2. Chronic liver injury immune cell phenotyping panel v.2*

| Laser | Filter | fluorochrome | Antibody | titrated vol (µL) | Supplier information |
|---|---|---|---|---|---|
| **Violet (405nM)** | 405-450/50 | eFluor 450 | CD45.2 | 1 | eBioscience 48-0454 |
| | 405-525/50 | eFluor 506 | Fixed Viability Dye | 1µL/mL | eBioscience 65-0866 |
| | 405-610/20 | Brilliant Violet 605 | Ly6G | 5 | BD 563005 |
| **Blue (488nM)** | 488-530/30 | AlexaFluor 488 | F4/80 | 1 | Serotec MCA497A488T |
| | 488-695/40 | PerCP-Cyanine5.5 | NK1.1 | | eBioscience 45-5941 |
| | 488-780/60 | PE-Cy7 | Ly6C | 1 | eBioscience 25-5932 |
| **Red (640nM)** | 640-670/14 | APC | CD11B | 1 | eBioscience 17-0112 |
| | 640-730/45 | AF700 | B220/CD45R | | eBioscience 56-0452 |
| | 640-780/60 | APC-eFluor 780 | CD3 | 1 | eBioscience 47-0032 |

**Table 2-6: Flow cytometry chronic liver injury immune cell phenotyping panel v.2, combined immune cell phenotyping panel**

### *2.8.2.3. Acute liver injury immune cell phenotyping panels*

Cell death was determined in a separate proportion of the isolated cells from each sample using Fixed Viability Dye labelled with eFluor 506 (eBioscience 65-0866).

| Laser | Filter | fluorochrome | Antibody | titrated vol (µL) | Supplier information |
|---|---|---|---|---|---|
| **Violet (405nM)** | 405-450/50 | eFluor 450 | CD45.2 | 1 | eBioscience 48-0454 |
| | 405-610/20 | Brilliant Violet 605 | Ly6G | 5 | BD 563005 |
| **Blue (488nM)** | 488-530/30 | AlexaFluor 488 | F4/80 | 1 | Serotec MCA497A488T |
| | 488-575/26 | PE | CD64 | 5 | BD 558455 |
| | 488-610/20 | PE-CF594 | CD11B | 1 | BD 562317 |
| | 488-780/60 | PE-Cy7 | Ly6C | 1 | eBioscience 25-5932 |
| **Red (640nM)** | 640-670/14 | APC | MerTK | 10 | R&D FAB5912A |

**Table 2-7: Flow cytometry acute liver injury immune cell phenotyping panel, macrophage panel**

Titrated vol = titrated volume per sample

| Laser | Filter | fluorochrome | Antibody | titrated vol (µL) | Supplier information |
|---|---|---|---|---|---|
| **Violet (405nM)** | 405-450/50 | eFluor 450 | CD45.2 | 1 | eBioscience 48-0454 |
| | 405-610/20 | Brilliant Violet 605 | Ly6G | 5 | BD 563005 |
| | 488-610/20 | PE-CF594 | CD11B | 1 | BD 562317 |
| **Blue (488nM)** | 488-695/40 | PerCP-Cyanine5.5 | NK1.1 | | eBioscience 45-5941 |
| **Red (640nM)** | 640-670/14 | APC | CD11B | 1 | eBioscience 17-0112 |
| | 640-730/45 | AF700 | B220/CD45R | | eBioscience 56-0452 |
| | 640-780/60 | APC-eFluor 780 | CD3 | 1 | eBioscience 47-0032 |

**Table 2-8: Flow cytometry acute liver injury immune cell phenotyping panel, non-macrophage immune cell panel**

### *2.8.3. Rationale for flow cytometry immune cell phenotyping panels*

#### *2.8.3.1. Background*

The innate immune system is composed of a number of different cells that provide a generic response to infection and inflammation that includes the recruitment of immune cells, activation of complement, phagocytosis and antigen presentation to cells of the adaptive immune system.

Monocytes and macrophages are one of the major constituents of the innate immune response. They are highly plastic cells that carry out a variety of functions depending on the stimulus and their surroundings. Due to their plasticity, defining different macrophage / monocyte populations based on their surface protein expression or even their gene expression is a highly contentious area of research.

Prior dogma categorised macrophages as classically activated pro-inflammatory ‘M1’or alternatively activated imunoregulatory ‘M2’ macrophages with the M2 category being sub-divided further into more specific groups such as tumour-associated macrophages. In the mouse the M1 macrophage expresses CD11b, F4/80, CD62L, CCR2, high levels of Gr-1 (an antibody to Ly6C/G) and low levels of CX3CR1. The M2 macrophage expresses CD11b, F4/80, low levels of Gr-1 and high levels of CX3CR1 but not CD62L and CCR2. However much of this classification system is based on *in-vitro* studies and it is now more widely accepted that *in-vivo* monocytes and macrophages exist in a spectrum of activation phenotypes and are able to class-switch from one phenotype to another (Murray & Wynn 2011)(Tacke & Randolph 2006).

In acute and chronic liver injury monocytes and macrophages have been shown to play a key role in initiation, propagation and resolution. In the liver these cells are categorised based on their origin (resident Kupffer cells with primitive derivation versus infiltrating monocytes and monocyte derived macrophages of bone marrow derivation) and / or their function associated cell surface markers and gene expression (Ramachandran et al. 2012)(Holt et al. 2008; Yona et al. 2013; Zigmond et al. 2014; Murray & Wynn 2011). However, these classification systems and their translation are still the basis of much research and debate.

#### *2.8.3.2. Markers used and rationale for their selection*

CD45 is a cell surface marker encoded by *ptprc*. It is also known as leukocyte common antigen (LCA) and is a protein tyrosine phosphatase receptor. CD45 is widely used to identify haematopoietic cells. Mice show strain dependant variations in nucleotide sequences resulting in amino acid changes in the extracellular domain. C57BL6/J used in this work are known to express the b variant of this gene/protein (Smith et al. 2014), also known as CD45.2. This marker (clone 104) was selected to identify immune cells from whole liver non-parenchymal cell isolates.

NK1.1 is a cell surface marker encoded by *Klrb1c*. It is killer cell lectin-like receptor subfamily B member 1c and is expressed on natural killer (NK) cells in some strains of mouse, including C57BL6/J used in this work (Smith et al.

2014). This marker (clone PK136) was selected to identify NK1.1+ NK cells in CD45.2+ liver immune cells (Table 2-9).

CD3 is a cell surface protein complex composed of ɣ, δ and ε chains. The CD3 complex is required for expression and function of the TCR complex. CD3 is expressed on thymocytes and all mature T-cells. This marker (clone 17A2) was selected to identify CD3+ T-cells in the CD45.2+ liver immune cells (Table 2-9).

CD45R/B220 is a cell surface marker encoded by *ptprc*. The specific antibody, CD45R/B220 (clone RA3-6B2) recognises an isoform of the protein that is expressed on B-cells (immature and mature) and some activated T-cells. This marker was selected to identify B-cells in the CD45.2+ liver immune cells (Table 2-9).

CD11b is a cell surface marker encoded by *Itgam*. It is a protein subunit of an integrin commonly known as Mac-1 that is involved in the complement system. It is expressed on all myeloid lineage cells. This marker (clone M1/70) was selected to identify myeloid cells in the CD45.2+ selected population. In addition, variations in expression of CD11b have been used in the identification of monocyte / macrophage subsets (Holt et al. 2008; Zigmond et al. 2014; Yona et al. 2013; Ramachandran et al. 2012; Murray & Wynn 2011).

Ly6G is a cell surface marker encoded by *Ly6g*. It is a lymphocyte antigen 6G or granulocyte differentiation antigen 1 and is expressed on granulocyte and

neutrophil populations. This marker (clone 1A8) was selected to identify CD11b+ neutrophils from other CD11b+ myeloid cells.

F4/80 is a cell surface marker encoded by *Emr1*. It is widely used in the identification of monocytes and macrophages in mice and variation in expression has been used to define monocyte / macrophage subsets. This marker (clone A3-1) was selected to identify monocytes and macrophages in CD11b+ myeloid cells. In the literature high expression of CD11b with low expression of F4/80 (CD11b hi F4/80 lo) has been used to define infiltrating monocyte derived macrophages and intermediate / low expression of CD11b with high expression of F4/80 (CD11b int F4/80 hi) has been used to define tissue resident macrophages or Kupffer cells (Holt et al. 2008; Zigmond et al. 2014; Yona et al. 2013; Ramachandran et al. 2012; Murray & Wynn 2011).

However in this work I was unable to identify a live CD11b int F4/80 hi population in an isolation process that did not use collagenase. Therefore, within the limits of this work, I used F4/80 expression to define macrophages and infiltrating monocyte-derived macrophages isolated from the liver as a single population. I have called this population “macrophages” as they were isolated from perfused tissue. This population is however, likely to be composed of resting tissue resident macrophages, activated tissue resident macrophages and infiltrating monocyte derived macrophages. In later work I used the expression of CD64 and MerTK to define a mature, tissue macrophage subset that was most likely to represent Kupffer cells.

CD64 is a cell surface marker encoded by *Fcgr1*. It is also known as FcγR1 and is an immunoglobulin receptor. Protein and gene expression studies has shown that CD64 expression is greatest in tissue macrophages (with some expression in dendritic cells) (Ikarashi et al. 2013; Gautier et al. 2012). This marker (clone X54-5/7.1) was selected to identify mature tissue macrophages in conjunction with MerTK.

MerTK is a cell surface marker encoded by *Mertk*. It is tyrosine kinase involved in efferocytosis. Protein and gene expression in F4/80+ cells has been associated with mature, possibly tissue resident macrophages and dendritic cells (Ikarashi et al. 2013; Gautier et al. 2012). This marker (clone 108928) was selected to identify mature tissue macrophages in conjunction with CD64.

Ly6C is a cell surface marker encoded by *Ly6c1*. It is lymphocyte antigen 6C and is enriched on monocytic myeloid cells. High expression of Ly6C on monocytes is associated with expression of CCR2. CCR2 is the receptor for CCL2 which is a chemokine associated with myelopoiesis and migration of monocytes from the bone marrow to the site of inflammation. This marker (clone HK1.4) was selected to phenotype “macrophages” isolated from perfused liver.

In acute liver injury liver macrophages with high expression of Ly6C ($Ly6C^{hi}$) have a pro-inflammatory phenotype and gene expression profile previously associated with the classically activated M1 phenotype. In chronic liver injury

Ly6C$^{hi}$ cells have been associated with a pro-fibrotic phenotype. Ly6C$^{hi}$ cells predominate during early acute liver injury and fibrogenesis and are therefore considered to be effector cells in the pro-inflammatory and pro-fibrotic phases of injury response (Murray & Wynn 2011; Zigmond et al. 2014; Ramachandran et al. 2012; Karlmark et al. 2009). Ly6C$^{hi}$ cells have been shown to switch to low expression of Ly6C (Ly6C$^{lo}$) and at baseline Ly6C$^{hi}$ cells are only seen transiently as they enter the tissue before they switch to Ly6C$^{lo}$ expression (Zigmond et al. 2014; Ramachandran et al. 2012)(Yona et al. 2013).

Ly6C$^{lo}$ expression is associated with loss of CCR2 expression and high expression of CX3CR1. CX3CR1 is the fractalkine receptor involved in cell adhesion and migration and Ly6C$^{lo}$ macrophages have been defined as having a 'patrolling' function (Geissmann et al. 2010)(Yona et al. 2013). In acute and chronic liver injury Ly6C$^{lo}$ cells also have a pro-resolution phenotype and gene expression profile (Zigmond et al. 2014; Ramachandran et al. 2012) and are therefore considered to be effector cells in the resolution phase of injury response.

In the literature there is a confusing array of definition of Ly6C expression by flow cytometry. In earlier work, Tacke et al, using the less specific Gr-1 antibody, producing a histogram with well defined peaks of low Ly6C expression and high expression with a trough of intermediate expression between the two – however this work was based only on blood monocytes (Tacke & Randolph 2006). Tackes' later work focuses onto two subsets –

Ly6C$^{hi}$ and Ly6C$^{lo}$ but gating strategies are not covered (Tacke & Zimmermann 2015; Ju & Tacke 2016). Karlmark et al also segregate cells as Gr-1(Ly6C)$^{hi}$ or Gr-1(Ly6C)$^{lo}$. Their paper shows only an overlay of Ly6C expression in CD11b+ F4/80+ or F4/80- negative cells and does not demonstrate their Ly6C gating strategy (Karlmark et al. 2009). Zigmond et al also refer to Ly6C$^{hi}$ and Ly6C$^{lo}$ populations but their paper also does not demonstrate their Ly6C gating strategy (Zigmond et al. 2014). Ramachandran et al refer to Ly6C$^{hi}$ and Ly6C$^{lo}$ populations and select a subset of cells with very high expression of Ly6C as their Ly6C$^{hi}$ population and everything else is termed Ly6C$^{lo}$ (Ramachandran et al. 2012). Yona et al refer to Ly6C+ or Ly6C- cells. Their Ly6C+ cells are functionally defined in similar fashion to Ly6C$^{hi}$ cells described by Karlmark, Tacke and Zigmond. Likewise, their Ly6C- cells seem to represent the Ly6C$^{lo}$ populations of the other authors. Figures and supplementary data in the paper by Yona et al demonstrate a scatter plot gating strategy where quadrants and box gates are used to define Ly6C expression and they appear to select a subset of cells with high expression of Ly6C, like Ramachandran et al as their Ly6C+ cells with everything else defined as Ly6C- (Yona et al. 2013).

In this work I chose to define Ly6C expression using the gating strategy demonstrated in Figure 2-6. I used an FMO to define Ly6C negative cells. Ly6C positive cells were divided into two groups, Ly6C$^{hi}$ and Ly6C$^{int/lo}$ based on scatter plot grouping and histogram peaks.

| Cell Surface Marker Combination | Cell Type Called | Notes |
|---|---|---|
| **CD45+ NK1.1+** | NK cells | Co-expression of NK1.1 and CD3 was seen in some cells likely to represent NK/T cells.<br>Some NK1.1 cells were positive for CD11b, indicting their myeloid origin. However these cells were F4/80 negative. |
| **CD45+ CD3+** | T cells | Co-expression of NK1.1 and CD3 was seen in some cells likely to represent NK/T cells. |
| **CD45+ B220+** | B cells | |
| **CD45+ CD11b+ Ly6G+** | Neutrophils | |
| **CD45+ CD11b+ Ly6G- F4/80+** | Macrophages | This marker combination is likely to identify both macrophages and infiltrating monocytes isolated from the liver after perfusion. |
| **CD45+ CD11b+ Ly6G- F4/80+ Ly6C$^{hi}$** | Pro-inflammatory or Pro-fibrotic macrophage | As Macrophages. |
| **CD45+ CD11b+ Ly6G- F4/80+ Ly6C$^{int/lo}$** | Pro-resolution or patrolling macrophage | As Macrophages. |
| **CD45+ CD11b+ Ly6G- CD64+ MerTK+** | Mature tissue macrophages | |

**Table 2-9: Flow cytometry cell surface marker combinations used to identify immune cell subsets**

| | |
|---|---|
| 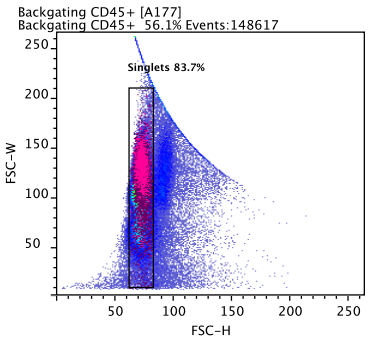 | **Selection of single cells based on width and height to cells**<br><br>FSC = forward scatter<br>W = width<br>H = height |
| 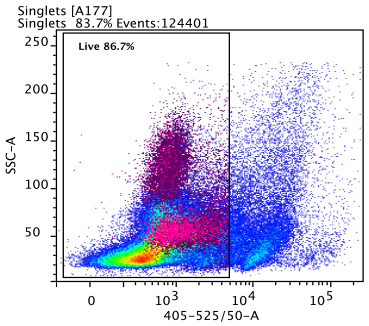 | **Selection of live cells based of live/dead marker staining**<br><br>SSC = side scatter<br>A = area<br>405-525/50-A = Channel used for detection of fixed viability dye with eFlour 506 fluorophore |
| 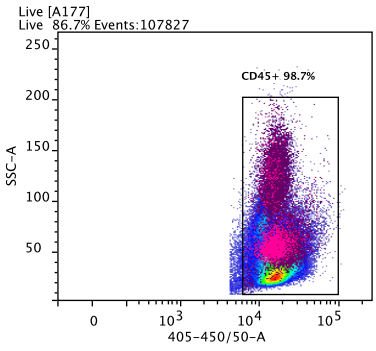 | **Selection of CD45+ cells**<br><br>405-450/50-A = Channel used for detection of CD45.2 antibody with eFluor 450 fluorophore |

**Figure 2-5: Flow cytometry gating strategy, selection of CD45+ live population**

Pink / purple cells are CD45+ CD11b+ F4/80+ macrophages

| | |
|---|---|
| 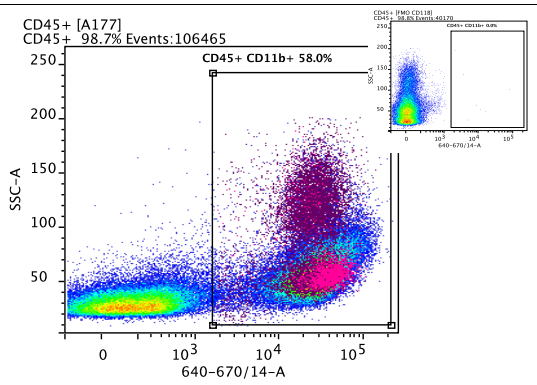 | **Selection of CD11b+ cells**<br><br>SSC = side scatter<br>A = area<br>640-670/14-A = Channel used for detection of CD11B with APC fluorophore<br><br>INSET: FMO used to determine gate boundaries |
| 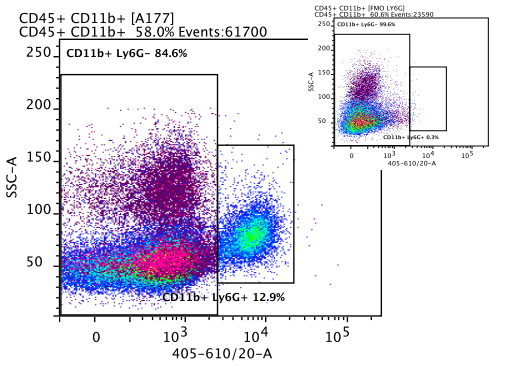 | **Selection of CD11b+ Ly6G- cells**<br><br>405-610/20-A = Channel used for detection of Ly6G with Brilliant Violet 605 fluorophore<br><br>INSET: FMO used to determine gate boundaries |
| 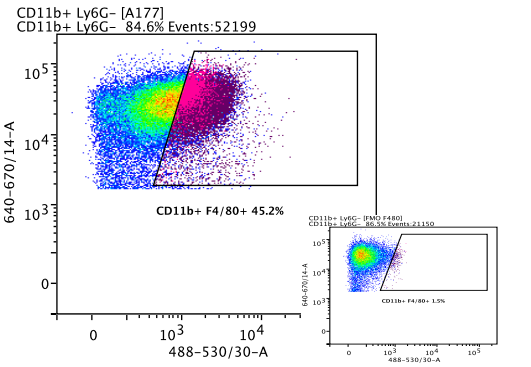 | **Selection of CD11b+ Ly6G- F4/80+ cells**<br><br>488-530/30-A = Channel used for detection of F4/80 with AlexaFluor 488 fluorophore<br><br>INSET: FMO used to determine gate boundaries |
| 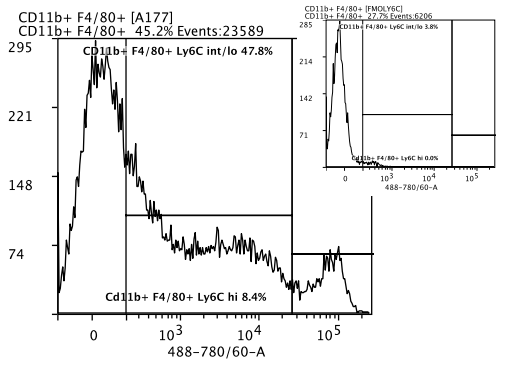 | **Histogram used to determineLy6C expression on CD11b+ Ly6G- F4/80+ cells**<br><br>488-780/30-A = Channel used for detection of Ly6C with PE-Cy7 fluorophore<br><br>INSET: FMO used to determine gate boundaries |

**Figure 2-6: Flow cytometry gating strategy, selection of macrophages after CD45 selection (Figure 2-5)**

Pink / purple cells are CD45+ CD11b+ F4/80+ macrophages.
FMO = fluorescence minus one.

| | |
|---|---|
| 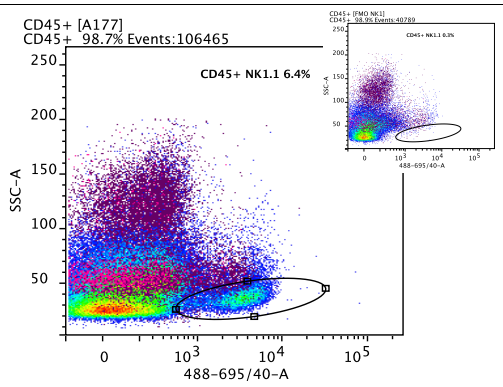 | **Selection of NK cells**<br><br>SSC = side scatter<br>A = area<br><br>488-695/40-A = Channel used for detection of NK with PerCP-Cy5.5 fluorophore<br><br>INSET: FMO used to determine gate boundaries |
| 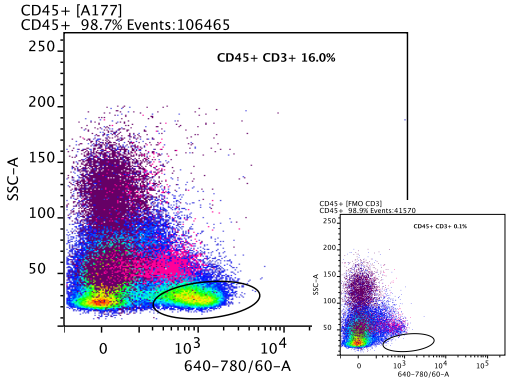 | **Selection of T cells**<br><br>640-780/60-A = Channel used for detection of CD3 with APC-eFluor 780 fluorophore<br><br>INSET: FMO used to determine gate boundaries |
| 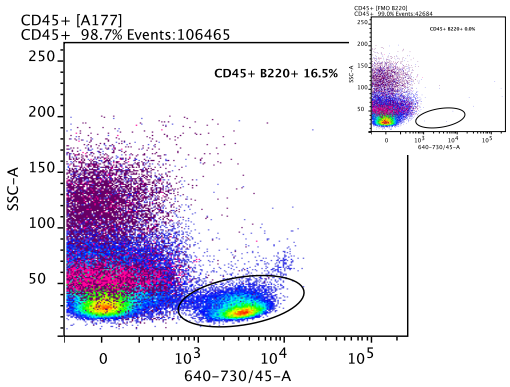 | **Selection of B cells**<br><br>640-730/45-A = Channel used for detection of B220 with AF700 fluorophore<br><br>INSET: FMO used to determine gate boundaries |

**Figure 2-7: Flow cytometry gating strategy, selection of non-macrophage immune cells after CD45 selection (Figure 2-5)**

Pink / purple cells are CD45+ CD11b+ F4/80+ macrophages.
FMO = fluorescence minus one.

## 2.9. Hydroxyproline colorimetric assay for liver collagen content

Hydroxyproline is an amino acid found in collagen and elastin. It is a direct measure of the amount of collagen or gelatin in the tissue examined. In the liver hydroxyproline has been found to correlate with quantification of Sirius red histochemical staining (James et al. 1990).

Snap frozen liver tissue was weighed and homogenised in 100µL of tissue for every 10mg of tissue in heat and acid resistant vials (Nunc cryovial) using a Fisherbrand™ disposable pestle system.

Samples were hydrolysed by adding equal volumes of concentrated hydrochloric acid (approximately 12N) to the homogenate and heating at 120°C for 3 hours.

After hydrolysis samples were allowed to cool and then spun at 10,000rpm for 3 minutes to pellet sediment. 10µL of the supernatant was placed in a 1.5mL microcentrifuge tube and placed in a vacuum concentrator at 60°C until the samples had evaporated to dryness.

Chloramine T concentrate and an oxidation buffer from the BioVision Hydroxyproline Colorimetric Assay Kit (K555-100) were combined and 100µL of this added to each dry sample for 5 minutes at room temperature. Each sample was transferred to a 96 well flat bottom microplate, suitable for use in a microplate reader.

DMAB concentrate and a perchloric acid/Isopropanol solution from the BioVision Hydroxyproline Colorimetric Assay Kit (K555-100) were combined and 100µL of this added to each sample and incubated at 60°C for 90 minutes. The plate was placed in a microplate reader and absorbance at 560nm recorded.

Sample absorbance was compared to a standard curve produced using serial dilutions (see Table 2-10) of a 1mg/mL hydroxyproline standard supplied with the BioVision Hydroxyproline Colorimetric Assay Kit (K555-100) that was pre-diluted to 0.1mg/mL with distilled water.

| Standard Concentration (µg/well) | Vol (µL) of 0.1mg/mL | Distilled Water (µL) |
|---|---|---|
| 0 | 0 | 50 |
| 0.025 | 0.25 | 49.75 |
| 0.05 | 0.5 | 49.5 |
| 0.1 | 1 | 49 |
| 0.2 | 2 | 48 |
| 0.4 | 4 | 46 |
| 0.6 | 6 | 44 |
| 0.8 | 8 | 42 |
| 1.0 | 10 | 40 |

**Table 2-10: Standard curve dilutions for Hydroxyproline colorimetric assay.**

The absorbance at 560nm was converted to µg/g using the straight line equation calculated from the standard curve (y=mx+b where m=gradient, x=sample absorbance and b=y intercept) in the equation:

$$\frac{[(x-b)/y] \times [\text{total volume of sample}/10]}{\text{weight of tissue used in g}}$$

Samples and standard curve were run in at least duplicate. A coefficient of variance (CV) was calculated for sample replicates and samples with a CV >10 were repeated or excluded.

## 2.10. Gene expression

Tissue RNA isolation, reverse transcription and PCR was used to quantify gene expression using a real time PCR system and semi-quantify gene expression in an end-point PCR product, gel electrophoresis band intensity analysis.

Sample preparation in gene expression analysis was carried out within a laminar flow hood in a designated room. Molecular grade, RNase free water (Life Technologies), RNase and DNase free filtered pipette tips, pipettors, 1.5mL microcentrifuge tubes and 0.2mL PCR tubes were UV irradiated prior to use. Where possible, reactions were carried out on ice or samples chilled to 4°C.

### *2.10.1. RNA isolation*

Approximately 5mg of snap frozen liver tissue harvested for RNA isolation was placed in 250µL of TRIzol® (Life Technologies) and homogenised using the Fisherbrand™ disposable pestle system in a 1.5mL microcentrifuge tube. Samples were allowed to rest at room temperature for at least 5 minutes.

50µL of chloroform was added to the TRIzol® and tissue homogenate and vigorously shaken for 15 seconds before incubating at room temperature for 3 minutes. Samples were then centrifuged at 13,000rpm for 15 minutes at 4°C.

The upper aqueous layer (containing isolated RNA) was aspirated and placed in a new microcentrifuge tube. 125µL of isopropanol (Sigma-Aldrich) was added to this, shaken gently and incubated at room temperature for 10 minutes. Samples were then centrifuged at 12,000rpm for 10 minutes at 4°C, forming a small white pellet.

The supernatant was aspirated and the pellet left to air dry for 10 minutes before resuspending in molecular grade, RNase free water (Life Technologies) and incubating at 55°C for 15 minutes.

### *2.10.2. DNase treatment*

RNA solutions were treated with Ambion® TURBO DNA-*free*™ kit (life Technologies). In a 0.2mL PCR tube, 1µL of 10X Turbo DNase buffer and 1µL of Turbo DNase was added to 10µL of RNA solution, gently mixed and incubated at 37°C for 30 minutes. The DNase reaction was halted by the addition of 1µL of DNase inactivation reagent.

The DNase treated RNA sample was then centrifuged at 10,000rpm for 90seconds and the supernatant transferred to a new 0.2mL PCR tube.

RNA concentration and purity was assessed by spectrophotometry. RNA purity was determined by 260nm/280nm absorption ratios, with a value of 1.8-2.0 indicating high purity RNA suitable for further experimentation.

RNA was diluted with molecular grade, RNase free water to produce a concentration of 1µg/µL.

### *2.10.3. Reverse transcription*

Reverse transcription of the DNase treated RNA to cDNA was carried out using the Ambion™ RETROscript® Reverse Transcription Kit (Life Technologies). 2µL of Oligo dT and 7µL molecular grade, RNase free water were combined with 3µL of DNase treated RNA in a 0.2mL PCR tube and incubated for 3 minutes at 80°C.

This mixture was combined with 2µL of 10X RT buffer, 4µL of dNTP mix, 1µL of RNase inhibitor and 1µL of MMLV-RT and incubated in a thermocycler at 44°C for 60 minutes, 92°C for 10 minutes before cooling to 4°C. This cDNA mixture was used immediately in gene expression analysis or stored at -20°C until needed.

### *2.10.4. Quantitative gene expression analysis*

Quantitative gene expression analysis was performed using TaqMan® assays and the StepOne® real time PCR system.

TaqMan® assays contain fluorogenic probes that produce a fluorescent signal only when the target DNA is amplified.

A mastermix of 2X TaqMan® Gene expression Master Mix (Life Technologies), molecular grade, RNase free water (Life Technologies) and 2X

TaqMan® Gene Expression Assay were made and added to 1µL of cDNA in a MicroAmp® 96 well plate (Life Technologies). Plates were sealed with MicroAmp® optical adhesive film (Life Technologies).

A comparative $C_T$ ($\Delta\Delta$ $C_T$) method of relative quantification was used for all assays and therefore plate set up was designed to include duplicates of two house-keeping genes and at least duplicates of genes of interest for each sample.

Plates were placed in the StepOne real time PCR system (Applied biosystems, Life Technologies) and the StepOne software v2.2 (Applied biosystems, Life Technologies) programmed for comparative CT TaqMan assay quantification with cycle parameters as follows: UDG activation for 2 minutes at 50°C. Polymerase activation for 10 minute at 95°C. Cycles of denaturation (15 seconds at 95°C) and annealing/extension (1 minute at 60°C) repeated as optimised for the individual TaqMan® Gene Expression Assay (see Table 2-11).

| Gene (Protein) | TaqMan® assay | Labelled with | Cycles |
|---|---|---|---|
| **GAPDH** | Mm99999915_g1 | FAM-MGB | As per gene of interest |
| **ActB (β actin)** | Mm00607939_s1 | VIC-MGB | As per gene of interest |
| **αSMA** | Mm00725412_s1 | FAM-MGB | 40 |
| **Col1a1** | Mm00801666_g1 | FAM-MGB | 40 |
| **F2r (PAR1)** | Mm00438851_m1 | FAM-MGB | 40 |
| **F2rII (PAR2)** | Mm00433160_m1 | FAM-MGB | 40 |
| **MMP-2** | Mm00439498_m1 | FAM-MGB | 40 |
| **MMP-9** | Mm00442991_m1 | FAM-MGB | 40 |
| **TIMP-1** | Mm00441818_m1 | FAM-MGB | 50 |

**Table 2-11: TaqMan® Gene Expression Assay and PCR cycle number**

#### *2.10.4.1. Comparative $C_T$ method of quantification*

The comparative $C_T$ method of quantitative PCR analysis compares the $C_T$ value of a gene of interest for a given sample standardised to the $C_T$ value of a house-keeping (ubiquitously expressed, unaffected by experimental intervention) gene in the same sample. The $C_T$ value is Cycle Threshold, the number of cycles required for the fluoresecent signal in the well to cross the (background) threshold. The $C_T$ value is inversely proportional to the amount of target cDNA in the sample. This method assumes that the reaction efficiency is close to 100% in the house-keeping gene as well as the gene of interest.

An alternative method for quantifying gene expression is the standard curve method where $C_T$ values of samples are compared to a standard curve created from known quantities of target gene cDNA. However the comparative $C_T$ method is useful where multiple genes of interest are to be examined in each sample as plate design allows for housekeeping genes to be used for

more than one gene of interest where a standard curve method requires a standard curve for each gene of interest on each plate.

In the comparative $C_T$ method the difference between the house-keeping gene $C_T$ value is subtracted from the gene of interest $C_T$ value to give the $\Delta C_T$ for each sample.

$$\Delta C_T = \text{gene of interest } C_T - \text{house-keeping } C_T$$

Once the $\Delta C_T$ for each sample has been calculated then the experimental and control groups can be compared to calculate the $\Delta\Delta C_T$.

$$\Delta\Delta C_T = \text{experimental } \Delta C_T - \text{control } \Delta C_T$$

The $\Delta\Delta C_T$ can then be expressed in terms of fold change from the control gene expression level by calculating the $2^{(-\Delta\Delta C_T)}$ value.

Graphical presentation and statistical analysis of this data, given that the $\Delta C_T$ data represents a reading from a reaction with exponential (base 2) amplification is complex and debated within the literature. Schmittgen and Livak produced a simple and well illustrated paper published in Nature Protocols in 2008 and I chose this method of analysis (Schmittgen & Livak 2008). Briefly, an individual $2^{-\Delta C_T}$ point for each animal or animal group was graphically presented on a Log 2 graph to demonstrate the level of gene expression. These figures were then used in statistical analysis. In addition, fold change was also noted in the text for direct comparisons between certain groups.

## 2.11. Statistics

Statistical analysis was performed using Microsoft Office for Mac 2011 Excel version 14.6.2 (last update) and Prism 6 for Mac OS X version 6.0 (last update).

As the bulk of this work is based on small groups it was not assumed that data followed a Gaussian distribution and therefore nonparametric tests were selected.

## 3. αSMA targeted expression of TFPI in acute liver injury

The genome of the transgenic mouse strain αSMA-TFPI contains a construct that initiates the expression of human TFPI when a cell expresses αSMA. The biological effect is therefore cell specific expression of TFPI beyond normal physiological expression.

### 3.1. Baseline parameters

The baseline (uninjured) liver phenotype of the αSMA-TFPI mice was defined to help analyse data from experimental studies.

#### *3.1.1. Plasma liver function tests*

Plasma markers of liver function are widely used as minimally invasive markers of liver injury and function. There were n=13 in the control group and n=14 in the αSMA-TFPI group (except for albumin values, where n=8 in the αSMA-TFPI group due to failed assays in one batch).

Alanine aminotransferase (ALT) is released from injured hepatocytes. Average ALT levels in C57BL6/J mice aged 6-16 weeks are 42-80IU/L (Grubb et al. 2014). Median ALT values for αSMA-TFPI and control mice in this work were both below this range.

There was no statistically significant difference in plasma ALT of αSMA-TFPI mice compared to control mice (Mann-Whitney U test, p=0.18. Figure 3-1. Graph A).

Alkaline phosphatase (ALP) is an enzyme produced by cholangiocytes and can be elevated when there is damage to these cells. Of note ALP is also produced by bone and can be elevated due to bone disease. Average ALP levels in C57BL6/J mice are 68-140IU/L (Grubb et al. 2014). Median ALP values for αSMA-TFPI and control mice in this work fell just below this range and there was no statistically significant difference in plasma ALP of αSMA-TFPI mice compared to control mice (Mann Whitney test, p=0.30. Figure 3-1. Graph B).

Total bilirubin measures unconjugated and conjugate bilirubin, the breakdown product of haemoglobin. The liver is responsible for conjugation and excretion of bilirubin. Elevated levels of total bilirubin suggest liver injury and decreased bilirubin metabolism, bile duct injury obstructing bilirubin excretion or increased breakdown of haemoglobin. Average total bilirubin levels in C57BL6/J mice aged 8-11 weeks are 0.48-1.35 μmol/L (Grubb et al. 2014). Median total bilirubin values for αSMA-TFPI and control mice in this work were above the normal range presented in the literature. However, there was no statistically significant difference in plasma total bilirubin of αSMA-TFPI mice compared to control mice (Mann Whitney test, p=0.28. Figure 3-1. Graph C).

Decreased levels of albumin can indicate chronic impairment of the livers synthetic function. Average albumin levels in C57BL6/J mice aged 8-11 weeks are 31-39g/L (Grubb et al. 2014). Median albumin values for αSMA-TFPI and control mice in this work were below the normal range presented in

the literature and there was no statistically significant difference in plasma albumin of αSMA-TFPI mice compared to control mice (Mann Whitney test, p=0.87. Figure 3-1. Graph D).

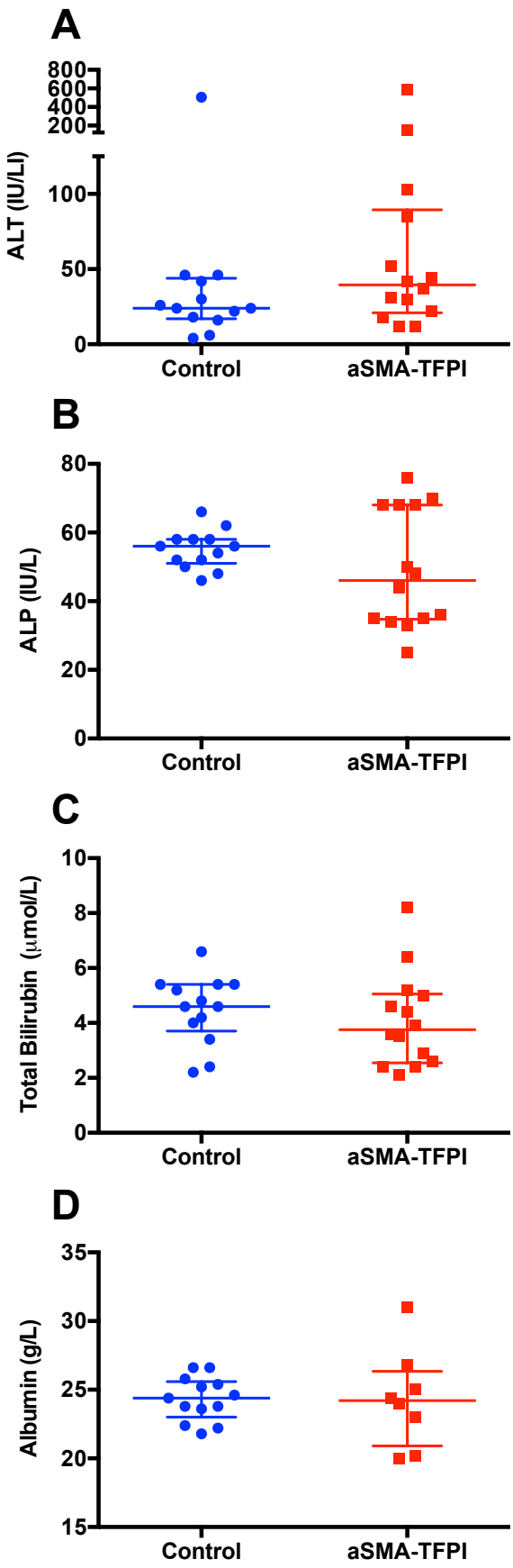


**Figure 3-1: Baseline plasma liver function test results**

Bars indicate median with interquartile range.

**Graph A**: Plasma ALT (IU/L). Median 24IU/L and 40IU/L in control and αSMA-TFPI strains respectively.

**Graph B:** Plasma ALP (IU/L). Median 56IU/L and 46IU/L in control and αSMA-TFPI strains respectively.

**Graph C:** Plasma total bilirubin (µmol/L). Median 4.6µmol/L and 3.8µmol/L in control and αSMA-TFPI strains respectively.

**Graph D:** Plasma albumin (g/L). Median 24.4g/L and 24.2g/L in control and αSMA-TFPI strains respectively.

### *3.1.2. Hepatic stellate cell activation*

Activated hepatic stellate cells are the predominant collagen producing cell in the liver during homeostasis and fibrosis. In the acute phase of liver injury there is initiation of hepatic stellate cells activation through paracrine stimulation from liver sinusoidal endothelial cells, liver macrophages, injured hepatocytes and platelets. The predominant mediators involved in this process are TGF- β, TRAIL and reactive oxygen species. Initiation of hepatic stellate cell activation is followed by perpetuation, where there is proliferation and migration of activated hepatic stellate cells accompanied by fibrogenesis (reviewed in (Scott L Friedman 2008)). Activated hepatic stellate cells express αSMA. Immunohistochemistry for αSMA in FFPE liver tissue sections is used as a surrogate for hepatic stellate cell activation.

Digital image analysis of FFPE liver sections stained using an antibody for αSMA showed no statistically significant difference in the number of activated hepatic stellate cells in the liver of αSMA-TFPI mice compared to C57BL6/J control mice (Mann Whitney test, p=0.10. **Figure 3-2**. Graph A). There were n=10 in the control group and n=11 in the αSMA-TFPI group.

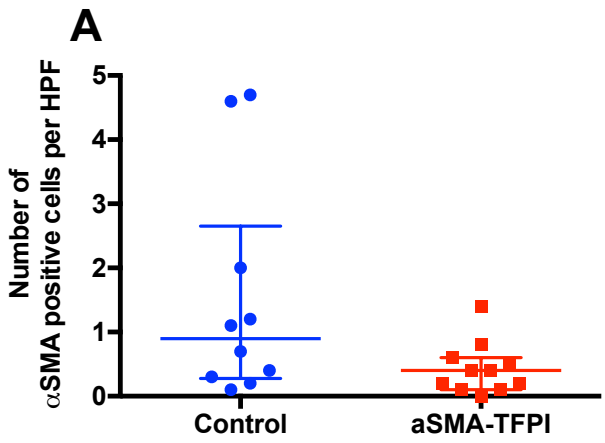


**Image 1**

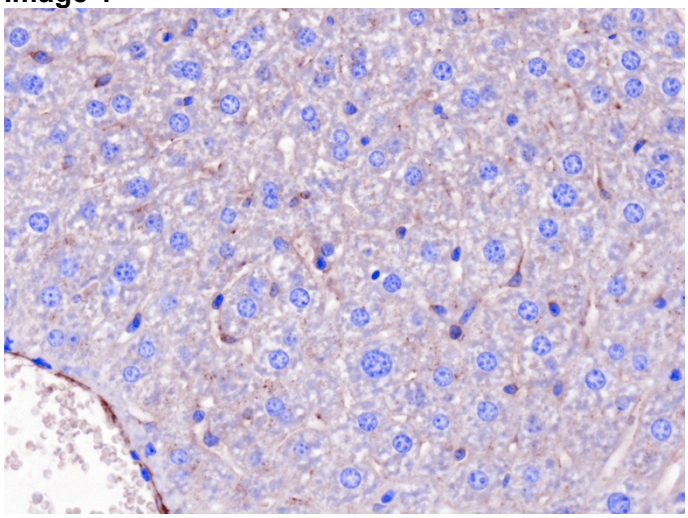

**Image 2**

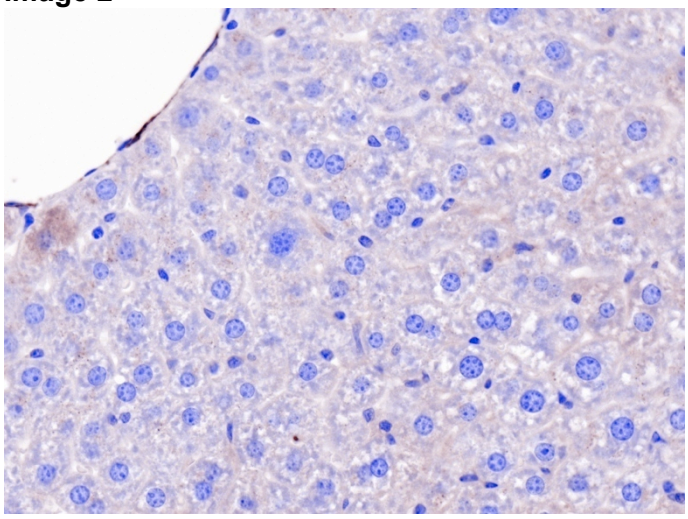

**Figure 3-2: Baseline αSMA immunohistochemistry**

Bars indicate median with interquartile range.

HPF = High power field, x400 magnification.

**Graph A**: Number of activated hepatic stellate cells in liver FFPE tissue sections as determined by αSMA immunohistochemistry. Median 0.9 cells per HPF and 0.4 cells per HPF in control and αSMA-TFPI strains respectively.

**Image 1:** Liver FFPE sections stained with αSMA from control mice. Original x400 magnification.

**Image 2:** Liver FFPE sections stained with αSMA from αSMA-TFPI mice. Original x400 magnification.

### *3.1.3. Liver immune cell composition*

The immune cell composition of the liver has been shown to affect the rate and progression of liver injury.

Macrophages are a key effector cell in acute and chronic liver injury. Immunohistochemistry for F4/80 in liver FFPE sections is used to identify macrophages.

Digital image analysis of liver FFPE sections stained using an antibody for F4/80 showed no statistically significant difference in the number of F4/80 positive cells in the livers of αSMA-TFPI mice compared to C57BL6/J control mice (Mann Whitney test, p=0.15. **Figure 3-3**. Graph A). There were n=5 in both the control and the αSMA-TFPI group. This was less than the power calculation sample number due to a failed assay in one batch and because flow cytometry was also used to determine the liver immune cell composition.

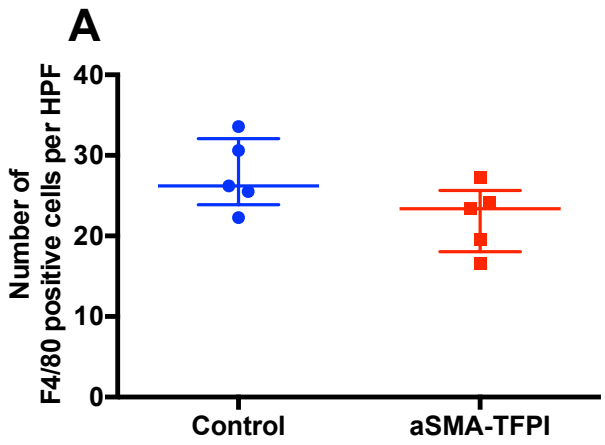


**Image 1**

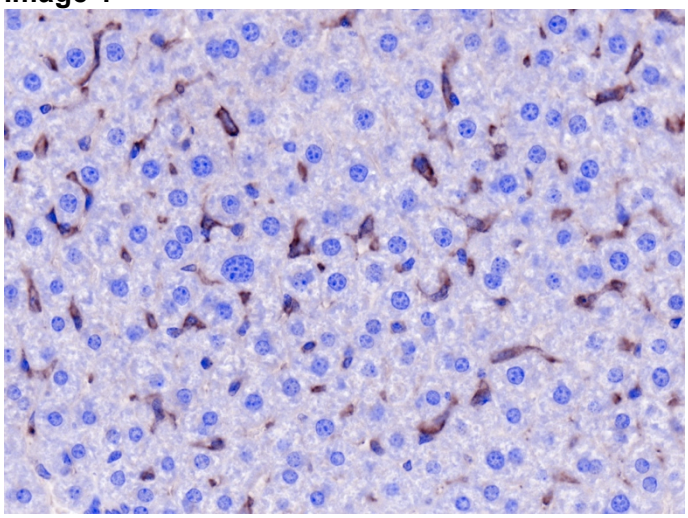

**Image 2**

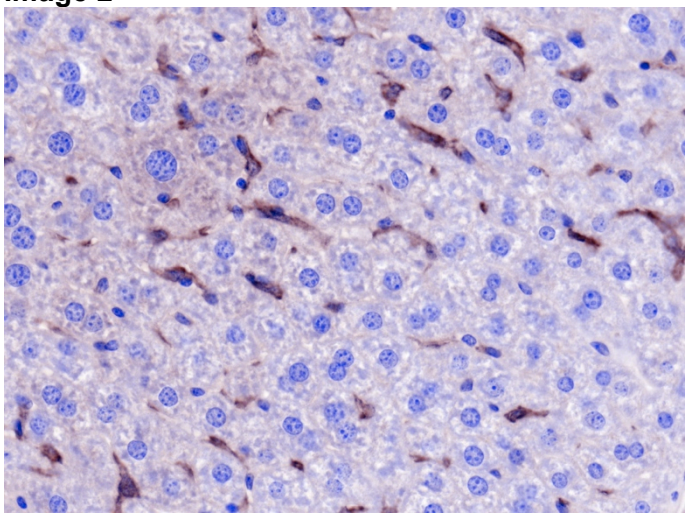

**Figure 3-3: Baseline F4/80 immunohistochemistry**

Bars indicate median with interquartile range.

HPF = High power field, x400 magnification.

**Graph A:** Number of macrophages in liver FFPE tissue sections as determined by F4/80 immunohistochemistry. Median 26 cells per HPF and 23 cells per HPF in control and αSMA-TFPI strains respectively.

**Image 1:** Liver FFPE sections stained with F4/80 from control mice. Original x400 magnification.

**Image 2:** Liver FFPE sections stained with F4/80 from αSMA -TFPI mice. Original x400 magnification.

Flow cytometry of fresh cells isolated from mouse liver was used to identify macrophages, neutrophils, T cells, B cells and NK cells. There were n=9 in both the control and the αSMA-TFPI group, except for data relating to the liver T cell, B cell and NK cell composition where n=3 in each group. This reduced number was due to an error with fluorophore selection and detection channels that was not picked up initially. It was subsequently felt inappropriate to repeat the experiment on animal welfare grounds, as it would require escalation of breeding and buying / transporting animals.

There was no statistically significant difference in the overall proportion of macrophages (CD45+ CD11b+ Ly6G- F4/80+ cells) in the livers of αSMA-TFPI mice compared to control mice at baseline (Mann Whitney test, p=0.43). However, there was a statistically significant increase in the proportion of macrophages that had intermediate / low Ly6C ($Ly6C^{int/lo}$) expression within this population in the αSMA-TFPI mice at baseline (Mann Whitney test, p=0.03. Figure 3-4. Graphs A-C).

There was no statistically significant difference in the proportion of mature macrophages (CD45+ CD11b+ Ly6G- CD64+ MerTK+ cells) in the livers of αSMA-TFPI mice compared to control mice at baseline (Mann Whitney test, p=0.18). There was no statistically significant difference in the proportions of mature macrophages with intermediate / low ($Ly6C^{int/lo}$) or high ($Ly6C^{hi}$) Ly6C expression in αSMA-TFPI mice compared to control mice (Mann Whitney test, p=0.90 and p=0.18 respectively. Figure 3-4. Graphs D-F).

There was no statistically significant difference in the proportion of neutrophils in the livers of αSMA-TFPI mice compared to control mice (Mann Whitney test, p=0.16. Figure 3-5. Graph A).

There was no statistically significant difference in the proportion of T cells, B cells or NK cells in the livers of αSMA-TFPI mice compared to control mice (Mann Whitney test, p=0.40, p=0.40 and p=0.10 respectively. Figure 3-5. Graphs B-D). Review of median and interquartile ranges for the data showed a trend towards decreased proportions of NK cells in αSMA-TFPI mice compared to control mice, however the numbers in each arm were small, limiting statistical analysis.

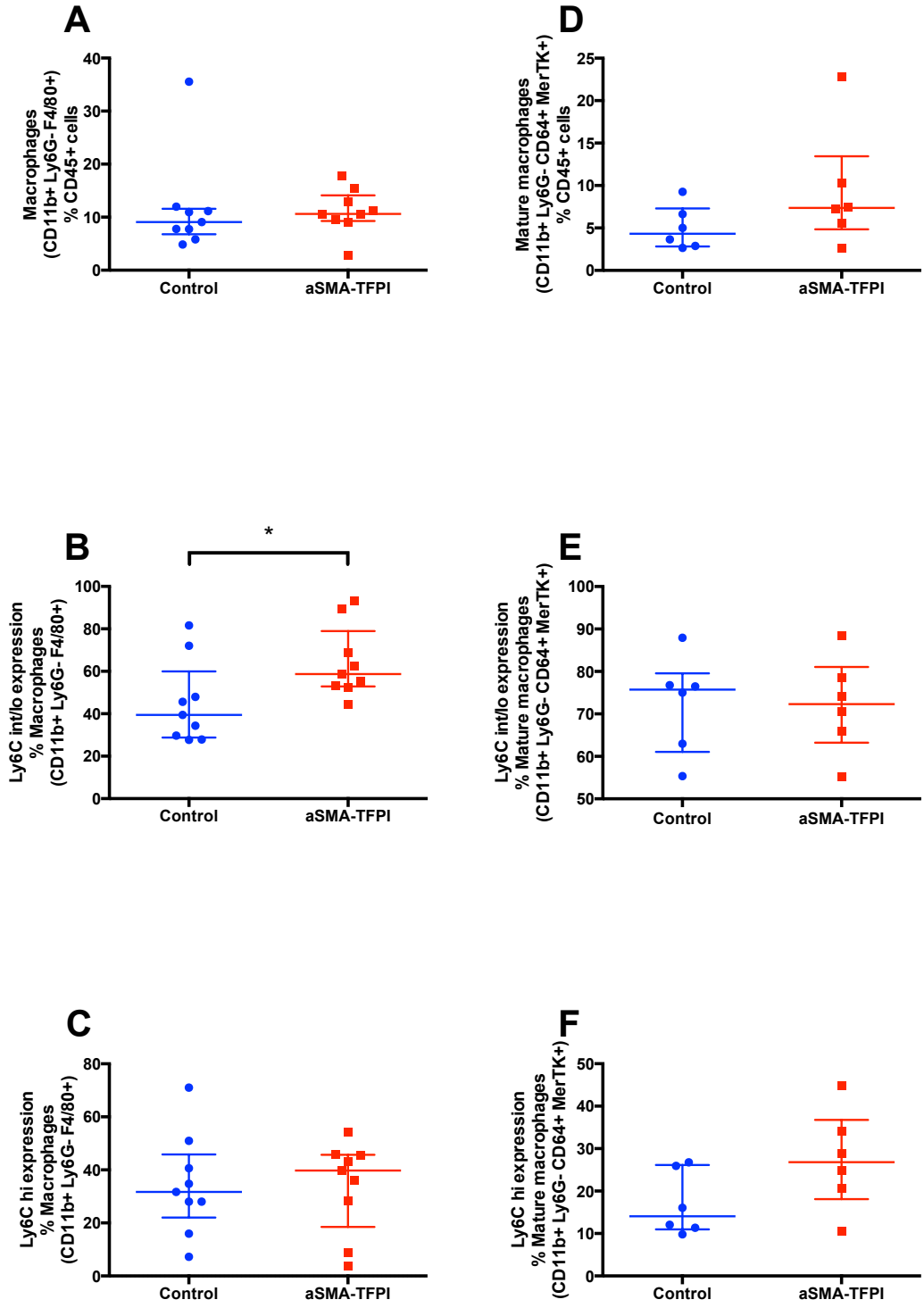


**Figure 3-4: Baseline liver macrophage composition**

Bars indicate median with interquartile range.

* p=<0.05

*Next page for figure legend.*

**Figure 3-4: Baseline liver macrophage populations**

**Graph A:** Macrophages (CD45+ CD11b+ Ly6G- F4/80+ cells) as a proportion of CD45+ (immune) cells. Median at baseline, 9% and 11% of CD45+ cells in control and αSMA-TFPI strains respectively.

**Graph B:** Macrophage expression of intermediate / low levels of Ly6C as a proportion of macrophages. Median at baseline, 39% and 59% macrophages in control and αSMA-TFPI strains respectively.

**Graph C:** Macrophage expression of high levels of Ly6C as a proportion of macrophages. Median at baseline, 32% and 40% of macrophages in control and αSMA-TFPI strains respectively.

**Graph D:** Mature macrophages (CD45+ CD11b+ Ly6G- CD64+ MerTK+ cells) as a proportion of CD45+ (immune) cells. Median at baseline, 4.3% and 7.4% of CD45+ cells in control and αSMA-TFPI strains respectively.

**Graph E:** Mature macrophage expression of intermediate / low levels of Ly6C as a proportion of macrophages. Median at baseline, 76% and 72% of CD45+ cells in control and αSMA-TFPI strains respectively.

**Graph F:** Mature macrophage expression of high levels of Ly6C as a proportion of macrophages. Median at baseline, 14% and 27% of CD45+ cells in control and αSMA-TFPI strains respectively.

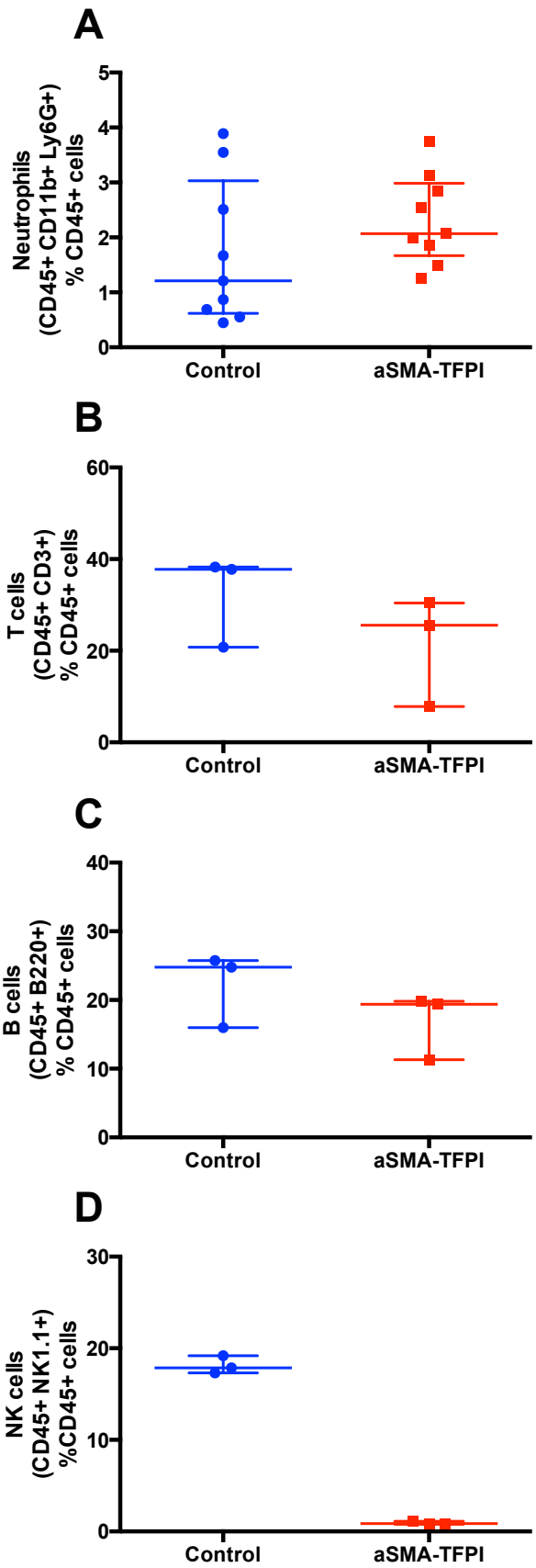


**Figure 3-5: Baseline liver neutrophil, T cell, B cell and NK cell composition**

Bars indicate median with interquartile range.

**Graph A:** Neutrophils (CD45+ CD11b+ Ly6G+ cells) as a proportion of CD45+ (immune) cells. Median at baseline, 1.2% and 2.1% of CD45+ cells in control and αSMA-TFPI strains respectively.

**Graph B:** T cells (CD45+ CD3+ cells) as a proportion of CD45+ (immune) cells. Median at baseline, 38% and 26% of CD45+ cells in control and αSMA-TFPI strains respectively.

**Graph C:** B cells (CD45+ B220+ cells) as a proportion of CD45+ (immune) cells. Median at baseline, 25% and 19% of CD45+ cells in control and αSMA-TFPI strains respectively.

**Graph D**: NK cells (CD45+ NK1.1+ cells) as a proportion of CD45+ (immune) cells. Median at baseline, 18% and 0.9% of CD45+ cells in control and αSMA-TFPI strains respectively.

### *3.1.4. Protease activated receptors*

Protease activated receptors (PAR) are transmembrane G-protein linked receptors that are activated when proteases cleave an extracellular amino-terminal. Activation leads to intracellular signalling including $IP_3$, MAPK and NF-κB pathways.

PAR1 and PAR2 gene expression infers the amount of receptor actively being transcribed in the sample. Quantitative PCR of cDNA reverse transcribed from whole liver homogenate RNA showed no statistically significant difference in PAR1 or PAR2 gene expression in the livers of αSMA-TFPI mice compared to control mice (Mann Whitney test, p=0.78 and p=0.99 respectively. Figure 3-6. Graphs A and B). There were n=8 in both the control and the αSMA-TFPI group for PAR1 gene expression assays. There were n=4 in the control group and n=6 in the αSMA-TFPI group in PAR2 gene expression assays due to failed assays.

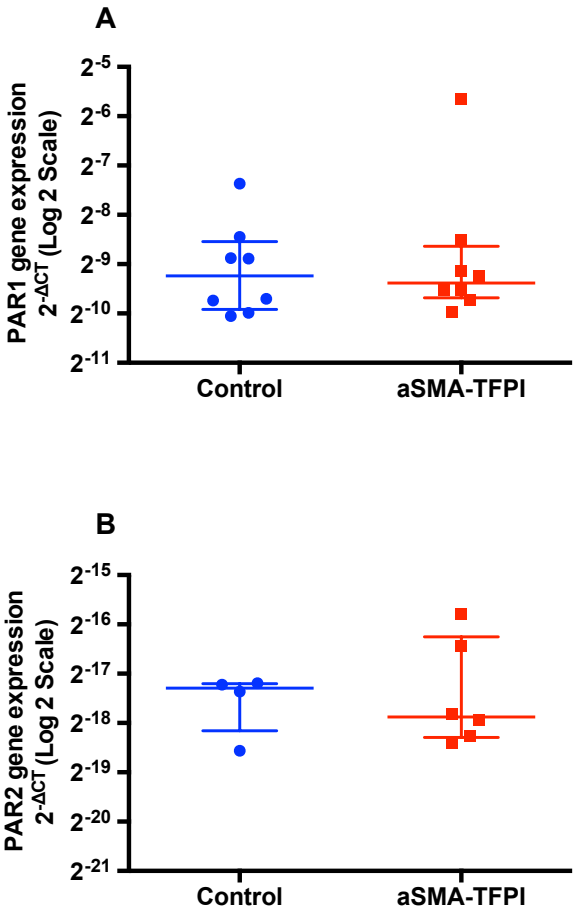


**Figure 3-6: Baseline PAR gene expression**

Bars indicate median with interquartile range.

**Graph A:** PAR1 gene expression in whole liver homogenates. At baseline the αSMA-TFPI strain had a 1.2 fold change (increase) in PAR1 gene expression compared to controls.

**Graph B:** PAR2 gene expression in whole liver homogenates. At baseline the αSMA-TFPI strain had a 1.1 fold change (increase) in PAR2 gene expression compared to controls.

### *3.1.5. Baseline transgenic TFPI expression*

Genomic carriage of the transgene was confirmed by end point PCR and gel electrophoresis of PCR products. Only mice with proven genomic carriage of the transgene were termed αSMA-TFPI mice and used in experiments.

Expression of the transgene was assessed using immunohistochemistry and / or PCR. Immunohistochemistry for human TFPI was performed on FFPE liver, kidney, spleen, lung and heart sections and end point PCR of cDNA reverse transcribed from whole liver homogenate DNAse treated RNA.

The anti-human TFPI antibody used in the immunohistochemistry was specific to amino acids 29-44 in the human protein, a portion of the protein present in the transgene that has only 31.25% homology with the mouse TFPI protein. Specificity was confirmed by negative staining in tissue from C57BL6/J control mice.

Strong DAB staining was seen in blood vessel walls in the FFPE liver, kidney, spleen and lung tissue (Figure 3-7, Image 1, 3, 4, 5). The distribution was consistent with transgenic TFPI expression in smooth muscle and associated with cellular αSMA expression (Figure 3-7. Image 1 and 2). Staining carried out on control mice showed no evidence of TFPI expression in keeping with the specificity of the antibody.

Gene expression was identified on gel electrophoresis of PCR products in 3/3 liver homogenate RNA derived cDNA samples from baseline αSMA-TFPI

mice (Figure 3-7. Image 6). The primer pairs used detect a unique portion of the transgenic fusion protein, preventing non-specific detection of non-transgenic TFPI.

The results from the immunohistochemistry and liver homogenate gene expression suggest a moderate amount of transgene expression in the livers of the αSMA-TFPI mice at baseline.

**Image 1**

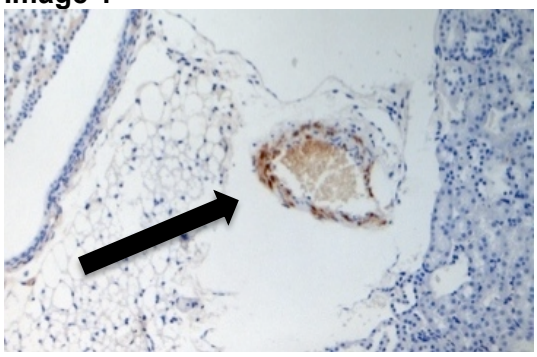

**Image 2**

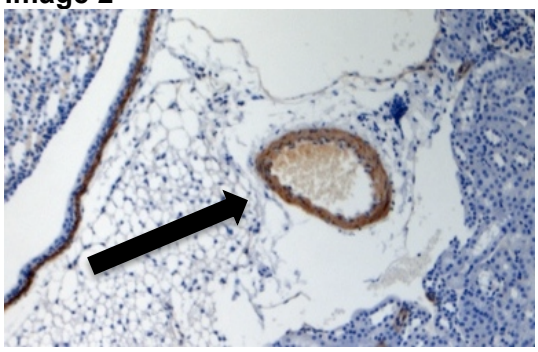

**Image 3**

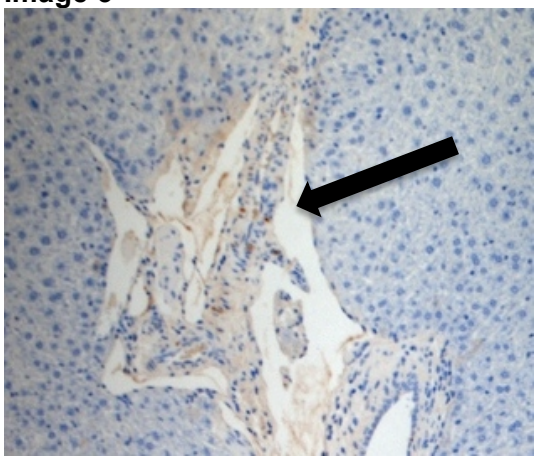

**Image 4**

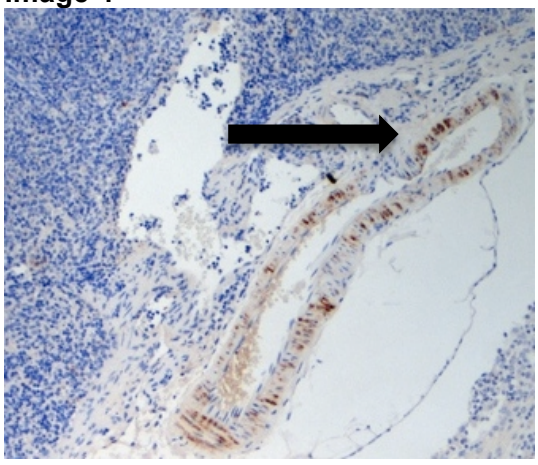

**Image 5**

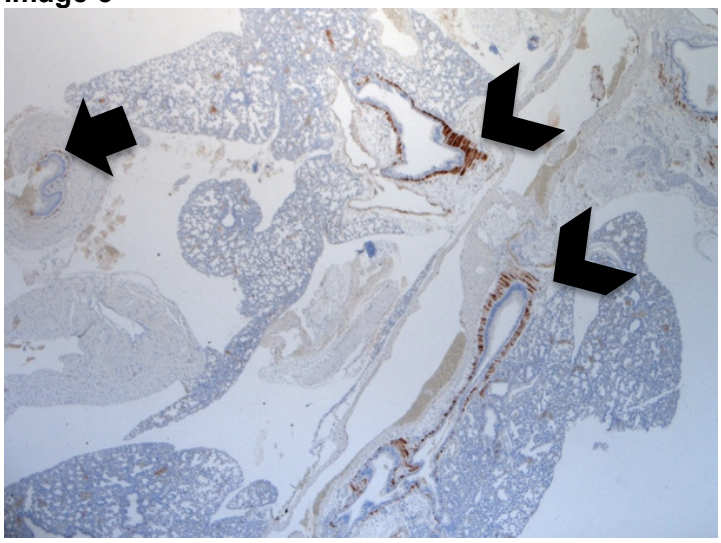

**Image 6**

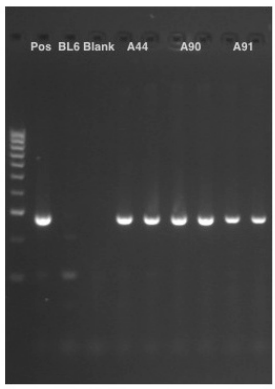


**Figure 3-7: Baseline transgenic TFPI expression**

*Next page for figure legend.*

**Figure 4-8: Baseline transgenic TFPI expression**

*Previous page for figures.*
*Arrow indicates typical staining pattern in vascular smooth muscle of vessels (Images 1-4, long arrow) or bronchial and oesophageal (Image 5, arrowheads and short arrow respectively).*

**Image 1:** Anti-human TFPI immunohistochemistry. αSMA-TFPI mouse. Kidney. Original x100 magnification.
**Image 2:** Anti-αSMA immunohistochemistry – matched to Image 1. αSMA-TFPI mouse. Kidney. Original x100 magnification.

Both images demonstrate DAB staining in smooth muscle cells of kidney vasculature. **Image 1** demonstrates TFPI staining and **Image 2** demonstrates αSMA staining – confirming the distribution of the transgenic protein to cells expressing αSMA.

**Image 3:** Anti-human TFPI immunohistochemistry. αSMA-TFPI mouse. Liver. Original x100 magnification.
**Image 4:** Anti-human TFPI immunohistochemistry. αSMA-TFPI mouse. Spleen. Original x100 magnification.
**Image 5:** Anti-human TFPI immunohistochemistry. αSMA-TFPI mouse. Lung and Oesophagus Original x20 magnification.

All images demonstrate DAB staining of the transgenic TFPI protein in a distribution consistent with cells expressing αSMA, being predominantly smooth muscle. In the liver there is patchy staining of cells making up the wall of a large vessel in the centre of the image (Image 3). In the spleen there is strong staining of cells making up the wall of large vessels at the bottom and right of the image (Image 4). In the lung there is strong staining of cells making up the wall of the bronchi (off-centre of the image) and oesophagus (top left of the image, Image 5).

**Image 6:** PCR product gel electrophoresis. αSMA-TFPI baseline samples (A44, A90 and A91). PCR of 1μL of cDNA transcribed from liver homogenate RNA.

Pos = genomic DNA positive control.
BL6 = control (C57BL6/J) liver homogenate cDNA (negative control).
Blank = non-template control.

### *3.1.6. Summary – Baseline parameters*

The αSMA-TFPI mice showed moderate amounts of transgenic TFPI gene and / or protein expression in the liver and other major organs at baseline (without liver injury). However, it appears that this expression did not alter many physiological and biological parameters of interest in the investigation of liver injury as there were no differences between αSMA-TFPI and control mice in plasma liver function tests, measures of hepatic stellate cell activation or protease activated receptor (PAR) gene expression. This is in keeping with previous work that showed no effect of the transgene on baseline bleeding times and circulating anticoagulant activity (Chen, Giannopoulos, et al. 2004; D Chen et al. 2006).

The reason for this, despite the moderate protein and gene expression seen, is likely to be because the transgenic construct was expressed on smooth muscle cells that were not in direct contact with the circulation (where clotting cascade factors are present at baseline) nor effector cells expressing PAR and thereby preventing biological activity.

αSMA-TFPI mice did demonstrate a statistically significant increase in the proportion of macrophages (CD45+ CD11b+ Ly6G- F4/80+ cells) with intermediate / low expression of Ly6C ($Ly6C^{int/lo}$) compared to control mice at baseline. These are the patrolling macrophages with high levels of $CX_3CR1$ and a pro-resolution phenotype. This difference was only identified in the general macrophage population, not within the CD64+ MerTK+ sub-population of mature tissue macrophages. Therefore the sub-set with the

greater proportion of Ly6C$^{int/lo}$ expression were the infiltrating, monocyte derived macrophages. This suggests that the transgenic TFPI expression might be affecting the recruitment of pro-resolution macrophages to the liver at rest, priming the liver for recovery after injury.

In the existing literature I have not been able to identify baseline proportions of Ly6C expression in hepatic macrophages (CD11b+ F4/80+ cells). Review of the supplementary data provided by Ramachandran et al suggests that Ly6C$^{int/lo}$ and Ly6C$^{hi}$ macrophages exist in a ratio of approximately 2:1 to 4:1 at baseline, depending on gating strategies (Ramachandran et al. 2012). Transgenic mice had similar proportions of Ly6C$^{hi}$ macrophages compared to control mice at baseline and even with the statistically significant difference in proportion of Ly6C$^{int/lo}$ macrophages, a ratio of approximately 2:1 was seen in control and transgenic mice. Therefore if the innate immune reaction to liver injury is determined by the balance of macrophage phenotype subsets and their ability to class switch in altered environments, then it may be that the differences seen between transgenic mice and control mice at baseline does not represent a biologically significant difference. Therefore I feel that the significance of this difference at baseline can only be interpreted in relation to liver injury models discussed later in this work.

The transgenic mice also demonstrated a decreased proportion of NK cells within the CD45+ immune cell population at baseline compared to control mice. It is possible that this is due to the small numbers in each cohort (due to experimental error – discussed in section 3.1.3). However the numbers were

quite striking. I cannot formulate a reason for this from the data collected. It is possible that the expression TFPI linked to αSMA positive activated hepatic stellate cells in the uninjured liver, acted to alter soluble and cell-cell ligand / receptor interactions, altering the NK cell population directly or via changes in the macrophage population discussed above. The cross talk between macrophages and NK cells is not well described in the published literature. Michel et al bring together a number of papers from studies in humans and mice in their review article, highlighting the role of cell-cell ligand / receptor interactions and soluble factors, concluding that the plasticity of macrophage phenotypes and tissue environments makes the understanding of the pathways implicated challenging (Michel et al. 2013).

Further work quantifying the liver content of cytokines, soluble factors and cell ligand / receptor expression may help determine how the expression of TFPI on αSMA positive cells may have reduced the liver NK cell population in the transgenic mice. As above, the significance of this difference at baseline will be interpreted in relation to liver injury models discussed later in this work.

Finally, both αSMA-TFPI and control mice in this study demonstrated plasma total bilirubin levels above the normal range. There was no indication that either strains of mice had bile duct injury (plasma ALP not elevated, no evidence of bile duct damage or bilirubinostasis on histology) and there was no identifiable reason for both strains to have an increased turnover of erythrocytes therefore the reason for the plasma total bilirubin result is likely to be associated with either diet or blood collection, processing and analysis

methods. Similarly the lower than normal range of plasma albumin levels seen in both αSMA-TFPI and control mice is likely to represent variation in either diet or blood collection, processing and analysis methods. As all mice were maintained on the same diet and all blood samples collected and processed in the same way it is unlikely that these findings would affect conclusions drawn from injury models.

## 3.2. Paracetamol induced acute liver injury

Paracetamol toxicity induces centrilobular hepatocellular necrosis with a marked inflammatory cell infiltrate.

300-350mg/kg of paracetamol was administered to mice via intraperitoneal injection. Mice were culled at 6, 12, 24, 48 and 72 hours after administration of paracetamol.

### *3.2.1. Plasma liver function tests*

*See* Table 3-1*and* Figure 3-8*, Graphs A-D.*

At 6 hours there were n=5 in both the control and the αSMA-TFPI group. At 12 hours there were n=4 in both the control and the αSMA-TFPI group. At 24 hours there were n=6 in the control group and n=5 in the αSMA-TFPI group. At 48 hours there were n=5 in both the control and the αSMA-TFPI group. At 72 hours there were n=6 in the control group and n=4 in the αSMA-TFPI group. Some of these sample numbers were less than the power calculation sample number due to failed assays. Baseline sample numbers were as previously noted in section 3.1.

At 6 hours after administration of paracetamol there was a statistically significant decrease in the plasma total bilirubin of αSMA-TFPI mice compared to C57BL6/J control mice (Mann Whitney test, $p = 0.03$). There was no statistically significant difference in the plasma ALT or ALP of αSMA-TFPI

mice compared to control mice (note: plasma albumin values were not recorded for this time point).

At 12 hours after administration of paracetamol there was a statistically significant decrease in the plasma ALP of αSMA-TFPI mice compared to control mice (Mann Whitney test, $p = 0.03$). There was no statistically significant difference in the plasma ALT, total bilirubin or albumin of αSMA-TFPI mice compared to control mice.

At 24 hours after administration of paracetamol there was a statistically significant decrease in the plasma ALT of αSMA-TFPI mice compared to control mice (Mann Whitney test, $p = 0.03$). There was no statistically significant difference in the plasma ALP, total bilirubin or albumin of αSMA-TFPI mice compared to control mice.

At 48 hours after administration of paracetamol there was a statistically significant decrease in the plasma ALT of αSMA-TFPI mice compared to control mice (Mann Whitney test, $p = 0.03$). There was no statistically significant difference in the plasma ALP, total bilirubin or albumin of αSMA-TFPI mice compared to control mice.

At 72 hours after administration of paracetamol there was a statistically significant decrease in the plasma ALT of αSMA-TFPI mice compared to control mice (Mann Whitney test, $p = 0.04$). There was no statistically

significant difference in the plasma ALP, total bilirubin or albumin of αSMA-TFPI mice compared to control mice.

| Median plasma values in each strain (fold change from baseline) | | Base-line | 6 hours | 12 hours | 24 hours | 48 hours | 72 hours |
|---|---|---|---|---|---|---|---|
| **ALT IU/L** | **Control** | 24 | 896 (37) | 4399 (183) | **2553 (106)** | **552 (23)** | **214 (9)** |
| | **αSMA-TFPI** | 40 | 532 (13) | 1306 (33) | **418 (10)** | **118 (3)** | **66 (1.7)** |
| **ALP IU/L** | **Control** | 56 | 112 (2.0) | **154 (2.8)** | 126 (2.3) | 116 (2.1) | 81 (1.5) |
| | **αSMA-TFPI** | 46 | 76 (1.7) | **95 (2.1)** | 76 (1.7) | 70 (1.5) | 86 (1.9) |
| **Total bilirubin µmol/L** | **Control** | 4.6 | **5.6 (1.2)** | 4.5 (-1.0) | 8.7 (1.9) | 5.4 (1.2) | 4.1 (-1.1) |
| | **αSMA-TFPI** | 3.8 | **3.1 (-1.2)** | 7.6 (2) | 5.8 (1.5) | 3.6 (-1.1) | 4.4 (1.2) |
| **Albumin g/L** | **Control** | 24.4 | | 28.5 (1.2) | 26.9 (1.1) | 25.2 (1.0) | 26.1 (1.1) |
| | **αSMA-TFPI** | 24.2 | | 27.0 (1.1) | 23.4 (-1.0) | 26.6 (1.1) | 25.4 (1.1) |

**Table 3-1: Paracetamol induced acute liver injury, median plasma liver function tests values and fold change from baseline**

**BOLD figures =** statistically significant decrease in value in αSMA-TFPI mice compared to control mice.

A fold change of 1.0 indicates a x1.0 increase in the value, or no change.
A negative fold change indicates a decrease in the value.

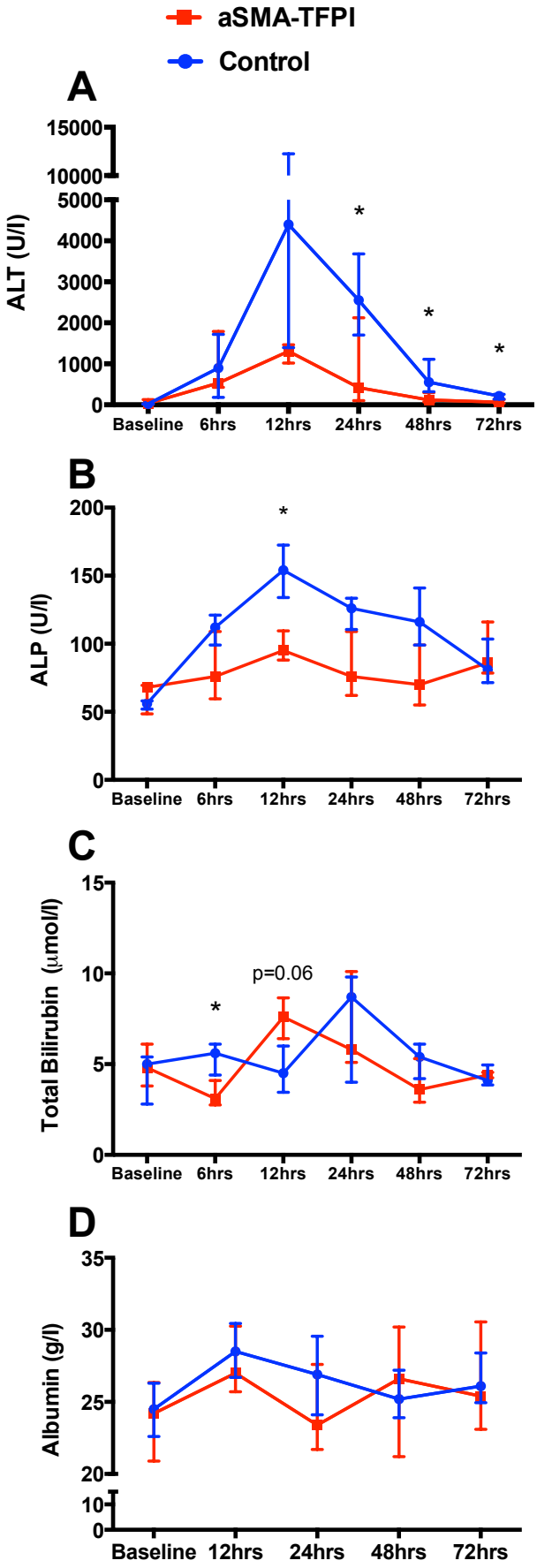


**Figure 3-8 Paracetamol induced acute liver injury, plasma liver function tests**

Symbols indicate median. Bars indicate interquartile range.

* p=<0.05.

*See* Table 3-1 *for median values.*

**Graph A**: Plasma ALT (IU/L).
**Graph B:** Plasma ALP (IU/L).

**Graph C:** Plasma total bilirubin (µmol/L).

**Graph D:** Plasma albumin (g/L).

### *3.2.2. Hepatocellular necrosis*

Digital image analysis of percentage area necrosis in H&E stained liver FFPE tissue sections showed a statistically significant decrease in αSMA-TFPI mice compared to C57BL6/J control mice at 24 and 48 hours after administration of paracetamol (Mann Whitney test, $p = 0.008$ at both time points. Figure 3-9. Graph A). Prior to this (at 2, 6 and 12 hours) there was no statistically significant difference in αSMA-TFPI mice compared to control mice. At 72 hours after administration of paracetamol control mice still showed evidence of hepatocellular necrosis whereas αSMA-TFPI mice demonstrated little or no necrosis (median 3% and 0% in control and αSMA-TFPI mice respectively. Figure 3-9. Graph A). However the difference was no longer statistically significant.

Graph A

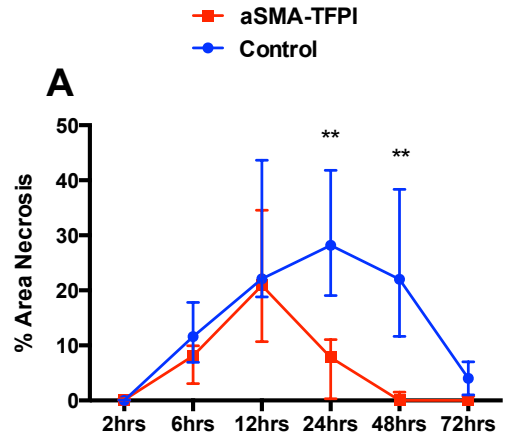


Image 1

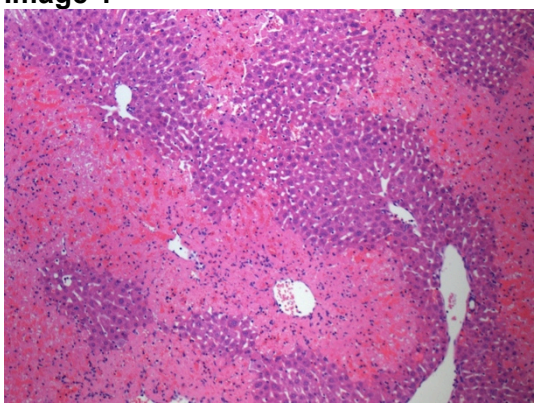

Image 2

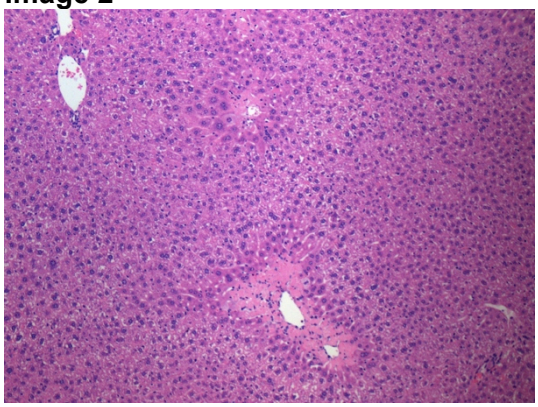

Image 3

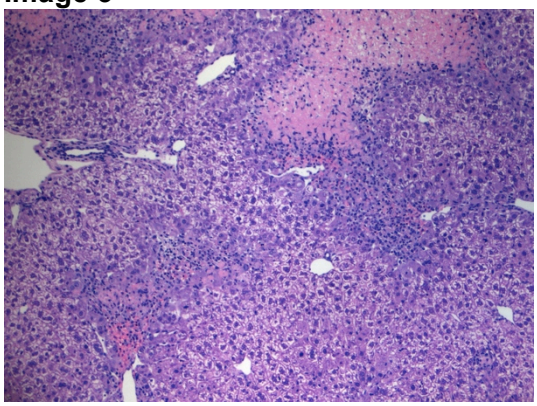

Image 4

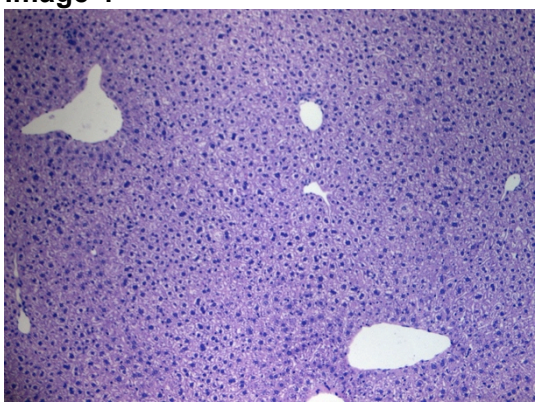

**Figure 3-9: Paracetamol induced acute liver injury, hepatocellular necrosis**

Symbols indicate median. Bars indicate interquartile range.
** p=<0.01.
**Graph A:** Percentage area necrosis in liver FFPE tissue sections. n=5 in each arm at each time point.
**Image 1:** Hepatocellular necrosis at 24 hours. Control mouse. Original x100 magnification. **Image 2:** Hepatocellular necrosis 24 hours. αSMA-TFPI mouse. Original x100 magnification.
**Image 3:** Hepatocellular necrosis at 72 hours. Control mouse. Original x100 magnification. **Image 4:** Hepatocellular necrosis at 72 hours. αSMA-TFPI mouse. Original x100 magnification.

### *3.2.3. Hepatic stellate cell activation*

Digital image analysis of FFPE liver sections stained using an antibody for αSMA showed a statistically significant increase in αSMA positive activated hepatic stellate cells in αSMA-TFPI mice at 12 hours after paracetamol administration (Mann Whitney test, p = 0.05. Figure 3-10. Graph A). This was followed by a reversal in trends with αSMA-TFPI mice subsequently demonstrating fewer αSMA positive activated hepatic stellate cells compared to controls (Table 3-2). This was statistically significant at 48 hours after administration of paracetamol (Mann Whitney test, p = 0.008. Figure 3-10. Graph A).

At 12 hours there were n=5 in both the control and the αSMA-TFPI group. At 24 hours there were n=4 in the control group and n=5 in the αSMA-TFPI group. At 48 hours there were n=5 in both the control and the αSMA-TFPI group. At 72 hours there were n=6 in the control group and n=4 in the αSMA-TFPI group. Some of these sample numbers were less than the power calculation sample number due to failed assays. Baseline sample numbers were as previously noted in section 3.1.

| Median number of αSMA+ cells (fold change from baseline) | Base-line | 12 hours | 24 hours | 48 hours | 72 hours |
|---|---|---|---|---|---|
| **Control** | 0.9 | **0.8 (-1.1)** | 2.5 (2.8) | **21.9 (24)** | 7.3 (8) |
| **αSMA-TFPI** | 0.4 | **1.2 (3)** | 1.7 (4) | **10.8 (27)** | 0.4 (1) |

**Table 3-2: Paracetamol induced acute liver injury, median number of activated hepatic stellate cells per HPF and fold change from baseline**

**BOLD figures =** statistically significant difference between αSMA-TFPI mice and control mice.

**Graph A**

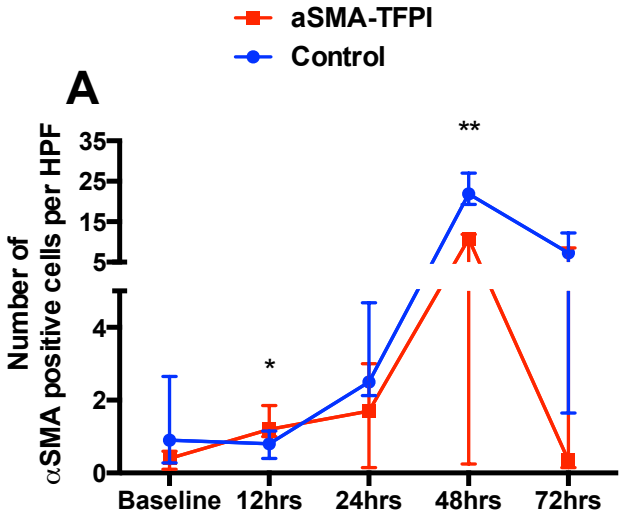


**Image 1**

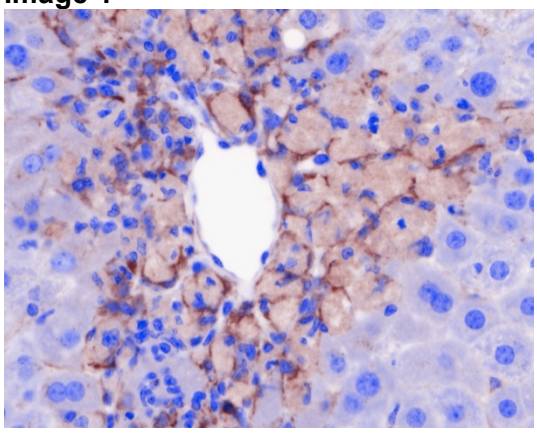

**Image 2**

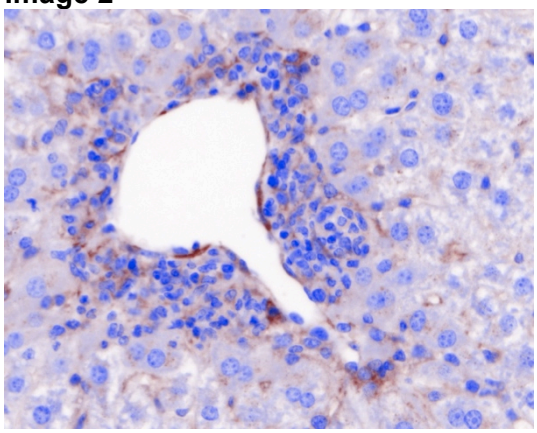

**Figure 3-10: Paracetamol induced acute liver injury, αSMA immunohistochemistry**

Symbols indicate median. Bars indicate interquartile range.
* p=<0.05. ** p=<0.01.
**Graph A:** Number of activated hepatic stellate cells in liver FFPE tissue sections as determined by αSMA immunohistochemistry.
**Image 1:** Anti-αSMA immunohistochemistry at 48 hours. Control mouse. Original x400 magnification. **Image 2:** Anti-αSMA immunohistochemistry at 48 hours. αSMA-TFPI mouse. Original x400 magnification.

### *3.2.4. Liver immune cell composition*

At baseline there were differences in the macrophage population phenotype (possibly due to gating strategies) and a trend towards decreased NK cells in αSMA-TFPI mice compared to C57BL6/J control mice (Section 3.1.3. Figure 3-4 and Figure 3-5).

Flow cytometry of fresh immune cells isolated from the liver showed that at 48 hours after administration of paracetamol there was a statistically significant decrease in the overall proportion of macrophages (CD45+ CD11b+ Ly6G- F4/80+ cells) in αSMA-TFPI mice compared to control mice (Mann Whitney test p = 0.01 Figure 3-11. Graph A). However there was no statistically significant difference at prior or subsequent time points. Assessment of macrophage Ly6C expression in this population showed no statistically significant difference in proportions of macrophages with intermediate / low Ly6C expression ($Ly6C^{int/lo}$) or high ly6C expression ($Ly6C^{hi}$) in the liver of αSMA-TFPI mice compared to control mice at any time point (Figure 3-11. Graphs B and C).

At 24 hours there were n=5 in the control group and n=6 in the αSMA-TFPI group. At 48 hours there were n=4 in the control and n=6 in the αSMA-TFPI group. At 72 hours there were n=6 in both the control and the αSMA-TFPI group. Some of these sample numbers were less than the power calculation sample number due to failed assays. Baseline sample numbers were as previously noted in section 3.1.

Assessment of mature macrophages (CD45+ CD11b+ Ly6G- CD64+ MerTK+ cells) showed a near significant decrease in the proportion of mature macrophages in αSMA-TFPI mice compared to control mice culled at 24 hours after administration of paracetamol (Mann Whitney test p = 0.07. Figure 3-12. Graph A). Assessment of macrophage Ly6C expression in this population showed a statistically significant decrease in the proportion of $Ly6C^{int/lo}$ mature macrophages and an increase in $Ly6C^{hi}$ mature macrophages in αSMA-TFPI mice compared to control mice (Figure 3-12. Graphs B and C). However there was no statistically significant difference at prior or subsequent time points.

At 24 hours there were n=7 in the control group and n=6 in the αSMA-TFPI group. At 48 hours there were n=4 in the control and n=6 in the αSMA-TFPI group. At 72 hours there were n=6 in both the control and the αSMA-TFPI group. Some of these sample numbers were less than the power calculation sample number due to failed assays. Baseline sample numbers were as previously noted in section 3.1.

Flow cytometry of fresh cells isolated from the liver showed no statistically significant difference in the proportions of neutrophils, T cells, B cells and NK cells in αSMA-TFPI mice compared to control mice culled any time point after administration of paracetamol (Figure 3-13. Graphs A-D). Review of median and interquartile ranges showed a trend towards an increased proportion of B cells in the livers of αSMA-TFPI mice compared to control mice culled at 24

hours after administration of paracetamol. However this did not reach statistical significance.

At 24 hours there were n=5 in the control group and n=6 in the αSMA-TFPI group. At 48 hours there were n=4 in the control and n=6 in the αSMA-TFPI group. At 72 hours there were n=6 in both the control and the αSMA-TFPI group. Some of these sample numbers were less than the power calculation sample number due to failed assays. Baseline sample numbers were as previously noted in section 3.1.

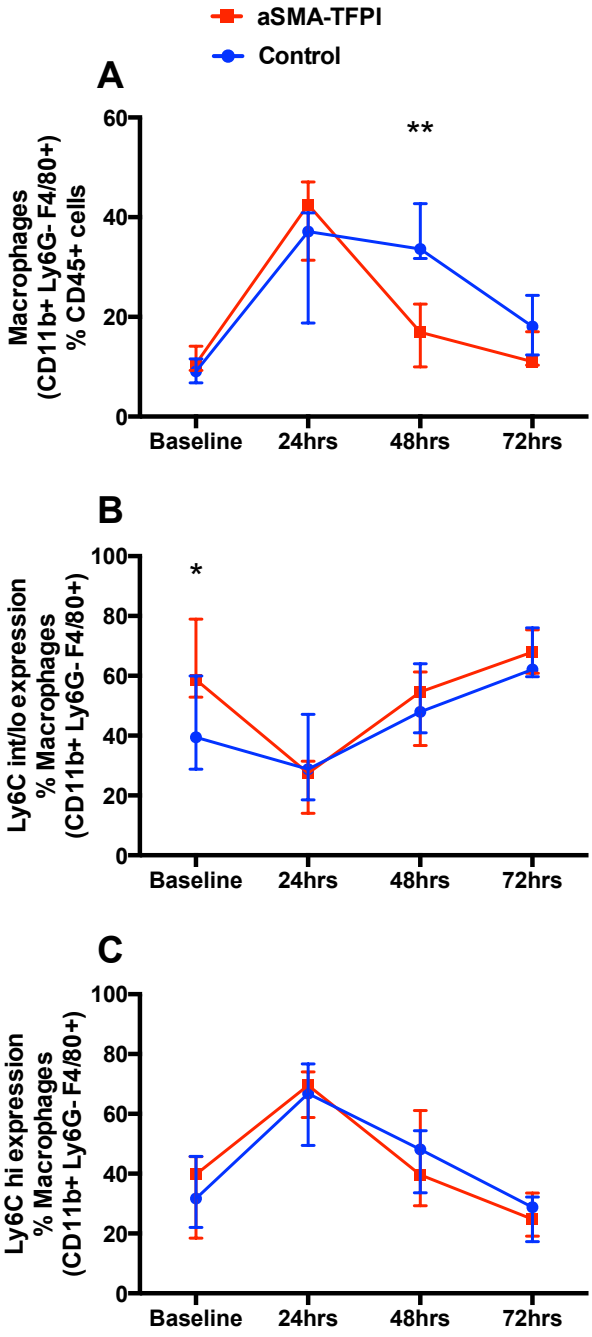


**Figure 3-11: Paracetamol induced acute liver injury, macrophage populations**

Symbols indicate median. Bars indicate interquartile range.

* p=<0.05. **p=<0.01.

*See* Table 3-3 *for median values.*

**Graph A:** Macrophages (CD45+ CD11b+ Ly6G- F4/80+ cells) as a proportion of CD45+ (immune) cells.

**Graph B:** Macrophage expression of intermediate or low levels of Ly6C as a proportion of macrophages.

**Graph C:** Macrophage expression of high levels of Ly6C as a proportion of macrophages.

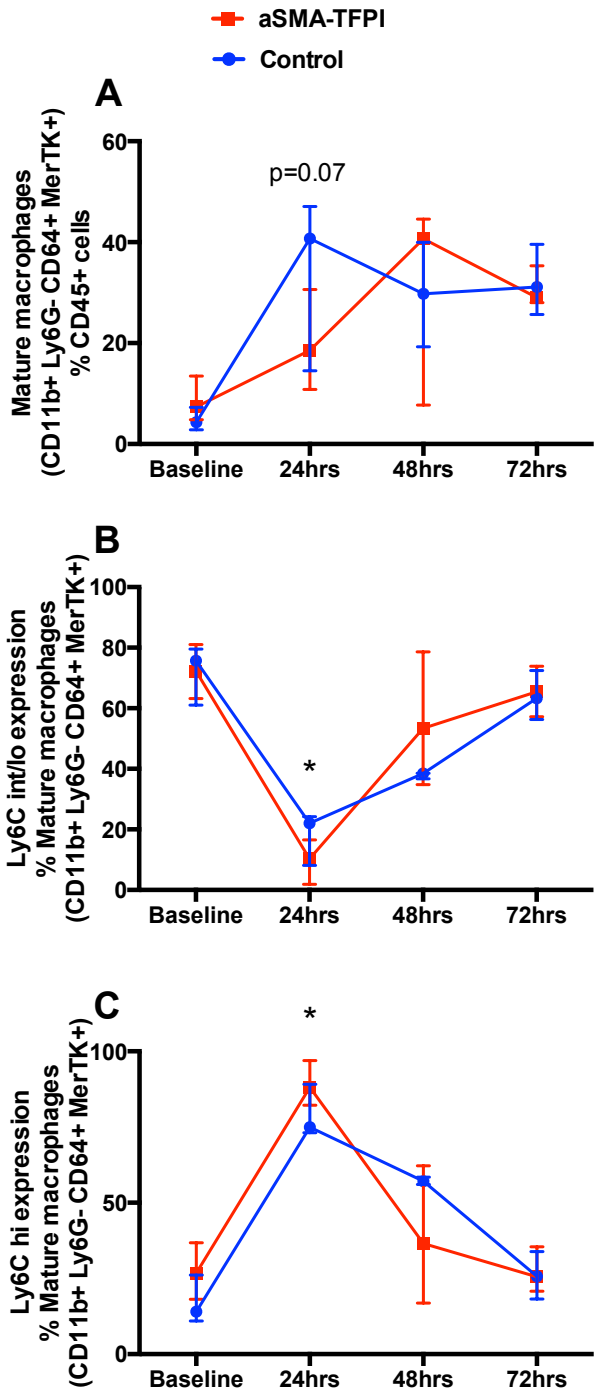


**Figure 3-12: Paracetamol induced acute liver injury, mature tissue macrophage populations**

Symbols indicate median. Bars indicate interquartile range.

* p=<0.05.

*See* Table 3-3 *for median values.*

**Graph A:** Mature macrophages (CD45+ CD11b+ Ly6G- CD64+ MerTK+ cells) as a proportion of CD45+ (immune) cells.

**Graph B:** Mature macrophage expression of intermediate / low levels of Ly6C as a proportion of mature macrophages.

**Graph C:** Mature macrophage expression of high levels of Ly6C as a proportion of mature macrophages.

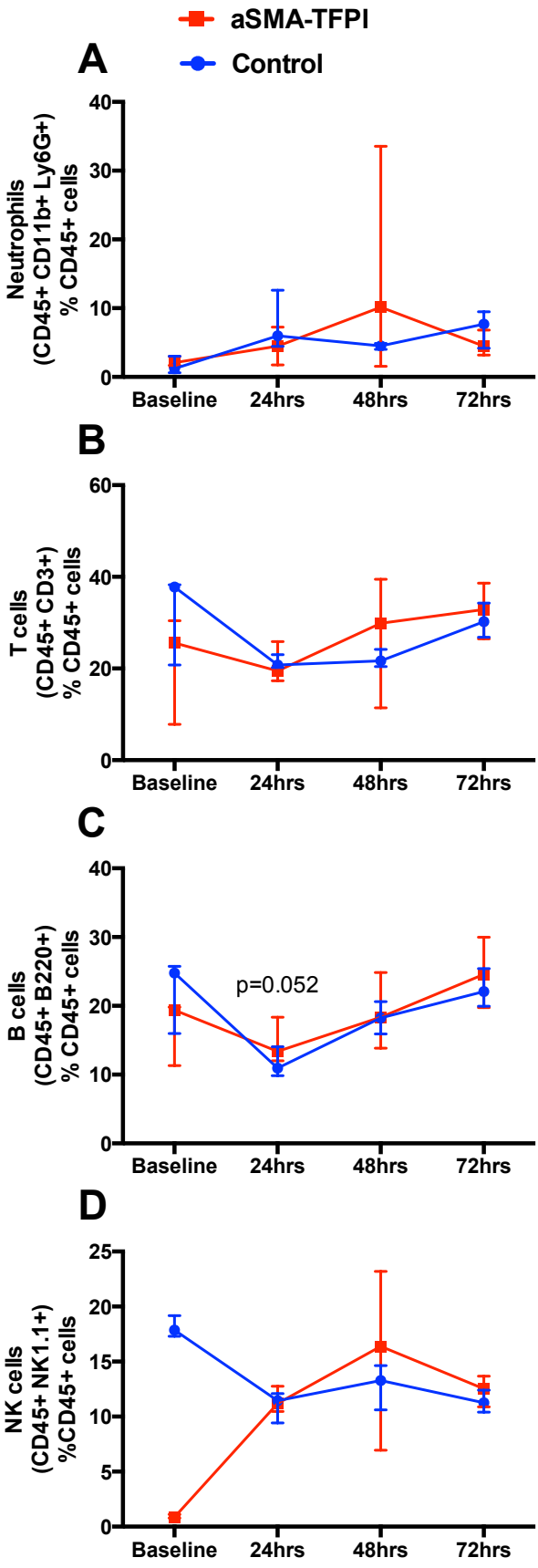


**Figure 3-13: Paracetamol induced acute liver injury, liver neutrophil, T cell, B cell and NK cell populations**

Symbols indicate median. Bars indicate interquartile range.

*See* Table 3-4 *for median values.*

**Graph A:** Neutrophils (CD45+ CD11b+ Ly6G+ cells) as a proportion of CD45+ (immune) cells.

**Graph B:** T cells (CD45+ CD3+ cells) as a proportion of CD45+ (immune) cells.

**Graph C:** B cells (CD45+ B220+ cells) as a proportion of CD45+ (immune) cells.

**Graph D**: NK cells (CD45+ NK1.1+ cells) as a proportion of CD45+ (immune) cells.

| Median macrophage population proportions in each strain (fold change from baseline) | | Baseline | 24 hours | 48 hours | 72 hours |
|---|---|---|---|---|---|
| **Overall macrophage proportions (% CD45+ immune cells)** | **Control** | 9 | 37 (4.1) | **34 (3.7)** | 18 (2.0) |
| | **αSMA-TFPI** | 11 | 43 (3.9) | **17 (1.5)** | 11 (1.0) |
| **Proportion of cells with Ly6C int/lo expression (% macrophages)** | **Control** | **39** | 31 (-1.3) | 48 (1.2) | 62 (1.6) |
| | **αSMA-TFPI** | **59** | 27 (-2.2) | 55 (-1.1) | 68 (1.2) |
| **Proportion of cells with Ly6C hi expression (% macrophages)** | **Control** | 32 | 67 (2.1) | 48 (1.5) | 29 (-1.1) |
| | **αSMA-TFPI** | 40 | 70 (1.8) | 40 (1.0) | 25 (-1.6) |
| **Overall mature macrophage proportions (% CD45+ immune cells)** | **Control** | 4.3 | **41 (9.5)** | 30 (7.0) | 31 (7.2) |
| | **αSMA-TFPI** | 7.4 | **19 (2.6)** | 41 (5.5) | 29 (3.9) |
| **Proportion of cells with Ly6C int/lo expression (% mature macrophages)** | **Control** | 76 | **22 (-3.5)** | 38 (-2.0) | 63 (-1.2) |
| | **αSMA-TFPI** | 72 | **10 (-7.2)** | 53 (-1.4) | 66 (-1.1) |
| **Proportion of cells with Ly6C hi expression (% mature macrophages)** | **Control** | 14 | **75 (5.4)** | 57 (4.2) | 26 (1.9) |
| | **αSMA-TFPI** | 27 | **88 (3.3)** | 37 (1.4) | 26 (-1.0) |

**Table 3-3: Paracetamol induced acute liver injury, liver macrophage populations, median values and fold change from baseline**

**BOLD figures =** statistically significant decrease in value in αSMA-TFPI mice compared to control mice.

| Median immune cell proportions in each strain (fold change from baseline) | | Baseline | 24 hours | 48 hours | 72 hours |
|---|---|---|---|---|---|
| **Overall neutrophil proportions (% CD45+ immune cells)** | **Control** | 1.2 | 5.7 (4.8) | 4.5 (3.8) | 7.7 (6.4) |
| | **αSMA-TFPI** | 2.1 | 4.5 (2.1) | 10 (4.8) | 4.5 (2.1) |
| **Overall T cell proportions (% CD45+ immune cells)** | **Control** | 38 | 21 (-1.8) | 22 (-1.7) | 30 (-1.3) |
| | **αSMA-TFPI** | 26 | 20 (-1.3) | 30 (1.2) | 33 (1.3) |
| **Overall B cell proportions (% CD45+ immune cells)** | **Control** | 25 | *11* (-2.3) | 18 (-1.4) | 22 (-1.1) |
| | **αSMA-TFPI** | 19 | *13* (-1.5) | 18 (-1.1) | 25 (1.4) |
| **Overall NK cell proportions (% CD45+ immune cells)** | **Control** | *18* | 11 (-1.6) | 13 (-1.4) | 11 (-1.6) |
| | **αSMA-TFPI** | *0.9* | 11 (12) | 16 (18) | 13 (14) |

**Table 3-4: Paracetamol induced acute liver injury, liver immune cell populations, median values and fold change from baseline**

**BOLD figures =** statistically significant decrease in value in αSMA-TFPI mice compared to control mice.

### *3.2.5. Cellular proliferation in the liver*

**Digital image analysis of liver FFPE sections stained using an antibody for MCM4 showed a statistically significant decrease in cellular proliferation at 24 and 48 hours after paracetamol administration in αSMA-TFPI mice compared to C57BL6/J control mice (Mann Whitney test, p = 0.008 at both time points.**

**Figure 3-14. Graph A). At 72 hours after paracetamol administration there was a decrease in cellular proliferation in αSMA-TFPI mice compared to control mice but this did not reach statistical significance (median 129 cells per HPF and 18.7 cells per HPF in control mice and αSMA-TFPI mice respectively.**

Figure 3-14. Graph A).

At 12 hours there were n=4 in the control group and n=5 in the αSMA-TFPI group. At 24 and 48 hours there were n=5 in both the control the αSMA-TFPI group. At 72 hours there were n=6 in the control group and n=4 in the αSMA-TFPI group. Some of these sample numbers were less than the power calculation sample number due to failed assays.

**Graph A**

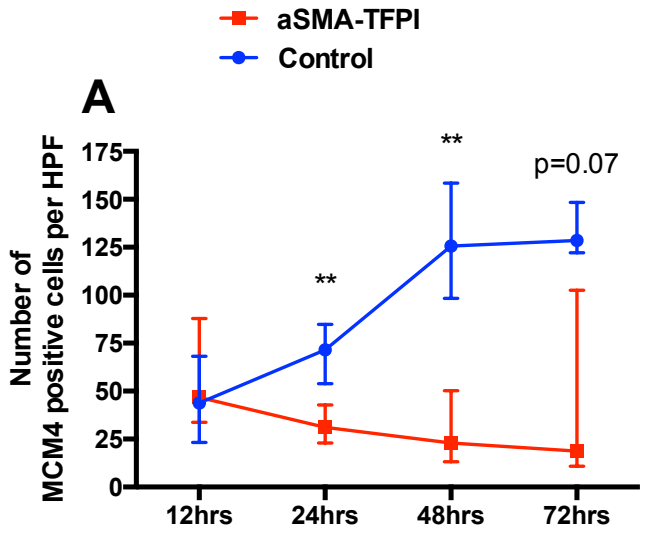


**Image 1**

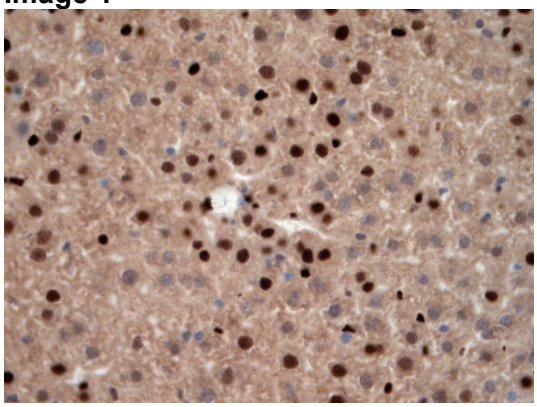

**Image 2**

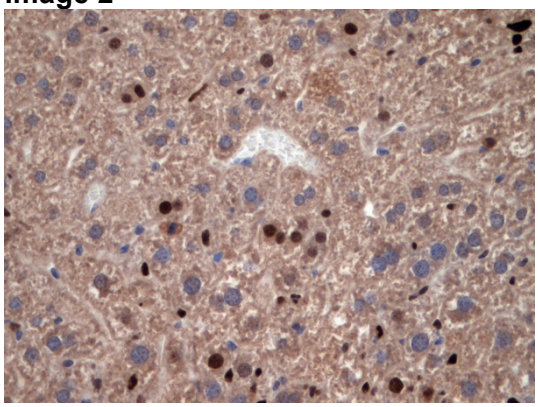

**Figure 3-14: Paracetamol induced acute liver injury, MCM4 immunohistochemistry**

Symbols indicate median. Bars indicate interquartile range.

** p=<0.01.

**Graph A:** MCM4 expression in liver FFPE tissue sections.

**Image 1:** Anti-MCM4 immunohistochemistry at 48 hours. Control mouse. Original x400 magnification. **Image 2:** Anti-MCM4 immunohistochemistry at 48 hours. αSMA-TFPI mouse. Original x400 magnification.

### *3.2.6. Fibrin deposition*

Fibrin deposition in the liver is associated with progression of paracetamol induced liver injury. At baseline there is little or no parenchymal deposition of fibrin in the liver but as parenchymal necrosis progresses there is greater deposition of fibrin (Dhar 2011).

Digital image analysis of liver FFPE sections stained using an anti-fibrin β chain antibody to identify fibrin deposition showed a statistically significant decrease in fibrin deposition in the livers of αSMA-TFPI mice compared to C57BL6/J control mice at 24 and 48 hours after paracetamol administration (Mann Whitney test, $p = 0.03$ and $p = 0.008$ respectively. Figure 3-15. Graph A). There was a trend towards less fibrin deposition at earlier (6 and 12 hours) time points, however this did not reach statistical significance. At 72 hours after the administration of paracetamol there was little or no fibrin deposition in either strains (both median 0% area fibrin staining).

At 6 and 48 hours there were n=4 in the control group and n=5 in the αSMA-TFPI group. At 12 hours there were n=3 in the control group and n=5 in the αSMA-TFPI group. At 24 hours there were n=4 in both the control the αSMA-TFPI group. At 72 hours there were n=6 in the control group and n=4 in the αSMA-TFPI group. Some of these sample numbers were less than the power calculation sample number due to failed assays.

Graph A

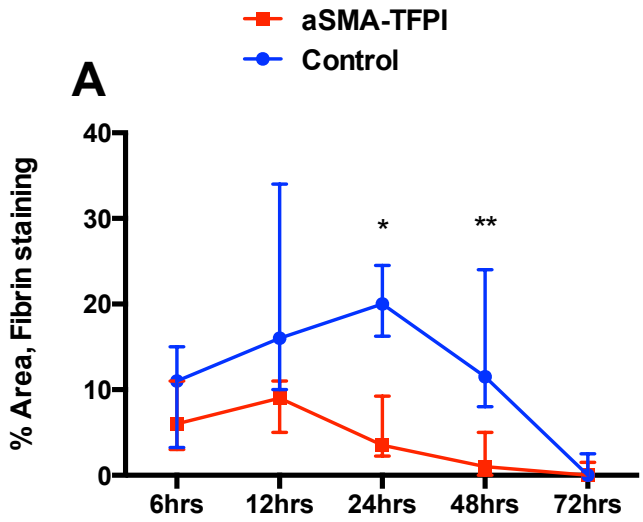


Image 1

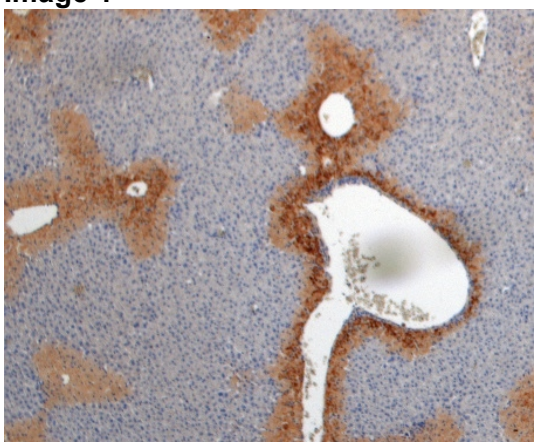

Image 2

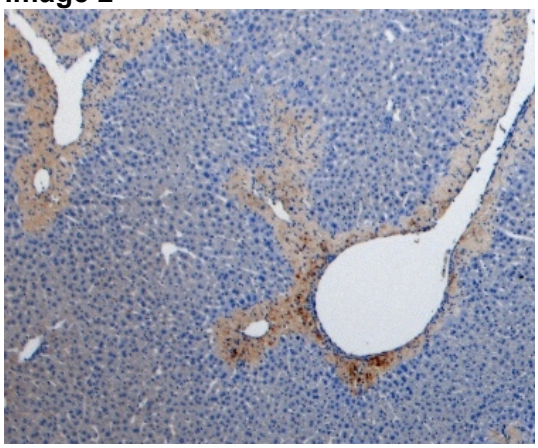

**Figure 3-15: Paracetamol induced acute liver injury, fibrin immunohistochemistry**

Symbols indicate median. Bars indicate interquartile range.

* p=<0.05. ** p=<0.01.

**Graph A**: Liver parenchymal fibrin deposition.

**Image 1:** Anti-Fibrin immunohistochemistry at 24 hours. Control mouse. Original x40 magnification. **Image 2:** Anti-MCM4 immunohistochemistry at 24 hours. αSMA-TFPI mouse. Original x40 magnification.

### *3.2.7. Protease activated receptors*

Quantitative PCR of cDNA reverse transcribed from whole liver homogenate RNA showed no statistically significant difference in PAR1 gene expression in the livers of αSMA-TFPI mice compared to C57BL6/J control mice at any time point after the administration of paracetamol (Figure 3-16. Graph A).

At 6 and 12 hours there were n=5 in both the control and the αSMA-TFPI group. At 24 hours there were n=6 in the control group and n=7 in the αSMA-TFPI group. At 48 hours there were n=5 in the control and n=7 in the αSMA-TFPI group. At 72 hours there were n=6 in both the control and the αSMA-TFPI group. Some of these sample numbers were less than the power calculation sample number due to failed assays. Baseline sample numbers were as previously noted in section 3.1.

Quantitative PCR of cDNA reverse transcribed from whole liver homogenate RNA showed a statistically significant difference in PAR2 gene expression the livers of αSMA-TFPI mice compared to control mice at 24 hours after the administration of paracetamol (Mann Whitney test, p = 0.02. Figure 3-16. Graph B).

At 6 hours there were n=4 in the control group and n=5 in the αSMA-TFPI group. At 12 hours there were n=4 in both the control and the αSMA-TFPI group. At 24 hours there were n=6 in both the control and the αSMA-TFPI group. At 48 hours there were n=5 in the control and n=7 in the αSMA-TFPI group. At 72 hours there were n=5 in the control group and n=6 in the αSMA-TFPI group. Some of these sample numbers were less than the power calculation sample number due to failed assays. Baseline sample numbers were as previously noted in section 3.1.

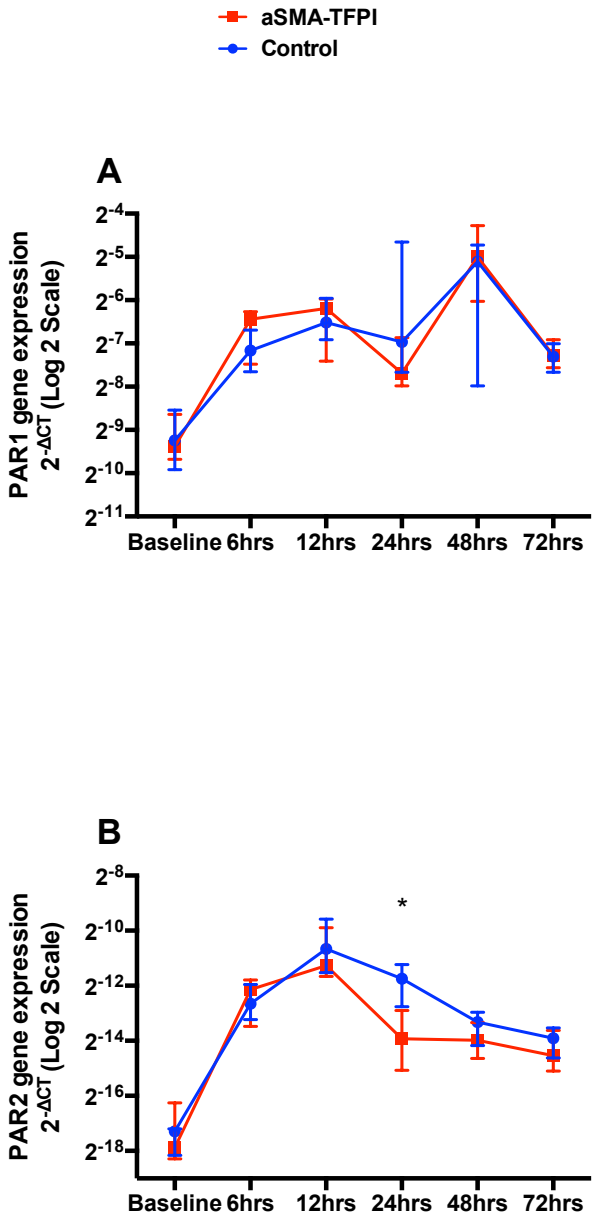


**Figure 3-16: Paracetamol induced acute liver injury, PAR gene expression**

Symbols indicate median. Bars indicate interquartile range.

* p=<0.05.

**Graph A:** PAR1 gene expression in whole liver homogenates.

**Graph B:** PAR2 gene expression in whole liver homogenates. At 24 hours after administration of paracetamol αSMA-TFPI mice had a 11 fold change (increase) in PAR2 gene expression compared to baseline and control mice had a 47 fold change (increase) compared to baseline.

### *3.2.8. Transgenic TFPI expression*

Expression of the transgene was assessed using immunohistochemistry and PCR.

No immunohistochemical staining was seen in 3/3 samples from αSMA-TFPI mice culled at 6 hours after administration of paracetamol. Of note, at this time point only liver sections were available for assessment and in baseline studies transgenic TFPI protein expression had been most easily identified in lung and large blood vessels.

At 12 hours and 24 hours after administration of paracetamol transgene expression was identified by immunohistochemical staining in all (5/5 and 3/3 respectively) samples from αSMA-TFPI mice. However, expression was predominantly seen in organs other than the liver (Figure 3-17. Images 1 and 2).

At 48 hours after administration of paracetamol transgene expression was identified by immunohistochemical staining in 2/2 samples from αSMA-TFPI mice. Positive staining was seen in aggregates of cells within the liver that were positive for αSMA and previously identified as activated hepatic stellate cells, indicating transgene expression in αSMA activated hepatic stellate cells within the liver (Figure 3-17. Images 3 and 4).

**Image 1**

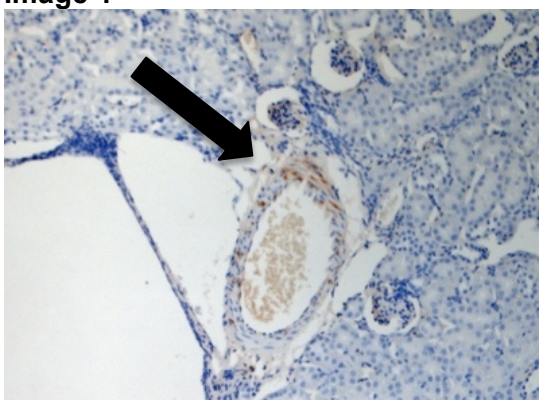

**Image 2**

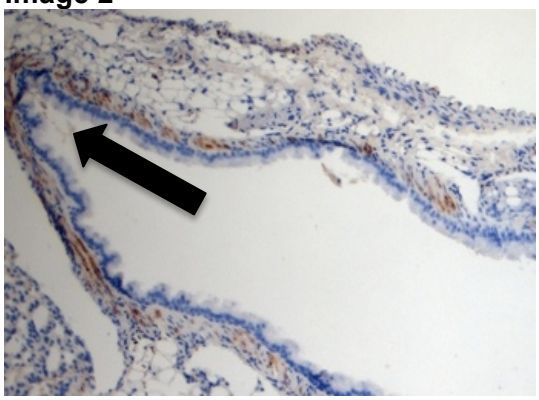

**Image 3**

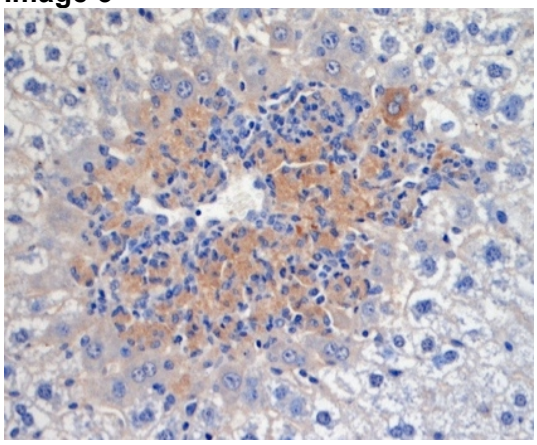

**Image 4**

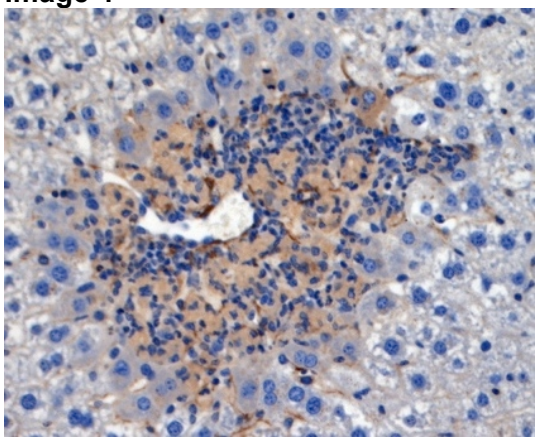

**Figure 3-17: Paracetamol induced acute liver injury, transgenic TFPI expression**

*Arrow indicates typical staining pattern in smooth muscle of vessels.*

**Image 1:** Anti-human TFPI immunohistochemistry. αSMA-TFPI mouse 24 hours after paracetamol administration. Kidney (vessel). Original x100 magnification.

**Image 2:** Anti-human TFPI immunohistochemistry. αSMA-TFPI mouse 24 hours after paracetamol administration. Lung (bronchial smooth muscle), Original x100 magnification.

**Image 3:** Anti-human TFPI immunohistochemistry. αSMA-TFPI mouse 48 hours after paracetamol administration. Liver (aggregate of activated hepatic stellate cells). Original x200 magnification.

**Image 4:** Anti-αSMA immunohistochemistry – matched to **Image 3**. αSMA-TFPI mouse 48 hours after paracetamol administration. Liver (aggregate of activated hepatic stellate cells). Original x200 magnification.

Expression of the TFPI transgene, as detected by PCR in liver samples, was identified in 4/5 samples from αSMA-TFPI mice culled at 6 hours after administration of paracetamol, 5/5 samples from αSMA-TFPI mice culled at 12 hours, 3/5 samples from αSMA-TFPI mice culled at 24 hours, 5/5 samples from αSMA-TFPI mice culled at 48 hours, and 6/6 samples from αSMA-TFPI mice culled at 72 hours after paracetamol administration. If strong gene expression can be interpreted as positivity after PCR of cDNA and weak gene expression as positivity after amplification of initial PCR products then the strongest gene expression was at 48 hours after administration of paracetamol.

Overall transgenic TFPI protein and gene expression was strongest at 48 hours after administration of paracetamol.

### *3.2.9. Model summary – paracetamol induced acute liver injury*

After paracetamol induced acute liver injury the overall picture in αSMA-TFPI mice was of decreased liver injury compared to control mice. This was associated with less fibrin deposition, decreased PAR2 gene expression, less hepatic stellate cell activation and a modified innate immune cell response. The recovery from liver injury in these mice appeared accelerated but, as the pattern of recovery was similar in transgenic and control mice, this is more likely to represent quicker recovery after less overall liver injury.

The presence of less fibrin in transgenic mice suggests that the transgenic TFPI was acting to inhibit activation of the coagulation cascade, decreasing clot formation. The association of decreased fibrin deposition with less liver injury suggests that the parenchymal extinction hypothesis of the role of the coagulation cascade in liver injury may be applicable to acute liver injury and suggests that TFPI is a key molecule in the coagulation cascade for regulating microvascular clot formation in paracetamol induced acute liver injury.

The pattern of decreased hepatocellular necrosis and decreased ALT (released from injured hepatocytes) is likely to be linked to the decreased MCM4 expression (indicating decreased cell proliferation).

The decreased gene expression of PAR2 in transgenic mice at 24 hours suggests that transgenic TFPI expression was associated with decreased production of PAR-2 receptors that also supports the PAR theory of the role of the coagulation cascade in liver injury. The reduction in PAR2 gene

expression was followed by a reduction in hepatic stellate cell activation and total hepatic macrophages at 48 hours after paracetamol induced acute liver injury which is in keeping with a reduction in PAR-2 associated pro-inflammatory stimuli (Adams et al. 2011; Knight et al. 2012; Gaca et al. 2002).

However, Kataoka et al showed that the blockade of PAR-2 alone is not sufficient to alter the degree of paracetamol induced liver injury (Kataoka et al. 2014) and it is likely that the effects of the transgenic TFPI in this work are due to its combined impact on PAR-2 and fibrin deposition.

Within the data collected there are two results that do not fit with the overall outcome of the model - the presence of increased activation of hepatic stellate cells in transgenic mice at 12 hours after paracetamol induced acute liver injury and the proportion of Ly6C expression in mature tissue macrophages at 24 hours.

It is possible that, because the transgene was predominantly expressed on activated hepatic stellate cells within the liver, there was not enough of the transgene present in the early stages of liver injury to affect the activation of hepatic stellate cells or immune cell composition. In addition, the central role of TF in the activation of the coagulation cascade during liver injury (Kerr 2003) might have meant that early in injury progression the transgenic TFPI was overwhelmed but, as propagation, rather than initiation, became the predominant phase of the coagulation cascade, there was enough transgenic TFPI available to affect a measurable impact beyond reduced fibrin deposition.

It is also possible that the increase in activated hepatic stellate cells at 12 hours was due to the decreased proportion of NK cells seen in transgenic mice at baseline. NK cells are key to activated hepatic stellate cell apoptosis (Radaeva et al. 2006) and a lack of these at the initiation of liver injury may have tipped the balance towards more activated hepatic stellate cells.

The impact of the baseline increase in pro-resolution Ly6C$^{int/lo}$ macrophages is difficult to ascertain from these results. Overall it seems to have been of benefit. It is also possible that at 24 hours the relative increase in the Ly6C$^{hi}$ expression within the mature tissue macrophage population represented a compensatory increase to overcome the initial pro-resolution macrophage phenotype dominance. Allowing the transgenic mice to develop an overall macrophage phenotype similar to that seen in control mice, including a peak in Ly6C$^{hi}$ pro-inflammatory macrophages.

The results from this set of experiments are also notable for not completely following the published literature. Although there is no published work that describes the effect of TFPI in paracetamol induced acute liver injury – there is work looking at low levels or lack of tissue factor (TF), the major constituents of the coagulation cascade that TFPI acts upon. Reduction of TF in models of paracetamol induced acute liver injury has shown a reduction in the degree of early (around 6 hours) liver injury but with no longer term affect on the progression of liver injury. The authors attributed this to the accumulation of fibrin to control levels over time, thought to be via activation

of other arms of the coagulation cascade and residual TF (Ganey et al. 2007; Sullivan et al. 2013). The difference between this work and the published literature may be due to the farther reaching effects of TFPI, which acts not only to bind TF but also factor VIIa and factor Xa.

### 3.3. α- naphthylisothiocyanate (ANIT) induced acute liver injury

ANIT (α-naphthylisothiocyanate) induces cholestatic, bile duct centric hepatocellular liver injury.

60mg/kg of ANIT was administered to mice via oral gavage. In this set of experiments mice were culled at 6, 24 and 48 hours after administration of ANIT.

#### *3.3.1. Plasma liver function tests*

At 6 hours after administration of ANIT there was a statistically significant decrease in ALP and plasma albumin in αSMA-TFPI mice compared to C57BL6/J control mice (Mann Whitney test, p = 0.02 and p = 0.04 respectively. Figure 3-18. Graph B and D). No other plasma liver function tests showed any statistically significant difference.

At 24 hours after administration of ANIT there was a statistically significant decrease in ALP and ALT in αSMA-TFPI mice compared to control mice (Mann Whitney test, p=0.02 for both. Figure 3-18. Graphs A and B). No other plasma liver function tests showed any statistically significant difference.

However, at 48 hours after administration of ANIT there was no statistically significant difference in any plasma liver function tests of αSMA-TFPI mice compared to control mice and review of the data shows similar median and interquartile ranges (Figure 3-18. Graphs A-D).

At 6 hours there were n=5 in both the control and the αSMA-TFPI group. At 24 hours there were n=5 in the control group and n=4 in the αSMA-TFPI group. At 48 hours there were n=4 in both the control and the αSMA-TFPI group. Some of these sample numbers were less than the power calculation sample number due to failed assays. Baseline sample numbers were as previously noted in section 3.1.

| **Median plasma values in each strain (fold change from baseline)** | | **Baseline** | **6 hours** | **24 hours** | **48 hours** |
|---|---|---|---|---|---|
| **ALT IU/L** | **Control** | 24 | 30 (1.3) | **102 (4.3)** | 145 (6.0) |
| | **αSMA-TFPI** | 40 | 46 (1.2) | **45 (1.1)** | 123 (3.1) |
| **ALP IU/L** | **Control** | 56 | 132 (2.4) | **98 (1.8)** | 73 (1.3) |
| | **αSMA-TFPI** | 46 | 104 (2.3) | **78 (1.7)** | 79 (1.7) |
| **Total bilirubin µmol/L** | **Control** | 4.6 | 9.4 (2.0) | 9.6 (2.1) | 10.6 (2.3) |
| | **αSMA-TFPI** | 3.8 | 9.6 (2.5) | 9.0 (2.4) | 9.2 (2.4) |
| **Albumin g/L** | **Control** | 24.4 | **25.4 (1.0)** | 21.6 (-1.1) | 21.2 (-1.2) |
| | **αSMA-TFPI** | 24.2 | **23.6 (-1.0)** | 21.6 (-1.1) | 23.8 (-1.0) |

**Table 3-5: ANIT induced acute liver injury, median plasma liver function tests values and fold change from baseline**

**BOLD figures =** statistically significant decrease in value in αSMA-TFPI mice compared to control mice.

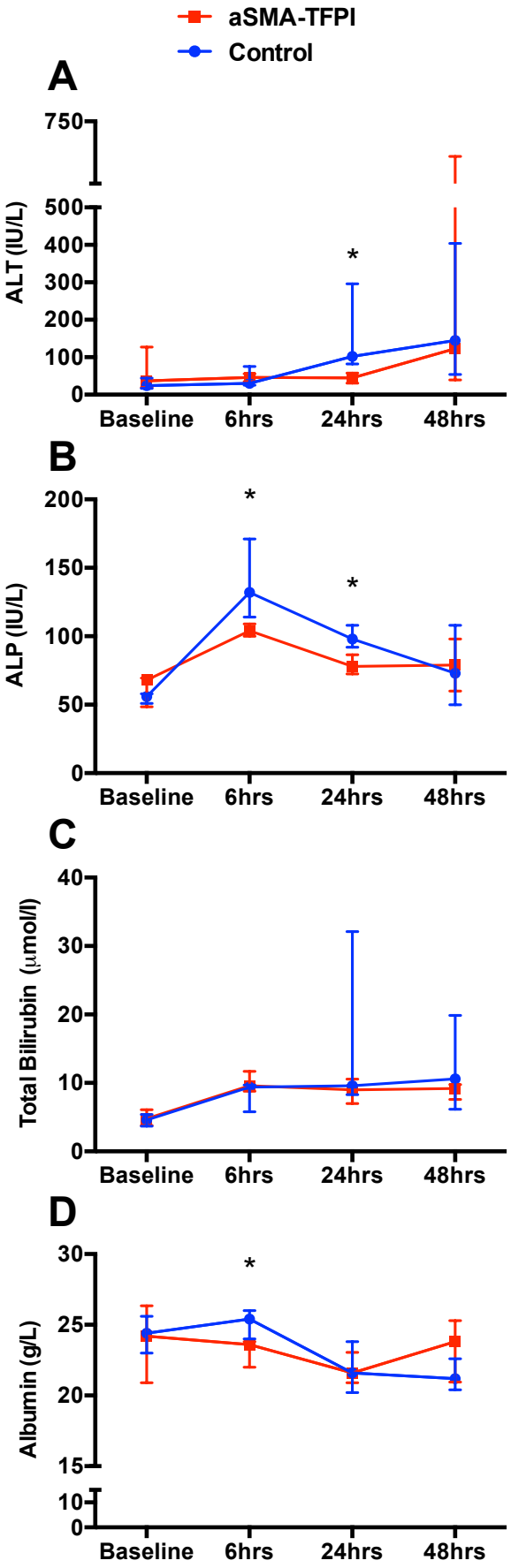


**Figure 3-18: ANIT induced acute liver injury, plasma liver function tests**

Symbols indicate median, bars indicate interquartile range.

* p=<0.05.

*See* Table 3-5 *for median values*

**Graph A**: Plasma ALT (IU/L).

**Graph B:** Plasma ALP (IU/L).

**Graph C:** Plasma total bilirubin (µmol/L).

**Graph D:** Plasma albumin (g/L).

### *3.3.2. Liver injury*

Analysis of H&E stained liver FFPE tissue sections showed no evidence of liver injury at 6 hours in both αSMA-TFPI and C57BL6/J control mice.

Digital image analysis of percentage area hepatocellular liver injury in H&E stained liver FFPE tissue sections showed no statistically significant difference in αSMA-TFPI mice compared to C57BL6/J control mice after ANIT administration at any time point (Figure 3-19. Graph A).

Review of the data showed that there was a trend towards less injury, bile duct centric hepatocellular necrosis/apoptosis, in the αSMA-TFPI mice at 24 and 48 hours compared to control mice (median at 24 hours 1.0% and 0.1% in control and αSMA-TFPI mice respectively; median at 48 hours 5.3% and 0.9% in control and αSMA-TFPI mice respectively) however this did not reach statistical significance. At 48 hours there were only 4 mice in the αSMA-TFPI mice (n = 7 control mice) and there was quite marked variation in both strains at the time point (coefficient of variation at 48 hours, 80% and 139% in control and αSMA-TFPI mice respectively), both of which may have limited statistical analysis.

At 6 hours there were n=5 in both the control and the αSMA-TFPI group. At 24 hours there were n=6 in the control group and n=4 in the αSMA-TFPI group. At 48 hours there were n=7 in the control and n=4 in the αSMA-TFPI group. Some of these sample numbers were less than the power calculation sample number due to failed assays.

**Graph A**

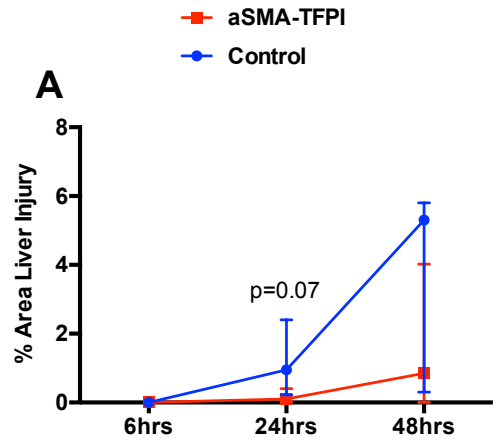


**Image 1**

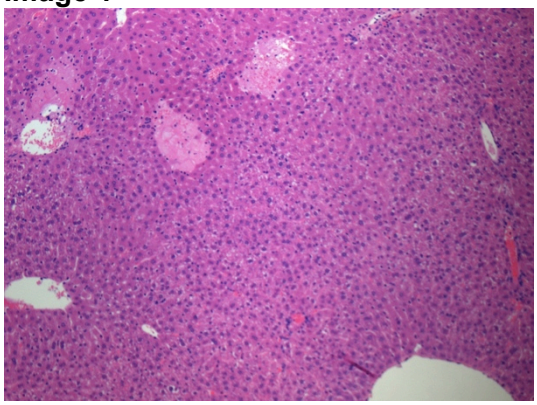

**Image 2**

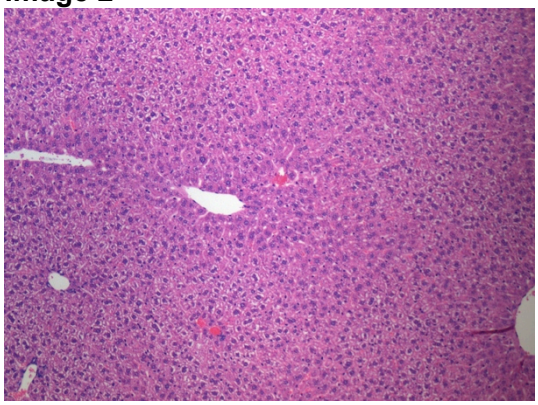

**Image 3**

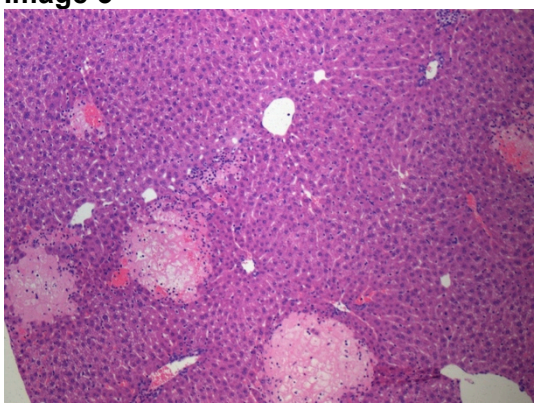

**Image 4**

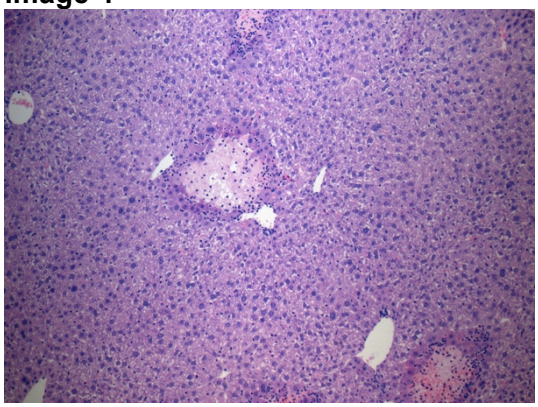

**Figure 3-19: ANIT induced acute liver injury**

Symbols indicate median. Bars indicate interquartile range.

**Graph A:** Percentage area liver injury in liver FFPE tissue sections.

**Image 1:** Hepatocellular injury at 24 hours. Control mouse. Original x100 magnification. **Image 2:** Hepatocellular injury at 24 hours. αSMA-TFPI mouse. Original x100 magnification.

**Image 3:** Hepatocellular injury at 48 hours. Control mouse. Original x100 magnification. **Image 4:** Hepatocellular injury at 48 hours. αSMA-TFPI mouse. Original x100 magnification.

### *3.3.3. Model summary - ANIT induced acute liver injury*

There was some variability in this model and the 48 hour time point was underpowered due to a lack of suitable transgenic mice. However αSMA-TFPI mice did display a significant reduction in plasma markers of liver injury (ALP and ALT) and a trend of decreased in liver parenchymal injury. These findings indicate that the transgenic expression of TFPI did alter the progression of acute cholestatic liver injury and acts to reinforce the results from the paracetamol model of acute liver injury.

Further work is required to elucidate the reason for these results but it is likely mechanism of action is that, as in the paracetamol model, inhibition of the TF / VIIa / Xa complex by the transgenic TFPI limited microvascular clot formation and protease activated receptor (PAR) activation, diminishing the impact of ANIT hepatocellular and bile duct injury.

Luyendyk et al confirmed that the coagulation cascade was activated in ANIT induced cholestatic liver injury. They showed that TF did play a role in the progression of injury as low level expression of TF was associated with less liver injury (Luyendyk et al. 2009). This supports the hypothesis that the reason for the differences between the transgenic and control model were due to the action of TFPI in relation to TF.

They attributed the impact of low-TF on the progression of ANIT liver injury to three possible mechanisms:

1. Disruption of fibrin microvascular clot formation and hepatic parenchymal hypoxia.
2. Disruption of fibrin clot scaffold formation, reducing the accumulation of platelets and neutrophils key to ANIT induced injury (Sullivan, Wang, et al. 2010)(Dahm et al. 1991)(Kodali et al. 2006).
3. Reduced thrombin associated PAR-1 signalling (Copple et al. 2003).

In addition, the apparent role of PAR-2 in the paracetamol induced acute liver injury model suggests that the role of PAR-2 in ANIT induced acute liver injury should also be examined. Future investigation of the role of TFPI in ANIT induced acute liver injury using the αSMA-TFPI transgenic model should be guided by these findings and include assessment of PAR expression, review of liver immune cell composition and assessment of the inflammatory cytokine profile of the liver during injury progression.

## 3.4. Chapter Results Summary Table

| Parameter measured | Paracetamol acute liver injury model vs. control (2, 6, 12, 24, 48 and 72 hours) | ANIT acute liver injury model vs. control (6, 24 and 48 hours) |
|---|---|---|
| **Liver injury** | Decreased injury at 24-48 hours (complete injury resolution at 72 hours).<br>Decreased ALT from 12 – 72 hours.<br>Decreased ALP at 12 hours (and 24 - 48 hours).<br>Decreased bilirubin at 6 hours (and 24 – 48 hours). Increased at 12 hours.<br>Decreased cellular proliferation. | Decreased injury.<br>Decreased ALP at 6 and 24 hours.<br>Decreased ALT at 24 hours. |
| **Fibrin deposition** | Decreased fibrin deposition (until resolution at 72 hours). | Not completed due to lack of significance in the degree of injury on H&E stained sections when controls were compared with transgenic mice. Limited time and reagents also played a role in this decision. |
| **PAR expression** | Decreased PAR2 expression at 24 hours. | |
| **Liver immune cell composition** | Decreased proportion of macrophages at 48 hours.<br>Decreased proportion of mature tissue macrophages at 24 hours with greater Ly6C$^{hi}$ expression. | |
| **Hepatic stellate cell activation** | Increased activation at 12 hours.<br>Decreased activation at 48 hours. | |

**Table 3-6: Comparison of acute liver injury models in αSMA targeted expression of TFPI**

Text in grey = non significant ($p<0.05$) trend

## 4. αSMA targeted expression of TFPI in chronic liver injury

### 4.1. Additional baseline parameters

Further parameters in the baseline (uninjured) liver phenotype of the αSMA-TFPI mice were defined to help analyse data from experimental studies in chronic liver injury.

Baseline liver function tests (3.1.1), hepatic stellate cell activation (3.1.2), liver immune cell composition (3.1.3), protease activated receptor gene expression (3.1.4) and baseline transgenic TFPI expression (3.1.5) were described in **section 3.1**.

The additional baseline measurements taken for investigation of chronic liver injury were baseline liver collagen content (4.1.1) and baseline liver collagen turnover (4.1.2).

#### *4.1.1. Liver collagen content*

Sirius red histochemical staining detects type I and Type III collagen in formalin fixed paraffin embedded (FFPE) tissue on light microscopy. Collagen is the predominant extracellular matrix protein deposited in liver and as such is often used as a surrogate for liver fibrosis.

Digital image analysis of liver sections stained with Sirius red showed no statistically significant difference in the percentage of collagen in liver tissue of αSMA-TFPI mice compared to C57BL6/J control mice (Mann Whitney test,

p=0.20. Figure 4-1. Graph A). There were n=10 in the control group and n=11 in the αSMA-TFPI group

Collagen 1α1 gene expression infers the amount of collagen I actively being transcribed in the sample. Quantitative PCR of cDNA reverse transcribed from whole liver homogenate RNA showed no statistically significant difference in collagen 1α1 gene expression in the livers of αSMA-TFPI mice compared to control mice (Mann Whitney test, p=0.99. Figure 4-1. Graph B). There were n=10 in the control group and n=9 in the αSMA-TFPI group

Note: Hydroxyproline quantification of liver collagen content was also used to evaluate liver fibrosis, however baseline measurements were not made due to lack of difference in Sirius red histochemistry and collagen 1α1 gene expression already demonstrated at baseline and the limited resources associated with the hydroxyproline assay.

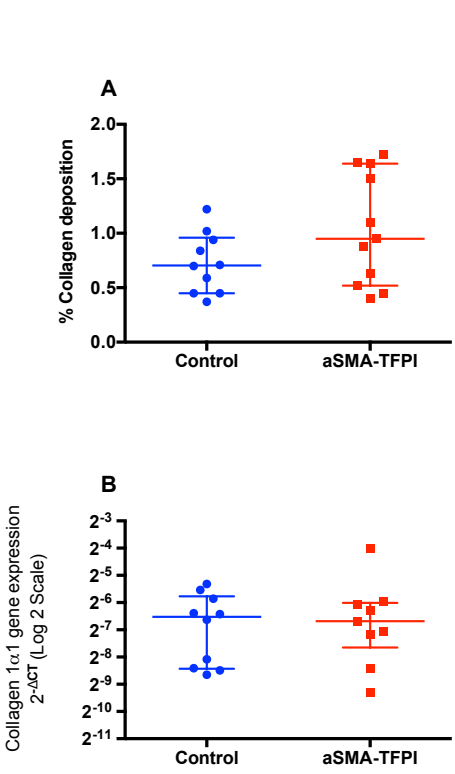


**Image 1**

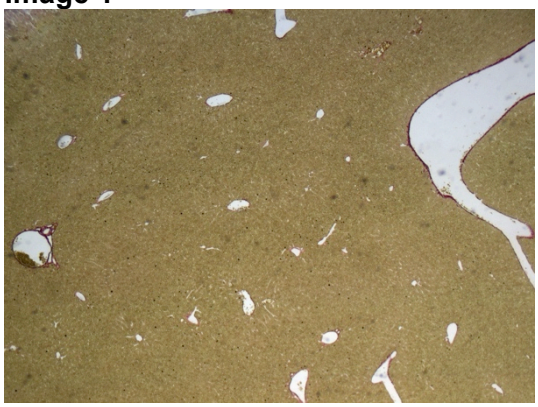

**Image 2**

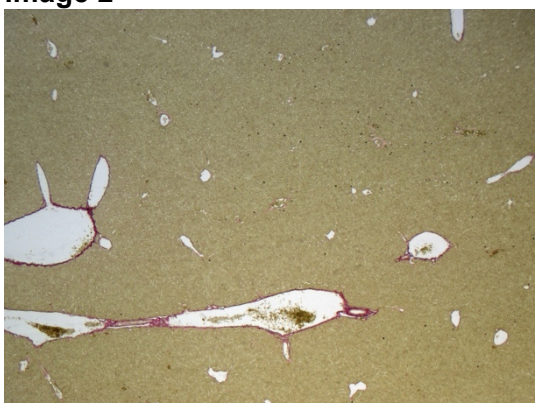

**Figure 4-1: Baseline liver collagen content**

Bars indicate median with interquartile range.

**Graph A:** Percentage Sirius red staining in liver FFPE tissue sections. Median 0.7% and 1.0% in control and αSMA-TFPI strains respectively.

**Graph B:** Collagen 1α1 gene expression in whole liver homogenates. At baseline the αSMA-TFPI strain had a -1.2 fold change (decrease) in collagen 1α1 gene expression compared to controls.

**Image 1:** Sirius red staining. Control mouse. Original x40 magnification.
**Image 2:** Sirius red αSMA-TFPI mouse. Original x40 magnification.

### *4.1.2. Collagen turnover*

Matrix metalloproteinases (MMP) and tissue inhibitors of metalloproteinases (TIMP) are proteases and protease inhibitors that regulate the degradation of collagen in the liver. MMP2, MMP9 and TIMP1 gene expression infers the amount of these proteins actively being transcribed in the sample.

Quantitative PCR of cDNA reverse transcribed from whole liver homogenate RNA showed no statistically significant difference in MMP2, MMP9 or TIMP1 gene expression in the livers of αSMA-TFPI mice compared to control mice (Mann Whitney test, p=0.86, p=0.87 and p=0.50 respectively. Figure 4-2. Graphs A-C).

There were n=6 in the control group and n=10 in the αSMA-TFPI group for MMP2 expression. There were n=7 in both the control and the αSMA-TFPI group for MMP9 expression. There were n=8 in the control group and n=10 in the αSMA-TFPI group for TIMP1 expression.

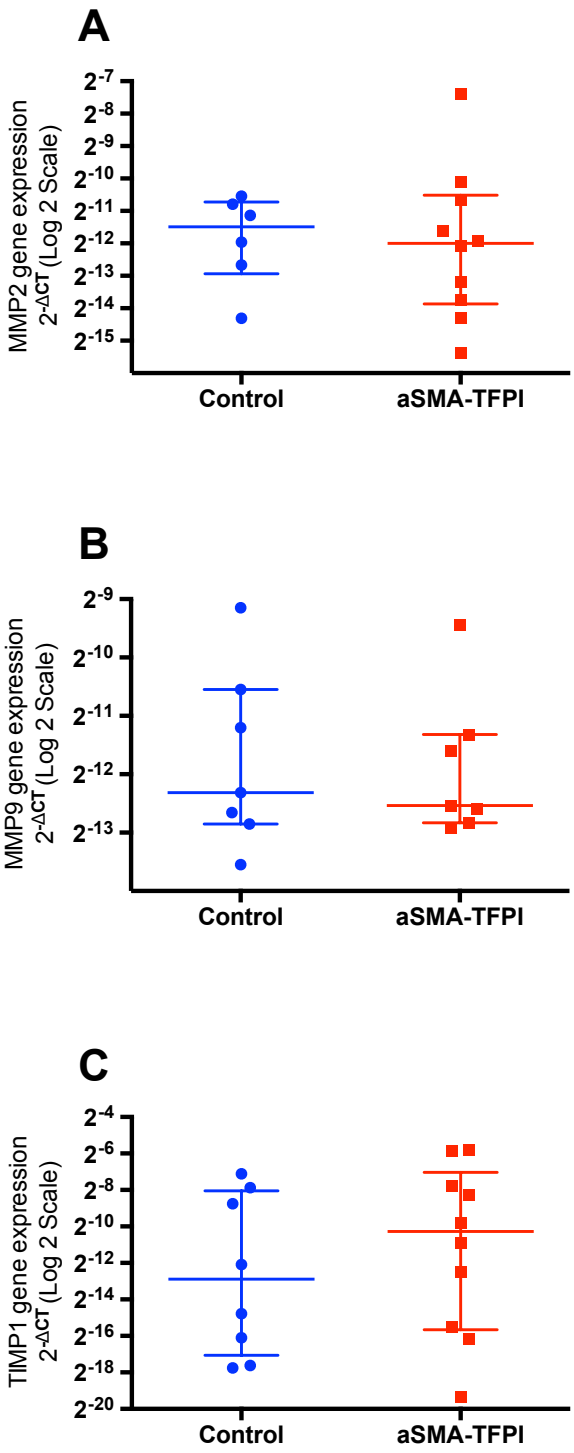


**Figure 4-2: Baseline matrixmetalloproteinase and TIMP gene expression**

Bars indicate median with interquartile range.

**Graph A:** MMP2 gene expression in whole liver homogenates. At baseline the αSMA-TFPI strain had a -1.1 fold change (decrease) in MMP2 gene expression compared to controls.

**Graph B:** MMP9 gene expression in whole liver homogenates. At baseline the αSMA-TFPI strain had a -1.1 fold change (decrease) in MMP9 gene expression compared to controls.

**Graph C:** TIMP1 gene expression in whole liver homogenates. At baseline the αSMA-TFPI strain had a 2.9 fold change (increase) in TIMP1 gene expression compared to controls.

### *4.1.3. Summary – Additional baseline parameters*

As shown in section 3.1.5 the αSMA-TFPI mice showed moderate amounts of TFPI protein and / or gene expression in the liver and other major organs at baseline. However, it appears that this expression did not alter many physiological and biological parameters of interest in the investigation of chronic liver injury as there were no differences between αSMA-TFPI and control mice in plasma liver function tests, measures of hepatic stellate cell activation, MMP, TIMP or protease activated receptor (PAR) gene expression. This is in keeping with previous work that showed no effect of the transgene on baseline bleeding times and circulating anticoagulant activity (Chen, Giannopoulos, et al. 2004; D Chen et al. 2006).

The αSMA-TFPI mice did show an altered liver innate immune cell composition (as described in section 3.1.3 and discussed in section 3.1.6) and these differences at baseline have been taken into account when analysing injury model data.

## 4.2. Carbon tetrachloride ($CCl_4$) induced chronic liver injury

Repeated doses of carbon tetrachloride ($CCl_4$) cause chronic liver injury with fibrosis. Early fibrosis has a centrilobular pattern but progresses to centri-portal bridging, and nodule formation. With cessation of $CCl_4$ fibrosis resolution occurs.

Staggered doses of 0.125mL – 1mL/kg of $CCl_4$ was administered to mice via intraperitoneal injection for 4 weeks. Mice were culled at 24, 48, 72 and 96 hours after the last injection of $CCl_4$.

### *4.2.1. Plasma liver function tests*

There was no statistically significant difference in any plasma liver function tests of αSMA-TFPI mice compared to C57BL6/J control mice at any time point after the last injection of $CCl_4$ (Figure 4-3. Graphs A-D).

Review of the data shows that at 24 hours after the last dose of $CCl_4$ transgenic mice had an ALT one third of that seen in the control mice (Mann Whitney test, p=0.14). At this time point statistical analysis may have been limited by the number of transgenic animals (n=4, power calculations recommended 6 animals per arm).

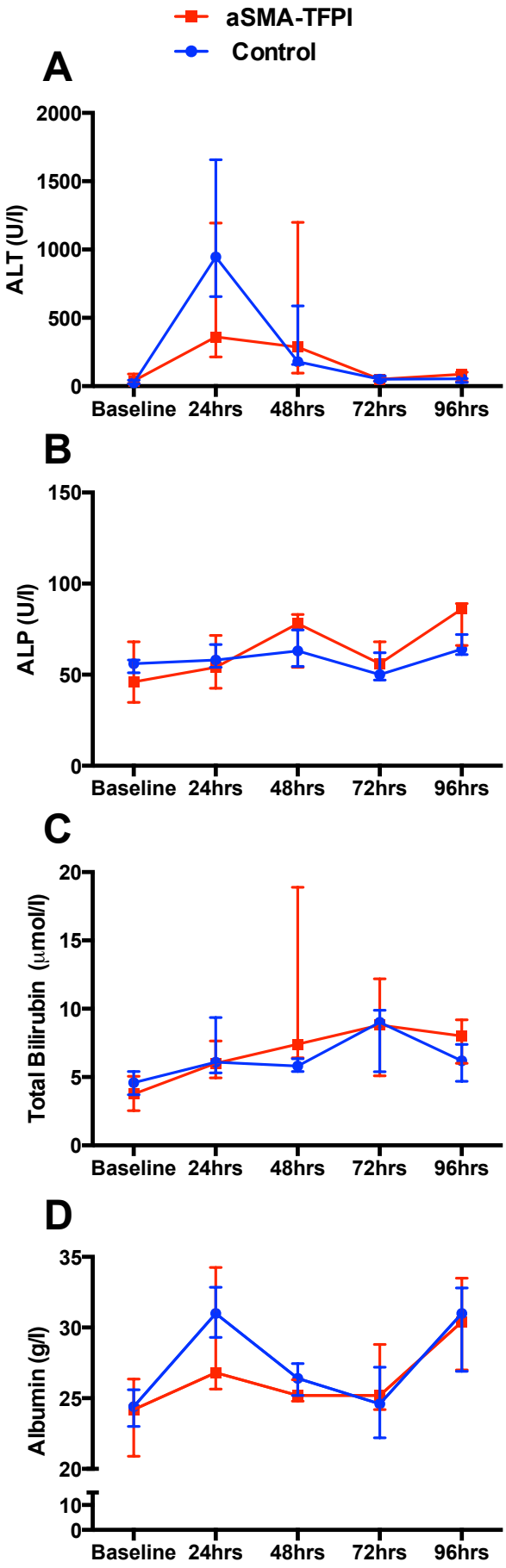


**Figure 4-3: $CCl_4$ induced chronic liver injury, plasma liver function tests**

Symbols indicate median, bars indicate interquartile range.

*See* Table 4-1 *for median values.*

**Graph A**: Plasma ALT (IU/L).

**Graph B:** Plasma ALP (IU/L).

**Graph C:** Plasma total bilirubin (µmol/L).

**Graph D:** Plasma albumin (g/L).

| Median plasma values in each strain (fold change from baseline) | | Baseline | 24 hours | 48 hours | 72 hours | 96 hours |
|---|---|---|---|---|---|---|
| **ALT IU/L** | **Control** | 24 | 946 (39) | 179 (7.5) | 50 (2.1) | 54 (2.3) |
| | **αSMA-TFPI** | 40 | 361 (9.0) | 286 (7.2) | 50 (1.3) | 88 (2.2) |
| **ALP IU/L** | **Control** | 56 | 58 (1.0) | 63 (1.1) | 50 (-1.1) | 64 (1.1) |
| | **αSMA-TFPI** | 46 | 54 (1.2) | 78 (1.7) | 56 (1.2) | 86 (1.9) |
| **Total bilirubin µmol/L** | **Control** | 4.6 | 6.1 (1.3) | 5.8 (1.3) | 9.0 (2.0) | 6.2 (1.4) |
| | **αSMA-TFPI** | 3.8 | 6 (1.6) | 7.4 (2.0) | 8.8 (2.3) | 8.0 (2.1) |
| **Albumin g/L** | **Control** | 24.4 | 31.0 (1.3) | 26.4 (1.1) | 24.6 (1.0) | 31.0 (1.3) |
| | **αSMA-TFPI** | 26.2 | 26.8 (1.0) | 25.2 (-1.0) | 25.2 (-1.0) | 30.4 (1.2) |

**Table 4-1: $CCl_4$ induced chronic liver injury, median plasma liver function tests values and fold change from baseline**

At 24 hours there were n=10 in the control group and n=4 in the αSMA-TFPI group. At 48 hours there were n=4 in the control group and n=5 in the αSMA-TFPI group. At 72 and 96 hours there were n=5 in both the control and the αSMA-TFPI group. Some of these sample numbers were less than the power calculation sample number due to failed assays. Baseline sample numbers were as previously noted in section 3.1.

### *4.2.2. Liver collage content*

Digital image analysis of liver FFPE sections stained with Sirius red from mice culled at 24, 48, 72 and 96 hours after the last injection of $CCl_4$ showed no statistically significant difference in liver collagen deposition in αSMA-TFPI mice compared to C57BL6/J control mice (Figure 4-4. Graph A). At 24 hours there were n=10 in the control group and n=9 in the αSMA-TFPI group. At 48, 72 and 96 hours there were n=5 in both the control and the αSMA-TFPI group. Some of these sample numbers were less than the power calculation sample number due to failed assays. Baseline sample numbers were as previously noted in section 4.1.

Hydroxyproline quantification of the collagen content of livers from mice culled at 24, 48, 72 and 96 hours after the last injection of $CCl_4$ showed no statistically significant difference in liver collagen content in αSMA-TFPI mice compared to control mice (Figure 4-4. Graph B). At 24 hours there were n=4 in the control group and n=5 in the αSMA-TFPI group. At 48, 72 and 96 hours there were n=5 in both the control and the αSMA-TFPI group. Some of these sample numbers were less than the power calculation sample number due to failed assays.

Quantitative PCR of cDNA reverse transcribed from whole liver homogenate RNA from mice culled at 24, 48, 72 and 96 hours after the last injection of $CCl_4$ showed no statistically significant difference in collagen 1$\alpha$1 gene expression in the livers of αSMA-TFPI mice compared to control mice (Figure 4-4. Graph C). At 24 hours there were n=14 in the control group and n=13 in

the αSMA-TFPI group. At 48, 72 and 96 hours there were n=5 in both the control and the αSMA-TFPI group. Some of these sample numbers were less than the power calculation sample number due to failed assays. Baseline sample numbers were as previously noted in section 4.1.

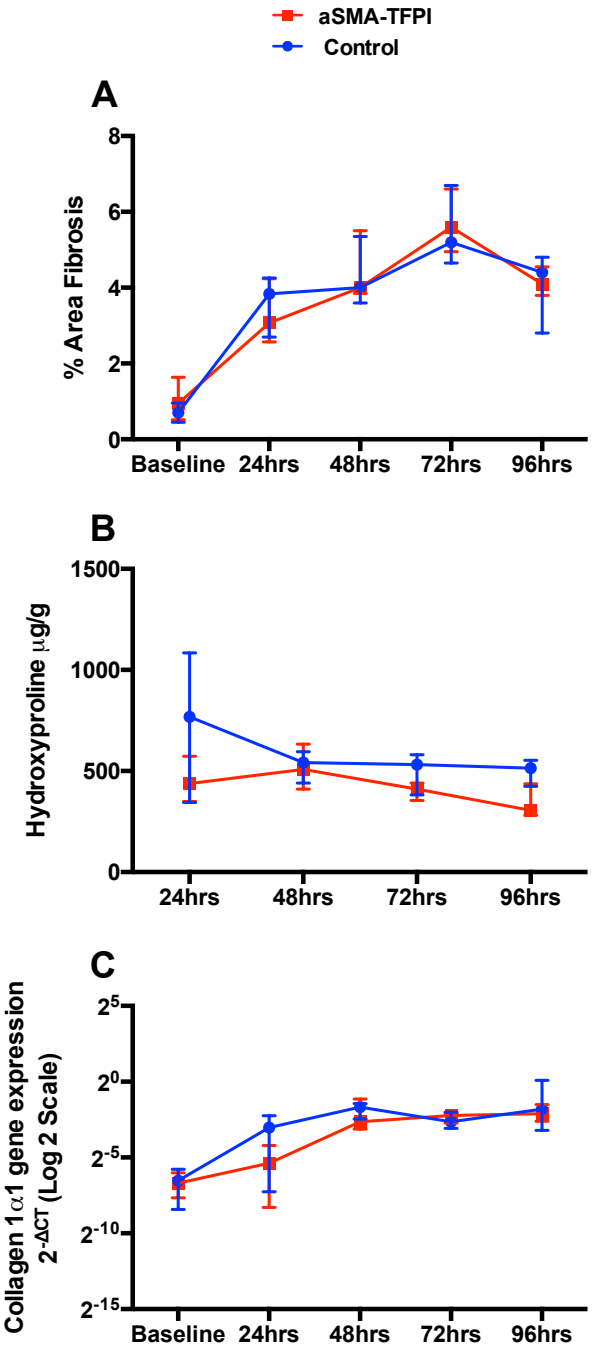


Image 1

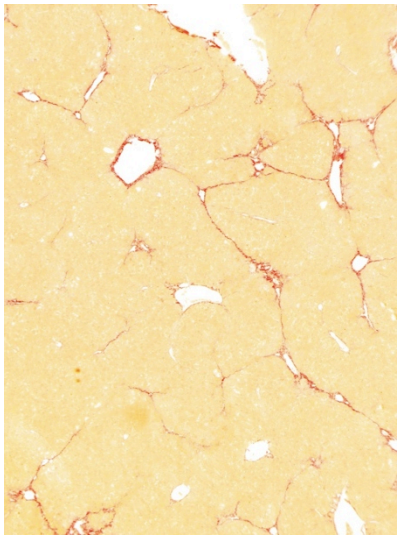

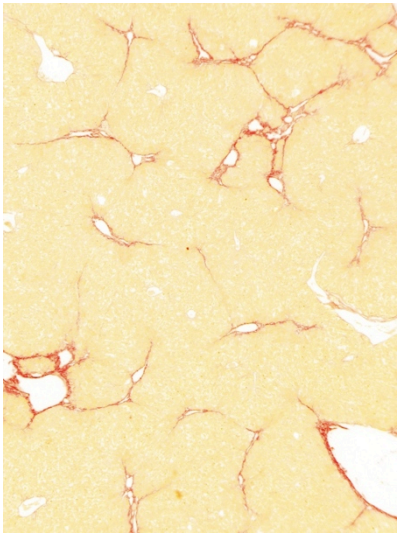

Image 2

**Figure 4-4: $CCl_4$ induced chronic liver injury, liver collagen content**

Symbols indicate median. Bars indicate interquartile range.

**Graph A:** Percentage Sirius red staining in liver FFPE tissue sections.
**Graph B:** Hydroxyproline content (µg/g of liver).
**Graph C:** Collagen 1α1 gene expression in whole liver homogenates.

**Image 1:** Sirius red at 48 hours. Control mouse. Original x40 magnification.
**Image 2:** Sirius red at 48 hours. αSMA-TFPI mouse. Original x40 magnification.

### *4.2.3. Hepatic stellate cell activation*

Digital image analysis of FFPE liver sections from mice culled at 24, 48, 72 and 96 hours after the last injection of $CCl_4$ were stained using an antibody for αSMA and showed a statistically significant decrease in the number of activated hepatic stellate cells in the livers of αSMA-TFPI mice compared to C57BL6/J control mice at 24 hours only (Mann Whitney test $p = 0.003$) but no significant difference at subsequent time points.

Review of the fold change in numbers of activated hepatic stellate from baseline showed a slightly different pattern. At 24 hours, the fold change from baseline was similar in both transgenic and control mice. Between 48 and 72 hours transgenic mice demonstrated a more pronounced increase in activated stellate cells – reaching a peak of 52 times that at baseline (compared to a peak of 26 times baseline in the control mice). At 72 hours transgenic mice still demonstrate a greater fold change in activated hepatic stellate cells from baseline, although not as marked as previous time points.

At 24 hours there were n=10 in the control group and n=9 in the αSMA-TFPI group. At 48, 72 and 96 hours there were n=5 in both the control and the αSMA-TFPI group. Some of these sample numbers were less than the power calculation sample number due to failed assays. Baseline sample numbers were as previously noted in section 3.1.

| Median number of αSMA+ cells (fold change from baseline) | Base-line | 24 hours | 48 hours | 72 hours | 96 hours |
|---|---|---|---|---|---|
| **Control** | 0.9 | **17.3 (19)** | 23.4 (26) | 16.8 (19) | 4.7 (5) |
| **αSMA-TFPI** | 0.4 | **9.2 (23)** | 19.8 (50) | 20.6 (52) | 5.7 (14) |

**Table 4-2: $CCl_4$ induced chronic liver injury, median number of activated hepatic stellate cells per HPF and fold change from baseline**

**BOLD figures =** statistically significant difference between αSMA-TFPI mice and control mice.

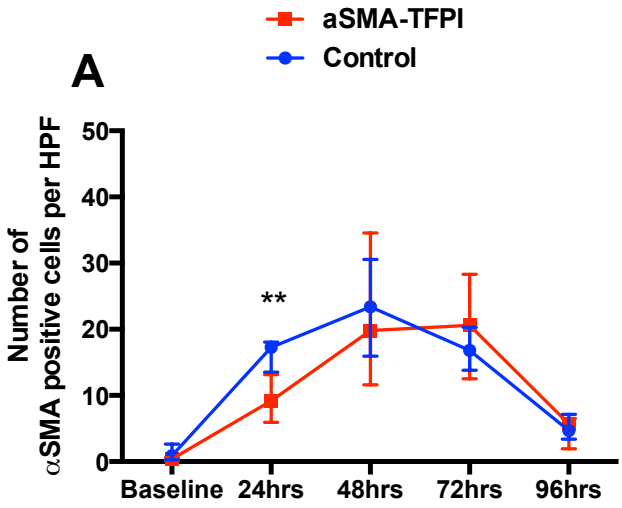


**Image 1**

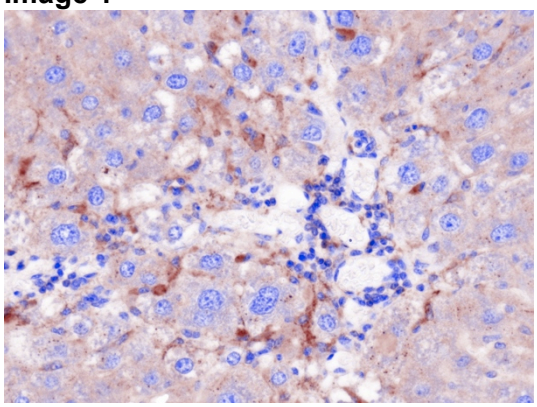

**Image 2**

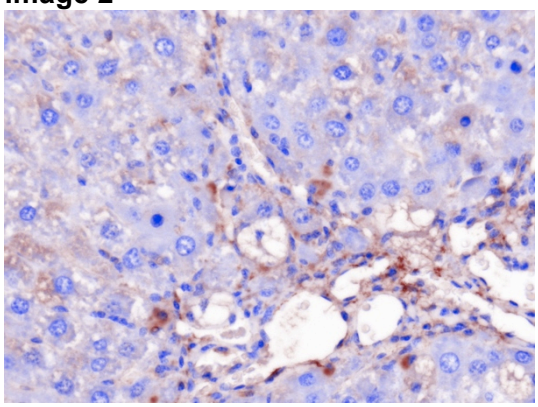

**Figure 4-5: $CCl_4$ induced chronic liver injury, αSMA immunohistochemistry**

Symbols indicate median. Bars indicate interquartile range.
** p=<0.01.
*See* Table 4-2 *for median values*

**Graph A:** Number of activated hepatic stellate cells in liver FFPE tissue sections as determined by αSMA immunohistochemistry.

**Image 1:** Anti-αSMA immunohistochemistry at 24 hours. Control mouse. Original x400 magnification. **Image 2:** Anti-αSMA immunohistochemistry at 24 hours. αSMA-TFPI mouse. Original x400 magnification.

### *4.2.4. Collagen turnover*

Quantitative PCR of cDNA reverse transcribed from whole liver homogenate RNA from mice culled at 24, 48, 72 and 96 hours after the last injection of $CCl_4$ showed no statistically significant difference in MMP2, MMP9 or TIMP1 gene expression in αSMA-TFPI mice compared to C57BL6/J control mice (Figure 4-6. Graphs A-C).

At 24 hours there were n=6 in the control group and n=9 in the αSMA-TFPI group for MMP2 expression. At 48, 72 and 96 hours there were n=5 in both the control and the αSMA-TFPI group for MMP2 expression.

At 24 hours there were n=9 in the control group and n=5 in the αSMA-TFPI group for MMP9 expression. At 48, 72 and 96 hours there were n=5 in both the control and the αSMA-TFPI group for MMP9 expression.

At 24 hours there were n=6 in the both control and the αSMA-TFPI group for TIMP1 expression. At 48 and 96 hours there were n=5 in both the control and the αSMA-TFPI group for TIMP1 expression. At 72 hours there were n=5 in the control group and n=5 in αSMA-TFPI group for TIMP1 expression.

Some of these sample numbers were less than the power calculation sample number due to failed assays. Baseline sample numbers were as previously noted in section 4.1.

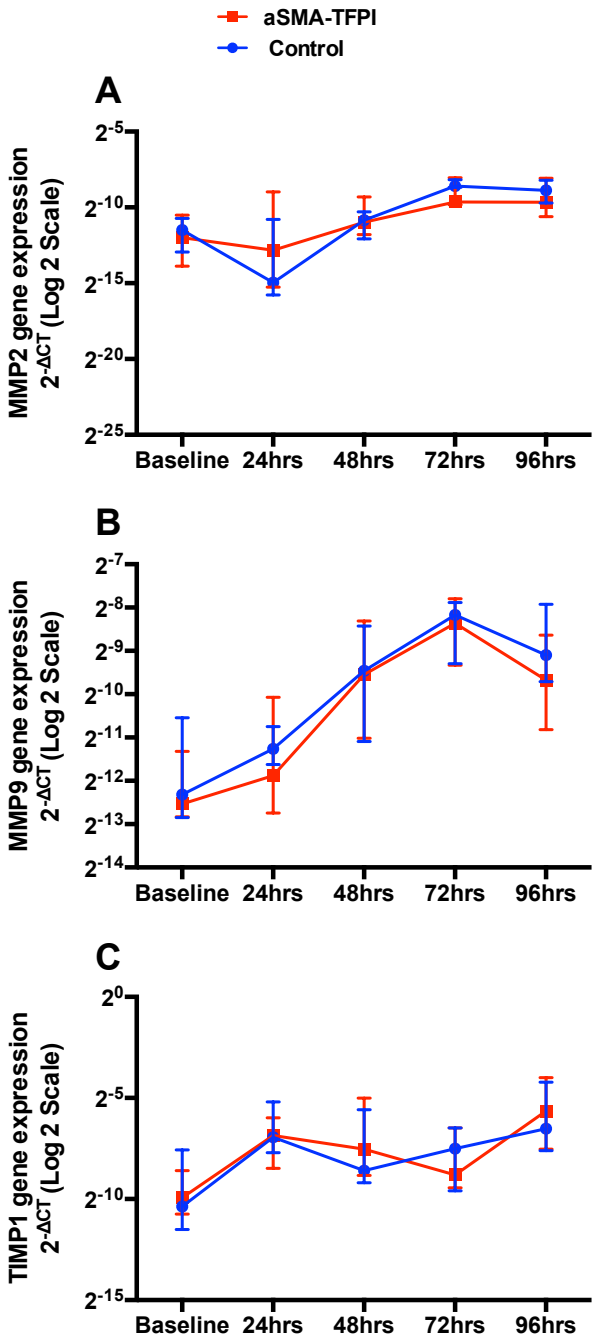


**Figure 4-6: $CCl_4$ induced chronic liver injury, matrixmetalloproteinase and TIMP gene expression**

**Graph A:** MMP2 gene expression in whole liver homogenates.

**Graph B:** MMP9 gene expression in whole liver homogenates.

**Graph C:** TIMP1 gene expression in whole liver homogenates.

### *4.2.5. Liver immune cell composition*

At baseline there were differences in the macrophage population phenotype and a trend towards decreased NK cells in αSMA-TFPI mice compared to C57BL6/J control mice (Section 3.1.3. Figure 3-4 and Figure 3-5).

Flow cytometry of fresh cells isolated from the liver showed a statistically significant decrease in the proportion of macrophages (CD45+ CD11b+ Ly6G- F4/80+ cells) in αSMA-TFPI mice compared to control mice culled at 24 hours after the last injection of $CCl_4$ (Mann Whitney test p = 0.02. Figure 4-7. Graph A). However, there was no statistically significant difference at subsequent time points.

Flow cytometric assessment of macrophage Ly6C expression showed no statistically significant difference in proportions of macrophages with intermediate / low or high Ly6C expression in αSMA-TFPI mice compared to control mice at any time point (Figure 4-7. Graphs B and C).

Flow cytometry of fresh cells isolated from the liver showed a statistically significant increase in the proportions of neutrophils in αSMA-TFPI mice compared to control mice culled at 24 hours after the last injection of $CCl_4$ (Mann Whitney test p = 0.008. Figure 4-7. Graph D). However, there was no statistically significant difference at subsequent time points.

Flow cytometry of fresh cells isolated from the liver showed a statistically significant decrease in the proportions of NK cells in αSMA-TFPI mice

compared to control mice culled at 24 hours after the last injection of $CCl_4$ (Mann Whitney test p = 0.008. Figure 4-8. Graph C). However, there was no statistically significant difference at subsequent time points.

There was no statistically significant difference in the proportions of T cells and B cells in αSMA-TFPI mice compared to control mice at any time point (Figure 4-8. Graphs A and B).

At 24, 48, 72 and 96 hours there were n=5 in both the control and the αSMA-TFPI group. Some of these sample numbers were less than the power calculation sample number due to failed assays. Baseline sample numbers were as previously noted in section 3.1.

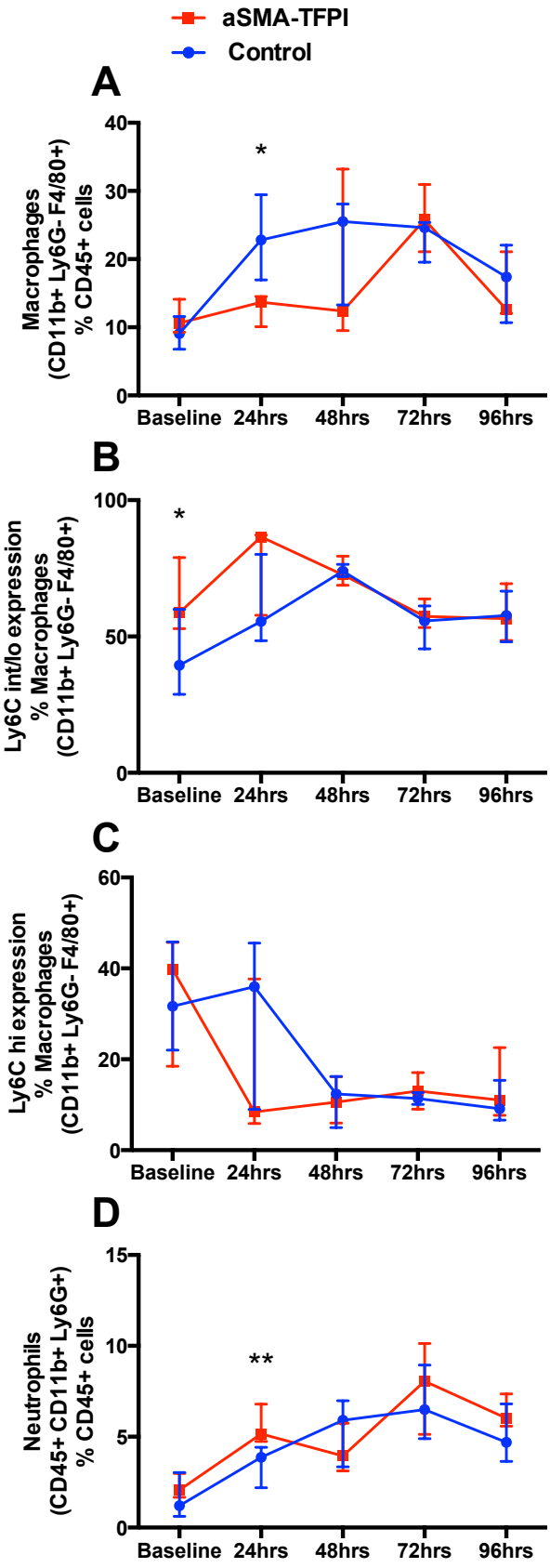


**Figure 4-7: $CCl_4$ induced chronic liver injury, liver macrophage and neutrophil populations**

Symbols indicate median. Bars indicate interquartile range.

* p=<0.05, ** p=<0.01

*See* Table 4-3 *for median values.*

**Graph A:** Macrophages (CD45+ CD11b+ Ly6G- F4/80+ cells) as a proportion of CD45+ (immune) cells.

**Graph B:** Macrophage expression of intermediate or low levels of Ly6C as a proportion of macrophages.

**Graph C:** Macrophage expression of high levels of Ly6C as a proportion of macrophages.

**Graph D:** Neutrophils (CD45+ CD11b+ Ly6G+ cells) as a proportion of CD45+ (immune) cells.

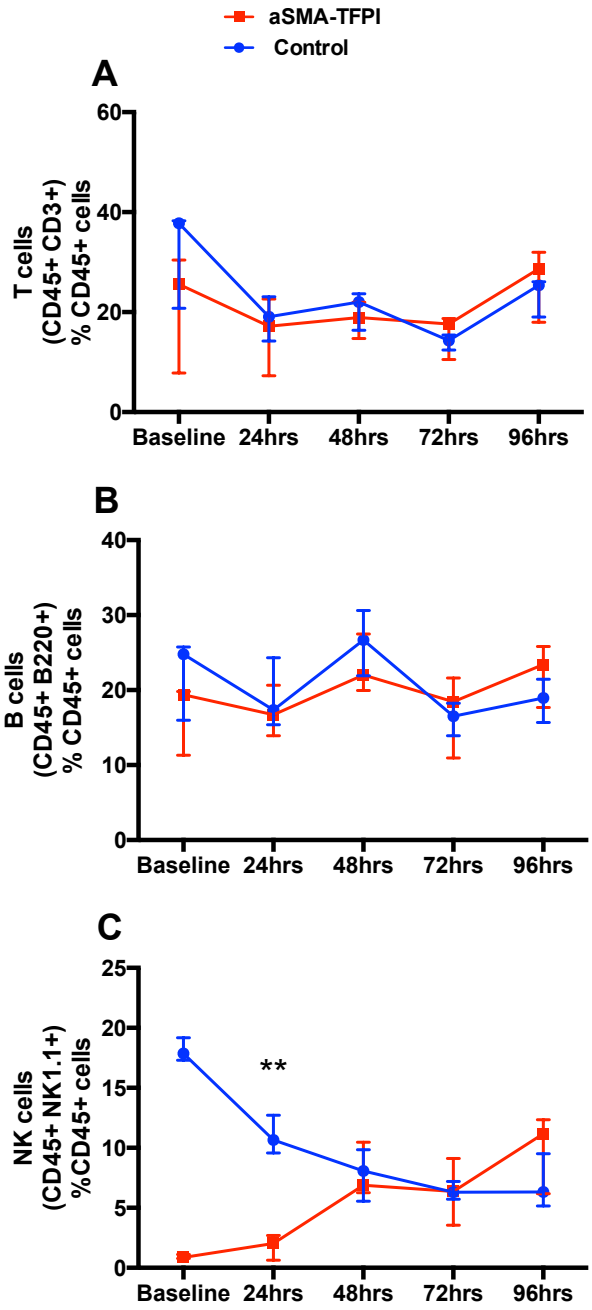


**Figure 4-8: $CCl_4$ induced chronic liver injury, liver T cell, B cell and NK cell populations**

Bars indicate median with interquartile range.

** p=<0.01

*See* Table 4-3 *for median values.*

**Graph A:** T cells (CD45+ CD3+ cells) as a proportion of CD45+ (immune) cells.

**Graph B:** B cells (CD45+ B220+ cells) as a proportion of CD45+ (immune) cells.

**Graph C**: NK cells (CD45+ NK1.1+ cells) as a proportion of CD45+ (immune) cells.

| Median immune cell proportions in each strain (fold change from baseline) | | Baseline | 24 hours | 48 hours | 72 hours | 96 hours |
|---|---|---|---|---|---|---|
| **Overall macrophage proportions (% CD45+ immune cells)** | **Control** | 9 | **23 (2.6)** | 26 (2.9) | 25 (2.8) | 17 (1.9) |
| | **aSMA-TFPI** | 11 | **14 (1.3)** | 12 (1.1) | 26 (2.4) | 13 (1.2) |
| **Proportion of cells with Ly6C int/lo expression (% macrophages)** | **Control** | **39** | 56 (1.4) | 74 (1.9) | 56 (1.4) | 58 (1.5) |
| | **aSMA-TFPI** | **59** | 87 (3.0) | 73 (1.2) | 57 (-1.0) | 57 (-1.0) |
| **Proportion of cells with Ly6C hi expression (% macrophages)** | **Control** | 32 | 36 (1.1) | 12 (-2.7) | 11 (-2.9) | 9 (-3.6) |
| | **aSMA-TFPI** | 40 | 8 (-5.0) | 11 (-3.6) | 13 (-3.1) | 11 (-3.6) |
| **Overall neutrophil proportions (% CD45+ immune cells)** | **Control** | 1.2 | **3.9 (3.3)** | 5.9 (4.9) | 6.5 (5.4) | 4.7 (3.9) |
| | **aSMA-TFPI** | 2.1 | **5.2 (2.5)** | 4.9 (2.3) | 8.1 (3.9) | 6.0 (2.9) |
| **Overall T cell proportions (% CD45+ immune cells)** | **Control** | 38 | 19 (-2.0) | 22 (-1.7) | 14 (-2.7) | 25 (-1.5) |
| | **aSMA-TFPI** | 26 | 17 (-1.5) | 19 (-1.4) | 18 (-1.4) | 29 (1.1) |
| **Overall B cell proportions (% CD45+ immune cells)** | **Control** | 25 | 17 (-1.5) | 27 (1.1) | 17 (-1.5) | 19 (-1.3) |
| | **aSMA-TFPI** | 19 | 17 (-1.1) | 22 (1.2) | 18 (-1.1) | 23 (1.2) |
| **Overall NK cell proportions (% CD45+ immune cells)** | **Control** | 18 | **11 (-1.6)** | 8.1 (-2.2) | 6.3 (-2.9) | 6.3 (-2.9) |
| | **aSMA-TFPI** | 0.9 | **2.0 (2.2)** | 6.9 (7.7) | 6.4 (7.1) | 11 (12) |

**Table 4-3: $CCl_4$ induced chronic liver injury, liver immune cell populations, median values and fold change from baseline.**

### *4.2.6. Transgenic TFPI expression*

Expression of the transgene was assessed using gel electrophoresis of PCR products from cDNA transcribed from DNase treated whole liver homogenate RNA.

Expression of the TFPI transgene was identified in 2/5 samples from αSMA-TFPI mice culled at 24 hours after the last injection of $CCl_4$; 5/5 samples from αSMA-TFPI mice culled at 48 hours after the last injection of $CCl_4$; 5/5 samples from αSMA-TFPI mice culled at 72 hours after the last injection of $CCl_4$ and 5/5 samples from αSMA-TFPI mice culled at 96 hours after the last injection of $CCl_4$.

Due to the lack of difference in the progression and resolution of liver fibrosis in the transgenic mice compared to the control mice, coupled with limited amounts of the transgene specific antigen for immunohistochemistry, only PCR detection of transgene expression was used.

### *4.2.7. Model summary - $CCl_4$ induced chronic liver injury*

After carbon tetrachloride ($CCl_4$) induced chronic liver injury the overall picture in αSMA-TFPI mice was of no significant difference in liver fibrosis or fibrosis resolution. The pattern of αSMA expression, indicative of the number of activated hepatic stellate cells, was similar to that in the published literature, although a peak was observed at 48 hours as opposed to 72 hours (see Figure 1-2). Liver fibrosis and resolution also followed a similar pattern to the published literature with peak Sirius red area staining at 72 hours (Ramachandran et al. 2012).

However αSMA-TFPI mice did demonstrate some changes at 24 hours that mirror those seen in the paracetamol induced acute liver injury model, further supporting the role of TFPI and the coagulation cascade in liver injury.

At 24 hours after the last dose of $CCl_4$, transgenic mice showed a statistically significant decrease in hepatic stellate cell activation and a global decrease in macrophages within the liver with a greater predominance of (although not statistically significant) the $Ly6C^{int/lo}$ pre-resolution population.

This relationship was seen at 48 hours in the paracetamol induced acute liver injury experiments and has also been demonstrate in PAR-2 knockout mice, PAR-1 knockout mice, low-TF mice and mice administered a thrombin antagonist (Sullivan, Weinreb, et al. 2010; Kallis et al. 2014; Duplantier et al. 2004). The published literature suggests that the loss of PAR-1 activation (knockout model or loss of thrombin induced activation) prevents or limits a

pro-fibrotic microenvironment (including reduced TGF-β signalling) and inflammatory cell recruitment to the liver (possibly via reduced MCP-1 signalling). Kallis et al specifically saw a decrease in the recruitment bone marrow derived macrophages with the loss of PAR-1 signalling. Loss of PAR-2 activation was also associated with a decreased in hepatic macrophages and loss of TGF-β signalling.

It could therefore be hypothesised that the changes seen in the αSMA-TFPI model at 24 hours represents the action of transgenic TFPI, via alteration of the coagulation cascade and PAR activation (blockade of TF action, prevention of TF / VIIa / Xa PAR-2 signalling or reduced thrombin or Xa PAR-1 activation) but that the effect is not of the same magnitude as that seen in other models. The reason for this reduced effect may be due to the cell specific expression of the transgenic TFPI compared to the global knockout / reduced expression / molecule blockade in the other models.

At 24 hours after the last dose of $CCl_4$, transgenic mice showed a statistically significant increase in neutrophils and decrease in NK cells compared to controls. At baseline, transgenic mice had a lower proportion of NK cells compared to controls and so this significant decrease at 24 hours may simply represent a lower starting point for transgenic mice compared to control mice with adequate / control equivalent recruitment of NK cells to the liver. In the setting of chronic liver injury however this is surprising as there had been repeated / on going stimuli for NK cell recruitment. It is not possible to fully elucidate the reason for this result from this work and further investigation of

inflammatory cytokines may help explain the recruitment of cells to the liver in these models.

Neutrophils are responsible for tissue injury and a pro-inflammatory microenvironment. The reasons for the increase in neutrophils at 24 hours cannot be elucidated from the results in this work however their role in promoting a pro-inflammatory environment might explain the transition of the transgenic model from a comparatively pro-resolution phenotype to one that mirrored the control mice. As with the NK cell result further investigation of inflammatory cytokines may help explain the recruitment of cells to the liver in these models.

## 4.3. Chapter Results Summary Table

| Parameter measured | $CCl_4$ chronic liver injury model vs. control (24, 48, 72 and 96 hours) |
|---|---|
| **Liver collagen content** | No difference. |
| **Hepatic stellate cell activation** | Decreased activation at 24 hours. |
| **MMP2 / MMP9 gene expression** | No difference. |
| **TIMP1 gene expression** | No difference. |
| **Liver Immune cell composition** | Decreased proportion of macrophages at 24 (and 48) hours.<br>Macrophage population at 24 hours with proportionally greater $Ly6C^{int/lo}$ expression.<br>Decreased proportion of neutrophils at 24 hours.<br>Decreased proportion of NK cells at 24 hours (reduced at baseline also). |
| **Liver injury** | Decreased ALT at 24 hours. |

**Table 4-4: Summary of chronic liver injury models in αSMA targeted expression of TFPI**

Text in grey = non significant ($p<0.05$) trend

## 5. CD31 targeted expression of TFPI in acute liver injury

The genome of the transgenic mouse strain CD31-TFPI contains a construct that initiates the expression of human TFPI when a cell expresses CD31. The biological effect is therefore cell specific expression of TFPI beyond normal physiological expression.

### 5.1. Baseline parameters

The baseline (uninjured) liver phenotype of the CD31-TFPI mice was defined to help analyse data from experimental studies.

#### *5.1.1. Plasma liver function tests*

Plasma markers of liver function are widely used as minimally invasive markers of liver injury and function.

There were n=13 in the control group and n=16 in the CD31-TFPI group (except for albumin values, where n=8 in the CD-TFPI group due to failed assays in one batch).

Alanine aminotransferase (ALT) is released from injured hepatocytes. Average ALT levels in C57BL6/J mice aged 6-16 weeks are 42-80IU/L (Grubb et al. 2014). Median ALT values for CD31-TFPI mice fell within this range but median ALT values for C57BL6/J control mice were below this range.

There was a statistically significant (Mann Whitney U test; $p = 0.01$) increase in plasma ALT of CD31-TFPI mice compared to control mice (Figure 5-1.

Graph A). There were a number of outliers within the ALT results. Removal of these outliers did not affect the significance of the result. Examination of the individual cases showed that these elevated readings were not associated with sample haemolysis or elevation of other liver function parameters and the median ALT value for this group remained within the normal range.

Alkaline phosphatase (ALP) is an enzyme produced by cholangiocytes and can be elevated when there is damage to these cells. Of note ALP is also produced by bone and can be elevated due to bone disease. Average ALP levels in C57BL6/J mice are 68-140IU/L (Grubb et al. 2014). Median ALP values for CD31-TFPI and control mice in this work fell just below this range and there was no statistically significant difference in plasma ALP of CD31-TFPI mice compared to control mice (Mann Whitney test, p=0.52. Figure 5-1. Graph B).

Total bilirubin measures unconjugated and conjugate bilirubin, the breakdown product of haemoglobin. The liver is responsible for conjugation and excretion of bilirubin. Elevated levels of total bilirubin suggest liver injury and decreased bilirubin metabolism, bile duct injury obstructing bilirubin excretion or increased breakdown of haemoglobin. Average total bilirubin levels in C57BL6/J mice aged 8-11 weeks are 0.48-1.35 μmol/L (Grubb et al. 2014). Median total bilirubin values for CD31-TFPI and control mice in this work were above the normal range presented in the literature. However, there was no statistically significant difference in plasma total bilirubin of CD31-TFPI mice

compared to C57BL6/J control mice (Mann Whitney test, p=0.63. Figure 5-1. Graph C).

Decreased levels of albumin can indicate chronic impairment of the livers synthetic function. Average albumin levels in C57BL6/J mice aged 8-11 weeks are 31-39g/L (Grubb et al. 2014). Median albumin values for CD31-TFPI and control mice in this work were below the normal range presented in the literature and there was a statistically significant (Mann Whitney U test, p=0.004) increase in plasma albumin of CD31-TFPI mice compared to control mice (Figure 5-1. Graph D).

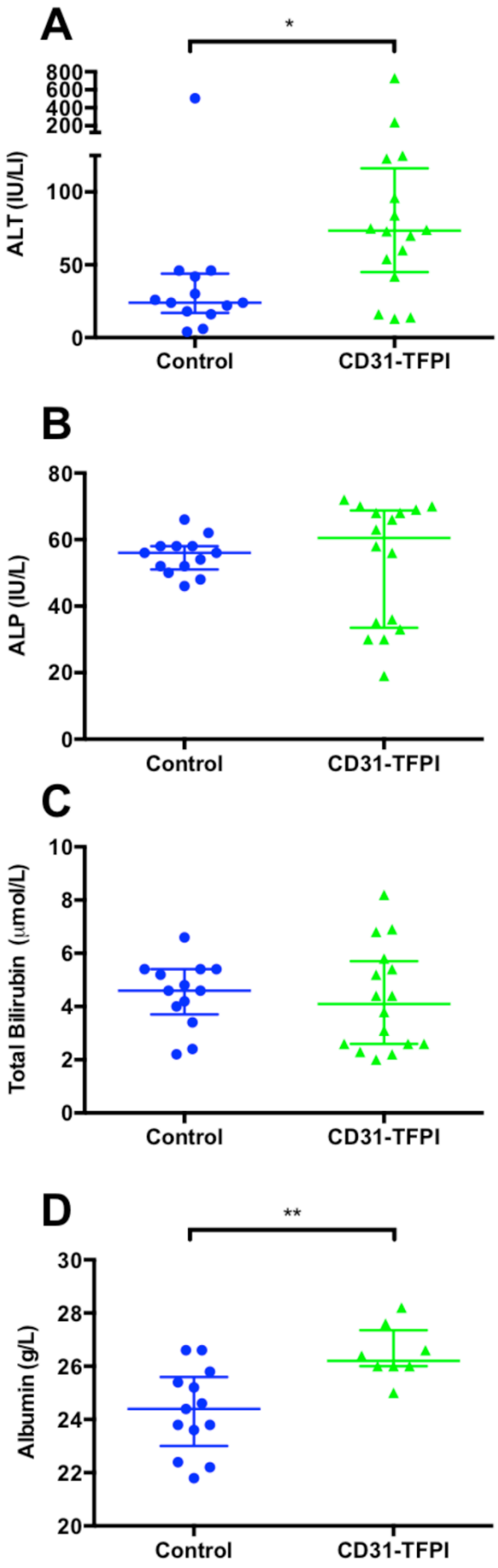


**Figure 5-1: Baseline plasma liver function test results**

Bars indicate median with interquartile range.

* p=<0.05; ** p=<0.01

**Graph A**: Plasma ALT (IU/L). Median 24IU/L and 74IU/L in control and CD31-TFPI strains respectively.

**Graph B:** Plasma ALP (IU/L). Median 56IU/L and 61IU/L in control and CD31-TFPI strains respectively.

**Graph C:** Plasma total bilirubin (μmol/L). Median 4.6μmol/L and 4.1μmol/L in control and CD31-TFPI strains respectively.

**Graph D:** Plasma albumin (g/L). Median 24.4g/L and 26.2g/L in control and CD31-TFPI strains respectively.

### *5.1.2. Baseline transgenic TFPI expression*

Genomic carriage of the transgene was confirmed by end point PCR and gel electrophoresis of PCR products. Only mice with proven genomic carriage of the transgene were termed CD31-TFPI mice and used in experiments.

Expression of the transgene was assessed using immunohistochemistry and / or PCR. Immunohistochemistry for human TFPI was performed on FFPE liver, kidney, spleen, lung and heart sections. End point PCR was performed on cDNA reverse transcribed from whole liver homogenate DNAse treated RNA.

The anti-human TFPI antibody used in the immunohistochemistry was specific to amino acids 29-44 of the human TFPI protein, a portion of the protein present in the transgene that has only 31.25% homology with the mouse TFPI protein. Specificity was confirmed by negative staining in tissue from C57BL6/J control mice.

FFPE tissue from the spleens of CD31-TFPI mice demonstrated staining consistent with expression of the transgene in CD31 positive sinusoidal endothelial cells and dendritic cells / macrophages but not the endothelium of the splenic arterioles (faint, non-specific staining seen, **Figure 5-2**. Image 1 and 2). No expression of the transgene was seen in liver, kidney, lung or heart.

Gene expression was identified on gel electrophoresis of PCR products in 1 in 5 liver homogenate samples from baseline CD31-TFPI mice. Further amplification of PCR products from the 4 negative liver homogenate samples

showed gene expression in 3 of these samples (total 4/5 positive). At both steps there was no expression detected in control samples (**Figure 5-2**. Image 3 and 4).

The results from the immunohistochemistry and liver homogenate gene expression suggest very low levels of transgene expression in the livers of the CD31-TFPI mice at baseline.

**Image 1**

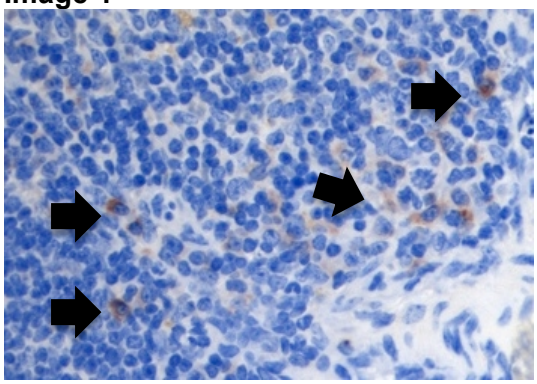

**Image 2**

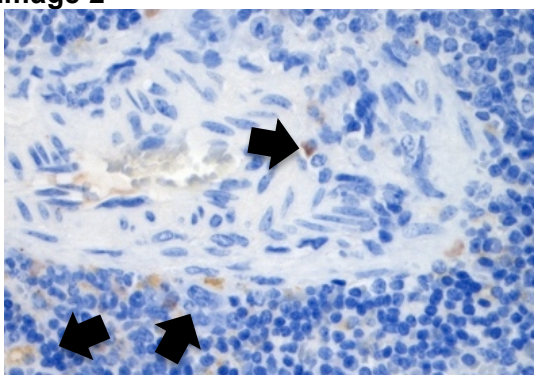

**Image 3**

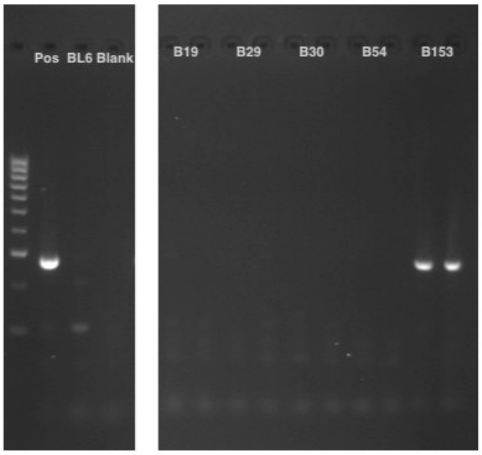


**Image 4**

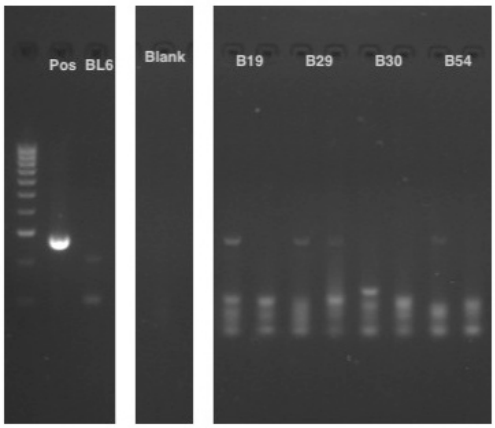


**Figure 5-2:** Baseline transgenic TFPI expression

**Image 1:** Anti-human TFPI immunohistochemistry. Splenic sinusoidal endothelial cells and macrophages. CD31-TFPI mouse. Spleen. Original x400 magnification.
**Image 2:** Anti-human TFPI immunohistochemistry. Splenic sinusoidal endothelial cells and macrophages. CD31-TFPI mouse. Spleen. Original x400 magnification.

**Image 3:** PCR product gel electrophoresis. CD31-TFPI baseline samples (B19, B29, B30, B54, B153). PCR of 1µL of cDNA transcribed from liver homogenate RNA. B153 shows strong positive bands.
**Image 4:** PCR product gel electrophoresis. CD31-TFPI baseline samples (B19, B29, B30, B54). PCR of 1.5µL of PCR product amplified from the PCR product produced in Image 3. Positive bands seen in samples B19, B29 and B54.

Pos = genomic DNA positive control.
BL6 = control (C57BL6/J) liver homogenate cDNA (negative control).
Blank = non-template control.

### *5.1.3. Summary – Baseline parameters*

The CD31-TFPI mice showed little or no transgenic TFPI gene expression in the liver and very low levels of protein expression in only the spleen at baseline. Given the transgene expression model (surface expression of TFPI when CD31 is expressed at the cell membrane) the low level of transgenic TFPI expression is likely to be due to low levels of cell surface CD31 expression in the liver. In the liver CD31 is predominantly expressed on activated liver sinusoidal endothelial cells (LSEC) and in the uninjured liver their cell surface expression of CD31 is low (DeLeve et al. 2004). This was confirmed by CD31 immunohistochemical staining of uninjured liver (see Appendix). Other CD31 positive cells in the liver include Kupffer cells, platelets and other immune cells in relatively low numbers.

Despite this, the CD31-TFPI mice did had an elevated average plasma ALT compared to control mice. This average was however within physiological range for the background C57BL6/J strain. All blood samples were collected and stored in the same way and each set of plasma tests was performed on the same machine in one batch. Routine health screening undertaken by the animal care facility where the mice were housed showed no evidence of mouse hepatitis virus in CD31-TFPI mice. In addition measurements of cellular proliferation and hepatic stellate cell activation were not elevated in CD31-TFPI mice compared to controls (see section 6.1 on baseline parameters in chronic liver injury) and plasma ALP and bilirubin levels were similar between the strains. Therefore although the results represent a true difference between the CD31-TFPI and control mice (and not analysis

artefact), the impact of this baseline difference may be of no physiological significance.

Both CD31-TFPI and control mice in this study demonstrated plasma total bilirubin levels above the normal range. There was no indication that either strains of mice had bile duct injury (plasma ALP not elevated, no evidence of bile duct damage or bilirubinostasis on histology) and there was no identifiable reason for both strains to have an increased turnover of erythrocytes therefore the reason for the plasma total bilirubin result is likely to be associated with either diet or blood collection, processing and analysis methods. As all mice were maintained on the same diet and all blood samples collected and processed in the same way it is unlikely that this finding would affect conclusions drawn from experimental models.

Similarly the lower than normal range of plasma albumin levels seen in both CD31-TFPI and control mice is likely to represent variation in either diet or blood collection, processing and analysis methods. The elevated plasma albumin seen in CD31-TFPI mice compared to control mice was physiologically small (only 1.8g/L difference in median values) and is likely to represent the fact that although brought in control mice were housed in the same room as the CD31-TFPI mice and acclimatised to their surroundings for at least 5 days prior to cull, their diet prior to arrival and the stress of transport (disrupting feeding patterns) may have negatively affected the control mice plasma albumin levels. Of note, brought in control mice used in experiments (as opposed to baseline animals) tended to have a greater delay between

transportation / arrival in the unit and the date they were culled (time from arrival to experimental cull ranged from 6 days to 84 days in control mice, depending on the experimental protocols they underwent).

These baseline differences have been taken into consideration when analysing injury model data.

## 5.2. Paracetamol induced acute liver injury

Paracetamol toxicity induces centrilobular hepatocellular necrosis with a marked inflammatory cell infiltrate.

300-350mg/kg of paracetamol was administered to mice via intraperitoneal injection. Mice were culled at 6, 12 and 24 hours after administration of paracetamol.

### *5.2.1. Plasma liver function tests*

As previously noted, there were statistically significant differences in baseline ALT and albumin in CD31-TFPI transgenic mice compared to control mice (Figure 5-1. Graphs A and D, CD31-TFPI mice had elevated plasma ALT and albumin compared to controls).

At 6 hours there were n=5 in both the control and the CD31-TFPI group. At 12 hours there were n=4 in both the control and the CD31-TFPI group. At 24 hours there were n=6 in the control group and n=7 in the CD31-TFPI group for ALP and total bilirubin, n=6 in the CD31-TFPI group for ALT and n=5 in the CD31-TFPI group for albumin. Some of these sample numbers were less than the power calculation sample number due to failed assays. Baseline sample numbers were as previously noted in section 5.1.

At 6 hours after administration of paracetamol there was no statistically significant difference in any plasma liver function tests of CD31-TFPI mice compared to control mice. There was a trend towards a lower plasma ALT in

the CD31-TFPI mice compared to control mice, with median ALT values of 118IU/L and 896IU/L respectively. A single high outlier in the CD31-TFPI group (ALT 13044IU/L, Figure 5-3. Graph A) was identified. Removal of this outlier from statistical analysis did not alter the significance of the results and it is possible that for this parameter the statistical analysis may have been limited by the number per group.

At 12 hours after administration of paracetamol there was a statistically significant decrease in the plasma ALT, ALP and albumin of CD31-TFPI mice compared to control mice (Mann Whitney U test, ALT p=0.03, ALP p=0.03, Albumin, p=0.03; Figure 5-3. Graphs A, B and D respectively).

At 24 hours after administration of paracetamol there was no statistically significant difference in any plasma liver function tests of CD31-TFPI mice compared to control mice and review of the data shows similar median and interquartile ranges.

| Median plasma values in each strain (fold change from baseline) | | Baseline | 6 hours | 12 hours | 24 hours |
|---|---|---|---|---|---|
| **ALT IU/L** | **Control** | **24** | 896 (37) | **4399 (183)** | 2553 (106) |
| | **CD31-TFPI** | **74** | 118 (1.6) | **182 (2.5)** | 2806 (38) |
| **ALP IU/L** | **Control** | 56 | 112 (2.0) | **154 (2.8)** | 126 (2.3) |
| | **CD31-TFPI** | 61 | 141 (2.3) | **92 (1.5)** | 100 (1.6) |
| **Total bilirubin µmol/L** | **Control** | 4.6 | 5.6 (1.2) | 4.5 (1.0) | 8.7 (1.9) |
| | **CD31-TFPI** | 4.1 | 5.7 (1.4) | 5.9 (1.4) | 6.6 (1.6) |
| **Albumin g/L** | **Control** | **24.4** | | **28.5 (1.2)** | 26.9 (1.1) |
| | **CD31-TFPI** | **26.2** | | **24.7 (-1.1)** | 30.4 (1.2) |

**Table 5-1: Paracetamol induced acute liver injury, median plasma liver function tests values and fold change from baseline**

**BOLD figures =** statistically significant decrease in value in CD31-TFPI mice compared to control mice.

A fold change of 1.0 indicates a x1.0 increase in the value, or no change.
A negative fold change indicates a decrease in the value.

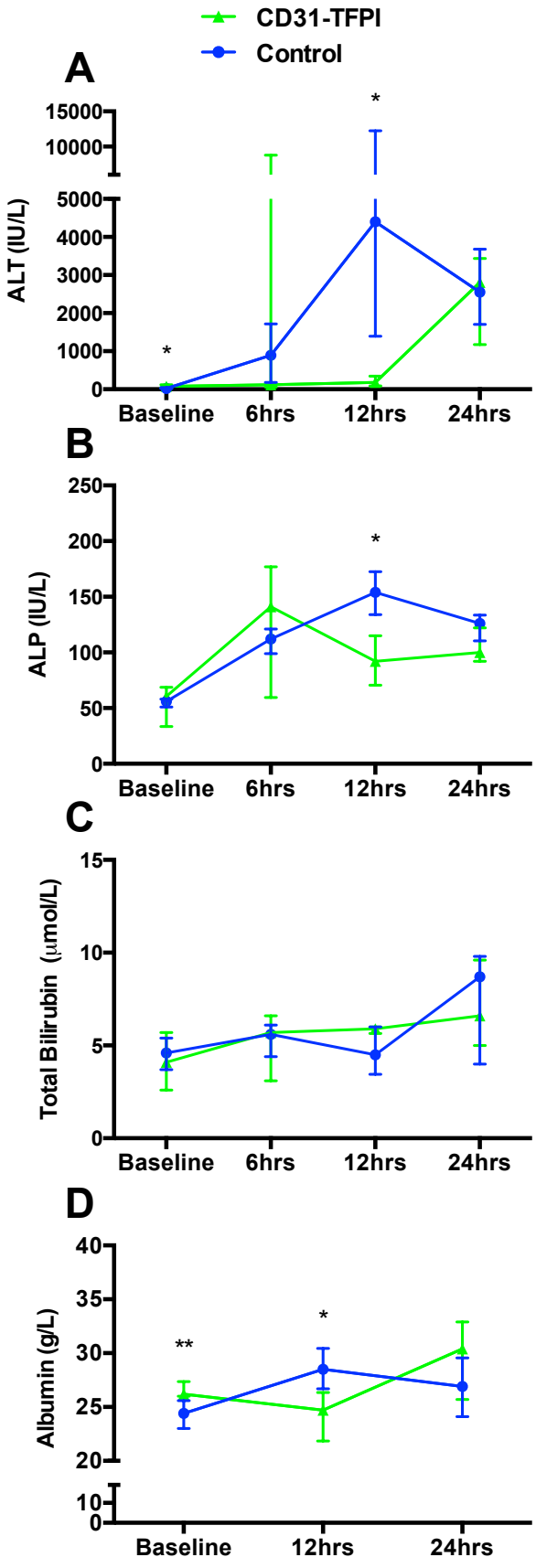


**Figure 5-3: Paracetamol induced acute liver injury, plasma liver function tests**

Symbols indicate median. Bars indicate interquartile range.

* p=<0.05. ** p=<0.01.

*See* Table 5-1 *for median values.*

**Graph A**: Plasma ALT (IU/L).

**Graph B:** Plasma ALP (IU/L).

**Graph C:** Plasma total bilirubin (µmol/L).

**Graph D:** Plasma albumin (g/L).

### *5.2.2. Hepatocellular necrosis*

Digital image analysis of percentage area necrosis in H&E stained liver FFPE tissue sections showed no statistically significant difference in CD31-TFPI mice compared to control mice. There were n=5 in both the control and the CD31-TFPI group at each time point.

There was a trend towards less necrosis in the CD31-TFPI mice compared to control mice at 6 hours with median percentage area necrosis of 0.2% and 11.6% respectively. A single outlier was identified in the CD31-TFPI group (35% necrosis, Figure 5-4. Graph A). Removal of this outlier from statistical analysis did not alter the significance of the results and it is possible that for this parameter the statistical analysis may have been limited by the number per group.

There was a trend towards less necrosis at 12 hours in the CD31-TFPI mice compared to control mice with median percentage area necrosis of 8.5% and 22.1% respectively. At this time point there was quite variable results in both experimental arms (ranges of 1.1-23.2% in CD31-TFPI and 18.4-51.1% in control mice) and again, and it is possible that for this parameter the statistical analysis may have been limited by the number per group (CD31-TFPI n=5, control n=5).

At 24 hours there was a trend towards more necrosis in the CD31-TFPI mice compared to control mice with median percentage area necrosis of 49.6% and 28.2% respectively. At this time point there was quite variable results in both

experimental arms (ranges of 11.7-85.9% in CD31-TFPI and 17.3-50.9% in control mice) and again, it is possible that for this parameter the statistical analysis may have been limited by the number per group (CD31-TFPI n=5, control n=5).

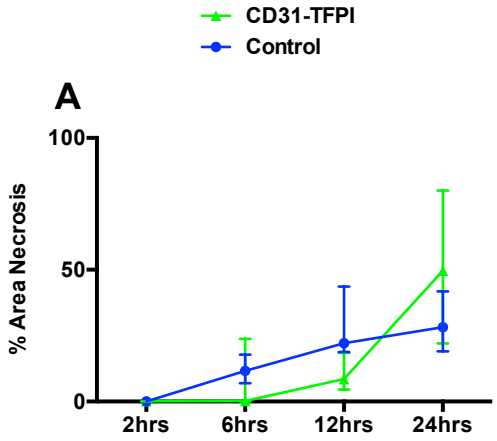


**Image 1**

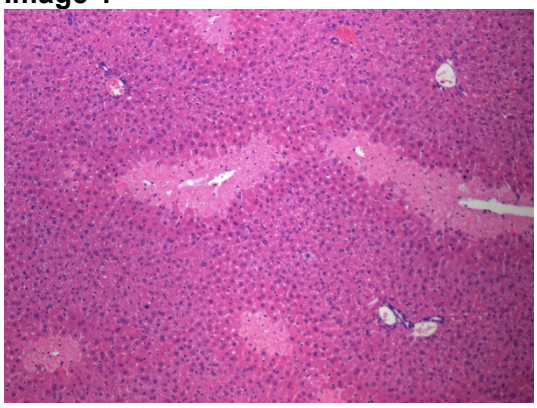

**Image 2**

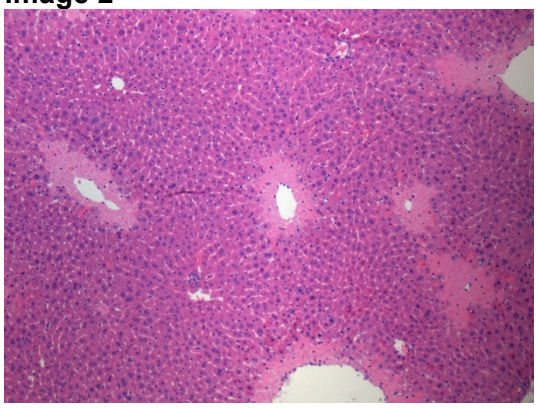

**Image 3**

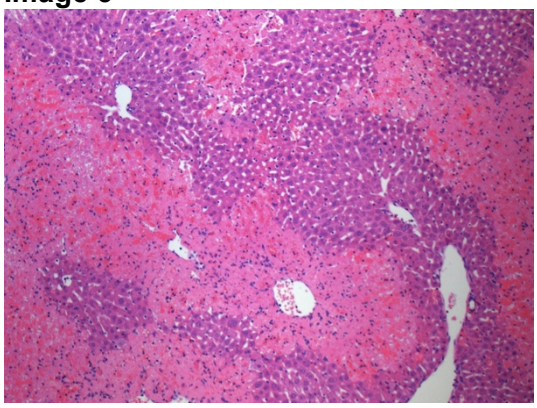

**Image 4**

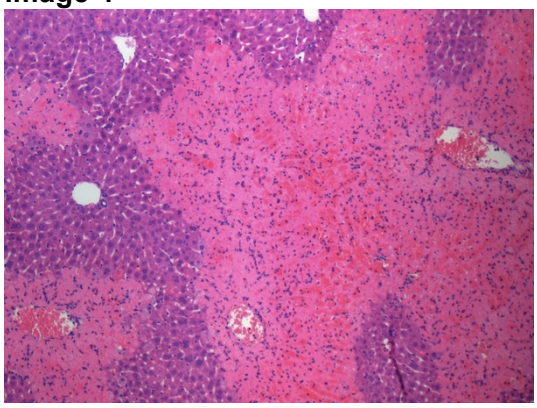

**Figure 5-4: Paracetamol induced acute liver injury, hepatocellular necrosis**

Symbols indicate median. Bars indicate interquartile range.

**Graph A:** Percentage area necrosis in liver FFPE tissue sections.

**Image 1:** Hepatocellular necrosis at 6 hours. Control mouse. Original x100 magnification. **Image 2:** Hepatocellular necrosis 6 hours. CD31-TFPI mouse. Original x100 magnification.

**Image 3:** Hepatocellular necrosis at 24 hours. Control mouse. Original x100 magnification. **Image 4:** Hepatocellular necrosis at 24 hours. CD31-TFPI mouse. Original x100 magnification.

### *5.2.3. Transgenic TFPI expression*

Expression of the transgene was assessed using PCR. Gene expression of the TFPI transgene was identified in 0/5 samples from CD31-TFPI mice culled 24 hours after administration of paracetamol, before and after amplification of initial PCR products.

Due to the lack of significant difference in the degree of hepatocellular injury / necrosis in the transgenic mice compared to the control mice, coupled with limited amounts of the transgene specific antigen for immunohistochemistry and no detection of the transgene by PCR, only PCR detection of transgene expression was used.

### *5.2.4. Model summary - paracetamol induced acute liver injury*

After paracetamol induced acute liver injury the overall picture in CD31-TFPI mice was of delayed but overall equivalent hepatocellular necrosis compared to controls. Data from this project and the literature suggests hepatocellular necrosis peaks at 24 hours after paracetamol administration and that plasma liver function tests peak at 12-24 hours (Jaeschke et al. 2014). Taken together with the lack of evidence to suggest transgenic TFPI was being expressed in the liver of these mice at 24 hours the model was halted at the 24 hours time point. Despite this, the model provided further evidence to suggest that TFPI does alter the progression acute liver injury when the result were considered alongside those of the αSMA-TFPI model.

The pattern of injury suggests that in the CD31-TFPI mice the inhibition of the TF / VIIa / Xa complex by the transgenic TFPI expressed on CD31+ cells limited early but not late acute liver injury. This is most striking at 12 hours when there is a marked decrease in plasma markers of acute liver injury in the CD31-TFPI mice. This corresponded with decreased but not statistically significant, hepatocellular necrosis. The reason for this difference (plasma vs. H&E stained FFPE liver sections) may be due to lobar heterogeneity of hepatocellular necrosis after paracetamol induced liver injury. Plasma markers are more representative of the overall extent of liver injury but are not necessarily specific for liver injury. Whereas H&E stained FFPE sections of the liver are specific for liver injury but dependant on sampling and may suffer from sampling error (selection of less injured areas).

Every effort was made to address sampling errors between experimental groups through systematic sampling of the liver (see Methods 2.4.1 and Figure Figure 2-1), however this may not have fully accounted for variable distribution of hepatocellular necrosis.

This pattern of injury seen in the CD31-TFPI mice (limited early but not late acute liver injury) differs from the results seen when TFPI expression was targeted at αSMA+ cells. The difference may be due to the earlier injury / activation of liver sinusoidal endothelial cells and tissue resident CD31+ Kupffer cells in paracetamol induced liver injury. Ito et al described their activation between 0.5 to 6 hours and 0.5 to 12 hours respectively (compared to maximal activation of αSMA+ hepatic stellate cells between 48 and 72 hours) (Ito et al. 2003).

This pattern of early protection from paracetamol induced acute liver injury is in keeping with the pattern of liver injury seen in low-TF mice, mice administered heparin or lepirubin (to inhibit thrombin) and PAR-1 knockout mice (Ganey et al. 2007; Miyakawa et al. 2015). Ideally, it would have been useful to demonstrate the distribution and extent of fibrin clot formation, to support the impact of transgenic TFPI expression acting through its role in reducing microvascular clot formation. However, due to limited time and resources (fibrin antibody for immunohistochemistry) and the overall lack of statistical significance in this model, this was not undertaken.

In these papers the authors attributed the pattern of injury and loss of protection at 24 hours to coagulation cascade propagation with clot formation despite low levels of tissue factor (TF) or thrombin inhibition and in turn the activation of PAR-1. The reason for the time limited effect of PAR-1 loss was not explored by the authors but it could be hypothesised that control level liver injury was the result of microvascular thrombus associated hypoxia and alternate PAR activation.

The impact of the increased baseline plasma ALT and albumin in CD31-TFPI mice compared to control mice is hard to evaluate as the transgenic strain demonstrated less elevation of these parameters compared to controls. It is therefore likely, as discussed in section 5.1.3, that the biological impact of the baseline differences was minimal.

This set of experiments was at times limited by the number of animals per group. A power calculation had suggested that 6 animals per arm would provide the data to evaluate the model however in some analyses there was not data from 6 animals per arm; the plasma liver function tests especially suffered from sample exclusion due to haemolysis. Repetition of experimental groups could have addressed this but because the model had provided data supporting published work and the body of work from the αSMA-TFPI model, plus the overall lack of difference in the degree of liver injury at 24 hours, I felt that the repetition of work in this way was contrary to the 3Rs of animal research (refinement, replacement and reduction) and would not add significantly to the scientific value of the data already collected.

## 5.3. Alpha-naphthylisothiocyanate (ANIT) induced acute liver injury

ANIT (α-naphthylisothiocyanate) induces cholestatic, bile duct centric liver injury.

60mg/kg of ANIT was administered to mice via oral gavage. Mice were culled at 6, 24 and 48 hours after administration of ANIT.

### *5.3.1. Plasma liver function tests*

As previously noted, there were statistically significant differences in baseline ALT and albumin in CD31-TFPI transgenic mice compared to control mice (Figure 5-1. Graphs A and D, CD31-TFPI mice had elevated plasma ALT and albumin compared to controls).

At 6 hours there were n=5 in both the control and the CD31-TFPI group. At 24 hours there were n=5 in the control group and n=7 in the CD31-TFPI group. At 48 hours there were n=4 in the control group and n=7 in the CD31-TFPI. Some of these sample numbers were less than the power calculation sample number due to failed assays. Baseline sample numbers were as previously noted in section 5.1.

At 6 hours after administration of ANIT there was a statistically significant decrease in ALP in CD31-TFPI mice compared to C57BL6/J control mice (Mann Whitney U test, $p = 0.02$. Figure 5-5. Graph B). No other plasma liver function tests showed any statistically significant difference. Review of the data showed that there was a trend towards decreased plasma albumin in the

CD31-TFPI mice compared to controls but that there were only 5 mice in each arm and this may have limited the statistical analysis.

At 24 hours after administration of ANIT there was a statistically significant decrease in ALT, ALP and total bilirubin in CD31-TFPI mice compared to control mice (Mann Whitney U test, $p = 0.003$, $p = 0.003$ and $p = 0.01$ respectively). Figure 5-5. Graphs A, B and C respectively).

At 48 hours after administration of ANIT there was no statistically significant difference in any plasma liver function tests of CD31-TFPI mice compared to control mice. Review of the data showed a trend towards increased ALT and decreased plasma bilirubin in CD31-TFPI mice compared to control mice, however there were only 4 mice in each arm and this may have limited statistical analysis (Table 5-2. Figure 5-5. Graphs A-D). Of note, given the baseline difference in ALT in CD31-TFPI mice, at 48 hours after administration of ANIT the fold change from baseline was 2.6 and 6.0 in CD31-TFPI mice compared to control mice respectively but this did represent a marked worsening (increase) plasma ALT in the CD31-TFPI mice.

| Median plasma values in each strain (fold change from baseline) | | Baseline | 6 hours | 24 hours | 48 hours |
|---|---|---|---|---|---|
| **ALT IU/L** | **Control** | **24** | 30 (1.3) | **102 (4.3)** | 145 (6.0) |
| | **CD31-TFPI** | **74** | 56 (-1.3) | **38 (-1.9)** | 192 (2.6) |
| **ALP IU/L** | **Control** | 56 | **132 (2.4)** | **98 (1.8)** | 73 (1.3) |
| | **CD31-TFPI** | 61 | **106 (1.7)** | **60 (1.0)** | 64 (1.0) |
| **Total bilirubin µmol/L** | **Control** | 4.6 | 9.4 (2.0) | **9.6 (2.1)** | 10.6 (2.3) |
| | **CD31-TFPI** | 4.1 | 9.6 (2.3) | **6.0 (1.5)** | 5.8 (1.4) |
| **Albumin g/L** | **Control** | **24.4** | 25.4 (1.0) | 21.6 (-1.1) | 21.2 (-1.2) |
| | **CD31-TFPI** | **26.2** | 23.8 (-1.1) | 20.8 (-1.3) | 20.4 (-1.3) |

**Table 5-2: ANIT induced acute liver injury, median plasma liver function tests values and fold change from baseline**

**BOLD figures =** statistically significant decrease in value in CD31-TFPI mice compared to control mice.

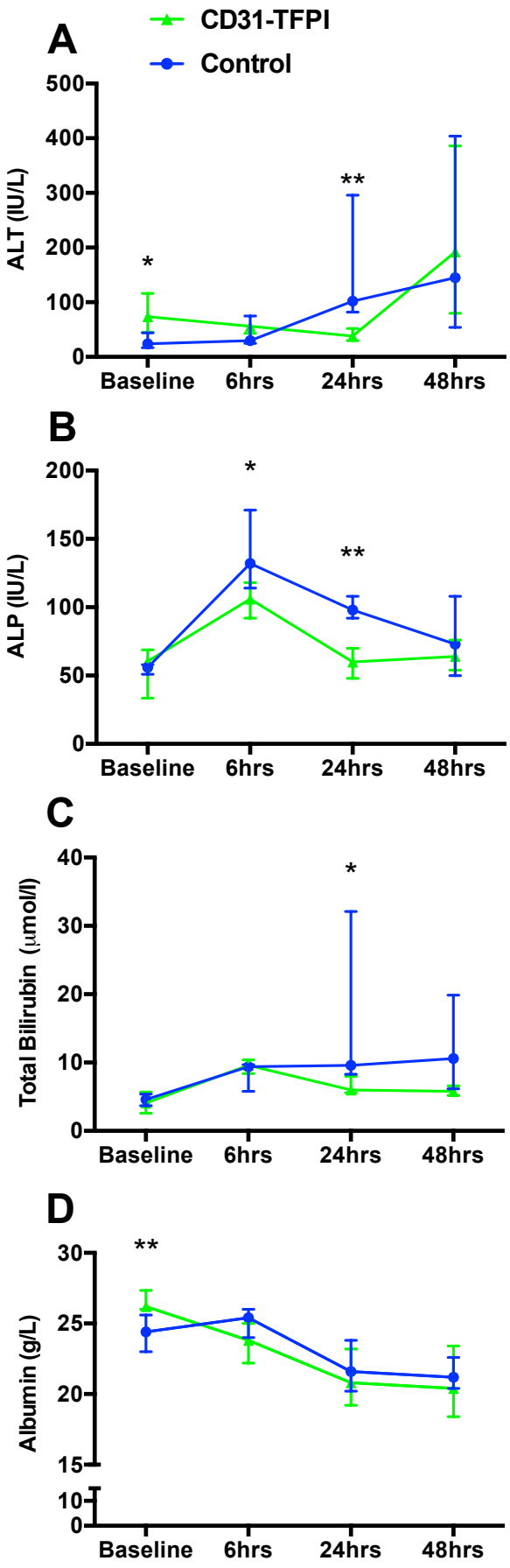


**Figure 5-5: ANIT induced acute liver injury, plasma liver function tests**

Symbols indicate median, bars indicate interquartile range.

* p=<0.05. ** p=<0.01.

*See* Table 5-2 *for median values.*

**Graph A**: Plasma ALT (IU/L).

**Graph B:** Plasma ALP (IU/L).

**Graph C:** Plasma total bilirubin (µmol/L).

**Graph D:** Plasma albumin (g/L).

### *5.3.2. Liver Injury*

Analysis of H&E stained liver FFPE tissue sections showed no evidence of liver injury at 6 hours in both CD31-TFPI and C57BL6/J control mice. There were n=5 in both the control and the CD31-TFPI group.

At 24 hours there was a statistically significant decrease in percentage area liver injury in CD31-TFPI mice compared to control mice (Mann Whitney U test, p = 0.005. Figure 5-6. Graph A. Median 0.9% and 0% in control and CD31-TFPI strains respectively). There were n=6 in the control group and n=7 in the CD31-TFPI group.

At 48 hours there was no statistically significant difference in percentage area liver injury in CD31-TFPI mice compared to control mice. Review of the data showed that there was a trend towards decreased injury in CD31-TFPI mice compared to control mice (median 5.3% and 0.7% in control and CD31-TFPI strains respectively) however the experiment was adequately powered (n=7 in each arm) and therefore variability in the model limited the statistical analysis (coefficient of variation at 48 hours, 80% and 143% in control and CD31-TFPI mice respectively).

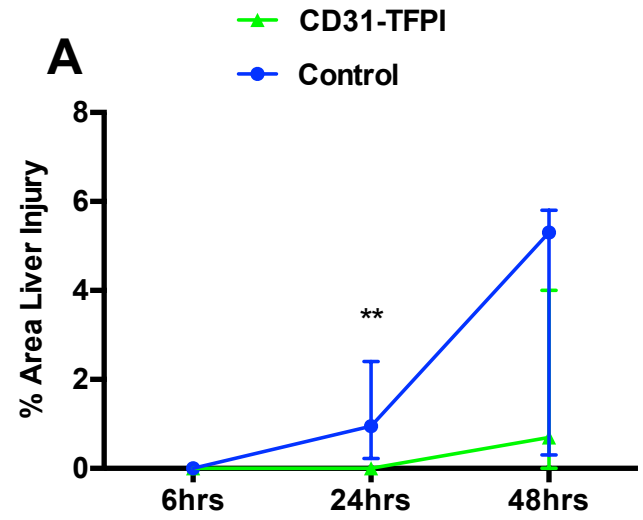


Image 1

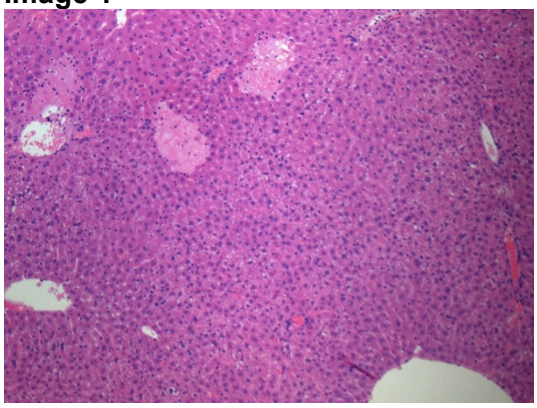

Image 2

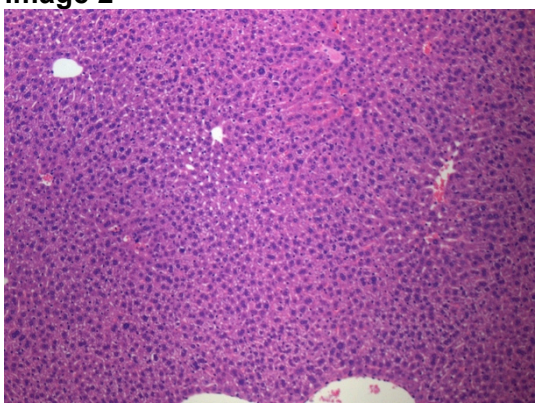

Image 3

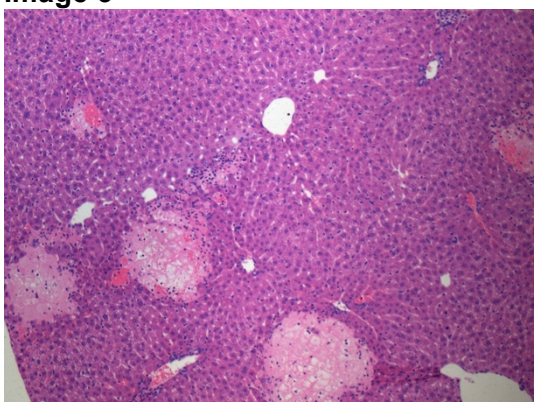

Image 4

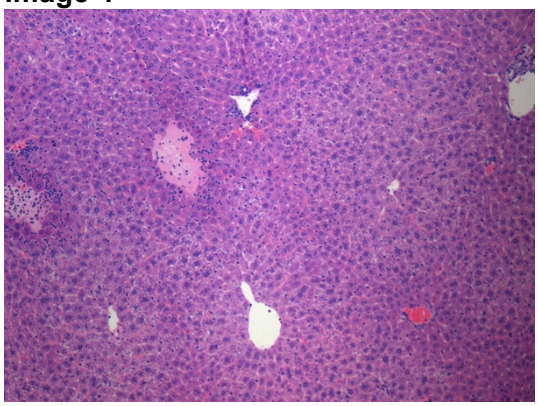

**Figure 5-6: ANIT induced acute liver injury**

Symbols indicate median. Bars indicate interquartile range.
** p=<0.01
**Graph A:** Percentage area liver injury in liver FFPE tissue sections.

**Image 1:** Hepatocellular injury at 24 hours. Control mouse. Original x100 magnification. **Image 2:** Hepatocellular injury at 24 hours. CD31-TFPI mouse. Original x100 magnification.

**Image 3:** Hepatocellular injury at 48 hours. Control mouse. Original x100 magnification. **Image 4:** Hepatocellular injury at 48 hours. CD31-TFPI mouse. Original x100 magnification.

### *5.3.3. Model summary - ANIT induced acute liver injury*

Overall CD31-TFPI mice displayed a reduction in liver injury as a result of ANIT administration as demonstrated by reduced hepatocellular necrosis and decreased plasma ALP and total bilirubin. This was most prominent at 24 hours after administration or ANIT but was also seen at 48 hours. The pattern of ANIT induced acute liver injury in this CD31-TFPI model directly mirrors that seen in the αSMA-TFPI model.

The likely mechanism of action is that inhibition of the tissue factor (TF) / VIIa / Xa complex by the transgenic TFPI expressed on CD31+ cells prevents microvascular clot formation and protease activated receptor (PAR) activation, diminishing the impact of ANIT hepatocellular and bile duct injury.

As discussed in Chapter 3 Luyendyk et al showed that TF did play a role in the progression of ANIT induced cholestatic liver injury (Luyendyk et al. 2009). This supports the hypothesis that the reason for the differences between the transgenic and control model were due to the action of TFPI in relation to TF. In Luyendyk et al's work the low-TF mice demonstrated a more significant decrease in liver injury at 48 hours after administration of ANIT, compared to the CD31-TFPI mice that demonstrated a more significant decrease 24 hours.

Luydendyk et al attributed the impact of low-TF on the progression of ANIT liver injury to three possible mechanisms:

- Disruption of fibrin microvascular clot formation and hepatic parenchymal hypoxia.

- Disruption of fibrin clot scaffold formation, reducing the accumulation of platelets and neutrophils key to ANIT induced injury (Sullivan, Wang, et al. 2010)(Dahm et al. 1991)(Kodali et al. 2006).
- Reduced thrombin associated PAR-1 signalling (Copple et al. 2003).

Given the apparent role of PAR-2 in the paracetamol induced acute liver injury model means that the role of PAR-2 in ANIT induced acute liver injury should also be examined.

As in the paracetamol induced acute liver injury model the earlier reduction in ALP, ALT, bilirubin and parenchymal injury seen in the CD31-TFPI mice may be due to the expression profile of CD31 during liver injury.

This set of experiments was at times limited by the number of animals per group. A power calculation had suggested that 6 animals per arm would provide the data to evaluate the model however in some analyses there was not data from 6 animals per arm; the plasma liver function tests especially suffered from sample exclusion due to haemolysis. However, I felt that the repetition of work to provide plasma data only, in light of the liver parenchymal injury data, was contrary to the 3Rs of animal research (refinement, replacement and reduction) and would not add significantly to the scientific value of the data already collected.

As in the paracetamol model it would have been ideal to demonstrate the distribution and extent of fibrin clot formation, to support the impact of

transgenic TFPI expression acting through its role in reducing microvascular clot formation. However, due to limited time and resources (fibrin antibody for immunohistochemistry) and the overall lack of statistical significance in this transgenic model, this was not undertaken.

## 5.4. Chapter Results Summary Table

| Parameter measured | Paracetamol acute liver injury model vs. controls (2, 6, 12 and 24 hours) | ANIT acute liver injury model vs controls (6, 24 and 48 hours) |
|---|---|---|
| **Liver injury** | Decreased liver injury at 6 and 12 hours.<br>Decreased ALP at 12 hours.<br>Decreased ALT at 6 and 12 hours. | Decreased liver injury.<br>Decreased ALP at 6 and 24 hours.<br>Decreased total bilirubin at 24 hours and 48 hours.<br>Decreased ALT at 24 hours. |

**Table 5-3: Comparison of acute liver injury models in CD31 targeted expression of TFPI**

Text in grey = non significant ($p<0.05$) trend

## 6. CD31 targeted expression of TFPI in chronic liver injury

### 6.1. Additional baseline parameters

Further parameters in the baseline (uninjured) liver phenotype of the CD31-TFPI mice were defined to help analyse data from experimental studies in chronic liver injury.

Baseline liver function tests (5.1.1) and baseline transgenic TFPI expression (5.1.2) were described in **section 5.1**.

The additional baseline measurements taken for the investigation of chronic liver injury were baseline liver collagen content (6.1.1) hepatic stellate cell activation (6.1.2), liver collagen turnover (6.1.3) and liver immune cell composition (6.1.4).

#### *6.1.1. Liver collagen content*

Sirius red histochemical staining detects type I and Type III collagen in formalin fixed paraffin embedded (FFPE) tissue on light microscopy. Collagen is the predominant extracellular matrix protein deposited in liver and as such is often used as a surrogate for liver fibrosis.

Digital image analysis of liver sections stained with Sirius red showed no statistically significant difference in the percentage of collagen in liver tissue of CD31-TFPI mice compared to C57BL6/J control mice (Mann Whitney test,

p=0.98. Figure 6-1. Graph A). There were n=10 in the control group and n=13 in the CD31-TFPI group.

Collagen 1α1 gene expression infers the amount of collagen I actively being transcribed in the sample. Quantitative PCR of cDNA reverse transcribed from whole liver homogenate RNA showed no statistically significant difference in collagen 1α1 gene expression in the livers of CD31-TFPI mice compared to control mice (Mann Whitney test, p=0.78. Figure 6-1. Graph B). There were n=10 in both the control and in the CD31-TFPI group.

Note: Hydroxyproline quantification of liver collagen content was also used to evaluate liver fibrosis, however baseline measurements were not made due to lack of difference in Sirius red histochemistry and collagen 1α1 gene expression already demonstrated at baseline and the limited resources associated with the hydroxyproline assay.

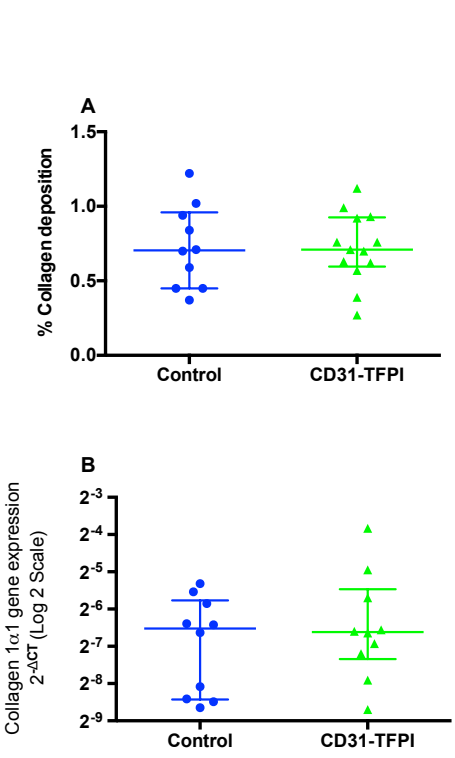


**Image 1**

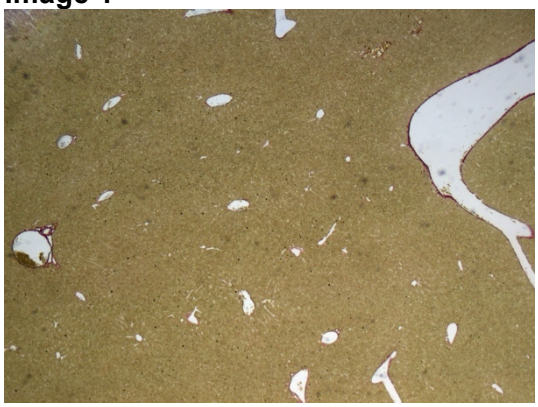

**Image 2**

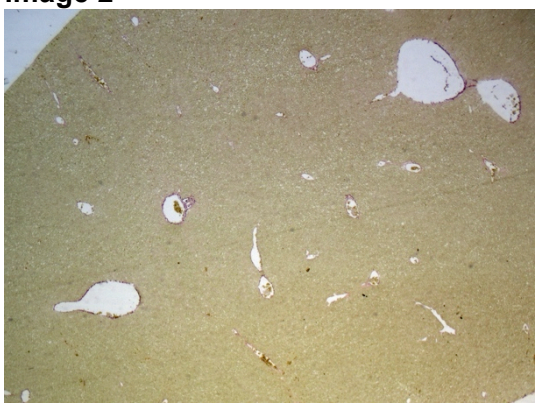

**Figure 6-1: Baseline liver collagen content**

Bars indicate median with interquartile range.

**Graph A:** Percentage Sirius red staining in liver FFPE tissue sections. Median 0.7% in both control and CD31-TFPI strains.

**Graph B:** Collagen 1α1 gene expression in whole liver homogenates. At baseline the CD31-TFPI strain had a -1.4 fold change (decrease) in collagen 1α1 gene expression compared to controls.

**Image 1:** Sirius red staining. Control mouse. Original x40 magnification.
**Image 2:** Sirius red CD31-TFPI mouse. Original x40 magnification.

### *6.1.2. Hepatic stellate cell activation*

Activated hepatic stellate cells are the predominant collagen producing cell in the liver during homeostasis and injury. Activated hepatic stellate cells express αSMA. Immunohistochemistry for αSMA in FFPE liver tissue sections is used as a surrogate for hepatic stellate cell activation.

Digital image analysis of FFPE liver sections stained using an antibody for αSMA showed a statistically significant decrease in the number of activated hepatic stellate cells in the liver of CD31-TFPI mice compared to C57BL6/J control mice (Mann Whitney U test; p=0.001.**Figure 6-2**. Graph A). Graphically, there were a number of outliers within the data collected for the control group. Removal of these outliers did not affect the significance of the result. There were n=10 in the control group and n=13 in the CD31-TFPI group.

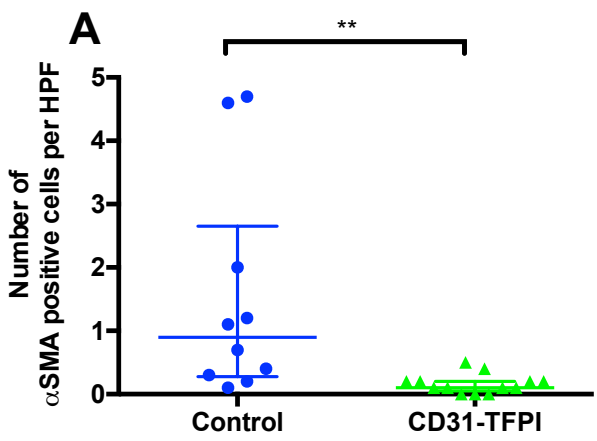


**Image 1**

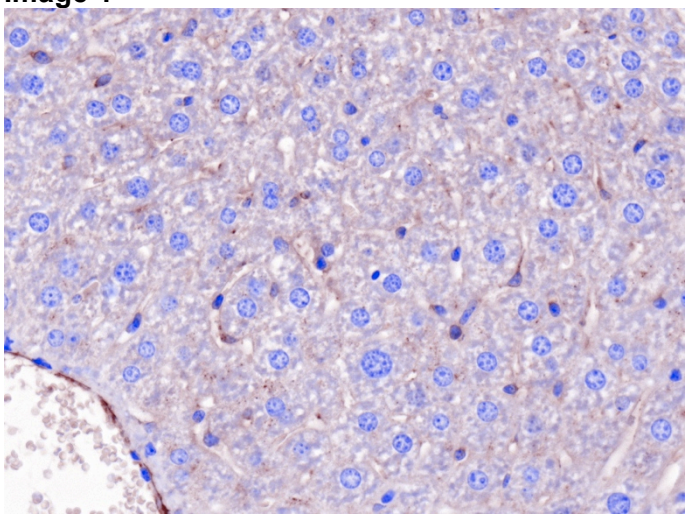

**Image 2**

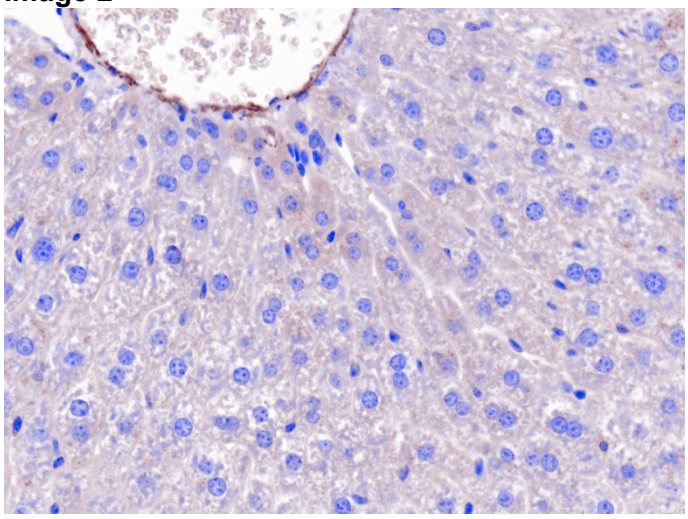

**Figure 6-2: Baseline αSMA immunohistochemistry**

Bars indicate median with interquartile range.

HPF = High power field, x400 magnification.

** p=<0.01.

**Graph A:** Number of activated hepatic stellate cells in liver FFPE tissue sections as determined by αSMA immunohistochemistry. Median 0.9 cells per HPF and 0.1 cells per HPF in control and CD31-TFPI strains respectively.

**Image 1:** Liver FFPE sections stained with αSMA from control mice. Original x400 magnification.

**Image 2:** Liver FFPE sections stained with αSMA from CD31-TFPI mice. Original x400 magnification.

### *6.1.3. Collagen turnover*

Matrix metalloproteinases (MMP) and tissue inhibitors of metalloproteinases (TIMP) are proteases and protease inhibitors that regulate the degradation of collagen in the liver. MMP2, MMP9 and TIMP1 gene expression infers the amount of these proteins actively being transcribed in the sample. There were n=6 in the control group and n=7 in the CD31-TFPI group for MMP2 expression. There were n=7 in the control group and n=6 in the CD31-TFPI group for MMP9 expression. There were n=8 in both the control and the CD31-TFPI group for TIMP1 expression.

Quantitative PCR of cDNA reverse transcribed from whole liver homogenate RNA showed a statistically significant increase in the expression of MMP2 in the liver of CD31-TFPI mice compared to C57BL6/J control mice (Mann Whitney U test; p=0.02. Figure 6-3. Graph A). However there was no statistically significant difference in MMP9 or TIMP1 gene expression in the livers of CD31-TFPI mice compared to control mice (Mann Whitney test, p=0.23 and p=0.70 respectively. Figure 6-3. Graphs B and C).

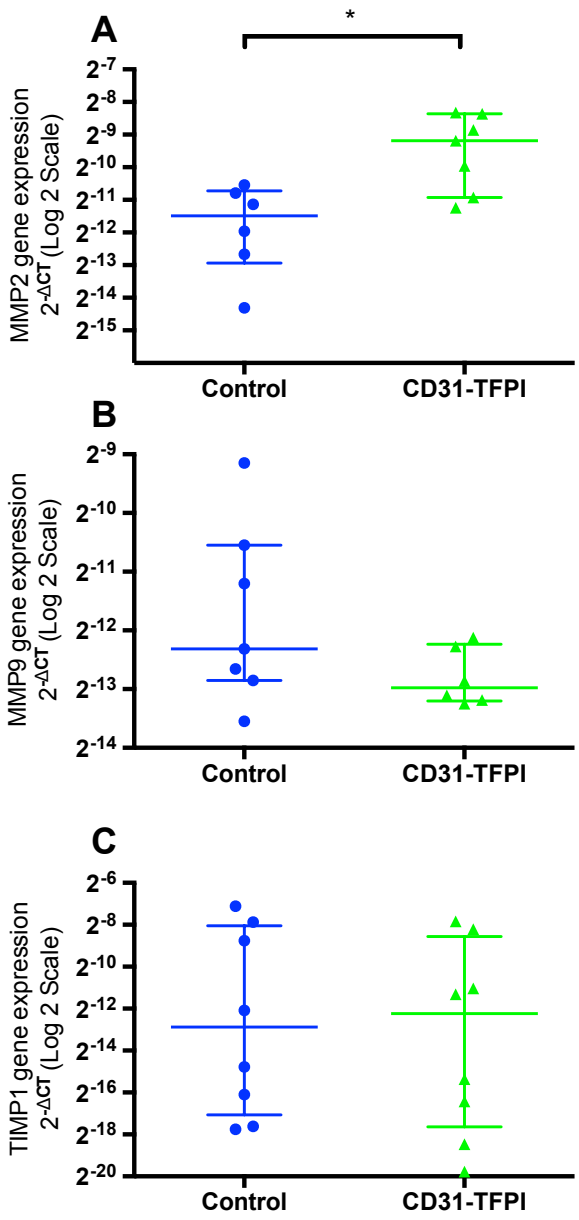


**Figure 6-3: Baseline matrixmetalloproteinase and TIMP gene expression**

Bars indicate median with interquartile range.

* p=<0.05

**Graph A:** MMP2 gene expression in whole liver homogenates. At baseline the CD31-TFPI strain had a 5 fold change (increase) in MMP2 gene expression compared to controls.

**Graph B:** MMP9 gene expression in whole liver homogenates. At baseline the CD31-TFPI strain had a -2 fold change (decrease) in MMP9 gene expression compared to controls.

**Graph C:** TIMP1 gene expression in whole liver homogenates. At baseline the CD31-TFPI strain had a -1.7 fold change (decrease) in TIMP1 gene expression compared to controls.

### *6.1.4. Liver immune cell composition*

The immune cell composition of the liver has been shown to affect the rate and progression of liver injury.

Macrophages are a key effector cell in acute and chronic liver injury. Immunohistochemistry for F4/80 in liver FFPE sections is used to identify macrophages.

Digital image analysis of liver FFPE sections stained using an antibody for F4/80 (**Figure 6-4**. Images 1 and 2) showed no statistically significant difference in the number of F4/80 positive cells in the livers of CD31-TFPI mice compared to C57BL6/J control mice (Mann Whitney test, p=0.31. **Figure 6-4**. Graph A). There were n=5 in both the control and the CD31-TFPI group.

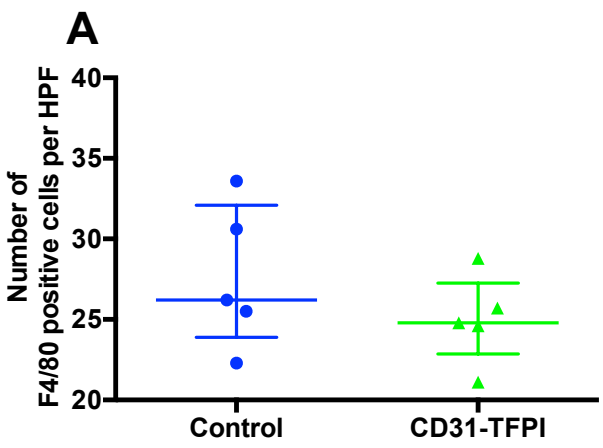


**Image 1**

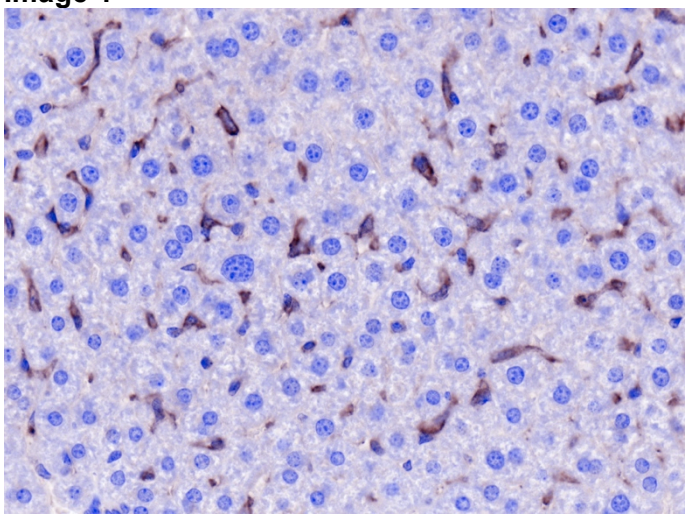

**Image 2**

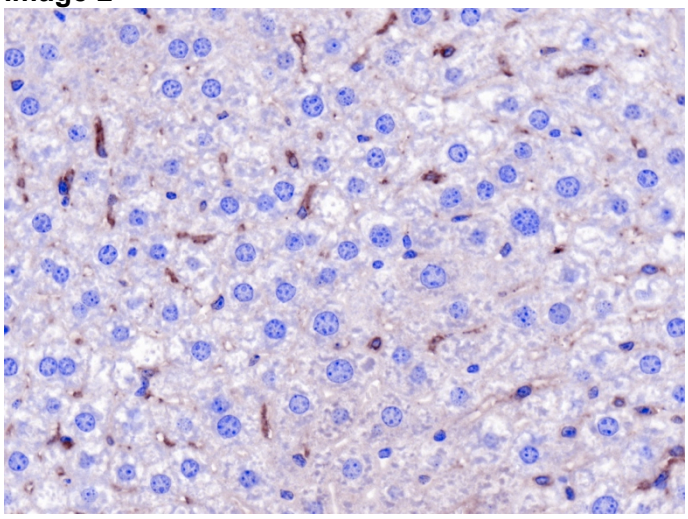

**Figure 6-4: Baseline F4/80 immunohistochemistry**

Bars indicate median with interquartile range.

HPF = High power field, x400 magnification.

n = 5 per arm.

**Graph A:** Number of macrophages in liver FFPE tissue sections as determined by F4/80 immunohistochemistry. Median 26 cells per HPF and 25 cells per HPF in control and CD31-TFPI strains respectively.

**Image 1:** Liver FFPE sections stained with F4/80 from control mice. Original x400 magnification.

**Image 2:** Liver FFPE sections stained with F4/80 from CD31-TFPI mice. Original x400 magnification.

Flow cytometry of fresh cells isolated from mouse liver was also used to identify macrophages, neutrophils, T cells, B cells and NK cells. Unfortunately data relating to the liver immune composition was available from only a small number of CD31-TFPI mice at baseline for all parameters (n = 3 in the CD31-TFPI group compared to n=9 in the control group for macrophages and n=3 in the control group for T cells, B cells and NK cells) due to failed assays. This limited statistical analysis.

There was no statistically significant difference in the proportion of macrophages (CD45+ CD11b+ Ly6G- F4/80+ cells) in the livers of CD31-TFPI mice compared to control mice (Mann Whitney test, p=0.28. Figure 6-5. Graphs A). Within this population there was no statistically significant difference in the proportions of macrophages with intermediate / low ($Ly6C^{int/lo}$) or high ($Ly6C^{hi}$) Ly6C expression in CD31-TFPI mice compared to control mice (Mann Whitney test, p=0.73 and p=0.37 respectively. Figure 6-5. Graphs B and C).

There was no statistically significant difference in the proportion of neutrophils in the livers of CD31-TFPI mice compared to control mice (Mann Whitney test, p=0.28. Figure 6-5. Graph D).

There was no statistically significant difference in the proportion of T cells, B cells or NK cells in the livers of CD31-TFPI mice compared to control mice (Mann Whitney test, p=0.40, p=0.90 and p=0.70 respectively. Figure 6-6. Graphs A-C).

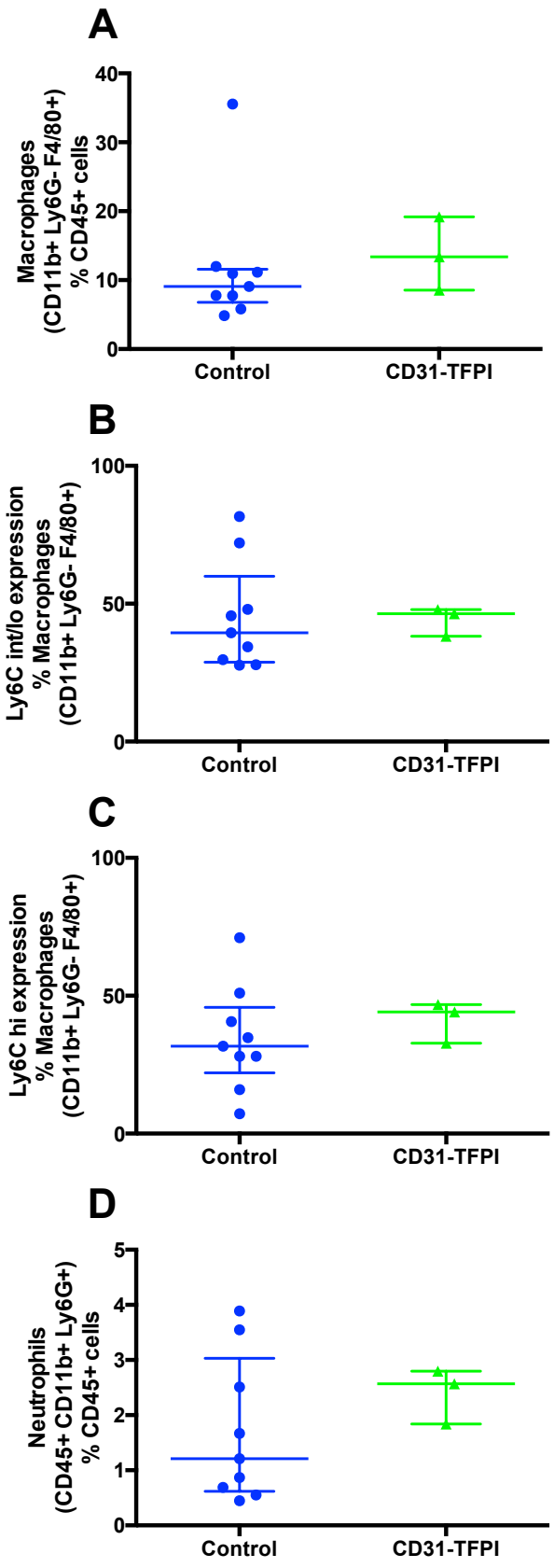


**Figure 6-5: Baseline liver macrophage and neutrophil composition**

Bars indicate median with interquartile range.

n = 3 per arm.

**Graph A:** Macrophages (CD45+ CD11b+ Ly6G- F4/80+ cells) as a proportion of CD45+ (immune) cells. Median at baseline, 9% and 13% of CD45+ cells in control and CD31-TFPI strains respectively.

**Graph B:** Macrophages expression intermediate or lo levels of Ly6C as a proportion of macrophages. Median at baseline, 39% and 46% macrophages in control and CD31-TFPI strains respectively.

**Graph C:** Macrophages expression high levels of Ly6C as a proportion of macrophages. Median at baseline, 32% and 44% of macrophages in control and CD31-TFPI strains respectively.

**Graph D:** Neutrophils (CD45+ CD11b+ Ly6G+ cells) as a proportion of CD45+ (immune) cells. Median at baseline, 1.2% and 2.6% of CD45+ cells in control and CD31-TFPI strains respectively.

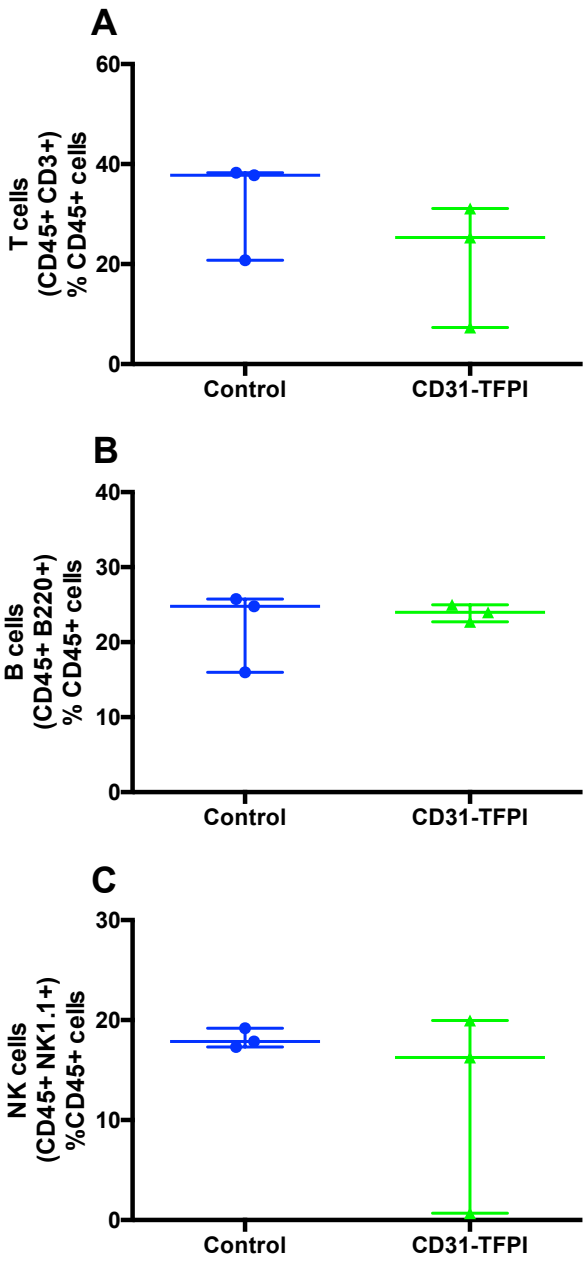


**Figure 6-6: Baseline liver T cell, B cell and NK cell composition**

Bars indicate median with interquartile range.

**Graph A:** T cells(CD45+ CD3+ cells) as a proportion of CD45+ (immune) cells. Median at baseline, 38% and 25% of CD45+ cells in control and CD31-TFPI strains respectively.

**Graph B:** B cells (CD45+ B220+ cells) as a proportion of CD45+ (immune) cells. Median at baseline, 25% and 24% of CD45+ cells in control and CD31-TFPI strains respectively.

**Graph C**: NK cells (CD45+ NK1.1+ cells) as a proportion of CD45+ (immune) cells. Median at baseline, 18% and 16% of CD45+ cells in control and CD31-TFPI strains respectively.

### *6.1.5. Summary – Additional baseline parameters*

As shown in section 5.1.2, the CD31-TFPI mice showed little or no transgenic TFPI gene expression in the liver and very low levels of protein expression in only the spleen at baseline. However differences were seen in baseline plasma liver function tests (discussed in section 5.1.3), hepatic stellate cell activation and MMP2 expression.

In the uninjured liver hepatic stellate cell αSMA expression is low (Knittel et al. 1999). Both CD31-TFPI and control mice demonstrated low levels of expression at baseline. CD31-TFPI mice had significantly lower αSMA expression compared to control mice at baseline and it is therefore possible that this was due to the effect of transgenic TFPI even though expression levels were low.

It is not possible to determine the mechanism by which this could have occurred from the data collected, however it is possible that the transgenic expression of TFPI targeted to CD31 positive endothelium or CD31 positive hepatic macrophages altered the crosstalk between these cells and hepatic stellate cells residing within the space of Disse (and therefore in close proximity to each other) in the uninjured liver. A possible pathway for this would be a reduction in the activation of PAR (PAR-1, PAR-2 and PAR-4) through TFPI inhibition / blockade of TF / VIIa / Xa, resulting in reduced hepatic stellate cell activation (Shi et al. 2007; Knight et al. 2012).

In CD31-TFPI mice there was a 5 fold increase in the baseline expression of MMP-2 compared to control mice. MMP-2 gene expression in uninjured liver has been reported in the literature (Smith et al. 2014) although MMP-2 expression is more commonly associated with activated hepatic stellate cells (Iredale et al. 2013). Work by Hartland et al has shown that active MMP-2 promotes apoptosis in cultured hepatic stellate cells in a dose dependent manner (Hartland et al. 2009). Therefore it could be hypothesised that the increase in MMP-2 seen in the CD31-TFPI mice was the reason for the relative decrease in activated hepatic stellate cells compared to controls at baseline.

I am unable to explain why there was an increase in the baseline MMP2 gene expression seen in the CD31-TFPI mice. It is worth noting that in this work the gene expression of MMP2 has been measured but this is not a direct reflection of the amount or activity of MMP-2 in the tissue, which is derived from proteolytic cleavage pro-MMP-2 protein. However, Knittel et al mapped the gene expression of MMP2 and MMP9 in acute and chronic liver injury and found that gene expression did correspond to changes in the protein level (Knittel et al. 2000).

## 6.2. Carbon tetrachloride ($CCl_4$) induced chronic liver injury

Repeated doses of carbon tetrachloride ($CCl_4$) cause chronic liver injury with fibrosis. Early fibrosis has a centrilobular pattern but progresses to centri-portal bridging, and nodule formation. With cessation of $CCl_4$ fibrosis resolution occurs.

Staggered doses of 0.125mL – 1mL/kg of $CCl_4$ was administered to mice via intraperitoneal injection for 4 weeks. Mice were culled at 24 hours after the last injection of $CCl_4$.

This model was halted at 24 hours due to the results demonstrated below and the lack of effect of transgenic TFPI to alter the progression and resolution of liver fibrosis in the α-SMA-TFPI mice administered $CCl_4$ (who were followed up along a time course of progression and resolution until 96 hours after the last injection of $CCl_4$).

### *6.2.1. Plasma liver function tests*

As previously noted, there were statistically significant differences in baseline ALT and albumin in CD31-TFPI transgenic mice compared to control mice (Figure 5-1. Graphs A and D, CD31-TFPI mice had elevated plasma ALT and albumin compared to controls).

At 24 hours there were n=10 in the control group and n=4 in the CD31-TFPI. Sample numbers were less than the power calculation sample number due to

failed assays. Baseline sample numbers were as previously noted in section 5.1.

At 24 hours after the last injection of $CCl_4$ there was no statistically significant difference in any plasma liver function tests of CD31-TFPI mice compared to control mice (Figure 6-7.Graphs A-D). Review of the data showed a trend towards decreased ALT in CD31-TFPI transgenic mice compared to controls (median 413IU/L and 946IU/L respectively). Taking into account the baseline increase in the plasma ALT of CD31-TFPI mice, the relative lack of increase in CD31-TFPI mice after $CCl_4$ induced chronic liver injury suggests that this trend is biologically significant. It is also worth noting that the statistical analysis of this marker was under powered in the CD31-TFPI arm (n=4).

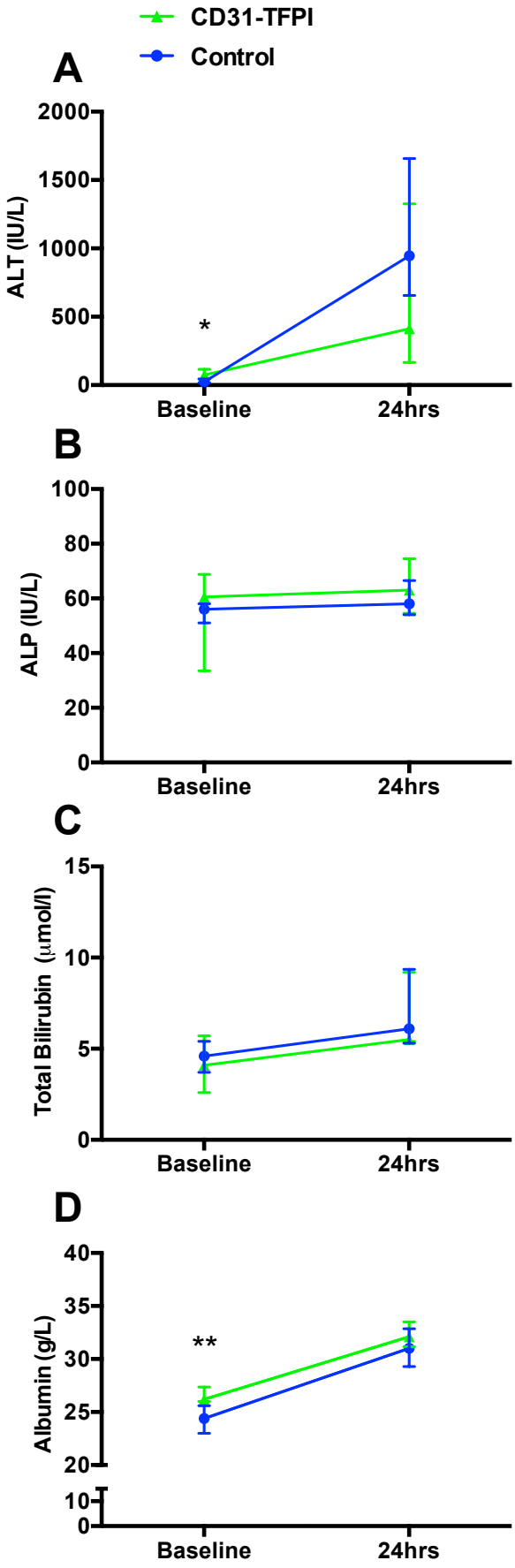


**Figure 6-7: $CCl_4$ induced chronic liver injury, plasma liver function tests**

Symbols indicate median, bars indicate interquartile range.

* p=<0.05. ** p=<0.01.

**Graph A**: Plasma ALT (IU/L). Median at 24 hours after last injection of $CCl_4$, 946U/L and 413IU/L (39 and 5.6 fold change from baseline) in control and CD31-TFPI strains respectively.

**Graph B:** Plasma ALP (IU/L). Median at 24 hours after last injection of $CCl_4$, 58IU/L and 66IU/L (1.0 and 1.0 fold change from baseline) in control and CD31-TFPI strains respectively.

**Graph C:** Plasma total bilirubin (µmol/L). Median at 24 hours after last injection of $CCl_4$, 6.1µmol/L and 5.5µmol/L (1.3 and 1.3 fold change from baseline) in control and CD31-TFPI strains respectively.

**Graph D:** Plasma albumin (g/L). Median at 24 hours after last injection of $CCl_4$, 31g/L and 32g/L (1.3 and 1.2 fold change from baseline) in control and CD31-TFPI strains respectively.

.

### *6.2.2. Liver collagen content*

Digital image analysis of liver FFPE sections stained with Sirius red from mice culled at 24 hours after the last injection of $CCl_4$ showed no statistically significant difference in liver collagen deposition in CD31-TFPI mice compared to control mice (**Figure 6-8**. Graph A). There were n=10 in the control group and n=9 in the CD31-TFPI group. Baseline sample numbers were as previously noted in section 6.1.

Hydroxyproline quantification of the collagen content of livers from mice culled 24 hours after the last injection of $CCl_4$ showed no statistically significant difference in liver collagen content in CD31-TFPI mice compared to control mice (**Figure 6-8**. Graph B). However there was a trend towards decreased liver hydroxyproline in the livers of CD31-TFPI mice with a median hydroxyproline measurement of 300µg/g compared to 768µg/g in control mice livers. Here the statistical analysis appears to be limited by the number per group (both n = 4).

Quantitative PCR of cDNA reverse transcribed from whole liver homogenate RNA from mice culled 24 hours after the last injection of $CCl_4$ showed a statistically significant decrease in collagen 1$\alpha$1 gene expression in the livers of CD31-TFPI mice compared to control mice (Mann Whitney U, p = 0.008. **Figure 6-8**. Graph C). There were n=14 in the control group and n=10 in the CD31-TFPI group. Baseline sample numbers were as previously noted in section 6.1.

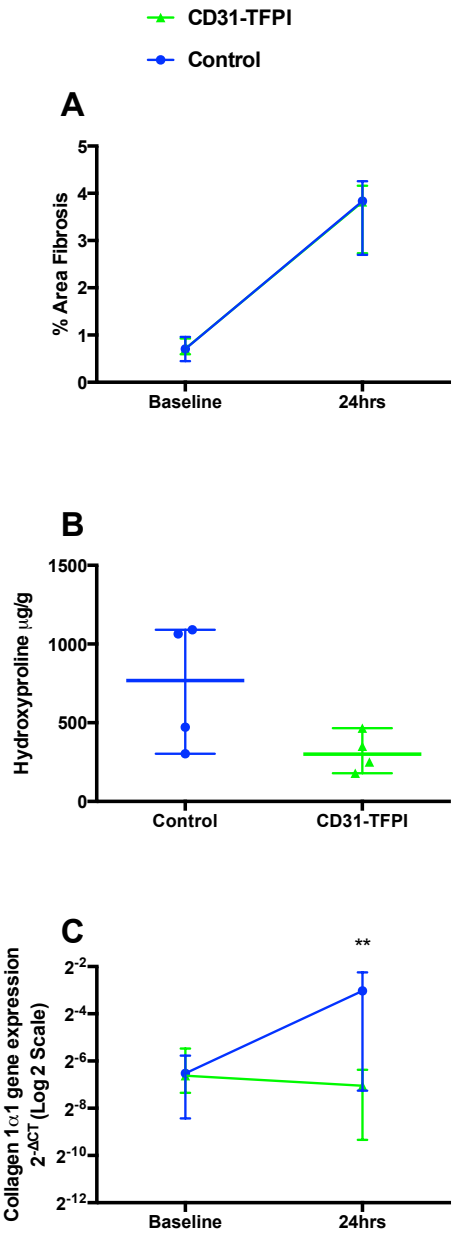


**Figure 6-8: $CCl_4$ induced chronic liver injury, liver collagen content**

Symbols indicate median. Bars indicate interquartile range.

** p=<0.01.

**Graph A:** Percentage Sirius red staining in liver FFPE tissue sections from mice administered $CCl_4$. At 24 hours after last injection of $CCl_4$, median 3.8% in both control and CD31-TFPI strains.

**Graph B:** Hydroxyproline content (µg/g of liver) in livers from mice culled 24 hours after the last injection of $CCl_4$. Median 768µg/g and 300µg/g in control and CD31-TFPI strains respectively. *Bars indicate median with interquartile range.*

**Graph C:** Collagen 1α1 gene expression in whole liver homogenates. CD31-TFPI mice had a -2.5 fold change (decrease) in collagen 1α1 gene expression at 24 hours after the last injection of $CCl_4$ compared to baseline. Control mice had a 5.4 fold change (increase) in collagen 1α1 gene expression compared to baseline.

**Image 1:** Sirius Red at 24 hours. Control mouse. Original x40 magnification.
**Image 2:** Sirius Red at 24 hours. CD31-TFPI mouse. Original x40 magnification.

**Image 1**

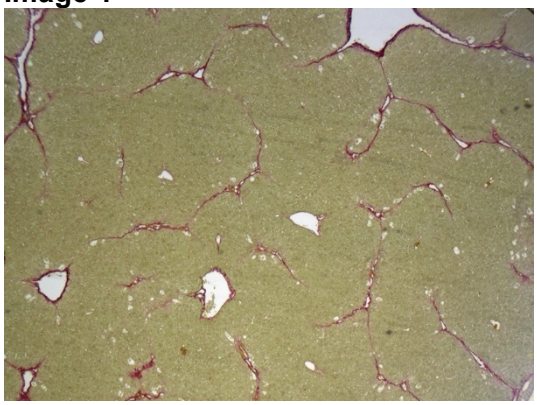

**Image 2**

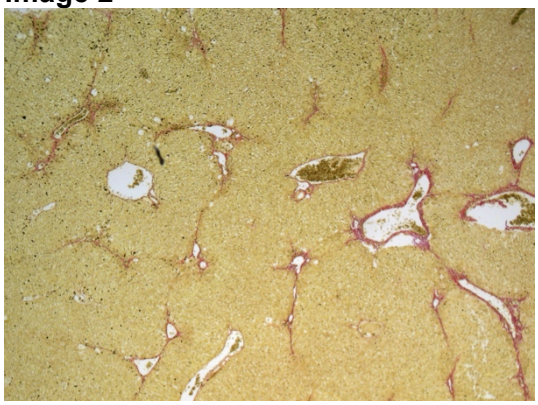

### *6.2.3. Hepatic stellate cell activation*

As previously noted, at baseline there was a statistically significant decrease in the number of activated hepatic stellate cells in the liver of CD31-TFPI mice compared to control mice (**Figure 6-2**. Graph A).

Digital image analysis of FFPE liver sections from mice culled 24 hours after the last injection of $CCl_4$ were stained using an antibody for αSMA and showed a statistically significant decrease in the number of activated hepatic stellate cells in the livers of CD31-TFPI mice compared to control mice (Mann Whitney U test; p=0.001.

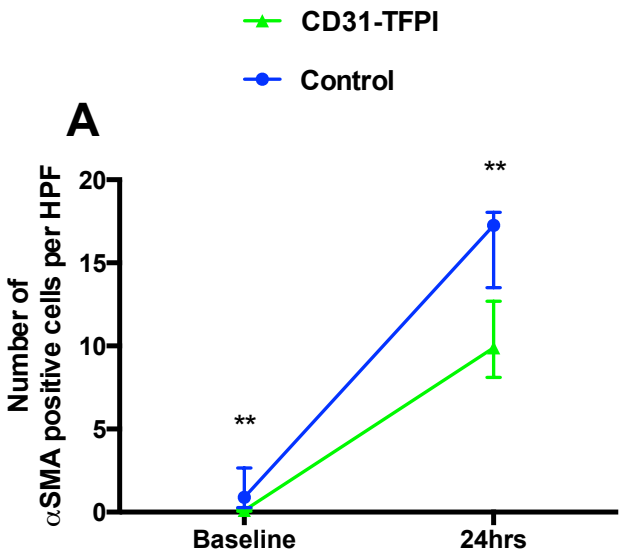


**Image 1**

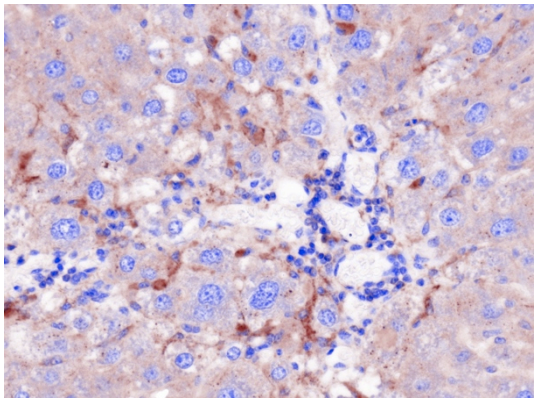

**Image 2**

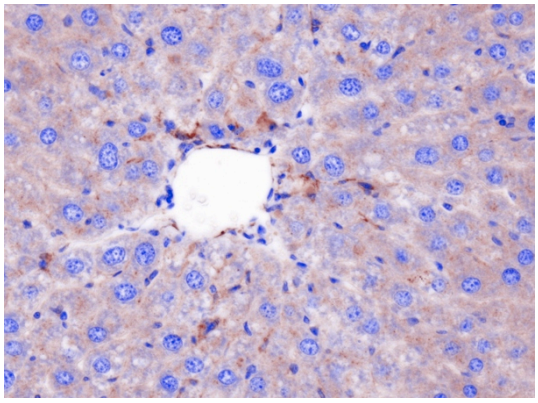

Figure 6-9. Graph A). However, given the baseline differences seen in the number of activate hepatic stellate cells, CD31-TFPI mice demonstrated a 99 fold increase in the number of hepatic stellate cells from baseline and control mice demonstrated a 19 fold increase. There were n=10 in the control group and n=11 in the CD31-TFPI group. Baseline sample numbers were as previously noted in section 6.1.

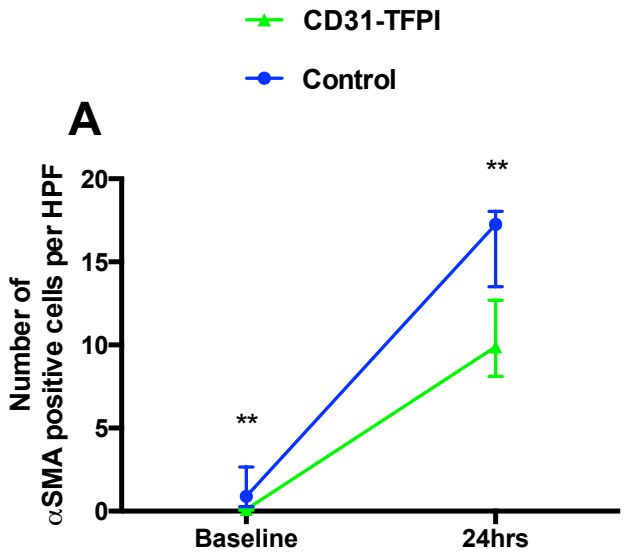


**Image 1**

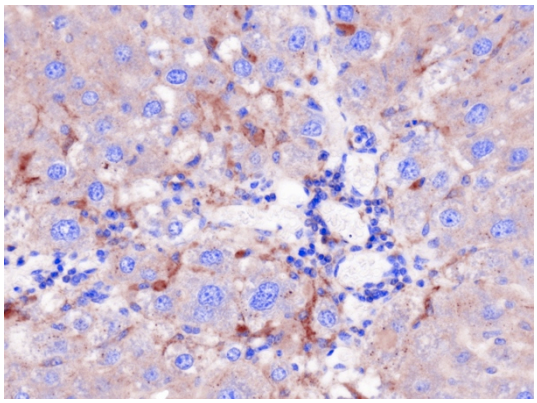

**Image 2**

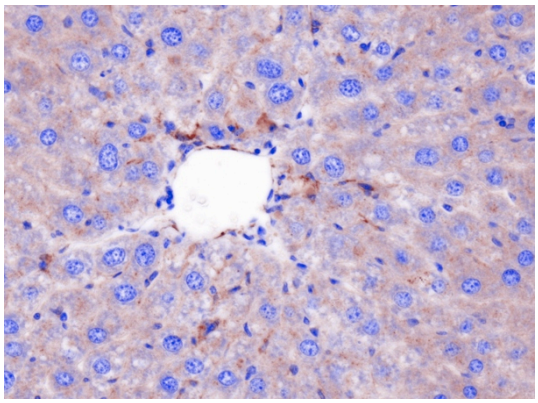

**Figure 6-9: $CCl_4$ induced chronic liver injury, αSMA immunohistochemistry**

Symbols indicate median. Bars indicate interquartile range.

** p=<0.01.

**Graph A:** Number of activated hepatic stellate cells in liver FFPE tissue sections as determined by αSMA immunohistochemistry. Median 17.3 cells per HPF and 9.9 cells per HPF in control and CD31-TFPI strains respectively.

**Image 1:** Anti-αSMA immunohistochemistry at 24 hours. Control mouse. Original x400 magnification. **Image 2:** Anti-αSMA immunohistochemistry at 24 hours. CD31-TFPI mouse. Original x400 magnification.

### *6.2.4. Collagen turnover*

As previously noted, at baseline there was a statistically significant increase in the expression of MMP2 in the liver of CD31-TFPI mice compared to control mice (Figure 6-3. Graph A).

Quantitative PCR of cDNA reverse transcribed from whole liver homogenate RNA from mice culled at 24 hours after the last injection of $CCl_4$ showed no statistically significant difference in MMP2, MMP9 or TIMP1 gene expression in CD31-TFPI mice compared to control mice (Figure 6-10. Graphs A-C). There were n=6 in the control group and n=7 in the CD31-TFPI group for MMP2 expression. There were n=9 in the control group and n=5 in the CD31-TFPI group for MMP9 expression. There were n=6 in the control group and n=8 in the CD31-TFPI group for TIMP1 expression. Sample numbers were less than the power calculation sample number due to failed assays. Baseline sample numbers were as previously noted in section 6.1.

At 24 hours after the last injection of $CCl_4$ both strains of mice showed decreased MMP2 gene expression and increased MMP9 gene expression compared to baseline. There was a trend towards decreased TIMP1 gene expression in CD31-TFPI mice compared to control mice, however this did not reach statistical significance (Mann Whitney U test; p=0.06) in adequately powered comparisons (n = 8 in CD31-TFPI arm and n = 6 in control arm). Review of the data showed little change in TIMP1 gene expression from baseline in CD31-TFPI mice but control mice should a 10 fold increase in TIMP1 gene expression from baseline.

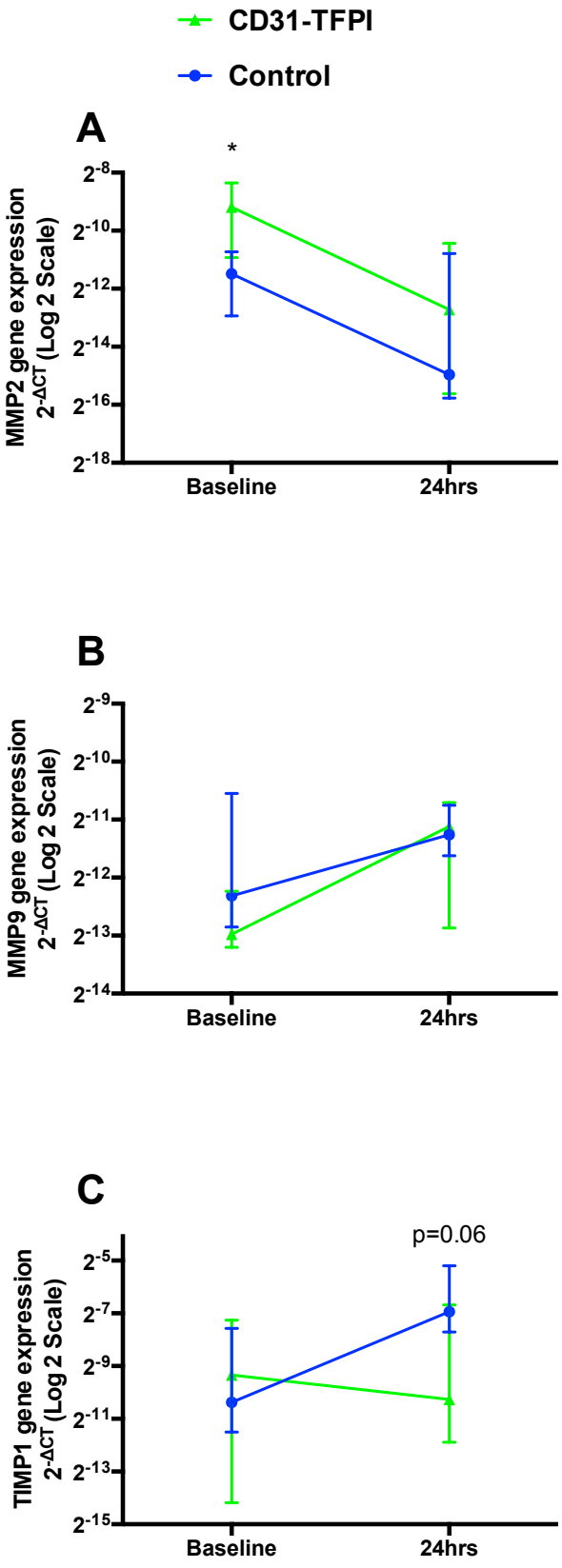


**Figure 6-10: $CCl_4$ induced chronic liver injury, matrixmetalloproteinase and TIMP gene expression**

**Graph A:** MMP2 gene expression in whole liver homogenates. CD31-TFPI mice had a -9.7 fold change (decrease) and control mice had a -5.0 fold change (decrease) in MMP2 gene expression at 24 hours after the last injection of $CCl_4$ compared to baseline.

**Graph B:** MMP9 gene expression in whole liver homogenates. CD31-TFPI mice had a 2.1 fold change (increase) and control mice had a 1.4 fold change (increase) in MMP9 gene expression at 24 hours after the last injection of $CCl_4$ compared to baseline.

**Graph C:** TIMP1 gene expression in whole liver homogenates. CD31-TFPI mice had a 1.3 fold change (increase) and control mice had a 10.2 fold change (increase) in TIMP1 gene expression at 24 hours after the last injection of $CCl_4$ compared to baseline.

### *6.2.5. Liver immune cell composition*

Digital image analysis of liver FFPE sections from mice culled 24 hours after the last injection of $CCl_4$ were stained using an antibody for F4/80 and showed no statistically significant difference in the number of F4/80 positive macrophages in the livers of CD31-TFPI transgenic mice compared to C57BL6/J control mice (Figure 6-11. Graph A). There were n=10 in the control group and n=11 in the CD31-TFPI group. Baseline sample numbers were as previously noted in section 6.1.

Flow cytometry of fresh cells isolated from the liver of mice culled 24 hours after the last injection of $CCl_4$ showed no statistically significant difference in the proportion of macrophages or macrophage subsets in the livers of CD31-TFPI mice compared to control mice (Figure 6-12. Graphs A-C).

Flow cytometry of fresh cells isolated from the liver of mice culled 24 hours after the last injection of $CCl_4$ showed no statistically significant difference in the proportion of neutrophils in the livers of CD31-TFPI mice compared to control mice (Figure 6-12. Graph D).

Flow cytometry of fresh cells isolated from the liver of mice culled 24 hours after the last injection of $CCl_4$ showed a statistically significant increase in the proportion of B cells in the livers of CD31-TFPI mice compared to control mice (Mann Whitney U test, $p = 0.03$. Figure 6-13. Graph B). There was no statistically significant difference in the proportion of T cells and NK cells in

the livers of CD31-TFPI mice compared to control mice (Figure 6-13. Graphs A and C).

There were n=5 in both the control and the CD31-TFPI group. Sample numbers were less than the power calculation sample number due to failed assays or insufficient numbers of transgenic animals. Baseline sample numbers were as previously noted in section 6.1.

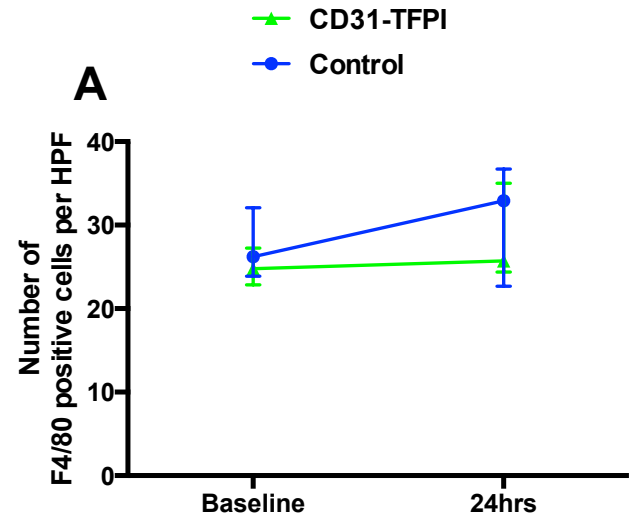


Image 1

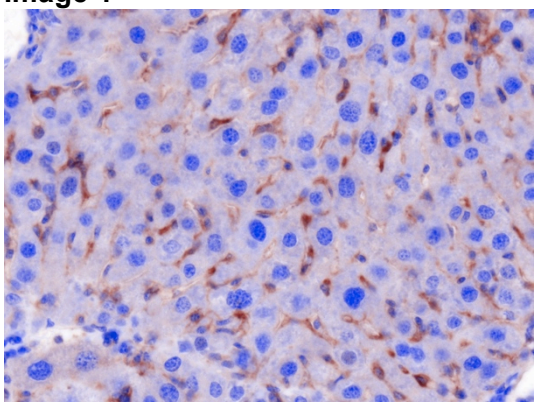

Image 2

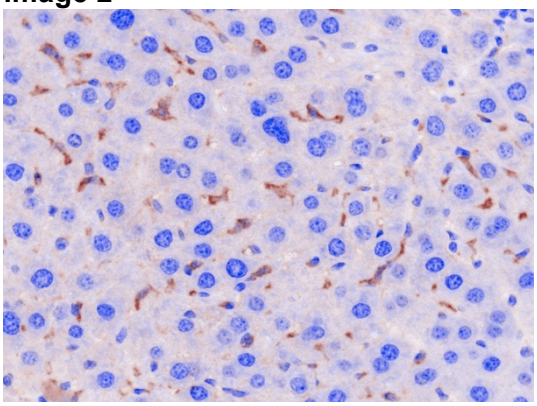

**Figure 6-11: $CCl_4$ induced chronic liver injury, F4/80 immunohistochemistry**
Symbols indicate median. Bars indicate interquartile range.

**Graph A:** Number of macrophages in liver FFPE tissue sections as determined by F4/80 immunohistochemistry. Median at 24 hours after last injection of $CCl_4$, 32.9 cells per HPF and 25.7 cells per HPF (1.3 and 1.0 fold change from baseline) in control and CD31-TFPI strains respectively.

**Image 1:** Anti-F4/80 immunohistochemistry at 24 hours. Control mouse. Original x400 magnification. **Image 2:** Anti-F4/80 immunohistochemistry at 24 hours. CD31-TFPI mouse. Original x400 magnification.

**Figure 6-12: $CCl_4$ induced chronic liver injury, liver macrophage and neutrophil composition**

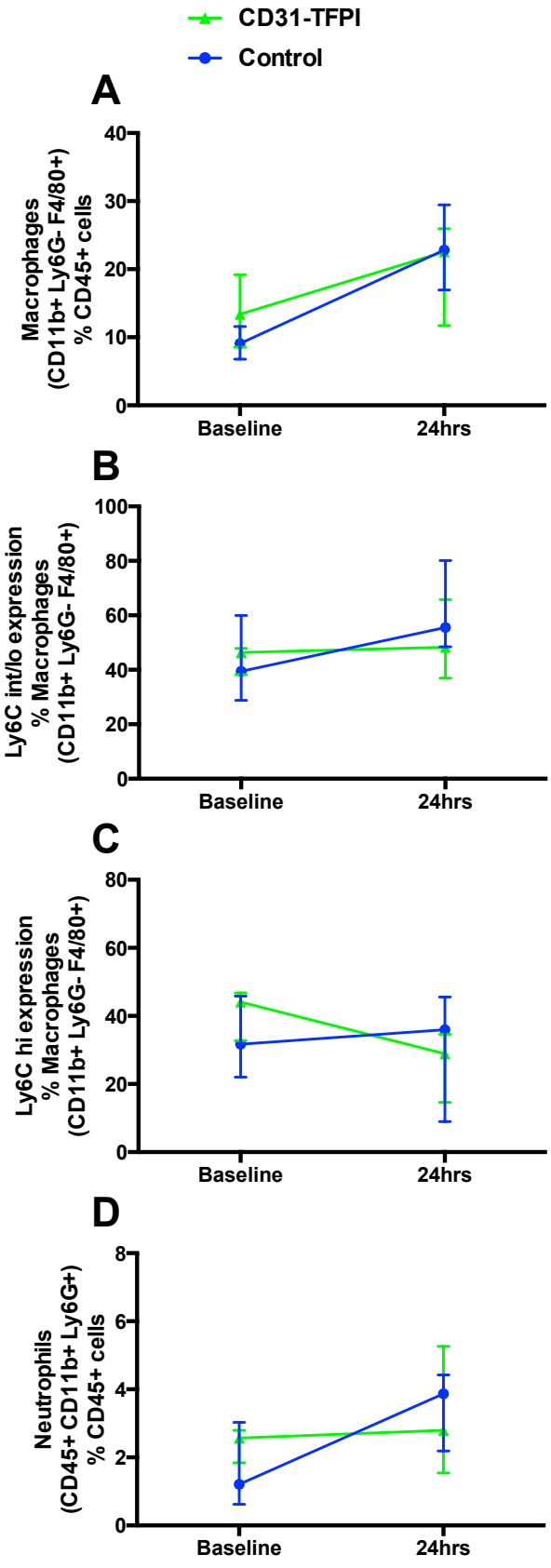


Symbols indicate median. Bars indicate interquartile range.

**Graph A:** Macrophages (CD45+ CD11b+ Ly6G- F4/80+ cells) as a proportion of CD45+ (immune) cells. Median at 24 hours after the last injection of $CCl_4$, 23% and 24% (2.5 and 1.7 fold change from baseline) in control and CD31-TFPI strains respectively.

**Graph B:** Macrophages expression intermediate or lo levels of Ly6C as a proportion of macrophages. Median at 24 hours after the last injection of $CCl_4$, 56% and 48% (1.4 and 1.0 fold change from baseline) in control and CD31-TFPI strains respectively.

**Graph C:** Macrophages expression high levels of Ly6C as a proportion of macrophages. Median at 24 hours after $CCl_4$, 36% and 29% (1.1 and -1.5 fold change from baseline) in control and CD31-TFPI strains respectively.

**Graph D:** Neutrophils (CD45+ CD11b+ Ly6G+ cells) as a proportion of CD45+ (immune) cells. Median at 24 hours after $CCl_4$, 3.9% and 2.8% (3.3 and 1.1 fold change from baseline) in control and CD31-TFPI strains respectively.

**Figure 6-13: $CCl_4$ induced chronic liver injury, liver T cell, B cell and NK cell composition**

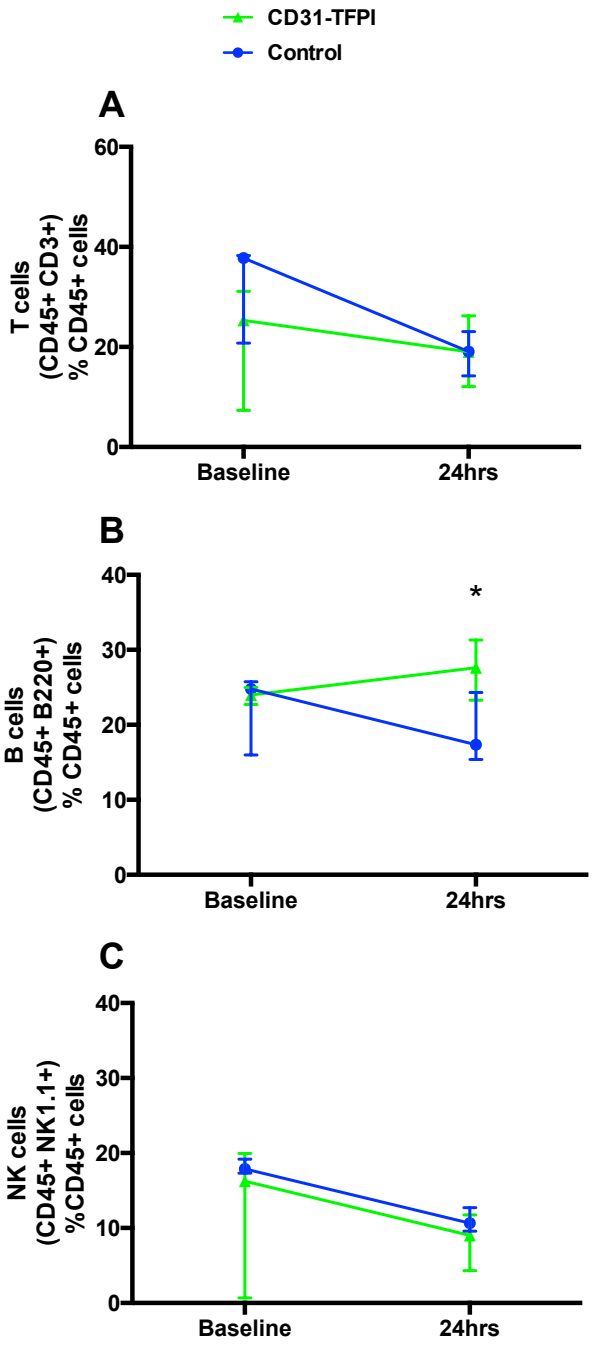


Bars indicate median with interquartile range.

* p=<0.05

**Graph A:** T cells (CD45+ CD3+ cells) as a proportion of CD45+ (immune) cells. Median at 24 hours after the last injection of $CCl_4$, 19% and 19% (-2.0 and -1.3 fold change from baseline) in control and CD31-TFPI strains respectively.

**Graph B:** B cells (CD45+ B220+ cells) as a proportion of CD45+ (immune) cells. Median at 24 hours after the last injection of $CCl_4$, 17% and 28% of CD45+ cells (-1.5 and 1.2 fold change from baseline) in control and CD31-TFPI strains respectively.

**Graph C**: NK cells (CD45+ NK1.1+ cells) as a proportion of CD45+ (immune) cells. Median at 24 hours after the last injection of $CCl_4$, 11% and 9% of CD45+ cells (-1.6 and -1.7 fold change from baseline) in control and CD31-TFPI strains respectively.

### *6.2.6. Transgenic TFPI expression*

Expression of the transgene was assessed using PCR. Gene expression of the TFPI transgene was identified in 0/5 samples from CD31-TFPI mice culled 24 hours after the last injection of $CCl_4$; before and after amplification of initial PCR products.

Due to the lack of statistically significant differences between in the transgenic and control mice, coupled with limited amounts of the transgene specific antigen for immunohistochemistry, only PCR detection of transgene expression was used.

### *6.2.7. Model summary - $CCl_4$ induced chronic liver injury*

Twenty four hours after carbon tetrachloride ($CCl_4$) induced chronic liver injury the overall picture in CD31-TFPI mice was of decreased liver injury and fibrosis in comparison to control mice.

In CD31-TFPI mice liver plasma ALT was decreased in real terms and in fold change from baseline compared to control mice but did not reach statistical significance. This suggests that the CD31-TFPI mice may have sustained less liver injury after $CCl_4$ induced chronic liver injury. In keeping with this CD31-TFPI demonstrated less hepatic stellate cell activation, less (not statistically significant) TIMP1 expression and in turn less fibrosis. However, baseline hepatic stellate cell activation was decreased and fold change from baseline showed that there was a similar or greater increase in the liver of CD31-TFPI mice compared to controls. The implication of this is that, while transgenic TFPI expression created an overall picture of decreased liver injury and fibrosis the effect was most likely due to baseline changes and not alteration in biological pathways during fibrogenesis. In keeping with this there was no detectable transgene expression in the liver of CD31-TFPI mice 24 hours after the last injection of $CCl_4$ in a $CCl_4$ induced chronic liver injury model.

In CD31-TFPI there was a 1.2 fold increase in the proportion of B cells from baseline and a statistically significant increase compared to control mice (control mice demonstrated a decrease in the proportion of B cells from baseline, consistent with published data (Novobrantseva et al. 2005)). The spleen acts as a major pool for lymphocytes, including B cell, that are

recruited to the liver during liver injury (Klugewitz et al. 2004). Given the relatively strong expression of transgenic TFPI in the spleen compared to the liver of CD31-TFPI at baseline, it may be that the transgene is acting outside of the liver to alter the B cell phenotype, promoting a pro-resolution or protective B cell phenotype. Of note, the published literature shows that, in a $CCl_4$ model of chronic liver injury, liver fibrosis is attenuated in absence of B cells because of their role producing pro-inflammatory cytokines and their role in the recruitment of innate immune mononuclear cells (Thapa et al. 2015; Novobrantseva et al. 2005).

This hypothesis (B cell priming in the spleen) required detailed studies of the B cell population in the transgenic mice. With constraints on time and resources I decided that the model, at 24 hours, had provided supportive evidence already collected on the beneficial role of TFPI in liver injury and further extension of the model, given the potentially complex baseline phenotype, would not be of benefit.

## 6.3. Chapter Results Summary Table

| Parameter measured | $CCl_4$ chronic liver injury model vs. control (to 24 hours only) |
|---|---|
| **Liver collagen content** | Decreased hydroxyproline content.<br>Decreased collagen 1α1 gene expression. |
| **Hepatic stellate cell activation** | Decreased hepatic stellate cell activation BUT RELATIVE INCREASE FROM BASELINE greater than controls. |
| **MMP2 / MMP9 gene expression** | No difference. |
| **TIMP1 gene expression** | Decreased expression. |
| **Liver Immune cell composition** | Increased proportion of B cells. |
| **Liver injury** | Relative decrease in fold change of ALT from baseline. |

**Table 6-1: Summary of chronic liver injury model in CD31 targeted expression of TFPI**

Text in grey = non significant ($p<0.05$) trend

## 7. The Role of TFPI in Liver Injury – Conclusions

This work sought to explore the role of TFPI in liver injury through exploration of the hypothesis "*Cell specific expression of TFPI in acute and chronic liver injury would limit the progression and extent of liver injury".*

Two transgenic strains of mice, selectively expressing TFPI on αSMA or CD31 positive cells (creating local, cell specific over expression of TFPI), were used to explore the role of TFPI in acute liver injury (paracetamol and α-naphthylisothiocyanate induced) and chronic liver injury (carbon tetrachloride induced).

### 7.1. Acute liver injury

Decreased liver injury was evident in all acute liver injury models. Therefore TFPI does modify the extent and progression of acute liver injury.

All models (mouse strain and liver injury type) were subjected to initial model screening consisting of assessment of plasma liver function tests and percentage area of liver injury visible on H&E stained sections of liver. The αSMA-TFPI paracetamol model was selected for more in depth investigation due to extensive differences between transgenic and control mice, less variability in results within experimental groups and the positive identification of the TFPI positive effector cell (αSMA positive hepatic stellate cells).

The presence of less fibrin in the liver confirmed that the transgenic TFPI was acting to inhibit activation of the coagulation cascade and that this was potent enough to overcome propagation steps of the cascade that may have otherwise resulted in fibrin production. The reduced fibrin deposition throughout the model time points, confirms that Wanless et al's parenchymal extinction theory of the role of the coagulation cascade in liver fibrosis is also applicable in acute liver injury (Wanless, Liu, et al. 1995).

The decreased gene expression of PAR2 at 24 hours suggests that transgenic TFPI expression was associated with decreased production of PAR-2 receptors. The reduction in PAR2 gene expression was followed by a reduction in hepatic stellate cell activation and total hepatic macrophages at 48 hours after paracetamol induced acute liver injury, in keeping with reduced

PAR-2 associated pro-inflammatory stimuli, particularly TNF-α (Adams et al. 2011). However this was a transient finding and it appears that there may have been the need for a threshold of transgenic TFPI expression to be exceeded for this to occur and that the action of the transgenic TPFI created a form of negative feedback where increased TFPI expression limited hepatic stellate cell activation, reducing further TFPI expression.

Furthermore, decreased liver injury and hepatocellular proliferation was notable from 24 hours onwards but changes in hepatic stellate activation and the innate immune cell composition were present only at the later time point of 48 hours, suggesting that mechanisms to reduce liver injury occurred prior to this and that the measurable effect on the hepatic stellate cell activation and liver immune cell composition was the result of reduced liver injury, possibly via a decrease in the release of danger associated molecular patterns (DAMPs) (Szabo & Petrasek 2015).

Therefore, the role of parenchymal extinction due to early microvascular clot formation may be a more important driver for acute liver injury. The role of tissue hypoxia / ischaemia was not investigated in this work and presents an opportunity for future investigation.

The positive impact of transgenic TFPI on the extent and progression of acute liver injury suggests that the administration of TFPI to humans during episodes of acute liver injury may act to reduce overall injury. Further work (see below, section 7.1.2) is required before any form of human trial could

proceed and my concern would be that the results from this work are based on localised cell specific ‘administration’ of TFPI potentially at the inception of liver injury that is different to how we could currently administer TFPI to humans. TFPI (for administration to humans) is only available in recombinant form, which is short acting and needs to be continuously administered via intravenous access resulting in systemic dosing. This is reliant on the individual seeking medical intervention, which is likely to only occur after inception of liver injury and usually not until symptoms of acute liver failure are present.

| Parameter measured | Paracetamol acute liver injury model vs. control | | ANIT acute liver injury model vs. control | |
|---|---|---|---|---|
| | **αSMA-TFPI (6, 12, 24, 48 and 72 hours)** | **CD31-TFPI (6, 12 and 24 hours)** | **αSMA-TFPI (6, 24 and 48 hours)** | **CD31-TFPI (6, 24 and 48 hours)** |
| **Liver injury** | Decreased injury at 24-48 hours (complete injury resolution at 72 hours).<br><br>Decreased ALT from 12 – 72 hours.<br><br>Decreased ALP at 12 hours (and 24 - 48 hours).<br><br>Decreased bilirubin at 6 hours (and 24 – 48 hours). Increased at 12 hours.<br><br>Decreased cellular proliferation. | Decreased liver injury at 6 and 12 hours.<br><br>Decreased ALT at 6 and 12 hours.<br><br>Decreased ALP at 12 hours. | Decreased injury.<br><br>Decreased ALT at 24 hours<br><br>Decreased ALP at 6 and 24 hours. | Decreased liver injury.<br><br>Decreased ALT at 24 hours.<br><br>Decreased ALP at 6 and 24 hours.<br><br>Decreased total bilirubin at 24 hours and 48 hours. |
| **Fibrin deposition** | Decreased fibrin deposition (until resolution at 72 hours). | | | |
| **PAR expression** | Decreased PAR2 expression at 24 hours. | | | |
| **Liver immune cell composition** | Decreased proportion of macrophages at 48 hours.<br>Decreased proportion of mature tissue macrophages at 24 hours with greater Ly6C hi expression. | | | |
| **Hepatic stellate cell activation** | Increased activation at 12 hours.<br>Decreased activation at 48 hours. | | | |

**Table 7-1: Summary of acute liver injury results**

Text in grey = non-significant ($p<0.05$) trend

### *7.1.1. Limitations*

A major limitation of this work was the presence of baseline differences between transgenic and control mice. The αSMA-TFPI mice had a decreased proportion of NK cells and a predominance of Ly6C$^{int/lo}$ pro-resolution macrophages at baseline with evidence of transgenic gene expression but not protein expression in the liver. The CD31-TFPI mice were less extensively investigated but showed a significant difference in baseline ALT compared to controls at baseline only and the median for the group tested was still within the normal range. No difference in liver immune cell composition was identified. The CD31-TFPI demonstrated very little evidence of transgenic gene expression in the liver.

The presence of baseline differences does not preclude the use of data obtained from these models, nor necessarily alter the impact of the results obtained as long as they are acknowledged in conclusions drawn from the work. The biggest impact of these baseline differences is on the translational value of the data. In this case, administration of TFPI as a therapeutic agent in liver injury could only occur after the injury, whereas baseline effects of the transgenic TFPI alter the environment in which the actual injury occurs.

In this work only PAR gene expression was analysed. As receptors, PAR do not need to be continuously produced in order for them to be active. Gene expression indicates the production of more PAR protein and any changes from baseline can indicate the increased or decreased production of PAR.

This can be extrapolated to indicate an increase or decrease in PAR activation, based on the assumption that with greater activation there is an increased need to replace activated proteins but it is not a direct marker of PAR activity. However, Jesmin et al did demonstrate that gene expression did mirror protein expression (Jesmin et al. 2006).

Finally in some experiments the number of animals, particularly transgenic animals, did not reach that suggested by power calculations performed during experimental planning.

### *7.1.2. Future work*

Based on the results demonstrated here, future work could include:

- Identification of the CD31+ effector cell expressing TFPI in the CD31-TFPI mice through:
    - double immunohistochemical / fluorescent staining of FFPE sections with light microscopic or confocal microscopy evaluation
    - and / or flow cytometry phenoptyping
    - use of cell suspension preparation methods that utilise cell enrichment techniques such as CD31 labelled magnetic microbeads and separation columns
    - and / or flow cytometry based cell sorting to select CD31 positive cells for further analysis
- Evaluation of PAR protein expression by:
    - Western blotting
    - Or ELISA
- Assessment of the liver inflammatory cytokine profile by:
    - Cytokine array panels that utilise membrane based antibodies for parallel detection of multiple cytokines and chemokines
- Assessment of makers of tissue hypoxia (e.g. hypoxia inducible factors, HIFs) using similar methods mentioned above for protein detection.
- Administration of TPFI via a continuous infusion pump to control animals undergoing procedures to induce acute liver injury (to better model how humans could be administered TFPI).

The results of these investigations would enable me to work out a biological mechanism for the results seen in this work as well as test *in vivo* the validity of TFPI as a therapy to modify the progression and extent of acute liver injury.

Some of the proposed future work could be carried out on samples collected from this body of work and could form the basis of a number of short projects for undergraduates. *In vivo* work would require a greater level of training and time to optimise and would be more suited to postgraduate research.

### 7.2. Chronic liver injury

No consistent effect on liver fibrosis was seen in transgenic mice compared to control mice and therefore this work can conclude that cell specific TFPI associated inhibition of the coagulation cascade does not present a useful avenue for the modification of chronic liver injury and fibrosis.

An important finding, which builds on results from the acute liver injury models, is the consistent decrease in hepatic stellate cell activation in αSMA-TFPI mice. TFPI expression was confirmed on αSMA positive hepatic stellate cells supporting a role for TFPI in the modification of hepatic stellate cell biology.

| Parameter measured | $CCl_4$ chronic liver injury model vs. control | |
|---|---|---|
| | **αSMA-TFPI (24, 48, 72 and 96 hours)** | **CD31-TFPI (24 hours only)** |
| **Liver collagen content** | No difference. | Decreased collagen 1α1 gene expression and hydroxyproline content. |
| **Hepatic stellate cell activation** | Decreased activation at 24 hours. | Decreased hepatic stellate cell activation (*but relative increase from baseline*) greater than controls. |
| **MMP2 / MMP9 expression** | No difference. | No difference. |
| **TIMP1 expression** | No difference. | Decreased expression. |
| **Liver Immune cell composition** | Decreased proportion of macrophages at 24 (& 48) hours.<br>Decreased proportion of neutrophils at 24 hours.<br>Decreased proportion of NK cells at 24 hours. | Increased proportion of B cells. |
| **Liver injury** | Decreased ALT at 24 hours. | |

**Table 7-2: Summary of chronic liver injury results**

Text in grey = non significant ($p<0.05$) trend

### *7.2.1. Limitations*

The major limitation to this work was the lack of another chronic liver injury model to support the findings in the $CCl_4$ model. During the course of the body of work a supporting thioacetamide model of chronic liver injury was planned and undertaken, however the model was found to be flawed due to the timing of tissue harvest and cessation of the administration of the xenobiotic causing chronic liver injury. Briefly, mice were continuously administered thioacetamide up until they were culled. This differs from the $CCl_4$ model where at least 24 hours is left between the final dose of xenobiotic and the first collection of tissue. The $CCl_4$ model is widely used in the literature and, although I cannot find a specific article describing why a 24 hour gap is left, I presume that this is to avoid sampling the liver during an episode of acute on chronic liver injury.

Results from these thioacetamide models (see Appendix A) were somewhat contradictory, demonstrating overall increased liver fibrosis / collagen content despite reduced hepatic stellate cell activation. This is likely to be due to the difference described above. Ideally this thioacetamide model would have been repeated but limitations on resources, the lack of positive findings in the $CCl_4$ model of chronic liver injury and consideration of the 3Rs of animal research lead to my decision not to repeat the work.

All the methods, data and analyses relating to the flawed thioacetamide model are included in Appendix A.

As mentioned above (section 7.1.1), another limitation of this work was the presence of baseline differences between transgenic and control mice. However, in a chronic liver injury model, compared to an acute liver injury model, the impact of any baseline differences may be less due to the repeated and extended period of liver injury prior to evaluation of specific markers.

Beyond the baseline differences mentioned above, the αSMA-TFPI mice showed no further baseline differences compared to controls. The CD31-TFPI showed additional differences including decreased hepatic stellate cell activation and decreased MMP2 gene expression. The differences in the CD31-TFPI mice did complicate the interpretation of the chronic liver injury models, especially the proportion of activated hepatic stellate cells, which is a key variable for the assessment of chronic liver injury and fibrosis.

Finally, MMP2, MMP9 and TIMP1 gene expression only were measured in this work. MMP-2, -9 and TIMP-1 are complex enzymes and their inhibitor that are produced by a number of cells in the liver in both active and inactive forms. Gene expression only indicates the production of more or less protein and not the activity of that protein. However, when Knittel et al mapped the gene expression of MMP2 and MMP9 in chronic liver injury they found that gene expression did correspond to changes in the protein level (Knittel et al. 2000).

### *7.2.2. Future work*

While the data in this work suggests that further investigation of TFPI in chronic liver injury would not be of value, the following work could reinforce or explain some of the findings:

- A 0 hour time point for the $CCl_4$ model of chronic liver injury.
- At least a 24 hour time point for the TAA model of chronic liver injury.
- Identification of the CD31+ effector cell expressing TFPI in the CD31-TFPI mice as described in section 7.1.2
- MMP protein expression and zymography to ascertain their activity.
- Evaluatio of TIMP-1 protein expression by:
    - Western blotting
    - Or ELISA
- Assessment of fibrin deposition as carried out in the acute liver injury models.
- PAR gene and protein expression as carried out in the acute liver injury models and as described in section 7.1.2
- Assessment of the liver inflammatory cytokine profile as described in section 7.1.2
- *Ex-vivo* isolation of αSMA-TFPI hepatic stellate cells by:
    - Flow cytometry based cell sorting
    - Or cell suspension preparation methods that utilise cell enrichment techniques such as antibody labelled magnetic microbeads and separation columns

- Followed by *in vitro* examination of TFPI expression, surface marker expression (including PAR) and assessment of cytokine, MMP and TIMP production.

The results of these investigations would enable me to work out biological mechanisms for the results, potentially revealing alternative coagulation cascade targets in chronic liver injury that may prove more effective in altering the progression and extent of chronic liver injury than TFPI.

Some of the proposed future work could be carried out on samples collected from this body of work and could form the basis of a number of short projects for undergraduates.

## References


Abumiya, T. et al., 1995. An anti-tissue factor pathway inhibitor (TFPI) monoclonal antibody recognized the third Kunitz domain (K3) of free-form TFPI but not lipoprotein-associated forms in plasma. *J Biochem*, 118(1), pp.178–182. Available at: http://www.ncbi.nlm.nih.gov/pubmed/8537308.

Adams, M.N. et al., 2011. Structure, function and pathophysiology of protease activated receptors. *Pharmacol Ther*, 130(3), pp.248–282. Available at: http://www.ncbi.nlm.nih.gov/pubmed/21277892.

Ameri, A. et al., 1992. Expression of tissue factor pathway inhibitor by cultured endothelial cells in response to inflammatory mediators. *Blood*, 79(12), pp.3219–3226. Available at: http://www.ncbi.nlm.nih.gov/pubmed/1596565.

Anstee, Q.M. et al., 2008. Coagulation status modulates murine hepatic fibrogenesis: implications for the development of novel therapies. *J Thromb Haemost*, 6(8), pp.1336–1343. Available at: http://www.ncbi.nlm.nih.gov/pubmed/18485088.

Arai, M. et al., 1995. Blood coagulation equilibrium in rat liver microcirculation as evaluated by endothelial cell thrombomodulin and macrophage tissue factor. *Thrombosis research*, 80(2), pp.113–123.

Arthur, M.J., 2000. Fibrogenesis II. Metalloproteinases and their inhibitors in liver fibrosis. *Am J Physiol Gastrointest Liver Physiol*, 279(2), pp.G245–9. Available at: http://www.ncbi.nlm.nih.gov/pubmed/10915630.

Bajaj, M.S. et al., 1990. Cultured normal human hepatocytes do not synthesize lipoprotein-associated coagulation inhibitor: evidence that endothelium is the principal site of its synthesis. *Proc Natl Acad Sci U S A*, 87(22), pp.8869–8873. Available at: http://www.ncbi.nlm.nih.gov/pubmed/2247459.

Bajaj, M.S., Steer, S., et al., 1999. Synthesis and expression of tissue factor pathway inhibitor by serum-stimulated fibroblasts, vascular smooth muscle cells and cardiac myocytes. *Thromb Haemost*, 82(6), pp.1663–1672. Available at: http://www.ncbi.nlm.nih.gov/pubmed/10613653.

Bajaj, M.S., Kuppuswamy, M.N., et al., 1999. Transcriptional expression of tissue factor pathway inhibitor, thrombomodulin and von Willebrand factor in normal human tissues. *Thromb Haemost*, 82(3), pp.1047–1052. Available at: http://www.ncbi.nlm.nih.gov/pubmed/10494762.

Bataller, R. et al., 2005. Systemic infusion of angiotensin II exacerbates liver

fibrosis in bile duct-ligated rats. *Hepatology*, 41(5), pp.1046–1055.

Bonis, P.A., Friedman, S.L. & Kaplan, M.M., 2001. Is liver fibrosis reversible? *N Engl J Med*, 344(6), pp.452–454. Available at: http://www.ncbi.nlm.nih.gov/pubmed/11172184.

Borensztajn, K. et al., 2008. Factor Xa stimulates proinflammatory and profibrotic responses in fibroblasts via protease-activated receptor-2 activation. *Am J Pathol*, 172(2), pp.309–320. Available at: http://www.ncbi.nlm.nih.gov/pubmed/18202198.

Borensztajn, K. et al., 2010. The coagulation factor Xa/protease activated receptor-2 axis in the progression of liver fibrosis: a multifaceted paradigm. *J Cell Mol Med*, 14(1-2), pp.143–153. Available at: http://www.ncbi.nlm.nih.gov/pubmed/19968736.

Brien, P.J.O. et al., 2000. Thrombin Responses in Human Endothelial Cells. *Biochemistry*, 275(18), pp.13502–13509.

Broze Jr., G.J. et al., 1994. Heterogeneity of plasma tissue factor pathway inhibitor. *Blood Coagul Fibrinolysis*, 5(4), pp.551–559. Available at: http://www.ncbi.nlm.nih.gov/pubmed/7841311.

Broze Jr., G.J. et al., 1988. The lipoprotein-associated coagulation inhibitor that inhibits the factor VII-tissue factor complex also inhibits factor Xa: insight into its possible mechanism of action. *Blood*, 71(2), pp.335–343. Available at: http://www.ncbi.nlm.nih.gov/pubmed/3422166.

Broze Jr., G.J., 1995. Tissue factor pathway inhibitor and the revised theory of coagulation. *Annu Rev Med*, 46, pp.103–112. Available at: http://www.ncbi.nlm.nih.gov/pubmed/7598447.

Broze Jr., G.J. & Miletich, J.P., 1987. Isolation of the tissue factor inhibitor produced by HepG2 hepatoma cells. *Proc Natl Acad Sci U S A*, 84(7), pp.1886–1890. Available at: http://www.ncbi.nlm.nih.gov/pubmed/3031657.

Caplice, N.M., Mueske, C.S., Kleppe, L.S., Peterson, T.E., et al., 1998. Expression of tissue factor pathway inhibitor in vascular smooth muscle cells and its regulation by growth factors. *Circ Res*, 83(12), pp.1264–1270. Available at: http://www.ncbi.nlm.nih.gov/pubmed/9851943.

Caplice, N.M., Mueske, C.S., Kleppe, L.S. & Simari, R.D., 1998. Presence of tissue factor pathway inhibitor in human atherosclerotic plaques is associated with reduced tissue factor activity. *Circulation*, 98(11), pp.1051–1057. Available at: http://www.ncbi.nlm.nih.gov/pubmed/9736590.

Carpenter-Deyo, L. et al., 1991. Involvement of glutathione in 1-naphthylisothiocyanate (ANIT) metabolism and toxicity to isolated hepatocytes. *Biochemical pharmacology*, 42(11), pp.2171–2180. Available at: http://www.ncbi.nlm.nih.gov/pubmed/1958235.

Chang, J.Y. et al., 1999. TFPIbeta, a second product from the mouse tissue factor pathway inhibitor (TFPI) gene. *Thromb Haemost*, 81(1), pp.45–49. Available at: http://www.ncbi.nlm.nih.gov/pubmed/9974373.

Chen, D., Weber, M., et al., 2004. Complete inhibition of acute humoral rejection using regulated expression of membrane-tethered anticoagulants on xenograft endothelium. *Am J Transplant*, 4(12), pp.1958–1963. Available at: http://www.ncbi.nlm.nih.gov/pubmed/15575897.

Chen, D., Giannopoulos, K., et al., 2004. Inhibition of intravascular thrombosis in murine endotoxemia by targeted expression of hirudin and tissue factor pathway inhibitor analogs to activated endothelium. *Blood*, 104(5), pp.1344–1349. Available at: http://www.ncbi.nlm.nih.gov/pubmed/15126322.

Chen, D. et al., 2012. Inhibition of thrombin receptor signaling on alpha-smooth muscle actin(+) CD34(+) progenitors leads to repair after murine immune vascular injury. *Arterioscler Thromb Vasc Biol*, 32(1), pp.42–49. Available at: http://www.ncbi.nlm.nih.gov/pubmed/22034512.

Chen, D., Reisbeck, K., Kemball-Cook, G., et al., 1999. Inhibition of tissue factor-dependant and independant coagulation by cell surface expression of novel anticoagulant fusion proteins. *Transplantation*, 67(3), pp.467–474.

Chen, D. et al., 2006. NK-cell-dependent acute xenograft rejection in the mouse heart-to-rat model. *Xenotransplantation*, 13(5), pp.408–414. Available at: http://www.ncbi.nlm.nih.gov/pubmed/16925664.

Chen, D. et al., 2006. Postinjury vascular intimal hyperplasia in mice is completely inhibited by CD34+ bone marrow-derived progenitor cells expressing membrane-tethered anticoagulant fusion proteins. *Journal of Thrombosis and Haemostasis*, 4, pp.2191–2198.

Chen, D. et al., 2008. Regenerative repair after endoluminal injury in mice with specific antagonism of protease activated receptors in CD34+ vascular progenitors. *Blood*, 111, pp.4155–4164. Available at: http://bloodjournal.hematologylibrary.org/content/111/8/4155.full.pdf.

Chen, D., Reisbeck, K., McVey, J.H., et al., 1999. Regulated inhibition of coagulation by porcine endothelial cells expressing P-Selectin tagged

hirudin and tissue factor pathway inhibitor fusion proteins. *Transplantation*, 68(6), pp.832–839.

Chen, V.M. et al., 2006. Evidence for activation of tissue factor by an allosteric disulfide bond. *Biochemistry*, 45(39), pp.12020–12028. Available at: http://www.ncbi.nlm.nih.gov/pubmed/17002301.

Codes, L. et al., 2007. Liver fibrosis in women with chronic hepatitis C: evidence for the negative role of the menopause and steatosis and the potential benefit of hormone replacement therapy. *Gut*, 56(3), pp.390–395. Available at: http://www.ncbi.nlm.nih.gov/pubmed/17005762.

Connolly, A.K. et al., 1988. Early changes in bile duct lining cells and hepatocytes in rats treated with alpha-naphthylisothiocyanate. *Toxicol Appl Pharmacol*, 93(2), pp.208–219. Available at: http://www.ncbi.nlm.nih.gov/pubmed/2895967.

Copple, B.L. et al., 2003. Thrombin and protease-activated receptor-1 agonists promote lipopolysaccharide-induced hepatocellular injury in perfused livers. *J Pharmacol Exp Ther*, 305(2), pp.417–425. Available at: http://www.ncbi.nlm.nih.gov/pubmed/12606620.

Coughlin, S.R., 2000. Thrombin signalling and protease-activated receptors. *Nature*, 407, pp.258–264.

Crawley, J. et al., 2000. Expression, localization, and activity of tissue factor pathway inhibitor in normal and atherosclerotic human vessels. *Arterioscler Thromb Vasc Biol*, 20(5), pp.1362–1373. Available at: http://www.ncbi.nlm.nih.gov/pubmed/10807755.

Dahm, L.J. & Roth, R.A., 1991. Protection against alpha-naphthylisothiocyanate-induced liver injury by decreased hepatic non-protein sulfhydryl content. *Biochem Pharmacol*, 42(6), pp.1181–1188. Available at: http://www.ncbi.nlm.nih.gov/pubmed/1679629.

Dahm, L.J., Schultze, A.E. & Roth, R.A., 1991. An antibody to neutrophils attenuates alpha-naphthylisothiocyanate-induced liver injury. *J Pharmacol Exp Ther*, 256(1), pp.412–420. Available at: http://www.ncbi.nlm.nih.gov/pubmed/1846424.

DeLeve, L.D. et al., 2004. Rat liver sinusoidal endothelial cell phenotype is maintained by paracrine and autocrine regulation. *Am J Physiol Gastrointest Liver Physiol*, 287(4), pp.G757–63. Available at: http://www.ncbi.nlm.nih.gov/pubmed/15191879.

Dell, R.B., Holleran, S. & Ramakrishnan, R., 2002. Sample size determination. *ILAR J*, 43(4), pp.207–213. Available at: http://www.ncbi.nlm.nih.gov/pubmed/12391396.

Desmet, V.J. & Roskams, T., 2004. Cirrhosis reversal: a duel between dogma and myth. *J Hepatol*, 40(5), pp.860–867. Available at: http://www.ncbi.nlm.nih.gov/pubmed/15094237.

Dhar, A., 2011. *the Role of the Coagulation System in the Pathogenesis of Liver Injury*.

Drake, T.A., Morrissey, J.H. & Edgington, T.S., 1989. Selective cellular expression of tissue factor in human tissues. Implications for disorders of hemostasis and thrombosis. *Am J Pathol*, 134(5), pp.1087–1097. Available at: http://www.ncbi.nlm.nih.gov/pubmed/2719077.

Duffield, J.S., 2003. The inflammatory macrophage: a story of Jekyll and Hyde. *Clinical Science*, 104, pp.27–38.

Duplantier, J.G. et al., 2004. A role for thrombin in liver fibrosis. *Gut*, 53(11), pp.1682–1687. Available at: http://www.ncbi.nlm.nih.gov/pubmed/15479692.

Ferro, D., Celestini, A. & Violi, F., 2009. Hyperfibrinolysis in liver disease. *Clin Liver Dis*, 13(1), pp.21–31. Available at: http://www.ncbi.nlm.nih.gov/pubmed/19150306.

Fiorucci, S. et al., 2004. PAR1 antagonism protects against experimental liver fibrosis. Role of proteinase receptors in stellate cell activation. *Hepatology*, 39(2), pp.365–375. Available at: http://www.ncbi.nlm.nih.gov/pubmed/14767989.

Flossel, C. et al., 1994. Immunohistochemical detection of tissue factor (TF) on paraffin sections of routinely fixed human tissue. *Histochemistry*, 101(6), pp.449–453. Available at: http://link.springer.com/10.1007/BF00269495.

Friedman, S.L., 2008. Hepatic fibrosis -- overview. *Toxicology*, 254(3), pp.120–129. Available at: http://www.ncbi.nlm.nih.gov/pubmed/18662740.

Friedman, S.L., 2008. Hepatic Stellate Cells: Protean, multifunctional, and enigmatic cells of the liver. *Physiol Rev*, 88, pp.125–172.

Fujiwara, K. et al., 1988. Antithrombin III concentrate in the treatment of fulminant hepatic failure. *Gastroenterologia Japonica*, 23(4), pp.423–427.

Gaca, M.D., Zhou, X. & Benyon, R.C., 2002. Regulation of hepatic stellate cell proliferation and collagen synthesis by proteinase-activated receptors. *J Hepatol*, 36(3), pp.362–369. Available at: http://www.ncbi.nlm.nih.gov/pubmed/11867180.

Gailani, D. & Renné, T., 2007. Intrinsic Pathway of Coagulation and Arterial Thrombosis. *Arteriosclerosis, Thrombosis, and Vascular Biology* , 27

(12 ), pp.2507–2513. Available at: http://atvb.ahajournals.org/content/27/12/2507.abstract.

Ganey, P.E. et al., 2007. Role of the coagulation system in acetaminophen-induced hepatotoxicity in mice. *Hepatology*, 46(4), pp.1177–1186. Available at: http://www.ncbi.nlm.nih.gov/pubmed/17654741.

Gautier, E.L. et al., 2012. Gene-expression profiles and transcriptional regulatory pathways that underlie the identity and diversity of mouse tissue macrophages. *Nature immunology*, 13(11), pp.1118–1128.

Geissmann, F. et al., 2010. Development of monocytes, macrophages, and dendritic cells. *Science*, 327(5966), pp.656–661. Available at: http://www.ncbi.nlm.nih.gov/pubmed/20133564.

Girard, T.J. et al., 1989. Functional significance of the Kunitz-type inhibitory domains of lipoprotein-associated coagulation inhibitor. *Nature*, 338(6215), pp.518–520. Available at: http://www.ncbi.nlm.nih.gov/pubmed/2927510.

Gori, A.M. et al., 1999. Tissue factor reduction and tissue factor pathway inhibitor release after heparin administration. *Thromb Haemost*, 81(4), pp.589–593. Available at: http://www.ncbi.nlm.nih.gov/pubmed/10235445.

Gottfried, E. et al., 2008. Expression of CD68 in non-myeloid cell types. *Scandinavian journal of immunology*, 67(5), pp.453–463.

Goulding, C. et al., 2007. The impact of inherited prothrombotic risk factors on individuals chronically infected with hepatitis C virus from a single source. *J Viral Hepat*, 14(4), pp.255–259. Available at: http://www.ncbi.nlm.nih.gov/pubmed/17381717.

Grubb, S.C., Bult, C.J. & Bogue, M.A., 2014. Mouse Phenome Database. *Nucleic Acids Research*, 42(D1).

Habib, M. et al., 2014. Evidence of rebalanced coagulation in acute liver injury and acute liver failure as measured by thrombin generation. *Liver international : official journal of the International Association for the Study of the Liver*, 34(5), pp.672–8. Available at: http://www.ncbi.nlm.nih.gov/pubmed/24164805.

Hague, S. et al., 2002. Protease activated receptor-1 is down regulated by levonorgestrel in endometrial stromal cells. *Angiogenesis*, 5(1-2), pp.93–98. Available at: http://www.ncbi.nlm.nih.gov/pubmed/12549865.

Han, X. et al., 1999. Structural requirements for TFPI-mediated inhibition of neointimal thickening after balloon injury in the rat. *Arterioscler Thromb Vasc Biol*, 19(10), pp.2563–2567. Available at:

http://www.ncbi.nlm.nih.gov/pubmed/10521388.

Hansen, J.B. et al., 2000. Rebound activation of coagulation after treatment with unfractionated heparin and not with low molecular weight heparin is associated with partial depletion of tissue factor pathway inhibitor and antithrombin. *Thromb Res*, 100(5), pp.413–417. Available at: http://www.ncbi.nlm.nih.gov/pubmed/11150584.

Hansen, J.B. et al., 1997. Tissue factor pathway inhibitor in complex with low density lipoprotein isolated from human plasma does not possess anticoagulant function in tissue factor-induced coagulation in vitro. *Thromb Res*, 85(5), pp.413–425. Available at: http://www.ncbi.nlm.nih.gov/pubmed/9076898.

Hartland, S.N. et al., 2009. Active matrix metalloproteinase-2 promotes apoptosis of hepatic stellate cells via the cleavage of cellular N-cadherin. *Liver International*, 29(7), pp.966–978.

Hemmann, S. et al., 2007. Expression of MMPs and TIMPs in liver fibrosis - a systematic review with special emphasis on anti-fibrotic strategies. *Journal of Hepatology*, 46(5), pp.955–975.

Henderson, N.C. & Iredale, J.P., 2007. Liver fibrosis: cellular mechanisms of progression and resolution. *Clin Sci (Lond)*, 112(5), pp.265–280. Available at: http://www.ncbi.nlm.nih.gov/pubmed/17261089.

Hinson, J.A., Roberts, D.W. & James, L.P., 2010. Mechanisms of acetaminophen-induced liver necrosis. *Handb Exp Pharmacol*, (196), pp.369–405. Available at: http://www.ncbi.nlm.nih.gov/pubmed/20020268.

Hitchman, E. et al., 2011. Effect of prolonged formalin fixation on immunohistochemical staining for the proliferation marker Ki67. *Histopathology*, 59(6), pp.1261–3. Available at: http://www.ncbi.nlm.nih.gov/pubmed/21939458.

Holt, M.P., Cheng, L. & Ju, C., 2008. Identification and characterization of infiltrating macrophages in acetaminophen-induced liver injury. *J Leukoc Biol*, 84(6), pp.1410–1421. Available at: http://www.ncbi.nlm.nih.gov/pubmed/18713872.

Hugenholtz, G.C. et al., 2013. TAFI deficiency promotes liver damage in murine models of liver failure through defective down-regulation of hepatic inflammation. *Thromb Haemost*, 109(5), pp.948–955. Available at: http://www.ncbi.nlm.nih.gov/pubmed/23467679.

Ikarashi, M. et al., 2013. Distinct development and functions of resident and recruited liver Kupffer cells/macrophages. *Journal of Leukocyte Biology*, 94(6), pp.1325–1336. Available at:

http://www.jleukbio.org/content/94/6/1325.abstract.

Iredale, J.P., Thompson, A. & Henderson, N.C., 2013. Extracellular matrix degradation in liver fibrosis: Biochemistry and regulation. *Biochimica et biophysica acta*, 1832(7), pp.876–83. Available at: http://www.sciencedirect.com/science/article/pii/S0925443912002530 [Accessed June 4, 2015].

Ito, Y. et al., 2003. Early hepatic microvascular injury in response to acetaminophen toxicity. *Microcirculation (New York, N.Y.: 1994)*, 10(5), pp.391–400.

Jacquemin, M. et al., 2006. FVIII production by human lung microvascular endothelial cells. *Blood*, 108(2), pp.515–517. Available at: http://www.ncbi.nlm.nih.gov/pubmed/16569771.

Jaeschke, H. & Bajt, M.L., 2006. Intracellular signaling mechanisms of acetaminophen-induced liver cell death. *Toxicological sciences : an official journal of the Society of Toxicology*, 89(1), pp.31–41.

Jaeschke, H., Xie, Y. & Mcgill, M.R., 2014. Review Article Acetaminophen-induced Liver Injury : from Animal Models to Humans. *Journal of Clinical Translational Hepatology*, 2, pp.153–161.

James, J. et al., 1990. Sirius red histophotometry and spectrophotometry of sections in the assessment of the collagen content of liver tissue and its application in growing rat liver. *Liver*, 10(1), pp.1–5.

Jesmin, S. et al., 2006. Chronological expression of PAR isoforms in acute liver injury and its amelioration by PAR2 blockade in a rat model of sepsis. *Thrombosis and Haemostasis*, 96(6), pp.830–838.

Johnston, G.I., Cook, R.G. & McEver, R.P., 1989. Cloning of GMP-140, a granule membrane protein of platelets and endothelium: sequence similarity to proteins involved in cell adhesion and inflammation. *Cell*, 56(6), pp.1033–1044. Available at: http://www.ncbi.nlm.nih.gov/pubmed/2466574.

Joshi, N. et al., 2015. Coagulation-driven platelet activation reduces cholestatic liver injury and fibrosis in mice. *Journal of Thrombosis and Haemostasis*, 13(1), pp.57–71.

Ju, C. & Tacke, F., 2016. Hepatic macrophages in homeostasis and liver diseases: from pathogenesis to novel therapeutic strategies. *Cellular and Molecular Immunology*, (October 2015), pp.1–12. Available at: http://www.nature.com/doifinder/10.1038/cmi.2015.104.

Kallis, Y.N. et al., 2014. Proteinase activated receptor 1 mediated fibrosis in a

mouse model of liver injury: a role for bone marrow derived macrophages. *PLoS One*, 9(1), p.e86241. Available at: http://www.ncbi.nlm.nih.gov/pubmed/24475094.

Karlmark, K.R. et al., 2009. Hepatic recruitment of the inflammatory Gr1+ monocyte subset upon liver injury promotes hepatic fibrosis. *Hepatology*, 50(1), pp.261–274. Available at: http://www.ncbi.nlm.nih.gov/pubmed/19554540.

Kataoka, H. et al., 2014. Evaluation of the Contribution of Multiple DAMPs and DAMP Receptors in Cell Death-Induced Sterile Inflammatory Responses. *PloS one*, 9(8), p.e104741. Available at: http://www.pubmedcentral.nih.gov/articlerender.fcgi?artid=4134227&tool=pmcentrez&rendertype=abstract.

Kerr, R., 2003. New insights into haemostasis in liver failure. *Blood Coagul Fibrinolysis*, 14 Suppl 1, pp.S43–5. Available at: http://www.ncbi.nlm.nih.gov/pubmed/14567536.

Klugewitz, K. et al., 2004. The composition of intrahepatic lymphocytes: Shaped by selective recruitment? *Trends in Immunology*, 25(11), pp.590–594.

Knight, V. et al., 2012. Protease-activated receptor 2 promotes experimental liver fibrosis in mice and activates human hepatic stellate cells. *Hepatology*, 55(3), pp.879–887. Available at: http://www.ncbi.nlm.nih.gov/pubmed/22095855.

Knittel, T. et al., 2000. Expression of matrix metalloproteinases and their inhibitors during hepatic tissue repair in the rat. *Histochemistry and cell biology*, 113(6), pp.443–453.

Knittel, T. et al., 1999. Localization of liver myofibroblasts and hepatic stellate cells in normal and diseased rat livers: Distinct roles of (myo-)fibroblast subpopulations in hepatic tissue repair. *Histochemistry and Cell Biology*.

Kodali, P. et al., 2006. ANIT toxicity toward mouse hepatocytes in vivo is mediated primarily by neutrophils via CD18. *American journal of physiology. Gastrointestinal and liver physiology*, 291(2), pp.G355–G363.

Kopec, A.K. & Luyendyk, J.P., 2014. Coagulation in liver toxicity and disease: Role of hepatocyte tissue factor. *Thrombosis Research*, 133(SUPPL. 1), pp.1–7.

Krenkel, O., Mossanen, J.C. & Tacke, F., 2014. Immune mechanisms in acetaminophen-induced acute liver failure. *Hepatobiliary surgery and nutrition*, 3(6), pp.331–43.

Langley, P.G. et al., 1993. Controlled trial of antithrombin III supplementation in fulminant hepatic failure. *Journal of hepatology*, 17(3), pp.326–331.

Lemoinne, S. et al., 2013. Origins and functions of liver myofibroblasts. *Biochim Biophys Acta*. Available at: http://www.ncbi.nlm.nih.gov/pubmed/23470555.

Levy, G.A. et al., 1983. The effect of mouse hepatitis virus infection on the microcirculation of the liver. *Hepatology*, 3(6), pp.964–973. Available at: http://www.ncbi.nlm.nih.gov/pubmed/6313508.

Levy, G.A., Leibowitz, J.L. & Edgington, T.S., 1982. Lymphocyte-instructed monocyte induction of the coagulation pathways parallels the induction of hepatitis by the murine hepatitis virus. *Prog Liver Dis*, 7, pp.393–409. Available at: http://www.ncbi.nlm.nih.gov/pubmed/6287526.

Lindahl, A.K., Sandset, P.M. & Abildgaard, U., 1992. The present status of tissue factor pathway inhibitor. *Blood Coagul Fibrinolysis*, 3(4), pp.439–449. Available at: http://www.ncbi.nlm.nih.gov/pubmed/1420819.

Liu, Y. et al., 2013. Animal models of chronic liver diseases. *Am J Physiol Gastrointest Liver Physiol*, 304(5), pp.G449–68. Available at: http://www.ncbi.nlm.nih.gov/pubmed/23275613.

Lupu, C., Kruithof, E.K., et al., 1999. Acute release of tissue factor pathway inhibitor after in vivo thrombin generation in baboons. *Thromb Haemost*, 82(6), pp.1652–1658. Available at: http://www.ncbi.nlm.nih.gov/pubmed/10613651.

Lupu, C., Poulsen, E., et al., 1999. Cellular effects of heparin on the production and release of tissue factor pathway inhibitor in human endothelial cells in culture. *Arterioscler Thromb Vasc Biol*, 19(9), pp.2251–2262. Available at: http://www.ncbi.nlm.nih.gov/pubmed/10479670.

Lupu, C. et al., 1995. Thrombin induces the redistribution and acute release of tissue factor pathway inhibitor from specific granules within human endothelial cells in culture. *Arterioscler Thromb Vasc Biol*, 15(11), pp.2055–2062. Available at: http://www.ncbi.nlm.nih.gov/pubmed/7583589.

Luyendyk, J.P. et al., 2009. Tissue factor-dependent coagulation contributes to alpha-naphthylisothiocyanate-induced cholestatic liver injury in mice. *Am J Physiol Gastrointest Liver Physiol*, 296(4), pp.G840–9. Available at: http://www.ncbi.nlm.nih.gov/pubmed/19179621.

Luyendyk, J.P., Mackman, N. & Sullivan, B.P., 2011. Role of fibrinogen and protease-activated receptors in acute xenobiotic-induced cholestatic liver

injury. *Toxicol Sci*, 119(1), pp.233–243. Available at: http://www.ncbi.nlm.nih.gov/pubmed/20974703.

Lwaleed, B.A. & Bass, P.S., 2006. Tissue factor pathway inhibitor: structure, biology and involvement in disease. *J Pathol*, 208(3), pp.327–339. Available at: http://www.ncbi.nlm.nih.gov/pubmed/16261634.

Mackman, N. et al., 1993. Murine tissue factor gene expression in vivo. Tissue and cell specificity and regulation by lipopolysaccharide. *Am J Pathol*, 143(1), pp.76–84. Available at: http://www.ncbi.nlm.nih.gov/pubmed/8317556.

Mann, K.G., Krudysz-Amblo, J. & Butenas, S., 2012. Tissue factor controversies. *Thromb Res*, 129 Suppl , pp.S5–7. Available at: http://www.ncbi.nlm.nih.gov/pubmed/22401799.

Mannucci, P.M. et al., 2001. Changes in health and disease of the metalloprotease that cleaves von Willebrand factor. *Blood*, 98(9), pp.2730–2735. Available at: http://www.ncbi.nlm.nih.gov/pubmed/11675345.

Maroney, S.A. & Mast, A.E., 2008. Expression of tissue factor pathway inhibitor by endothelial cells and platelets. *Transfus Apher Sci*, 38(1), pp.9–14. Available at: http://www.ncbi.nlm.nih.gov/pubmed/18261960.

Marra, F. et al., 1998. Expression of the thrombin receptor in human liver: up-regulation during acute and chronic injury. *Hepatology*, 27(2), pp.462–471.

Marra, F. et al., 2009. Mononuclear cells in liver fibrosis. *Seminars in Immunopathology*, 31(3), pp.345–358. Available at: http://link.springer.com/10.1007/s00281-009-0169-0.

Martinelli, A. et al., 2008. Effect of a thrombin receptor (protease-activated receptor 1, PAR-1) gene polymorphism in chronic hepatitis C liver fibrosis. *J Gastroenterol Hepatol*, 23(9), pp.1403–1409. Available at: http://www.ncbi.nlm.nih.gov/pubmed/18005014.

Mast, A.E. et al., 2000. Tissue factor pathway inhibitor binds to platelet thrombospondin-1. *J Biol Chem*, 275(41), pp.31715–31721. Available at: http://www.ncbi.nlm.nih.gov/pubmed/10922378.

McVey, J.H., 1994. Tissue factor pathway. *Baillieres Clin Haematol*, 7(3), pp.469–484. Available at: http://www.ncbi.nlm.nih.gov/pubmed/7841596.

Michel, T. et al., 2013. Consequences of the crosstalk between monocytes / macrophages and natural killer cells. , 3(January), pp.1–6.

Miyakawa, K. et al., 2015. *Platelets and protease-activated receptor-4*

*contribute to acetaminophen-induced liver injury in mice*, Available at: http://www.bloodjournal.org/cgi/doi/10.1182/blood-2014-09-598656.

Moles A Fau - Sanchez, A.M. et al., 2013. Inhibition of RelA-Ser536 phosphorylation by a competing peptide reduces mouse liver fibrosis without blocking the innate immune response. *Hepatology*, 57(2), pp.817–828.

van Montfoort, M.L. & Meijers, J.C.M., 2013. Anticoagulation beyond direct thrombin and factor Xa inhibitors: Indications for targeting the intrinsic pathway? *Thrombosis and Haemostasis*, 110(2), pp.223–232.

Mouse Genome Informatics, 2008. Alimentary canal removed to display lobes of the liver. From The Anatomy of the Laboratory Mouse by Margaret J. Cook. Available at: http://www.informatics.jax.org/cookbook/figures/figure60.shtml [Accessed June 26, 2013].

Muciño-Bermejo, J. et al., 2013. Coagulation abnormalities in the cirrhotic patient. *Annals of Hepatology*, 12(5), pp.713–724.

Murphy, F.R. et al., 2002. Inhibition of apoptosis of activated hepatic stellate cells by tissue inhibitor of metalloproteinase-1 is mediated via effects on matrix metalloproteinase inhibition: implications for reversibility of liver fibrosis. *J Biol Chem*, 277(13), pp.11069–11076.

Murray, P.J. & Wynn, T.A., 2011. Protective and pathogenic functions of macrophage subsets. *Nature Reviews Immunology*, 11(11), pp.723–737.

Nakanishi-Matsui, M. et al., 2000. PAR3 is a cofactor for PAR4 activation by thrombin. *Nature*, 404(6778), pp.609–613.

Novobrantseva, T.I. et al., 2005. Attenuated liver fibrosis in the absence of B cells. *Journal of Clinical Investigation*, 115(11), pp.3072–3082.

Novotny, W.F. et al., 1988. Platelets secrete a coagulation inhibitor functionally and antigenically similar to the lipoprotein associated coagulation inhibitor. *Blood*, 72(6), pp.2020–2025. Available at: http://www.ncbi.nlm.nih.gov/pubmed/3143429.

Novotny, W.F. et al., 1989. Purification and characterization of the lipoprotein-associated coagulation inhibitor from human plasma. *J Biol Chem*, 264(31), pp.18832–18837. Available at: http://www.ncbi.nlm.nih.gov/pubmed/2553722.

O'Grady, J.G., 2005. Acute liver failure. *Postgrad Med J*, 81(953), pp.148–154. Available at: http://www.ncbi.nlm.nih.gov/pubmed/15749789.

Oksuzoglu, G. et al., 1997. Tissue factor pathway inhibitor concentrations in

cirrhotic patients with and without portal vein thrombosis. *The American journal of gastroenterology*, 92(2), pp.303–306.

Ossovskaya, V.S. & Bunnett, N.W., 2004. Protease-activated receptors: contribution to physiology and disease. *Physiol Rev*, 84(2), pp.579–621. Available at: http://www.ncbi.nlm.nih.gov/pubmed/15044683.

Osterud, B. et al., 1995. Sites of tissue factor pathway inhibitor (TFPI) and tissue factor expression under physiologic and pathologic conditions. On behalf of the Subcommittee on Tissue factor Pathway Inhibitor (TFPI) of the Scientific and Standardization Committee of the ISTH. *Thromb Haemost*, 73(0340-6245 (Print)), pp.873–875.

Osterud, B., 2010. Tissue factor expression in blood cells. *Thromb Res*, 125 Suppl , pp.S31–4. Available at: http://www.ncbi.nlm.nih.gov/pubmed/20149415.

Osterud, B. & Rapaport, S.I., 1977. Activation of factor IX by the reaction product of tissue factor and factor VII: additional pathway for initiating blood coagulation. *Proc Natl Acad Sci U S A*, 74(12), pp.5260–5264. Available at: http://www.ncbi.nlm.nih.gov/pubmed/271951.

Ott, I. et al., 2001. Regulation of monocyte procoagulant activity in acute myocardial infarction: role of tissue factor and tissue factor pathway inhibitor-1. *Blood*, 97(12), pp.3721–3726. Available at: http://www.ncbi.nlm.nih.gov/pubmed/11389008.

Owens 3rd, A.P. & Mackman, N., 2011. Microparticles in hemostasis and thrombosis. *Circ Res*, 108(10), pp.1284–1297. Available at: http://www.ncbi.nlm.nih.gov/pubmed/21566224.

Palmier, M.O. et al., 1992. Clearance of recombinant tissue factor pathway inhibitor (TFPI) in rabbits. *Thromb Haemost*, 68(1), pp.33–36. Available at: http://www.ncbi.nlm.nih.gov/pubmed/1514170.

Papatheodoridis, G. V et al., 2003. Thrombotic risk factors and extent of liver fibrosis in chronic viral hepatitis. *Gut*, 52(3), pp.404–409. Available at: http://www.ncbi.nlm.nih.gov/pubmed/12584224.

Papatheodoridis, G. V et al., 2009. Thrombotic risk factors and liver histologic lesions in non-alcoholic fatty liver disease. *J Hepatol*, 51(5), pp.931–938. Available at: http://www.ncbi.nlm.nih.gov/pubmed/19726097.

Pellicoro, A. et al., 2014. Liver fibrosis and repair: immune regulation of wound healing in a solid organ. *Nature Reviews Immunology*, 14(3), pp.181–194. Available at: http://www.nature.com/doifinder/10.1038/nri3623.

PerkinElmer, 2012. *User's Manual for Nuance 3.0.2*, USA.

Piro, O. & Broze Jr., G.J., 2005. Comparison of cell-surface TFPIalpha and beta. *J Thromb Haemost*, 3(12), pp.2677–2683. Available at: http://www.ncbi.nlm.nih.gov/pubmed/16246254.

Piro, O. & Broze Jr., G.J., 2004. Role for the Kunitz-3 domain of tissue factor pathway inhibitor-alpha in cell surface binding. *Circulation*, 110(23), pp.3567–3572. Available at: http://www.ncbi.nlm.nih.gov/pubmed/15557366.

Possamai, L.A., 2010. Role of monocytes and macrophages in experimental and human acute liver failure. *World Journal of Gastroenterology*, 16(15), p.1811.

Possamai, L.A., 2015. *Susceptibilty factors in paracetamol-induced acute liver failure*. Imperial College London.

Poujol-Robert, A., Boelle, P.Y., et al., 2004. Factor V Leiden as a risk factor for cirrhosis in chronic hepatitis C. *Hepatology*, 39(4), pp.1174–1175. Available at: http://www.ncbi.nlm.nih.gov/pubmed/15057924.

Poujol-Robert, A., Rosmorduc, O., et al., 2004. Genetic and acquired thrombotic factors in chronic hepatitis C. *Am J Gastroenterol*, 99(3), pp.527–531. Available at: http://www.ncbi.nlm.nih.gov/pubmed/15056097.

Poynard, T. et al., 2001. Rates and risk factors of liver fibrosis progression in patients with chronic hepatitis c. *J Hepatol*, 34(5), pp.730–739. Available at: http://www.ncbi.nlm.nih.gov/pubmed/11434620.

Poynard, T., Bedossa, P. & Opolon, P., 1997. Natural history of liver fibrosis progression in patients with chronic hepatitis C. The OBSVIRC, METAVIR, CLINIVIR, and DOSVIRC groups. *Lancet*, 349(9055), pp.825–832. Available at: http://www.ncbi.nlm.nih.gov/pubmed/9121257.

Pradella, P. et al., 2011. Platelet production and destruction in liver cirrhosis. *J Hepatol*, 54(5), pp.894–900. Available at: http://www.ncbi.nlm.nih.gov/pubmed/21145808.

Pruitt, K.D. et al., 2012. NCBI Reference Sequences (RefSeq): current status, new features and genome annotation policy. *Nucleic Acids Res*, 40, pp.D130–5.

Radaeva, S. et al., 2006. Natural killer cells ameliorate liver fibrosis by killing activated stellate cells in NKG2D-dependent and tumor necrosis factor-related apoptosis-inducing ligand-dependent manners. *Gastroenterology*, 130(2), pp.435–452. Available at: http://www.ncbi.nlm.nih.gov/pubmed/16472598.

Rake, M.O. et al., 1971. EARLY AND INTENSIVE THERAPY OF INTRAVASCULAR COAGULATION IN ACUTE LIVER FAILURE. *The Lancet*, 298(7736), pp.1215–1218. Available at: http://www.thelancet.com/article/S014067367190540X/fulltext [Accessed September 23, 2015].

Ramachandran, P. et al., 2012. Differential Ly-6C expression identifies the recruited macrophage phenotype, which orchestrates the regression of murine liver fibrosis. *Proc Natl Acad Sci U S A*, 109(46), pp.E3186–95. Available at: http://www.ncbi.nlm.nih.gov/pubmed/23100531.

Ramaiah, S. & Jaeschke, H., 2007. Role of Neutrophils in the Pathogenesis of Acute Inflammatory Liver Injury. *Toxicologic Pathology*, 35(6), pp.757–766. Available at: http://tpx.sagepub.com/cgi/doi/10.1080/01926230701584163.

Rasband, W.., 2014. ImageJ 1.46r. Available at: http://imagej.nih.gov/ij/.

Rehg, J.E., Bush, D. & Ward, J.M., 2012. The Utility of Immunohistochemistry for the Identification of Hematopoietic and Lymphoid Cells in Normal Tissues and Interpretation of Proliferative and Inflammatory Lesions of Mice and Rats. *Toxicologic Pathology*, 40(2), pp.345–374.

Reinhardt, C. et al., 2008. Protein disulfide isomerase acts as an injury response signal that enhances fibrin generation via tissue factor activation. *Journal of Clinical Investigation*, 118(3), pp.1110–1122.

Rezaie, A.R., 2014. Protease-activated receptor signalling by coagulation proteases in endothelial cells. , pp.876–882.

Richards, J. a. et al., 2015. Acute Liver Injury Is Independent of B Cells or Immunoglobulin M. *Plos One*, 10(9), p.e0138688. Available at: http://dx.plos.org/10.1371/journal.pone.0138688.

Riesbeck, K. et al., 1998. Expression of hirudin fusion proteins in mammalian cells: a strategy for prevention of intravascular thrombosis. *Circulation*, 98(24), pp.2744–2752. Available at: http://www.ncbi.nlm.nih.gov/pubmed/9851962.

Riesbeck, K. et al., 1997. Human tissue factor pathway inhibitor fused to CD4 binds both FXa and TF/FVIIa at the cell surface. *Thromb Haemost*, 78(6), pp.1488–1494. Available at: http://www.ncbi.nlm.nih.gov/pubmed/9423800.

Rullier, A. et al., 2006. Expression of protease-activated receptors and tissue factor in human liver. *Virchows Archiv*, 448(1), pp.46–51.

Rullier, A. et al., 2008. Protease-activated receptor 1 knockout reduces

experimentally induced liver fibrosis. *Am J Physiol Gastrointest Liver Physiol*, 294(1), pp.G226–35. Available at: http://www.ncbi.nlm.nih.gov/pubmed/17962354.

Sandset, P.M., 1996. Tissue factor pathway inhibitor (TFPI)--an update. *Haemostasis*, 26 Suppl 4, pp.154–165. Available at: http://www.ncbi.nlm.nih.gov/pubmed/8979119.

Sandset, P.M., Abildgaard, U. & Larsen, M.L., 1988. Heparin induces release of extrinsic coagulation pathway inhibitor (EPI). *Thromb Res*, 50(6), pp.803–813. Available at: http://www.ncbi.nlm.nih.gov/pubmed/3413731.

Schaer, D.J. et al., 2001. Molecular cloning and characterization of the mouse CD163 homologue, a highly glucocorticoid-inducible member of the scavenger receptor cysteine-rich family. *Immunogenetics*, 53(2), pp.170–177.

Schmittgen, T.D. & Livak, K.J., 2008. Analyzing real-time PCR data by the comparative C(T) method. *Nature protocols*, 3(6), pp.1101–1108.

Shi, Y.-F. et al., 2007. Hypoxia induces the activation of human hepatic stellate cells LX-2 through TGF-beta signaling pathway. *FEBS letters*.

Shimizu, I., 2003. Impact of oestrogens on the progression of liver disease. *Liver Int*, 23(1), pp.63–69. Available at: http://www.ncbi.nlm.nih.gov/pubmed/12640729.

Shimokawa, T. et al., 2000. Down-regulation of murine tissue factor pathway inhibitor mRNA by endotoxin and tumor necrosis factor-alpha in vitro and in vivo. *Thromb Res*, 100(3), pp.211–221. Available at: http://www.ncbi.nlm.nih.gov/pubmed/11108908.

Singanayagam, A. & Bernal, W., 2015. Update on acute liver failure. *Current Opinion in Critical Care*.

Smith, C.M. et al., 2014. The mouse Gene Expression Database (GXD): 2014 update. *Nucleic Acids Research*, 42(D1).

Spicer, E.K. et al., 1987. Isolation of cDNA clones coding for human tissue factor: primary structure of the protein and cDNA. *Proc Natl Acad Sci U S A*, 84(15), pp.5148–5152. Available at: http://www.ncbi.nlm.nih.gov/pubmed/3037536.

Stephenne, X. et al., 2007. Tissue factor-dependent procoagulant activity of isolated human hepatocytes: relevance to liver cell transplantation. *Liver Transpl*, 13(4), pp.599–606. Available at: http://www.ncbi.nlm.nih.gov/pubmed/17394166.

Sullivan, B.P. et al., 2013. Hepatocyte tissue factor activates the coagulation

cascade in mice. *Blood*, 121(10), pp.1868–1874. Available at: http://www.ncbi.nlm.nih.gov/pubmed/23305736.

Sullivan, B.P., Wang, R., et al., 2010. Protective and damaging effects of platelets in acute cholestatic liver injury revealed by depletion and inhibition strategies. *Toxicol Sci*, 115(1), pp.286–294. Available at: http://www.ncbi.nlm.nih.gov/pubmed/20133375.

Sullivan, B.P., Weinreb, P.H., et al., 2010. The coagulation system contributes to alphaVbeta6 integrin expression and liver fibrosis induced by cholestasis. *Am J Pathol*, 177(6), pp.2837–2849. Available at: http://www.ncbi.nlm.nih.gov/pubmed/21037076.

Szabo, G. & Petrasek, J., 2015. Inflammasome activation and function in liver disease. *Nature Reviews Gastroenterology & Hepatology*, 12(7), pp.387–400. Available at: http://www.nature.com/doifinder/10.1038/nrgastro.2015.94.

Tacke, F. & Randolph, G.J., 2006. Migratory fate and differentiation of blood monocyte subsets. *Immunobiology*, 211(6-8), pp.609–18. Available at: http://www.sciencedirect.com/science/article/pii/S0171298506000751 [Accessed August 11, 2015].

Tacke, F. & Zimmermann, H.W., 2015. Macrophage heterogeneity in liver injury and fibrosis. *Journal of Hepatology*, 60(5), pp.1090–1096. Available at: http://dx.doi.org/10.1016/j.jhep.2013.12.025.

Thapa, M. et al., 2015. Supplementary material Liver fibrosis occurs through dysregulation of MyD88-dependent innate B cell activity Affiliations : , 30329(404), pp.2067–2079.

Tripodi, A. et al., 2009. An imbalance of pro- vs anti-coagulation factors in plasma from patients with cirrhosis. *Gastroenterology*, 137(6), pp.2105–2111. Available at: http://www.ncbi.nlm.nih.gov/pubmed/19706293.

Uhlén, M. et al., 2015. Tissue-based map of the human proteome. *Science*, 347(6220). Available at: http://www.sciencemag.org/content/347/6220/1260419.abstract.

Wanless, I.R., Wong, F., et al., 1995. Hepatic and portal vein thrombosis in cirrhosis: Possible role in development of parenchymal extinction and portal hypertension. *Hepatology*, 21(5), pp.1238–1247.

Wanless, I.R., Liu, J.J. & Butany, J., 1995. Role of thrombosis in the pathogenesis of congestive hepatic fibrosis (cardiac cirrhosis). *Hepatology*, 21(5), pp.1232–1237.

Warshawsky, I., Broze Jr., G.J. & Schwartz, A.L., 1994. The low density

lipoprotein receptor-related protein mediates the cellular degradation of tissue factor pathway inhibitor. *Proc Natl Acad Sci U S A*, 91(14), pp.6664–6668. Available at: http://www.ncbi.nlm.nih.gov/pubmed/7517557.

Weerasinghe, S. V et al., 2011. Fibrinogen-gamma proteolysis and solubility dynamics during apoptotic mouse liver injury: heparin prevents and treats liver damage. *Hepatology*, 53(4), pp.1323–1332. Available at: http://www.ncbi.nlm.nih.gov/pubmed/21480334.

Werling, R.W. et al., 1993. Distribution of tissue factor pathway inhibitor in normal and malignant human tissues. *Thromb Haemost*, 69(4), pp.366–369. Available at: http://www.ncbi.nlm.nih.gov/pubmed/8497849.

Williams, R. et al., 2014. Addressing liver disease in the UK: a blueprint for attaining excellence in health care and reducing premature mortality from lifestyle issues of excess consumption of alcohol, obesity, and viral hepatitis. *Lancet (London, England)*, 384(9958), pp.1953–97. Available at: http://www.sciencedirect.com/science/article/pii/S0140673614618389 [Accessed September 16, 2015].

Willingham, A.K. & Matschiner, J.T., 1989. The activation of factor X by hepatocyte plasma membranes. *Cell Mol Biol*, 35(4), pp.421–429. Available at: http://www.ncbi.nlm.nih.gov/pubmed/2611830.

Wojtukiewicz, M.Z. et al., 1999. Expression of tissue factor and tissue factor pathway inhibitor in situ in laryngeal carcinoma. *Thromb Haemost*, 82(6), pp.1659–1662. Available at: http://www.ncbi.nlm.nih.gov/pubmed/10613652.

Wright, M. et al., 2003. Factor V Leiden polymorphism and the rate of fibrosis development in chronic hepatitis C virus infection. *Gut*, 52, pp.1206–1210.

Wu, Z. et al., 2010. Acute liver failure: Mechanisms of immune-mediated liver injury. *Liver International*, 30(6), pp.782–794.

Wun, T.C. et al., 1988. Cloning and characterization of a cDNA coding for the lipoprotein-associated coagulation inhibitor shows that it consists of three tandem Kunitz-type inhibitory domains. *J Biol Chem*, 263(13), pp.6001–6004. Available at: http://www.ncbi.nlm.nih.gov/pubmed/2452157.

Wynn, T.A. & Barron, L., 2010. Macrophages: master regulators of inflammation and fibrosis. *Semin Liver Dis*, 30(3), pp.245–257. Available at: http://www.ncbi.nlm.nih.gov/pubmed/20665377.

Xu, J.W. et al., 2002. Estrogen reduces CCL4- induced liver fibrosis in rats. *World J Gastroenterol*, 8(5), pp.883–887. Available at: http://www.ncbi.nlm.nih.gov/pubmed/12378635.

Yona, S. et al., 2013. Fate Mapping Reveals Origins and Dynamics of Monocytes and Tissue Macrophages under Homeostasis. *Immunity*, 38(1), pp.79–91. Available at: http://www.ncbi.nlm.nih.gov/pubmed/23273845.

Zhang, J. et al., 2003. Glycosyl phosphatidylinositol anchorage of tissue factor pathway inhibitor. *Circulation*, 108(5), pp.623–627. Available at: http://www.ncbi.nlm.nih.gov/pubmed/12835228.

Zigmond, E. et al., 2014. Infiltrating monocyte-derived macrophages and resident kupffer cells display different ontogeny and functions in acute liver injury. *Journal of immunology (Baltimore, Md.: 1950)*, 193(1), pp.344–353.

Zimmermann, H.W., Trautwein, C. & Tacke, F., 2012. Functional role of monocytes and macrophages for the inflammatory response in acute liver injury. *Frontiers in physiology*, 3, p.56.

## Appendix A

This appendix contains all background information, data and analyses relating to the thioacetamide model of chronic liver injury carried out as supporting model for the $CCl_4$ model of chronic liver injury also used in the body of work but abandoned due to a flaw in experimental design.

## A.1. Background: Thioacetamide (TAA) chronic liver injury model

Thioacetamide (TAA) is another commonly used xenobiotic for the experimental induction of liver injury in mice. TAA is metabolised to thioacetamide-S-oxide that is a potent reactive oxygen species. Hepatocellular damage occurs in periportal and centrilobular hepatocytes and long term exposure results in progressive liver fibrosis through the activation of hepatic stellate cells, the expression of pro-fibrogenic and pro-inflammatory cytokines (including IL-1β, TGF- β, PDGF and TNF-α) and the production of MMP-9 by neutrophils and to a lesser extent, leukocytes and Kupffer cells (Liu et al. 2013; Salguero Palacios et al. 2008). With cessation of thioacetamide, fibrosis resolves.

## A.2. Methods: Thioacetamide induced liver injury

Under Home Office Licence 70/6493 and 70/8060, 6-8 week old transgenic and background strain matched wild type controls (C57BL6/J, Harlan UK) were administered 0.03% w/v thioacetamide (Sigma) dissolved in autoclaved drinking water for 8 weeks (Teixeira-Clerc et al. 2006) and then culled as described in section 2.4.

Vehicle only treated mice were administered autoclaved drinking water only.

Mice were monitored using minimally invasive parameters (observation of body condition and weight, minimal handling) and in accordance with guidance set out in the licence.

A power calculation based on pilot cohort Sirius red collagen staining data suggested 6 animals per experimental arm.

## A.3. Thioacetamide (TAA) induced chronic liver injury in αSMA targeted expression of TFPI

### *A.3.1. Plasma liver function tests*

After TAA administration there was a statistically significant decrease in plasma ALP and total bilirubin in αSMA-TFPI mice compared to C57BL6/J control mice (Mann Whitney test, $p = <0.0001$ and $p = 0.008$ respectively. Figure A 1. Graphs B and C). There was no statistically significant difference in plasma ALT in αSMA-TFPI mice compared to control mice (Figure A 1. Graph B). There were n=9 in the control group and n=7 in the αSMA-TFPI group. Baseline sample numbers were as previously noted in section 3.1.

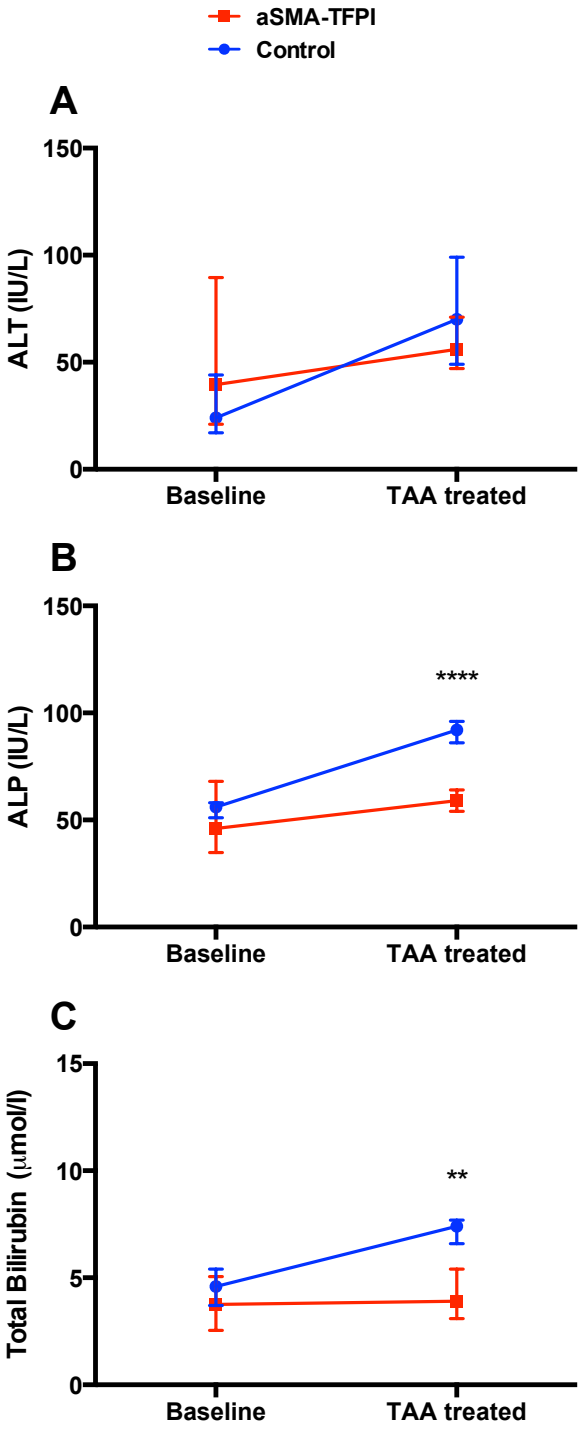


**Figure A 1: TAA induced chronic liver injury, plasma liver function tests**

Symbols indicate median. Bars indicate interquartile range.

** p=<0.01. **** p=<0.0001.

**Graph A**: Plasma ALT (IU/L). Median after TAA administration, 70IU/L and 56IU/L in (2.9 and 1.4 fold change from baseline) control and αSMA-TFPI strains respectively.

**Graph B:** Plasma ALP (IU/L). Median after TAA administration, 92IU/L and 59IU/L (1.6 and 1.2 fold change from baseline) in control and αSMA-TFPI strains respectively.

**Graph C:** Plasma total bilirubin (µmol/L). Median after TAA administration, 7.4µmol/L and 3.9µmol/L (1.6 and 1.0 fold change from baseline) in control and αSMA-TFPI strains respectively.

### *A.3.2. Liver collagen content*

Digital image analysis of liver FFPE sections stained with Sirius red from mice administered TAA showed no statistically significant difference in liver collagen deposition in αSMA-TFPI mice compared to C57BL6/J control mice (Figure A 2. Graph A). There were n=10 in both the control and the αSMA-TFPI group. Baseline sample numbers were as previously noted in section 4.1.

Hydroxyproline quantification of the collagen content of livers from mice administered TAA showed a statistically significant increase in liver collagen content in αSMA-TFPI mice compared to control mice (Mann Whitney test p = 0.03. Figure A 2. Graph B). There were n=5 in both the control and the αSMA-TFPI group. The sample number was below that suggested by the power calculation due to failed assays.

Quantitative PCR of cDNA reverse transcribed from whole liver homogenate RNA from mice culled after TAA administration showed no statistically significant difference in collagen 1α1 gene expression in the livers of αSMA-TFPI mice compared to control mice (Figure A 2. Graph C). There were n=10 in both the control and the αSMA-TFPI group. Baseline sample numbers were as previously noted in section 4.1.

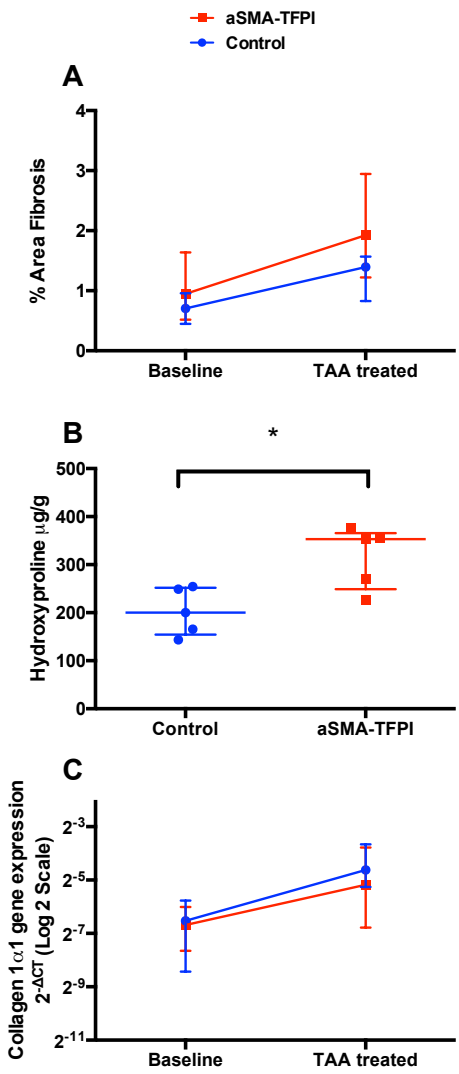


**Figure A 2: TAA induced chronic liver injury, liver collagen content**

Symbols indicate median. Bars indicate interquartile range.

* p=<0.05.

**Graph A:** Percentage Sirius red staining in liver FFPE tissue sections from mice administered TAA. Median 1.4% and 1.9% in control and αSMA-TFPI strains respectively.

**Graph B:** Hydroxyproline content (µg/g of liver) in livers from mice administered TAA. Median 200µg/g and 353µg/g in control and αSMA-TFPI strains respectively. *Bars indicate median with interquartile range.*

**Graph C:** Collagen 1α1 gene expression in whole liver homogenates. αSMA-TFPI mice had a 2.7 fold change (increase) in collagen 1α1 gene expression after TAA administration compared to baseline. Control mice had a 5.8 fold change (increase) compared to baseline.

**Image 1**

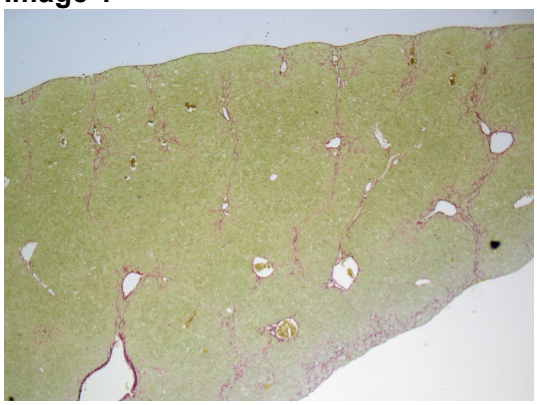

**Image 2**

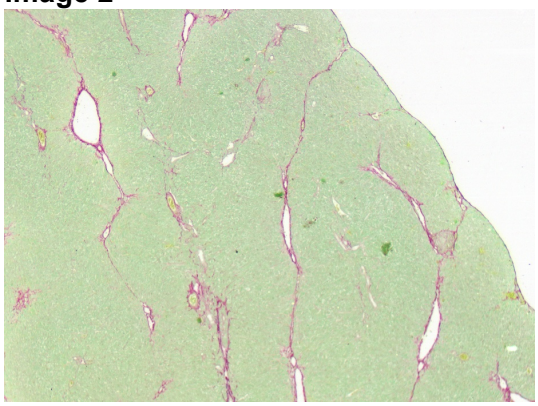

**Image 1:** Sirius Red. Control mouse. Original x40 magnification. **Image 2:** Sirius Red. αSMA-TFPI mouse. Original x40 magnification.

### *A.3.3. Hepatic stellate cell activation*

Digital image analysis of FFPE liver sections from mice culled after TAA administration were stained using an antibody for αSMA and showed a statistically significant decrease in the number of activated hepatic stellate cells in the livers of αSMA-TFPI mice compared to control mice (Mann Whitney test p = <0.0001.Figure A 3. Graph A). There were n=9 in the control group and n=10 in the αSMA-TFPI group. Baseline sample numbers were as previously noted in section 3.1.

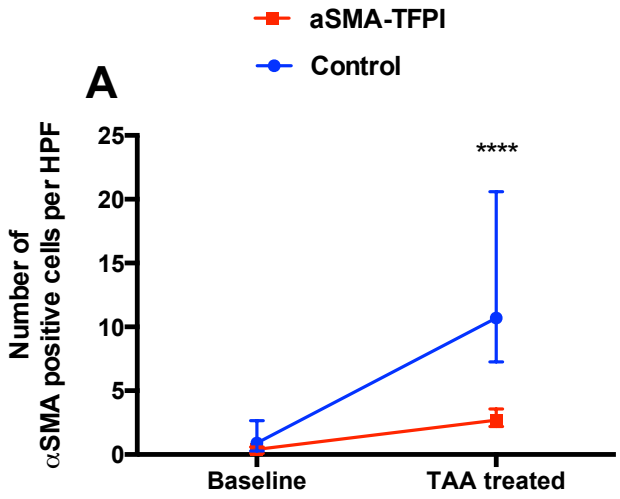


**Figure A 3: TAA induced chronic liver injury, αSMA immunohistochemistry**
Symbols indicate median. Bars indicate interquartile range.

**** p=<0.0001.

**Graph A:** Number of activated hepatic stellate cells in liver FFPE tissue sections as determined by αSMA immunohistochemistry. Median after TAA administration 10.7 cells per HPF and 2.7 cells per HPF (12 and 6.8 fold change from baseline) in control and αSMA-TFPI strains respectively.

### *A.3.4. Collagen turnover*

Quantitative PCR of cDNA reverse transcribed from whole liver homogenate RNA from mice administered TAA showed a statistically significant decrease in MMP9 gene expression and statistically significant increase in TIMP1 gene expression in αSMA-TFPI mice compared to C57BL6/J control mice (Mann Whitney test $p = 0.04$ and $p = 0.02$ respectively. Figure A 4. Graphs B and C). There was no statistically significant difference in MMP2 gene expression in αSMA-TFPI mice compared to control mice (Figure A 4. Graph A).

There were n=10 in both the control and the αSMA-TFPI group for all gene expression assays. Baseline sample numbers were as previously noted in section 4.1.

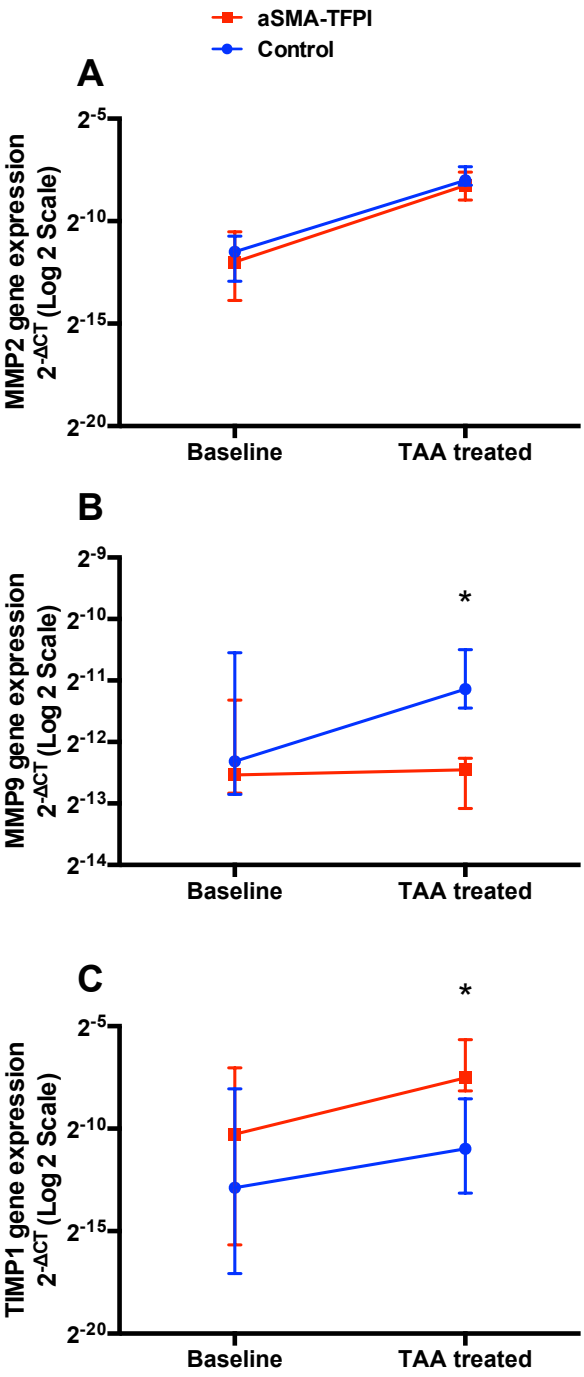


**Figure A 4: TAA induced chronic liver injury, matrixmetalloproteinase and TIMP gene expression**

**Graph A:** MMP2 gene expression in whole liver homogenates. αSMA-TFPI mice had a 13.7 fold change (increase) and control mice had a 17.9 fold change (increase) in MMP2 gene expression after TAA administration compared to baseline.

**Graph B:** MMP9 gene expression in whole liver homogenates. αSMA-TFPI mice had a -1.4 fold change (decrease) and control mice had a 1.5 fold change (increase) in MMP9 gene expression after TAA administration compared to baseline.

**Graph C:** TIMP1 gene expression in whole liver homogenates. αSMA-TFPI mice had a 9.8 fold change (increase) and control mice had a 4.1 fold change (increase) in TIMP1 gene expression after TAA administration compared to baseline.

### *A.3.5. Liver immune cell composition*

Digital image analysis of liver FFPE sections from mice administered TAA were stained using an antibody for F4/80 and showed no statistically significant difference in the number of F4/80 positive macrophages in the livers of αSMA-TFPI mice compared to C57BL6/J control mice (Figure A 5. Graph A). There were n=10 in both the control and the αSMA-TFPI group. Baseline sample numbers were as previously noted in section 3.1.

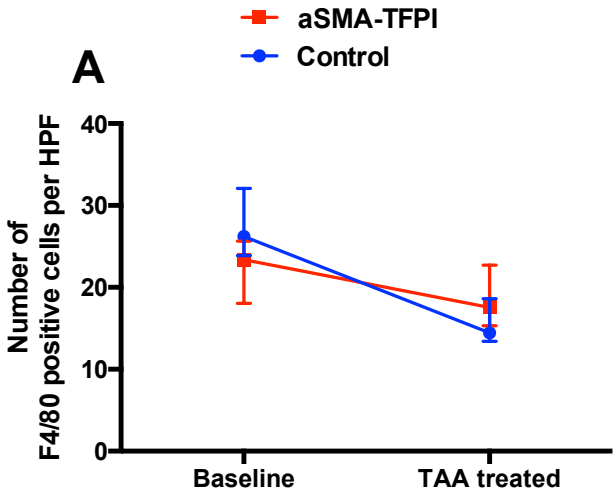


**Figure A 5: TAA induced chronic liver injury, F4/80 immunohistochemistry**
Symbols indicate median. Bars indicate interquartile range.

**Graph A:** Number of macrophages in liver FFPE tissue sections as determined by F4/80 immunohistochemistry. Median at 24 hours after TAA administration, 14.5 cells per HPF and 17.6 cells per HPF (-1.7 and -1.3 fold change from baseline) in control and αSMA-TFPI strains respectively.

### *A.3.6. Model summary - TAA induced chronic liver injury in αSMA targeted expression of TFPI*

This model was initiated to provide further evidence to support the data collected in the $CCl_4$ model of chronic liver injury, however it was abandoned after a single cohort because a flaw in the experimental design was identified. Mice were continuously administered thioacetamide (TAA) up until they were culled. This differs from the $CCl_4$ model where at least 24 hours is left between the final dose of xenobiotic and the first collection of tissue. The $CCl_4$ model is widely used in the literature and, although I cannot find a specific article describing why a 24 hour gap is left, I presume that this is to avoid sampling the liver during an episode of acute on chronic liver injury.

Due to the overall lack of impact of αSMA targeted TFPI expression on the progression of chronic liver injury in a $CCl_4$ model I felt it was inappropriate to repeat a modified version of the TAA model. However some brief conclusions have been drawn from the data collected from this TAA model of chronic liver injury.

Prior models have suggested a protective / pro-resolution effect of transgenic TFPI expression. Some of the results from the TAA model support this. The most notable result from this TAA model and all the other αSMA-TFPI models of liver injury is the reduction in hepatic stellate cell activation (not measured in the ANIT model of acute liver injury). This suggests that, if only on a cellular level, TFPI can act to reduce hepatic stellate activation.

In the TAA model of chronic liver injury there was reduced plasma ALP and total bilirubin in αSMA-TFPI mice compared to controls. The combination of changes in the plasma ALP and bilirubin does suggest some alteration in the extent of bile duct damage, but this was not seen histologically and, with a lack of histological evidence for reduced bile duct injury, these are non-specific markers (elevated / reduced in a number of disease processes) and the significance of this is uncertain within the limits of the data collected.

The MMP9, TIMP1 and hydroxyproline results in this model are difficult to interpret and are likely to be indicative of the model flaw described above. On one hand, comparatively reduced MMP-9 and increased TIMP-1 production suggests a pro-fibrotic environment, which is supported by the increased hydroxyproline result. However other markers of fibrosis did not confirm the hydroxylproline result and some studies have shown that MMP-9 production is not altered from baseline in chronic liver injury (Knittel et al. 2000; Hemmann et al. 2007), as was the case in this model. MMP-9 is produced by a number of cells including activated hepatic stellate cells and therefore it is also possible that the relatively decreased production fits with decreased hepatic stellate cell activation seen in transgenic mice compared to control mice.

TIMP-1 is predominantly expressed by activated hepatic stellate cells and therefore its relatively increased expression is contrary to the relatively decreased activation of hepatic stellate cells in the transgenic mice. It is possible that, in the setting of TAA induced chronic liver injury in mice expressing transgenic TFPI, alternate cell types such as macrophages are

induced to produce TIMP-1 (Hemmann et al. 2007). Immunohistochemical detection of TIMP-1 protein expression or flow cytometry phenotyping of TIMP-1 expressing cells may help to clarify this result. The role of TFPI in these results, other than its impact on hepatic stellate cell activation, cannot be elucidated from this work.

## A.4. Thioacetamide (TAA) induced chronic liver injury in CD31 targeted expression of TFPI

### *A.4.1. Plasma liver function tests*

As previously noted, there was a statistically significant increase in baseline ALT in CD31-TFPI transgenic mice compared to control mice (Figure A 6. Graphs A). Of note, plasma albumin was not measured for this experiment.

After TAA administration there was no statistically significant difference in any plasma liver function tests of CD31-TFPI mice compared to control mice (Figure A 6. Graphs A-C). There was a trend towards decreased plasma ALT and total bilirubin in CD31-TFPI mice compared to controls after TAA administration, and in each parameter this indicated no change or a small decrease from baseline measurements. However this did not reach statistical significance in adequately powered comparisons (n=7 in the CD31-TFPI group and n=9 in the control group).

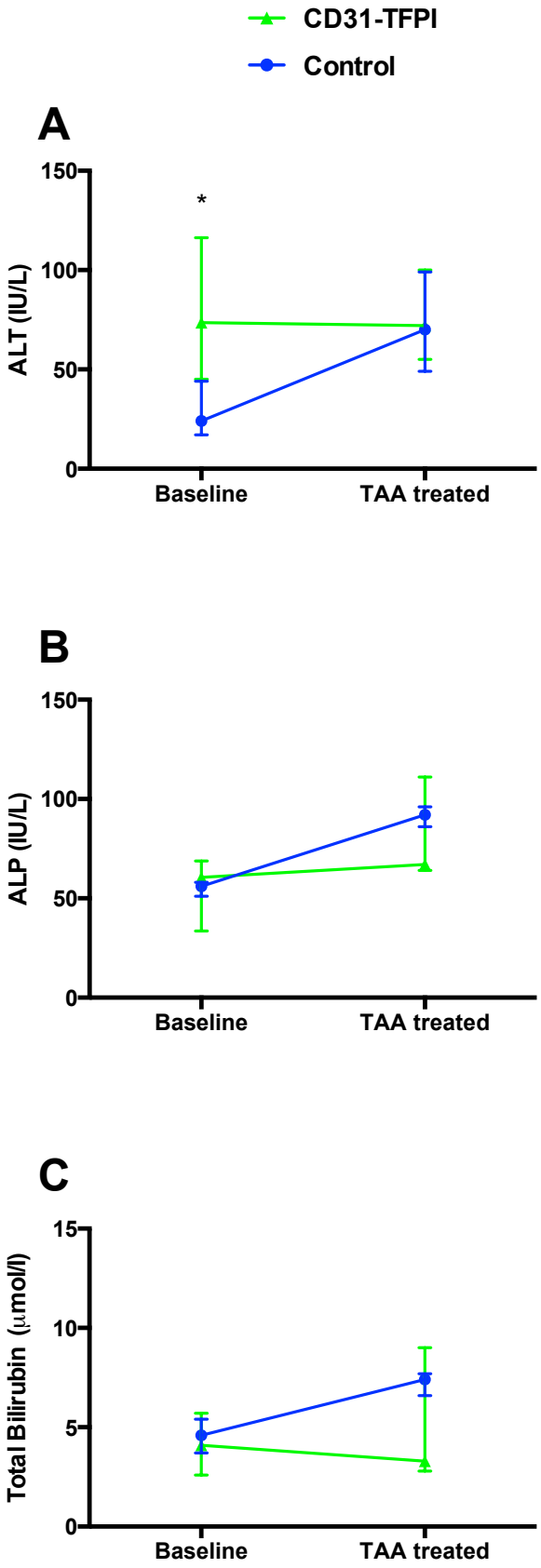


**Figure A 6: TAA induced chronic liver injury, plasma liver function tests**

Symbols indicate median. Bars indicate interquartile range.

* p=<0.05.

**Graph A**: Plasma ALT (IU/L). Median after TAA administration, 70IU/L and 72IU/L (2.9 and 1.0 fold change from baseline) in control and CD31-TFPI strains respectively.

**Graph B:** Plasma ALP (IU/L). Median after TAA administration, 92IU/L and 67IU/L (1.6 and 1.1 fold change from baseline) in control and CD31-TFPI strains respectively.

**Graph C:** Plasma total bilirubin (μmol/L). Median after TAA administration, 7.4μmol/L and 3.3μmol/L (1.6 and -1.2 fold change from baseline) in control and CD31-TFPI strains respectively.

### *A.4.2. Liver collagen content*

Digital image analysis of liver FFPE sections stained with Sirius red from mice administered TAA showed a statistically significant increase in liver collagen deposition in CD31-TFPI mice compared to controls (Mann Whitney U, p = 0.005. **Figure A 7**. Graph A). There were n=10 in both the control and the CD31-TFPI group. Baseline sample numbers were as previously noted in section 6.1.

Hydroxyproline quantification of the collagen content of livers from mice administered TAA showed a statistically significant increase in liver collagen content in CD31-TFPI mice compared to control mice (Mann Whitney U, p = 0.008. **Figure A 7**. Graph B). There were n=5 in both the control and the CD31-TFPI group. Sample numbers were less than the power calculation sample number due to failed assays or insufficient assay reagents.

Quantitative PCR of cDNA reverse transcribed from whole liver homogenate RNA from mice culled after TAA administration showed a statistically significant increase in collagen 1$\alpha$1 gene expression in the livers of CD31-TFPI mice compared to control mice (Mann Whitney U, p = 0.01. **Figure A 7**. Graph C). There were n=10 in both the control and the CD31-TFPI group. Baseline sample numbers were as previously noted in section 6.1.

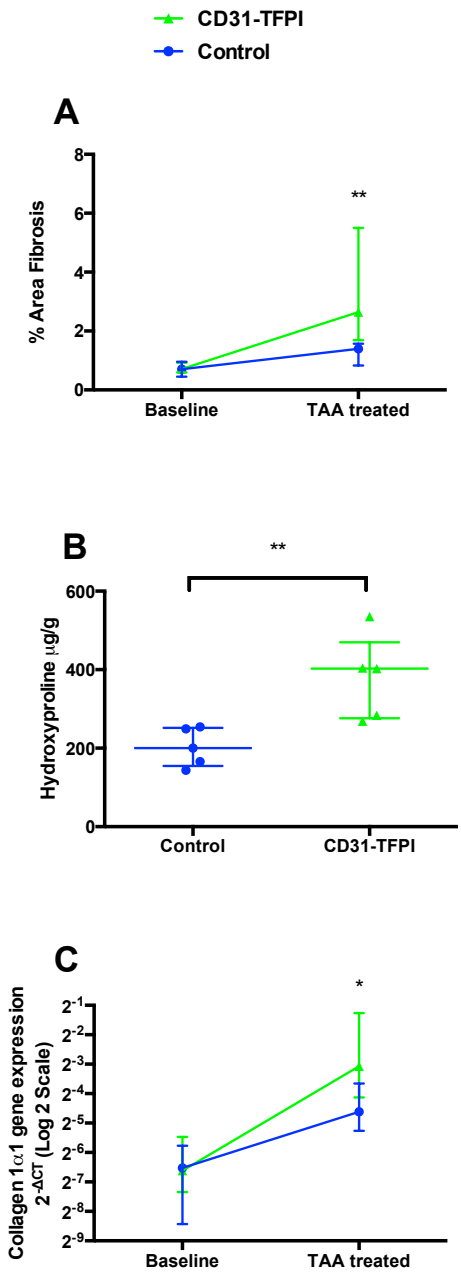


**Figure A 7: TAA induced chronic liver injury, liver collagen content**

Symbols indicate median. Bars indicate interquartile range.

* p=<0.05. ** p=<0.01.

**Graph A:** Percentage Sirius red staining in liver FFPE tissue sections from mice administered TAA. Median 1.4% and 2.6% in control and CD31-TFPI strains respectively.

**Graph B:** Hydroxyproline content (µg/g of liver) in livers from mice administered TAA. Median 200µg/g and 402µg/g in control and CD31-TFPI strains respectively. *Bars indicate median with interquartile range.*

**Graph C:** Collagen 1α1 gene expression in whole liver homogenates. CD31-TFPI mice had a 12.8 fold change (increase) in collagen 1α1 gene expression after TAA administration compared to baseline. Control mice had a 5.8 fold change (increase) in collagen 1α1 gene expression compared to baseline.

**Image 1:** Sirius Red. Control mouse. Original x40 magnification.

**Image 2:** Sirius Red. CD31-TFPI mouse. Original x40 magnification**.**

**Image 1**

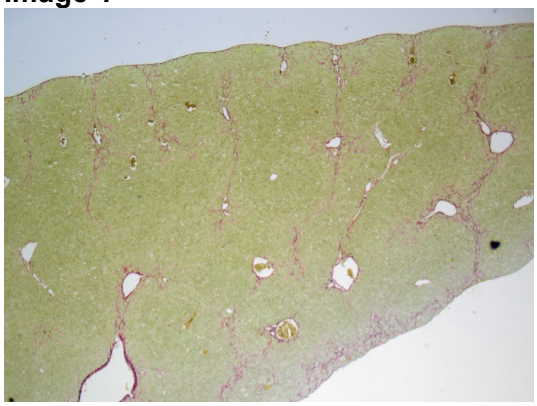

**Image 2**

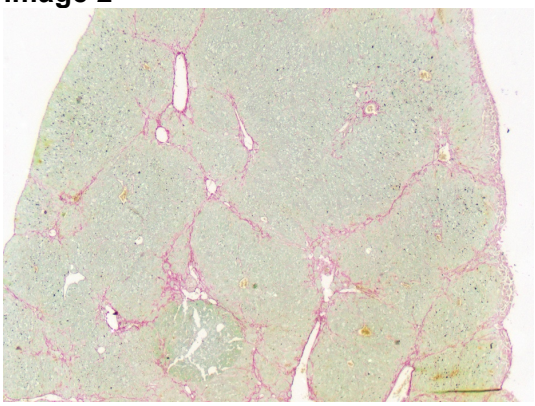

### *A.4.3. Hepatic stellate cell activation*

As previously noted, at baseline there was a statistically significant decrease in the number of activated hepatic stellate cells in the liver of CD31-TFPI mice compared to control mice (Figure A 8. Graph A).

Digital image analysis of FFPE liver sections from mice culled after TAA administration were stained using an antibody for αSMA and showed a statistically significant decrease in the number of activated hepatic stellate cells in the livers of CD31-TFPI mice compared to control mice (Mann Whitney U test; p = 0.006. Figure A 8. Graph A). However, given the baseline differences seen in the number of activate hepatic stellate cells, CD31-TFPI mice demonstrated a 38 fold increase in the number of hepatic stellate cells from baseline and control mice demonstrated only a 12 fold increase. There were n=9 in the control group and n=10 in the CD31-TFPI group. Baseline sample numbers were as previously noted in section 6.1.

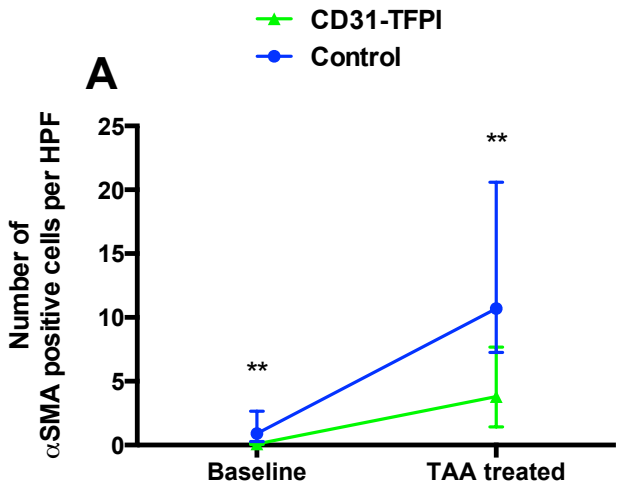


**Figure A 8: TAA induced chronic liver injury, αSMA immunohistochemistry**
Symbols indicate median. Bars indicate interquartile range.

** p=<0.01.

**Graph A:** Number of activated hepatic stellate cells in liver FFPE tissue sections as determined by αSMA immunohistochemistry. Median after TAA administration 10.7 cells per HPF and 3.8 cells per HPF (12 and 38 fold change from baseline) in control and CD31-TFPI strains respectively.

### *A.4.4. Collagen turnover*

As previously noted, at baseline there was a statistically significant increase in the expression of MMP2 in the liver of CD31-TFPI mice compared to control mice (Figure A 9. Graph A).

Quantitative PCR of cDNA reverse transcribed from whole liver homogenate RNA from mice administered TAA showed a statistically significant increase in MMP9 gene expression in CD31-TFPI mice compared to control mice (Mann Whitney U test; p = 0.03. Figure A 9. Graph B). No statistically significant difference was seen in MMP2 or TIMP1 gene expression in CD31-TFPI mice compared to control mice (**Error! Reference source not found.**. Graphs A and C).

There were n=10 in the control and in the CD31-TFPI group for all assays. Baseline sample numbers were as previously noted in section 6.1.

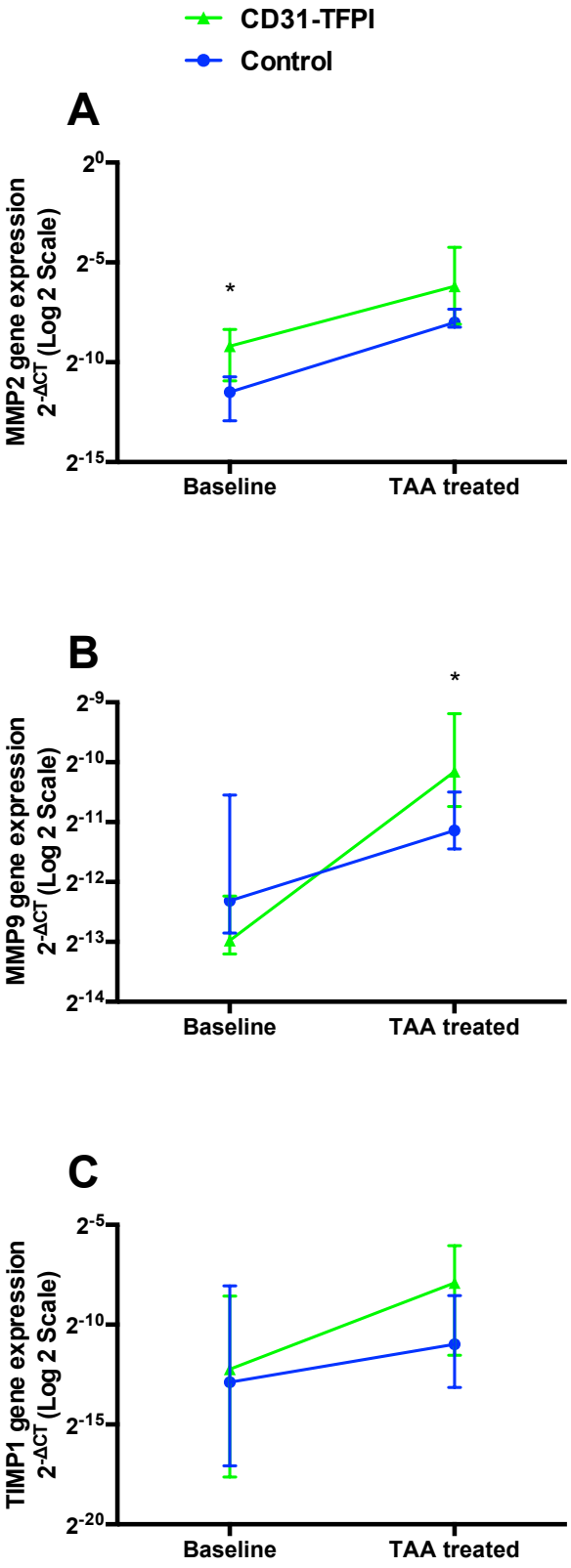


**Figure A 9: TAA induced chronic liver injury, matrixmetalloproteinase and TIMP gene expression**

**Graph A:** MMP2 gene expression in whole liver homogenates. CD31-TFPI mice had a 8.7 fold change (increase) and control mice had a 17.9 fold change (increase) in MMP2 gene expression after TAA administration compared to baseline.

**Graph B:** MMP9 gene expression in whole liver homogenates. CD31-TFPI mice had a 6.8 fold change (increase) and control mice had a 1.5 fold change (increase) in MMP9 gene expression after TAA administration compared to baseline.

**Graph C:** TIMP1 gene expression in whole liver homogenates. CD31-TFPI mice had a 22.3 fold change (increase) and control mice had a 4.1 fold change (increase) in TIMP1 gene expression after TAA administration compared to baseline.

### *A.4.5. Liver immune cell composition*

Digital image analysis of liver FFPE sections from mice administered TAA were stained using an antibody for F4/80 and showed no statistically significant difference in the number of F4/80 positive macrophages in the livers of CD31-TFPI mice compared to C57BL6/J control mice (Figure A 10. Graph A). There were n=10 in the control and in the CD31-TFPI group for all assays. Baseline sample numbers were as previously noted in section 6.1.

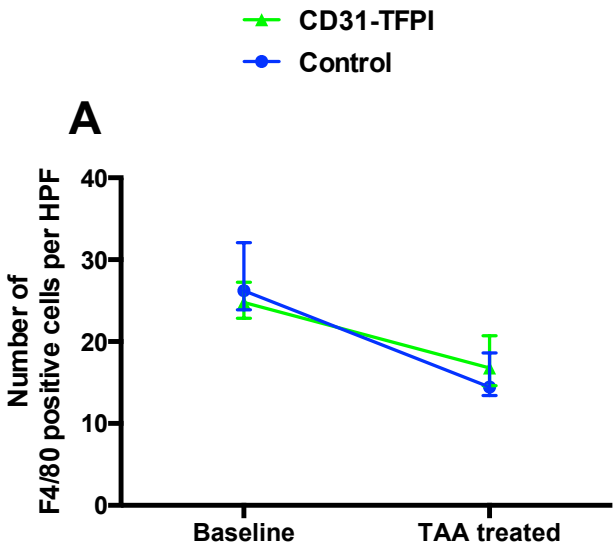


**Figure A 10: TAA induced chronic liver injury, F4/80 immunohistochemistry**
Symbols indicate median. Bars indicate interquartile range.

**Graph A:** Number of macrophages in liver FFPE tissue sections as determined by F4/80 immunohistochemistry. Median at 24 hours after TAA administration, 15 cells per HPF and 17 cells per HPF (-1.7 and -1.5 fold change from baseline) in control and CD31-TFPI strains respectively.

### *A.4.6. Model summary - TAA induced chronic liver injury in CD31 targeted expression of TFPI*

This model was initiated to provide further evidence to support the data collected in the $CCl_4$ model of chronic liver injury, however it was abandoned after a single cohort because of the flaw in the experimental design discussed in Chapter 4. Briefly, mice were continuously administered thioacetamide (TAA) up until they were culled creating a potential acute on chronic liver injury model as opposed to the intended chronic liver model.

After thioacetamide (TAA) induced chronic liver injury the overall picture in CD31-TFPI mice was of increased liver fibrosis in comparison to control mice. This was a somewhat surprising result as all prior models (acute and chronic liver injury) had suggested a protective or pro-resolution effect of transgenic TFPI expression and there had been a significant decrease in hepatic stellate cell activation in CD31-TFPI mice compared to control mice in this TAA model. However, as in the previous model ($CCl_4$ induced chronic liver injury) hepatic stellate cell activation had been decreased at baseline and fold change from baseline showed that there was a greater increase in hepatic stellate cell activation in the liver of CD31-TFPI mice compared to controls.

The relatively greater increase in hepatic stellate cell activation from baseline in the CD31-TFPI mice, in part, explains the increased fibrosis and relatively large fold increase in TIMP1 expression from baseline. The increase in hepatic stellate cell activation may have been associated with the increase in MMP9 expression seen in CD31-TFPI mice. MMP-9 has a role in TGF-β

associated hepatic stellate cell activation and collagen production. MMP-9 is expressed by Kupffer cells, hepatic stellate cells, lymphocytes and neutrophils during liver fibrosis and its activity and gene expression is not normally altered in liver fibrosis (Knittel et al. 2000)(Hemmann et al. 2007) therefore it is possible that, as in the $CCl_4$ model, priming of an effector cell may have occurred and in this model lead to increased MMP9 expression and a pro-fibrotic microenvironment. Unfortunately only F4/80 macrophage populations were quantified in this model. There was no difference between transgenic and control mice in the absolute numbers of these cells in the liver but their Ly6C expression profile was not investigated.

Due to limitations on time and resources and the incongruous results from this model I felt it was inappropriate to repeat a modified version of the TAA model to address the experimental design flaw.

| Parameter measured | TAA chronic liver injury model vs. control | |
|---|---|---|
| | **αSMA-TFPI** | **CD31-TPFI** |
| **Liver collagen content** | Increased hydroxyproline content. | Increased Sirius red staining, hydroxyproline content and collagen 1α1 gene expression. |
| **Hepatic stellate cell activation** | Decreased activation. | Decreased hepatic stellate cell activation (*but relative increase from baseline)* greater than controls. |
| **MMP2 / MMP9 expression** | Decreased (no change from baseline) MMP9 expression. | Increased MMP9 expression. |
| **TIMP1 expression** | Decreased expression. | Increased expression. |
| **Liver Immune cell composition** | No difference (F4/80 positive macrophages only measured). | No difference (F4/80 positive macrophages only measured). |
| **Liver injury** | Decreased ALP and total bilirubin. | No difference. Relative stability in LFT's compared to control increase. |

**Table A 1: Summary TAA chronic liver injury**

## Appendix A References

Hemmann, S. et al., 2007. Expression of MMPs and TIMPs in liver fibrosis - a systematic review with special emphasis on anti-fibrotic strategies. *Journal of Hepatology*, 46(5), pp.955–975.

Knittel, T. et al., 2000. Expression of matrix metalloproteinases and their inhibitors during hepatic tissue repair in the rat. *Histochemistry and cell biology*, 113(6), pp.443–453.

Liu, Y. et al., 2013. Animal models of chronic liver diseases. *Am J Physiol Gastrointest Liver Physiol*, 304(5), pp.G449–68. Available at: http://www.ncbi.nlm.nih.gov/pubmed/23275613.

Salguero Palacios, R. et al., 2008. Activation of hepatic stellate cells is associated with cytokine expression in thioacetamide-induced hepatic fibrosis in mice. *Lab Invest*, 88(11), pp.1192–1203. Available at: http://www.ncbi.nlm.nih.gov/pubmed/18794850.

Teixeira-Clerc, F. et al., 2006. CB1 cannabinoid receptor antagonism: a new strategy for the treatment of liver fibrosis. *Nat Med*, 12(6), pp.671–676. Available at: http://www.ncbi.nlm.nih.gov/pubmed/16715087.

## Appendix B

Below are images (original magnification x1000) of CD31 DAB immunohistochemical staining of liver sections from uninjured livers. The DAB labelled antibody demonstrates positive staining of vascular endothelial cells but not sinusoidal epithelial cells.

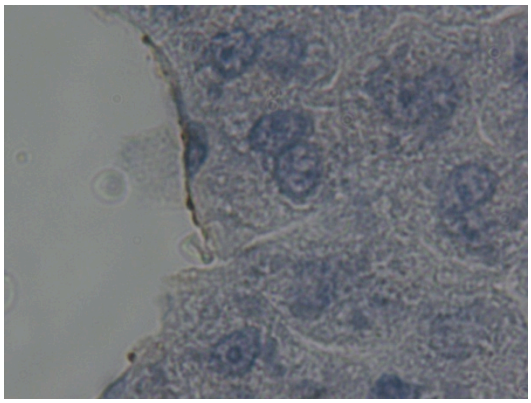

CD31 staining luminal vascular endothelial cells

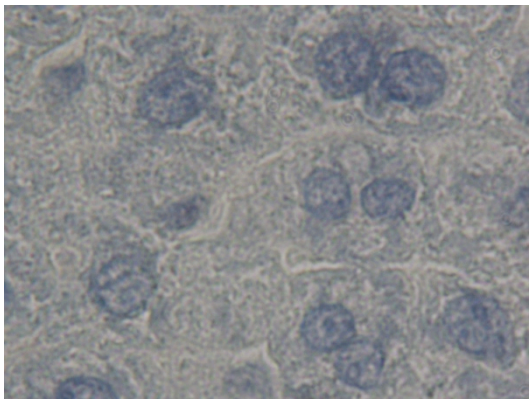

No staining of sinusoidal endothelial cells